

Camilla Gunnesdahl Jensen
Emile Dreyer Vetter

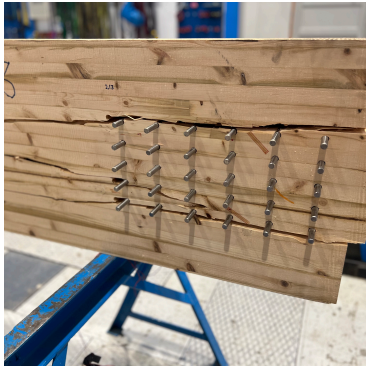
Experimental analysis of GLULAM specimens from Tretten bridge and related block failure and fatigue issues

Master's thesis in Civil and Environmental Engineering
Supervisor: Kjell Arne Malo
June 2023



Camilla Gunnesdahl Jenssen
Emile Dreyer Vetter

Experimental analysis of GLULAM specimens from Tretten bridge and related block failure and fatigue issues



Master's thesis in Civil and Environmental Engineering
Supervisor: Kjell Arne Malo
June 2023

Norwegian University of Science and Technology
Faculty of Engineering
Department of Structural Engineering



Norwegian University of
Science and Technology



MASTER THESIS 2023

SUBJECT AREA: Timber Structures	DATE: 08.06.2023	NO. OF PAGES: 89 + 190
------------------------------------	---------------------	---------------------------

TITLE:

Experimental analysis of GLULAM specimens from Tretten bridge and related block failure and fatigue issues

Eksperimentelle forsøk på limtreprøver fra Tretten bru og relaterte problemer med utmatting og blokkutrivning

BY:

Camilla Gunnesdahl Jenssen

Emile Dreyer Vetter



SUMMARY:

This Master's thesis aims at contributing to the ongoing investigation of the collapse of *Tretten* bridge with a particular emphasis on GLULAM's relations to block failure and fatigue. Various experimental tests are conducted on GLULAM specimens from diagonal element 13B to define static strength parameters for a fatigue-related case study. This thesis encompasses four tension tests, three tests focused on block failure, four four-point bending tests, and an additional ten compression tests. Block failure specimens experienced sudden rotations and dynamic displacement responses prior to failure, indicating a capacity limitation due to unsymmetrical failure. Nevertheless, data from the block failure test and bending test indicated consistent results of $f_{t,0}$ that varies between 32 to 33 MPa. Furthermore, $f_{c,0}$ and $E_{c,0}$ were defined as 39 MPa and 11420 MPa, respectively. Consequently, the results indicate that the material quality of the lamellas T14.5 used in diagonal 13B satisfies the qualities provided for GL32c in EN14080.

S-N curves were constructed based on a load scenario presumably similar to the one that led to the collapse of *Tretten* bridge. The results yield k_{fat} values of 0.7 and 0.8 for diagonal 6 and 7, respectively. The latter indicates a greater design stress level for diagonal 7, resulting in failure after 432 cycles. Additionally, diagonal 7 exhibits a steeper S-N curve than diagonal 6, indicating a lower number of cycles at the same stress level. Consequently, diagonal 7 is the critical diagonal.

RESPONSIBLE TEACHER: Kjell Arne Malo

SUPERVISOR(S): Kjell Arne Malo

CARRIED OUT AT: Department of Structural Engineering

Sammendrag

Målet med denne masteroppgaven er å belyse viktige temaer som kan ha bidratt til kollapsen av *Tretten* bru, med særlig vekt på trevirkets relasjon til blokkutrivning og utmatting. Det vil bli gjennomført eksperimentelle tester på tilsendte limtreprøver fra diagonalelement 13B for å definere relevante styrkeparametere. Resultatene fra eksperimentet vil senere bli brukt til å regne på kritiske forbindelser og deres kapasitet til utmattelse.

Kapittel 2 består av en teoridel som omhandler trevirkets unike egenskaper og karakteristikk. Bakgrunnen for denne delen er å skape et grunnlag for å forstå treets anvendelser og potensiale i brukonstruksjoner. De sterkt miljøavhengige materialegenskapene til trevirke vil bli beskrevet i relasjon til utfordringene som følger med dem.

Kapittel 3 inneholder en litteraturstudie av relevant forskning med fokus på faktorer som er relatert til kollapsen av *Tretten* bru. Informasjon om forskningsstudier relatert til syklisk og statisk utmattelse vil bli presentert. Videre inneholder kapittelet en oppsummering av de foreløpige rapportene utstedt av SHK (Statens havarikommisjon) angående bruens kollaps. I disse rapportene fremstår utmattelse og blokkutrivning av diagonalelementene som avgjørende svakheter i bruas strukturelle integritet.

Kapittel 4 omhandler gjennomførte eksperimenter. Rapporten inneholder gjennomgangen av 4 strekktester, 3 blokkutrivningstester, 4 firepunkts bøyningstester og ytterligere 10 trykktester. Prøvene for blokkutrivning opplevde rotasjoner og dynamiske forskyvninger før kollaps, noe som indikerer en kapasitetsbegrensning på grunn av asymmetrisk svikt. Likevel viste data samlet fra blokkutrivningstestene og bøyningstest konsistente resultater for $f_{t,0}$ som varierte mellom 32 til 33 MPa. Videre ble $f_{c,0}$ og $E_{c,0}$ definert som henholdsvis 39 MPa og 11420 MPa. Resultatene indikerer derfor at kvaliteten på lamellene T14.5 som ble brukt i diagonal 13B oppfyller kvalitetskravene som er angitt for GL32c i EN14080.

Kapittel 5 omhandler en *case-studie* av kapasitetsberegning til kritiske forbindelser i diagonal 6 og 7 relatert til blokkutrivning og utmatting. Resultatet indikerer k_{fat} verdier tilsvarende 0.7 og 0.8 for respektive diagonaler. S-N kurver ble så konstruert basert på disse verdiene, som videre beskriver at diagonal 7 er forventet å tåle 432 sykluser. S-N diagrammene illustrerer en brattere kurve for diagonal 7 i forhold til diagonal 6 ved samme spenningsnivå, dette impliserer at diagonal 7 er den kritiske diagonalen.

Abstract

This *Master's thesis* aims on contributing to the ongoing investigation of the collapse of *Tretten* bridge with a particular emphasis on GLULAM's relations to block failure and fatigue. Various experimental tests are conducted on GLULAM specimens from diagonal element 13B to define static strength parameters for a fatigue-related case study.

Chapter 2 consists of an in-depth examination of the unique properties and characteristics of timber, serving as a comprehensive foundation for understanding its utilization and potential in civil engineering. The highly environmentally dependent material properties of timber are elaborated, shedding light on the challenges that accompany them.

Chapter 3 conducts a *state-of-the-art* review of relevant literature focusing on topics that are plausibly related to the collapse of *Tretten* bridge. Noteworthy areas of investigation include prior research studies on cyclic and static fatigue. Furthermore, a summary of the preliminary reports issued by the Norwegian safety investigation authority (NSIA) regarding the bridge collapse is presented. From the latter, fatigue and block failure within the dowel connections emerges as decisive weaknesses in the bridge's structural integrity.

Chapter 4 presents the laboratory experiments conducted, including 4 tension tests, 3 tests focused on block failure, 4 four-point bending tests, and an additional 10 compression tests. Block failure specimens experienced sudden rotations and dynamic displacement responses prior to failure, indicating a capacity limitation due to unsymmetrical failure. Nevertheless, data from the block failure test and bending test indicated consistent results of $f_{t,0}$ that varies between 32 to 33 MPa. Furthermore, $f_{c,0}$ and $E_{c,0}$ was defined as 39 MPa and 11420 MPa, respectively. Consequently, the results indicate that the material quality of the lamellas T14.5 used in diagonal 13B does satisfy the qualities provided for GL32c in EN14080.

Chapter 5 contains a simplified case study on block capacity-related fatigue failure of critical connections in diagonal 6 and 7. A simplified design method for fatigue verification in EC5-2 is described and utilized in order of establishing S-N curves. The S-N curves are constructed based on a load scenario presumably similar to the one that led to the collapse of *Tretten* bridge. The results yield k_{fat} values of 0.7 and 0.8 for diagonals 6 and 7, respectively. This indicates a greater design stress level for diagonal 7, resulting in failure after 432 cycles. Additionally, diagonal 7 exhibits a steeper S-N curve than diagonal 6, indicating a lower number of cycles at the same stress level. Consequently, diagonal 7 is the critical diagonal.

Preface

This *Master's thesis* was conducted at the Faculty of Engineering Science and Technology in the Department of Structural Engineering at the Norwegian University of Science and Technology during the spring of 2023.

We would like to take this opportunity to express our gratitude to our supervisor, Kjell Arne Malo, for granting us the opportunity to participate in the investigation of the collapse of *Tretten* bridge, and for providing continuous guidance and support throughout the writing of this *Master's thesis*.

Additionally, we would like to express our appreciation to the lab technicians at the Department of Structural Engineering. Special thanks to Johan Fagervold and Gøran Loraas for their valuable help in assembling and operating the testing machines, Terje Petersen for his assistance with specimen cutting and reinforcement, and lastly Thomas Uhlving and Trond Auestad for their assistance and instructions on the test machines. We are also grateful to Wefag Alawd for her support in the laboratory and valuable insight related to this thesis.

Initially, this *Master's thesis* was intended to focus on the topic of fatigue of GLULAM beams. However, due to unforeseen circumstances, the designated test machine was out of order for the entire semester, rendering fatigue testing not possible. As a result, we decided to redirect the content of this thesis towards experimental testing of the *Tretten* bridge elements, with a lesser emphasis on fatigue than initially planned. Despite this alteration, we have chosen to include some of the work we conducted on the topic of fatigue with relevancy to the collapse of *Tretten* bridge, with the intention that it may serve as a valuable resource for future inquiries.

Table of Contents

Sammendrag	I
Abstract	I
Preface	II
Abbreviations	VII
Nomenclature	VII
1 Introduction	1
2 Background theory	3
2.1 Biological properties of timber	3
2.1.1 The anatomy of timber	3
2.1.2 Timber species	4
2.1.3 Composite material	4
2.1.4 Water transportation	5
2.2 Influences on material behaviour	6
2.2.1 Moisture content	6
2.2.2 Knots	6
2.2.3 Viscoelastic and mechano-sorptive properties	7
2.2.4 Accounting for uncertainties in laminated beams	7
2.3 Orientations in timber	9
2.3.1 Grain orientation	9
2.3.2 Critical stresses	10
3 State-of-the-art	12
3.1 Cyclic fatigue	12
3.1.1 S-N curves	13
3.1.2 The Palmgren-Miner rule	15
3.2 Static fatigue	15
3.2.1 Empirical models - The Madison and Pearson Curve	16
3.2.2 Theoretical models - The Nielsen and LEFM model	17

3.3	Tretten bridge	18
3.3.1	The bridge design	18
3.3.2	The current investigations	19
3.4	Capacity of dowel connections	20
3.4.1	Design guidelines in <i>EC5</i>	20
3.4.2	Correlation of block shear and tension in American standards	22
4	Experimental test of Tretten bridge elements	23
4.1	Introduction to experiments	24
4.1.1	Background analysis of <i>Tretten</i> bridge	24
4.1.2	Diagonal element of <i>Tretten</i> used for experiments	24
4.1.3	Details of dowel connections	25
4.2	Tension test of timber elements	28
4.2.1	Preparation for <i>S-tests</i>	28
4.2.2	Equipment and method of <i>S-tests</i>	30
4.2.3	Results of <i>S-tests</i>	32
4.2.4	Discussion of tensile tests and concluding remarks	34
4.3	Block failure test	35
4.3.1	Preparation for <i>B-tests</i>	35
4.3.2	Equipment and method of <i>B-tests</i>	36
4.3.3	Result of <i>B-tests</i>	39
4.3.4	Discussion of block failure tests and concluding remarks	44
4.4	Compression tests	45
4.4.1	Equipment and method of <i>C-tests</i>	45
4.4.2	Results of <i>C-tests</i>	47
4.5	Four-point bending test	50
4.5.1	Equipment and method of bending test	50
4.5.2	Result of bending tests	51
4.6	Specimen moisture and density calculations	55
4.6.1	Density	55
4.6.2	Moisture content	56
5	Fatigue life determination based on static strength	58

5.1	Analysis of critical connections	59
5.2	Fatigue verification according to <i>EC5-2</i>	63
5.3	S-N curves for Tretten bridge diagonals	64
5.4	Discussion on case study for diagonal 6 and 7	67
6	Conclusion	68
	Bibliography	70
	Appendix	72
A	Tension test	72
A.1	Specimen S1	74
A.2	Specimen S2	75
A.3	Specimen S3	76
A.4	Specimen S4	77
B	Block shear test	78
B.1	Specimen B1	80
B.2	Specimen B2	84
B.3	Specimen B3	88
C	Compression test	89
C.1	Specimen C1	91
C.2	Specimen C2	93
C.3	Specimen C3	95
C.4	Specimen C4	97
C.5	Specimen C5	99
C.6	Specimen C6	101
C.7	Specimen C7	103
C.8	Specimen C8	105
C.9	Specimen C9	107
C.10	Specimen C10	109
D	4-point bending test	111
D.1	Specimen S2	114
D.2	Specimen S3	116
D.3	Specimen S4	118

E	cross-section areas of specimens for <i>S</i> -tests	120
F	<i>Python</i> codes	122
F.1	S-tests	123
F.2	S1-test	125
F.3	S2-test	128
F.4	S3-test	131
F.5	S4-test	134
F.6	B-tests	137
F.7	B1-test	139
F.8	B2-test	145
F.9	B3-test	150
F.10	C-tests	152
F.11	4-point bending test	154
F.12	S-N curves	161
G	Pictures from <i>Tretten</i> bridge elements	162
G.1	Tension test specimens	162
G.2	Block failure test specimens	171
G.3	4-point bending specimens	189
H	Block from <i>Tretten</i> bridge	196
I	Drawings	201
I.1	Drawings of <i>Tretten</i>	201
I.2	Drawings of specimens for experiments	205
J	Report	211

Abbreviations

- B-test** specimen for block failure test.
- C-test** specimen for compression failure test.
- COG** centre of gravity.
- CSA** Canadian standards association.
- DOL** duration of load.
- DVM** damaged viscoelastic material.
- EC0** EN 1990: Basis of structural design.
- EC5** EN 1995: Design of timber structures.
- EC5-2** EN 1995-2: Design of timber structures - Part 2: Bridges.
- EMC** equilibrium moisture content.
- FEA** finite element analysis.
- FSP** fibre saturation point.
- GL32c** glued laminated timber, composite.
- GL32h** glued laminated timber, homogeneous.
- GLULAM** glued laminated timber.
- LEFM** linear elastic fracture mechanics.
- LVDT** linear variable differential transformers.
- LVL** laminated veneer lumber.
- MC** moisture content.
- MC-test** specimen for moisture content and density determination.
- NDS** national design specification.
- NOC** number of cycles.
- NSIA** Norwegian safety investigation authority.
- RH** relative humidity.
- S-test** specimen for tension failure test.
- SL** stress level.
- ULS** ultimate limit state.

Nomenclature

α	capillary suction
Δl	changes in length
Δl_0	changes in sectional length
δ	displacement
$\Delta\sigma$	stress range
ℓ_1	gauge length
γ_M	material partial safety factor for the material
γ_S	partial safety factor for design actions
$\rho_{05,i,min}$	lowest 5-percentile density of all sub-samples
$\rho_{05,i}$	5-percentile density of sub-sample i
ρ_k	characteristic density
σ_w	surface tension
σ_a	stress amplitude in cyclic load
σ_{max}	maximal stress in cyclic load
σ_{mean}	mean stress in cyclic load
σ_{min}	minimal stress in cyclic load
τ	shear stresses
A	slope of the S-N curve
a	fatigue coefficient depending on type of loading or connections
a_d	distance between a loading position and the nearest support in a bending test
a_1	distance between dowels in a row
A_{cs}	area of cross-section
A_{net}	net area
B	constant term for S-N curves
b	fatigue coefficient depending on type of loading or connections
d_i	inner diameter
e	dimensionless eccentricity
e_N	eccentricity of axial load
$E_{m,g}$	mean global modulus of elasticity
$E_{m,l}$	mean local modulus of elasticity
f_k	characteristic strength

f_m	mean strength
f_v	shear strength
$f_{c,0}$	compressive strength parallel to grain
$f_{c,el}$	elastic compression strength
$f_{c,pl}$	plastic compression strength
$F_{est,max}$	estimated maximum load
F_{Rk}	characteristic load-carrying capacity according to Johansen's theory
F_{Sk}	characteristic load-carrying capacity for splitting considering effective amount of dowels
$f_{t,0}$	tensile strength parallel to grain
G	shear modulus of elasticity
g	gravitational acceleration
h	height of cross-section
H_c	capillary height
I	second moment of inertia
I_{net}	net second moment of inertia
k_{fat}	reduction factor for fatigue loads
k_{mod}	reduction factor for static loads
k_n	factor to adjust for number of sub-samples in a density test
l	total length
l_0	gauge length
l_s	length between supports
L_{net}	total net length
l_{net}	sectional net length
M	moment
m_{init}	initial mass
m_{od}	oven dried mass
MC	moisture content
N	number of cycles
N_x	axial load
n_d	number of dowels
n_{ef}	effective number of dowels
n_j	number of specimens in sub-sample j
n_s	number of sub-samples

$N_{x,R}$	resistance to axial load
R	stress ratio
r	capillary radius
R_0	rotation around origin
R_d	design resistance value
R_k	characteristic resistance value
S_d	design value of load
S_k	characteristic value of load
t	specimen thickness
t_f	time until failure
w	width of cross-section
z_{max}	largest vertical distance from centre of gravity

1 Introduction

The *Hyperion*, a coast redwood located in California, is the tallest known living tree measuring 116 metres. In contrast, the tallest bearing timber building is *Ascent* in Wisconsin, standing at 87 metres. Humans frequently look to nature for guidance in solving complex issues, such as the development of new materials or the utilization of existing ones. Correspondingly, timber has arguably become the most important organic construction material that can be utilized for structures with great heights or large spans. Due to its high specific strength and low environmental impact, it holds the potential to replace widely employed materials that have a more significant ecological footprint.

Even though timber has been used in construction for many millennia, our effective knowledge of the material is surprisingly low. This lack of knowledge is evident in the ongoing investigations into the collapse of *Tretten* bridge in 2022. The current situation in Norway regarding the discontinuation of using timber for bridges after *Tretten's* collapse highlights the evident lack of comprehensive scientific guidelines in certain aspects of dimensioning timber structures within the *Eurocodes*. This *Master's thesis* is driven by the intention to contribute to filling this gap. Nonetheless, in correlation to a growing demand of environmentally friendly building materials, the demand for timber products has increased correspondingly, which implies the importance of scientific results in the field.

The subject being addressed in this *Master's thesis* is the complex interaction of fatigue loads and block failure capacity in dowel connections, specifically focusing on their potential role in the collapse of the *Tretten* bridge. This *Master's thesis* seeks to contribute towards enhancing the nation's infrastructure. By analyzing information from ongoing investigations, samples from the bridge's glued laminated timber (GLULAM) beams, and state-of-the-art theory, relevant strength parameters will be found and compared to qualities specified in design standards. The motivation of this work is effectively illustrated by the similarities observed between the conducted experiments and the critical section that likely led to the collapse of the bridge on Figure 1.



Figure 1: Decisive block failure from *Tretten* bridge and experiments.

Prior to delving into the case study's intricacies, it is essential to establish a solid theoretical understanding of timber. Chapter 2 will visit the background characteristics of timber's complex cellular structure, and how the latter influences material behaviour in various ways. Furthermore, a *state-of-the-art* review of relevant topics will be presented in Chapter 3. Chapter 4 will include experimental results, discussion, and partial conclusions related to samples sent from *Tretten* bridge. Lastly, Chapter 5 will present a case study focusing on the dowel connections of critical diagonals of *Tretten* bridge, shedding light on their potential contribution to the collapse of the bridge.

2 Background theory

Timber, and its derivative products, have various properties that should be exploited advantageously according to its field of application. Certain species of timber are dense and durable, making them particularly well-suited for use in furniture or as railroad ties. Other species, on the other hand, possess higher specific strength, which makes them more suitable for applications within construction. The unique characteristics of timber can however solely be attributed to its microstructure.

This chapter will provide an in-depth examination of the basic properties and characteristics of timber, serving as a comprehensive foundation for understanding its utilization and potential in civil engineering.

2.1 Biological properties of timber

2.1.1 The anatomy of timber

A tree will grow tall as a result of evolutionary principles, in order to maximize the amount of sunlight they receive and thus optimize the output from the process of photosynthesis. This is the reason why growth occurs primarily in the longitudinal direction, often referred to as primary growth. Growth in the radial direction is known as secondary growth and happens on a smaller scale. The cell walls and their structure contributes to major parts in characterisation of timber's anisotropic behaviour and moisture content dependency (Jenssen and Vetter 2022).

The cell structure of timber consists of layers of various chemical compounds serving different organic purposes. In the longitudinal direction, cellulose chains are bundled together in the shape of long, thin fibrils, held together by lignin. Analogously as for concrete structures, the cellulose serves as reinforcement bars, while hemicellulose acts like cement and lignin as glue (Booker and Sell 1998). Each of the cells includes, among other components, primary and secondary walls. The primary wall consists of fibrils with random orientations, while the secondary wall can be divided into three more structured subcategories denoted as *S1*, *S2*, and *S3* in Figure 2. The layers *S1* and *S3* has the microfibrils on large angles to cell direction, and has favorable effects for resisting buckling and compressive forces in the cell structure. *S2*, the thickest layer, has a smaller angle along the cell direction and serves well for resisting tension forces (Nygaard 2020).

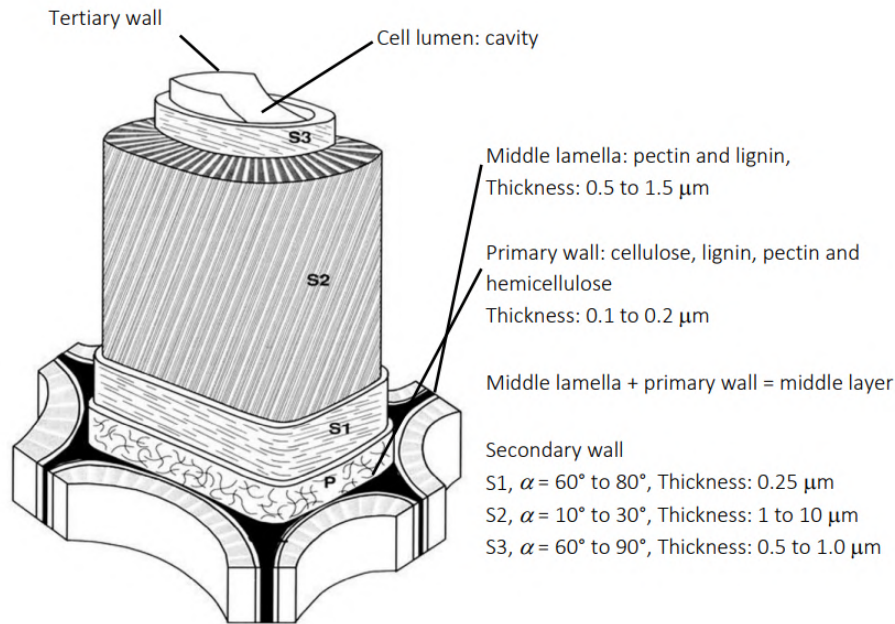


Figure 2: Schematic of cell wall structure (Booker and Sell 1998).

2.1.2 Timber species

Each timber species encompasses a broad variety of characteristics that must be taken into account in relation to their intended purpose and applications. EN 1995: Design of timber structures (EC5) and corresponding standards, often differentiate timber species into hardwood and softwood in order to define general resistance parameters. Some important distinctions between the species are their density, growth rate, fire resistance, and specific strength. Softwoods, such as spruce and pine, are generally lighter and less dense than most hardwoods. Softwoods are commonly used in construction, while hardwoods are often seen in high-quality furniture or used as crossties in railroads (Koehler 1917). Due to the latter, this thesis will mainly focus on the properties of softwood, more specifically pine.

2.1.3 Composite material

The growth of annual rings in softwoods is a product of alternating properties between earlywood and latewood due to seasonal climate changes. Earlywood, which forms early in the season, has a thin-walled and porous cell structure that serves the purpose of transporting water and nutrition in the trunk. In contrast to earlywood, latewood is a denser material heavily influenced by dry and cold climates and can be recognized as a darker ring in the cross-section of a wood trunk. Earlywood is less dense, hence it has a correspondingly lighter color. When the cells in a tree die, they dry out and become heartwood, which is the inner and oldest part of softwood as illustrated in Figure 3. In opposition to sapwood, heartwood is denser and is accompanied by better load resistance properties. Timber's complex composition of varying material densities gives it composite material-like behaviour, which can have decisive effects on load-carrying capacity and fracture surface for both static and cyclic loading (Harris 2003).

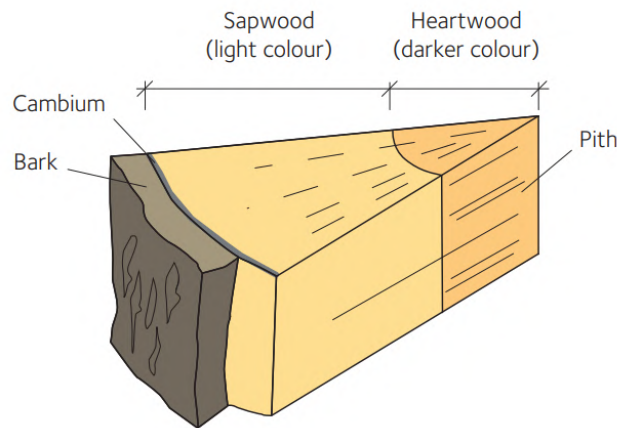


Figure 3: cross-section of a wood trunk of softwood (Swedish wood 2022).

2.1.4 Water transportation

Wood is capable of absorption and desorption of moisture in accordance with the ambient environment, hence defined as a hygroscopic material. The hygroscopic properties imply that the material behaviour is dependent on the relative humidity (RH) in the exposed environment. The consequences of the dependency will be elaborated in Section 2.2.1. Due to the cell composition in timber, changes in moisture content (MC) will occur until the material reaches the equilibrium moisture content (EMC). The point at which wood ceases to absorb moisture from or release moisture to the surrounding environment is defined as EMC.

Absorption and desorption are slow processes that depend on humidity changes over time. If one were to analyze the EMC by increasing the RH, and then reversing the process by decreasing the RH, one would observe that absorption and desorption curves will not coincide. This is a result of residue water after desorption resulting in a higher MC than for absorption, partly due to chemically bound water in the cell structure. The phenomenon is called hysteresis. Water content in wood comes as bound water and free water, where the ratio between them is influenced by transportation within the stem.

Transportation of water in timber occurs through three methods; osmosis, transpiration and, capillary suction, where the latter is most relevant in construction. Capillary suction is a phenomena that occurs in timber as well as any other material with straw-shaped compositions. For timber, there are electrostatics forces along the cell walls pulling on the concave surface membrane of water, and hence also the liquid column in the pore beneath it (Thue 2016). A force equilibrium in a vertical direction can be used to define Equation 1.

$$H_c = \frac{2\sigma_w \cos(\alpha)}{\rho_w r g} \quad (1)$$

Where,

H_c	is the capillary height;
r	is the capillary radius;
ρ_w	is the water density;
g	is the gravitational acceleration;
σ_w	is the surface membrane tension;
α	is the angle of capillary suction.

Equation 1 describes how water is transported in the trunk using capillary suction. For small capillary radii such as in the pores in timber, capillary heights may reach over hundred metres (Thue 2016).

2.2 Influences on material behaviour

2.2.1 Moisture content

Timber's cell structure makes its material properties susceptible to changes in water content. As a hygroscopic material, timber absorbs water in response to its environment. The amount of moisture in wood is measured as moisture content (MC). Equation 2 describes how MC is calculated in timber, where m_{init} is the initial mass and m_{od} is the oven-died mass of the specimen.

$$MC = \frac{m_{init} - m_{od}}{m_{od}} \quad (2)$$

In construction, variations in MC are undesirable as they can lead to reduced material durability, introduce stresses, and unpredictable material properties. This is especially the case when moisture is stored as free water in the lumen. The fibre saturation point (FSP) is the stage at which the cell walls are saturated with bound water, and the cell cavities are free of unbound water. The FSP for timber depends on the species, though often found between 25 % and 35 % (Tronstad 2000). For $MC \leq FSP$ the material properties are dependent on changes in MC. At this point free water is filling the cavities and the strength and stiffness of timber are significantly reduced, though constant for further increase of MC. The changes in behaviour due to MC are illustrated in Figure 4.

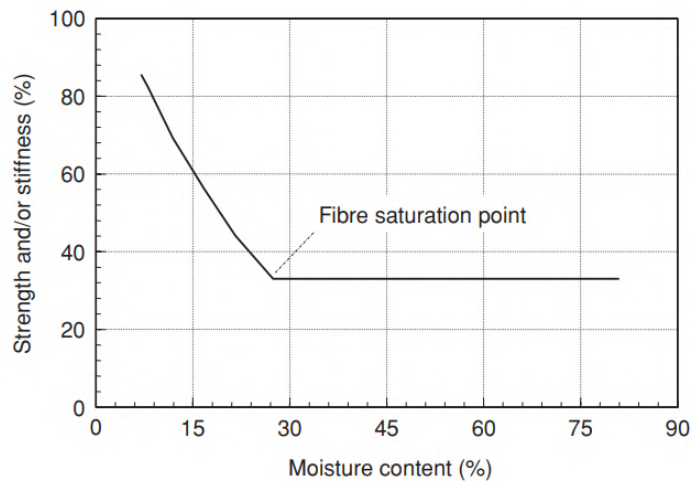


Figure 4: General relationship between stiffness and MC (Porteous and Kermani 2008).

2.2.2 Knots

Knots are the most common defect in timber and provide large uncertainties to the quality of the material. Knots arise when branches are cut off or removed and the exposed wood is left behind. They can also be formed from injuries to the tree caused by fungal infections. Knots result in local discontinuities in the grain direction of the wood, caused by the varying direction of branch growth in the logs. The significance of knots on the structural capabilities of timber depends on the location of the knot, size and, the loads the timber is supposed to resist.

Knots are usually considered as weak points that reduce the strength of timber structures under bending or tensile stresses. This is not the case for compression (Jockwer et al. 2017). Depending on the location of the knots, they could potentially strengthen a specimen subjected to certain loads by acting as reinforcements due to their high relative strength (Nygaard 2020). This is true when the knots are located centrally in the specimen. In instances where the knots are found on the edge of a specimen, they are likely to reduce the overall strength by early crack initialization. When exposed to excessive shear or tensile stresses perpendicular to grain, knots induce brittle behaviour in the timber material (Jockwer et al. 2017). The same brittle behaviours are found for specimens with knots subjected to tensile stresses parallel grain. In Figure 5 a timber specimen subjected to shear loads reach failure along grain direction with crack propagating initiated by the knot.

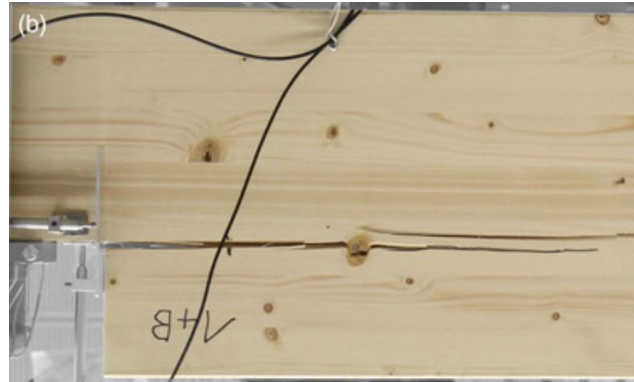


Figure 5: Crack propagation in wood subjected to shear (Jockwer et al. 2017).

2.2.3 Viscoelastic and mechano-sorptive properties

MC, knots and annual rings are a few of many factors that contribute to timber's somewhat unpredictable material behaviour. To make matters even more complicated, wood does not behave as a simple elastic material. Timber has time-dependent mechanical behaviour in addition to its elastic behaviour, which implies that wood is a viscoelastic material. When subjected to certain loads, wood experiences instantaneous elastic, delayed elastic and plastic or viscous deformations, where the two latter are time dependent. Plastic deformations are unrecoverable creep in opposition to delayed elastic deformations (Mårtensson 1994).

In addition to viscoelastic creep, timber experiences mechano-sorptive deformations due to the hygroscopic properties of wood. Variations of MC during mechanical loads induce deformations called mechano-sorptive creep (Nygaard 2020). Due to reduced strength and stiffness for $MC > FSP$, as discussed in Section 2.2.1, timber may experience additive effects with a mechano-sorptive creep for large values of MC.

2.2.4 Accounting for uncertainties in laminated beams

The design process for timber structures is complicated because of the intricate cellular structure and uneven behaviour of the material. As a result, a structural analysis must carefully consider the relationship between the loads applied and the material's response to ensure safety. For an arbitrary design problem, a probabilistic approach is used in order to acquire a safe relationship between subjected forces and structural resistance. Chapter 6.4 in EN 1990: Basis of structural design (EC0) introduces safety factors for design actions and for material resistance respectively denoted as γ_s and γ_M . Moreover, clause 6.4.2 in EC0 requires verification of Equation 3 for an ultimate limit state (ULS)

problem to achieve structural safety. Additionally, *EC5* introduces a modification factor k_{mod} to take account the effect of duration of load (DOL) and moisture content (MC) on timber.

$$S_d \leq R_d$$

$$S_k \gamma_S \leq k_{mod} \frac{R_k}{\gamma_M} \quad (3)$$

S_d and R_d are notations for design load and design resistance, respectively. Correspondingly, the same variable parameter with subscript k denotes the characteristic values. The partial safety factor for load actions accounts for uncertainty in load scenarios, which include permanent, variable, and accidental loads. The safety factor for resistance is based on the material used, with some materials having larger uncertainties and thus requiring a higher safety factor. For instance, γ_M for timber generally varies between 1.15 and 1.3 depending on the timber product that is used.

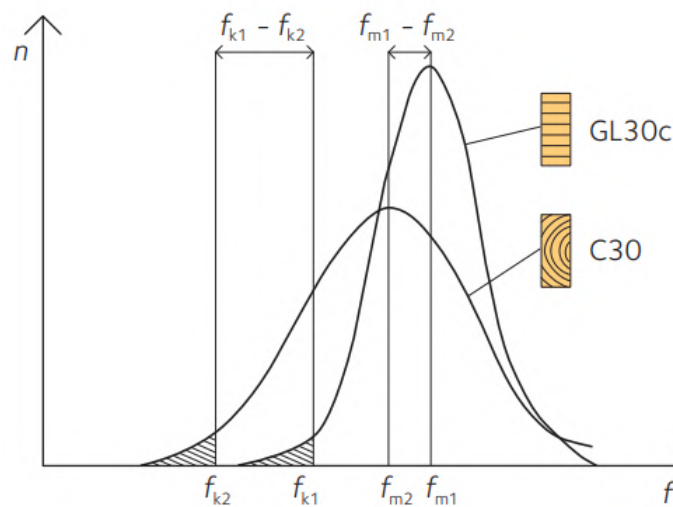


Figure 6: Probabilistic behaviour of GLULAM and solid timber (Swedish wood 2018).

Solid timber is more likely to have material imperfections such as knots and uneven grain patterns, resulting in a higher standard deviation of its properties. However, products like glued laminated timber (GLULAM) and laminated veneer lumber (LVL), which are made of layers of lamellas with stricter grading systems, have a more even distribution of imperfections and therefore more consistent properties. This is illustrated in Figure 6, where the y-axis represents the number of test specimens and f_k and f_m represent the specimens' characteristics and mean strengths. The latter notations may also include subscripts 90 or 0 which respectively refers to strength perpendicular and parallel to grain. Load-carrying capacity is hence generally higher for laminated beams than for solid timber of the same quality. GLULAM consists of multiple lamellas connected using finger-joints. According to *EC5* there are two classes of GLULAM, homogeneous and combined, with the latter using stronger lamellas on the outer edges for increased flexure resistance. The contribution of the lamellas to the second moment of area is found by multiplying its area and strength, with the distance from the centre of gravity (COG) squared. Thus, it is optimal to use high-strength lamellas in the outer zones of the laminates. An example of a GLULAM beam lay-up is seen in Figure 7.

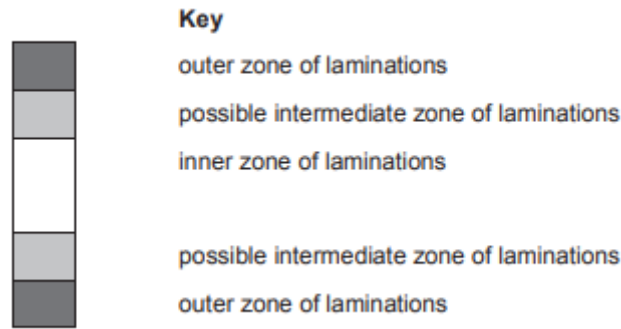


Figure 7: Example of a beam-layup of combined *GLULAM* (Standard Norge 2013).

2.3 Orientations in timber

2.3.1 Grain orientation

Orientation-based materials are referred to as anisotropic materials. Trees are, based on evolutionary principles, evolved to resist transverse wind loads that induce bending in form of in-plane tension and compression forces. This implies that they evolved to withstand loads parallel to grain direction and often have weaker properties perpendicular to it. As a result of having orientation-dependent strength properties, timber is referred to as an anisotropic material. The axis system for timber analysis is hence defined by the orientation of local grain direction that comprises of the longitudinal (L), radial (R), and tangential (T) axes, also known as the first, second, and third axes respectively (Jenssen and Vetter 2022). Figure 8 displays the relationships among them.

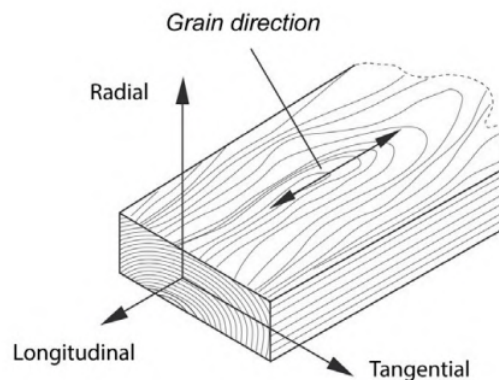


Figure 8: Orientation in timber (Fragkia and Foged 2020).

Loading on any timber surface is represented by two subscripts, with the primary subscript indicating the direction of the normal vector on the plane where the load acts and the secondary subscript giving the load's orientation. For example, a load imposed perpendicular to a cross-section is denoted as LL. Figure 9 illustrates the notations used for the stresses in the timber.

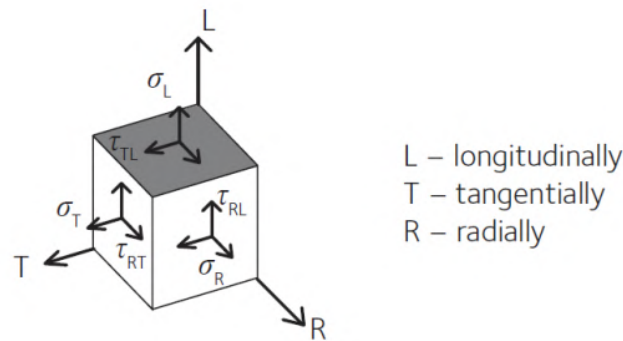


Figure 9: Notations of stresses (Fragkia and Foged 2020).

2.3.2 Critical stresses

The orientation of the grain in timber contributes to the anisotropic properties of timber. Due to the biological nature of trees mostly being subjected to loads in the longitudinal axis and is required to transport water vertically up the stem, grain direction is generally equivalent to the longitudinal direction. The first axis, commonly known as the strong axis, is both the strongest and stiffest. On the other hand, the second axis, which runs perpendicular to the grain, is relatively weaker and is therefore referred to as the weak axis. As a result of this, resistance parameters in timber need to be defined accordingly. For loads in the longitudinal axis, wood is given a corresponding tensile and compressive strength. For loads in the transverse direction, transversal strengths are defined accordingly.

Shear stresses in timber are defined in the material's local axis system. The stresses are denoted as τ_{TL} , τ_{RT} and, τ_{RL} and are always occurring in pairs. In order to respect the laws of equilibrium, the integral of the shear stresses over the area to which they are subjected to will coincide with the equivalent shear force on the opposite surface. For the same reason, $\tau_{TL} = \tau_{LT}$, $\tau_{RT} = \tau_{TR}$, and $\tau_{RL} = \tau_{LR}$ as illustrated in Figure 10. Correspondingly as for compression and tension, resistance parameters to shear forces are defined for timber. In timber structures, τ_{TL} and τ_{RL} are the most common shear stresses where shear strength values are found between 5 and 8 MPa. τ_{RT} is known as rolling shear with shear strength often as low as 3 MPa (Swedish wood 2022).

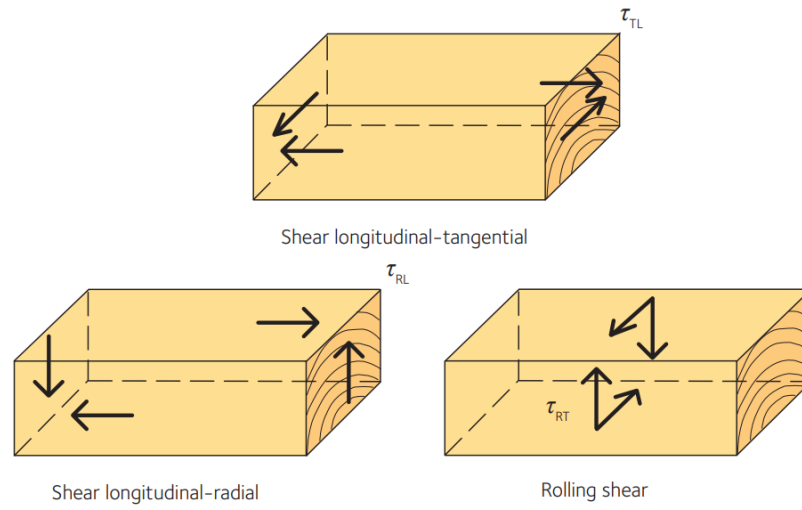


Figure 10: Shear stresses in timber (Swedish wood 2022).

3 State-of-the-art

Timber bridges are commonly used in many parts of the world, and they have a long history of providing safe and reliable transportation. However, these structures require careful design and maintenance to ensure their continued safety. The collapse of *Tretten* bridge has prompted concerns regarding the safety of timber truss bridges and emphasized the importance of conducting rigorous design checks. The investigation into the *Tretten* bridge collapse is ongoing, and experts are working to identify the underlying factors and safety issues that led to the failure. It is likely that fatigue and block failure of the dowel connections are critical causes of the collapse.

Fatigue in material science is the reduction of strength over time due to dynamic or static loads lower than the material strength. The capacity to resist fatigue loads, also but not necessarily referred to as cyclic loads, is determined by the number of cycles (NOC) until failure. The study of fatigue life began during the industrialization era of the early 19th century with the use of steel alloys in chains and railroads (Schütz 1996). Today, most fatigue studies are still focused on steel, as its failures produce a distinct fracture surface. Even though timber has been used as a structural material for centuries, information on the fatigue behaviour of wood is limited compared to metals and composite materials (Ansell and Bond 1998). It is hence imperative for this thesis to present current tools and guidelines for solving problems related to fatigue.

This *state-of-the-art* review will include a brief overview of cyclic and static fatigue and some of its simplified calculation models. Additionally, a summary of the preliminary reports by the Norwegian safety investigation authority regarding the collapse of *Tretten* bridge will be presented. Lastly, a review of current guidelines on capacity calculations of dowel connections according to Annex A in *EC5* will be presented.

3.1 Cyclic fatigue

Cyclic loading defines a load situation where the loads are continuously and repeatedly applied, which weakens the material and ultimately leads to fatigue. To analyze such loading sequences, it is necessary to define maximum stress, represented as σ_{max} , and minimum stress, represented as σ_{min} . The ratio between them is called the stress ratio, denoted R in Equation 4. A value of $R < 0$ indicates alternating loads, where σ_{max} and σ_{min} have opposite signs, and the load alternates between tension and compression. The most critical loading mode for wood is $R = -1$ (K. Malo et al. 2022).

$$R = \frac{\sigma_{min}}{\sigma_{max}} \quad (4)$$

The stress range, $\Delta\sigma$, is the difference between the maximum and minimum stresses as defined in Equation 5.

$$\Delta\sigma = \sigma_{max} - \sigma_{min} \quad (5)$$

Furthermore, the mean stress, σ_{mean} , is the mean value of the maximum and minimum stresses as defined in Equation 6.

$$\sigma_{mean} = \frac{1}{2}(\sigma_{max} + \sigma_{min}) = \frac{\Delta\sigma}{2} \frac{1+R}{1-R} \quad (6)$$

Lastly, the alternating stress, σ_a , is the amplitude of the cyclic load wave, thus the difference between maximum and minimum stresses as defined in Equation 7.

$$\sigma_a = \frac{1}{2}(\sigma_{max} - \sigma_{min}) \quad (7)$$

These equations are graphically visualized in Figure 11.

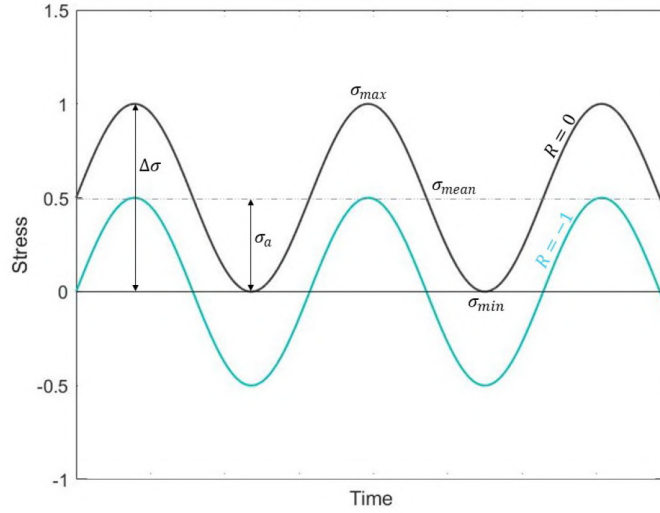


Figure 11: Cyclic load with stress as load parameter (Nygaard 2020).

Several models exist to describe cyclic fatigue, and the following sub-chapters will present two of them.

3.1.1 S-N curves

S-N diagrams are a tool commonly used to analyze the fatigue behaviour of a material. Basquin (1910) developed the S-N curve by utilizing Wöhler's experiments and work on fatigue behaviour (Schütz 1996). S-N curves in timber represent the reduction in strength level, f , caused by cyclic stresses. The curves are typically illustrated on a logarithmic scale such that the stress level is linearly proportional to NOC until failure, N (K. Malo et al. 2022). The formula for the S-N curve is given in Equation 8.

$$f = B - A \cdot \log_{10}(N) \quad (8)$$

Where f denotes the strength level, B is the constant term, and N is the number of cycles (NOC). The slope of the curve is dependent on the stress ratio and is denoted by parameter A as defined according to Equation 9. The constants a and b are dependent on the type of loading or connection scenario for a structure. Values for the constants are defined by the informative Annex A in EN 1995-2: Design of timber structures - Part 2: Bridges (EC5-2) (CEN 2004), presented in Table 1. By inserting the constants of the type of loading, S-N curves may be constructed. Figure 12 and Figure 13 illustrate the S-N curves' dependency on stress ratio. Note that for $R = -1$, parameter A is significantly higher than for other values. This is reasonable because it arises in a situation where $\sigma_{max} = -\sigma_{min}$, indicating a fully alternating load with $\sigma_{mean} = 0$. This situation is illustrated earlier in Figure 11.

$$A = \frac{1 - R}{a \cdot (b - R)} \quad (9)$$

Table 1: Parameters for a and b from EC5-2 (CEN 2004).

Type of loading or connections	a	b
Compression parallel or perpendicular to grain	2.0	9.0
Bending or tension	9.5	1.1
Shear	6.7	1.3
Connection with dowels $d \leq 12 \text{ mm}$	6.0	2.0
Connection with nails	6.9	1.2

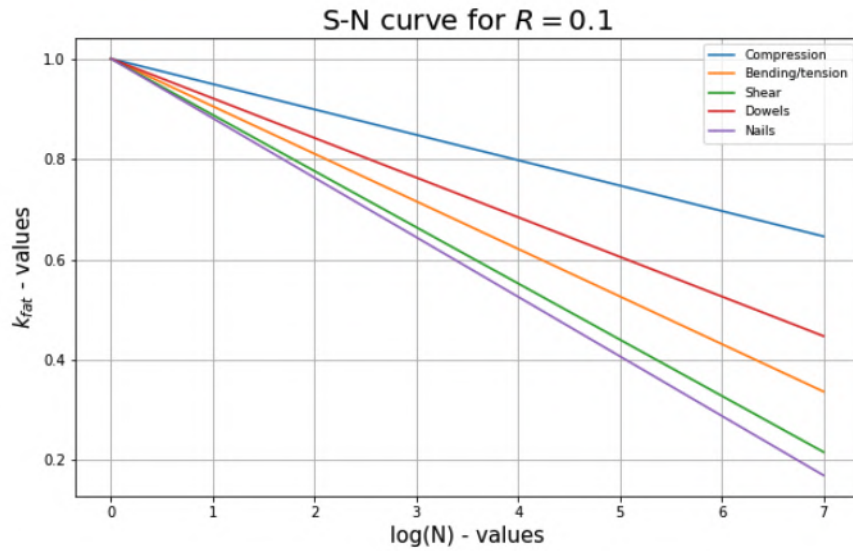


Figure 12: S-N curve for $R = 0.1$ (Jenssen and Vetter 2022).

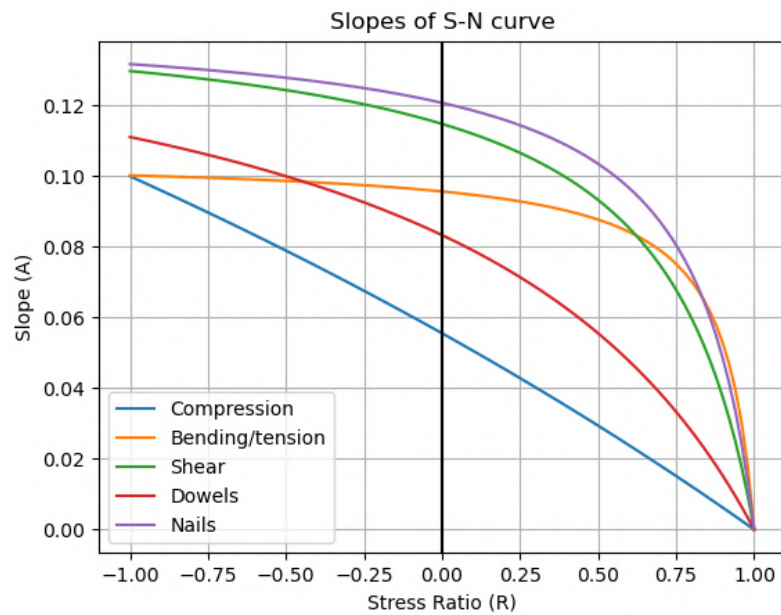


Figure 13: The slope parameter A for various values of R .

To determine the starting point for the S-N curve, static tests must be performed on the test specimen to ascertain its static capacity. Subsequently, the stress level corresponding to the material's static strength can be identified. At this stress level, the material will fail due to fatigue after 0.25 load cycles. Hence, the starting value for the S-N curve can be obtained by $\log(N) = -0.6 = \log(0.25)$ (K. Malo et al. 2022).

3.1.2 The Palmgren-Miner rule

The Palmgren-Miner rule is based on the principle established by Palmgren (1924) and Miner (1945) that fatigue damage accumulates over time and the total damage is a sum of partial damage caused by each loading cycle. Equation 10 can be used to predict failure due to cumulative damage over time. When the sum of all fractions equals unity, failure is expected to occur. Miner conducted experiments to verify this concept for an aluminum alloy, employing various specimen types, stress ratios, and loading cycle combinations (Miner 1945). The experimental findings revealed the minimum and maximum values observed were 0.61 and 1.45, respectively. The average test sum was 0.98, approximately unity.

$$D = \sum_{i=1}^k \frac{n_i}{N_i} = 1 \quad (10)$$

k denotes the number of different stress levels during the load history. n_i is the number of cycles at stress level i . N_i is the number of cycles required to cause failure at each stress level i , according to the S-N curve.

Schijve (2009) stated that the Palmgren-Miner rule is somewhat primitive in its approach. The rule assumes that fatigue damage can be expressed by a single damage parameter, which is inconsistent with current understanding of how fatigue damage accumulates. The Palmgren-Miner rule, at most, provides a weighted indication of the load spectrum, but it fails to convey the intensity or severity of the load spectrum.

3.2 Static fatigue

Timber design typically involves recognizing that the strength of the material is dependent on how long it is under stress, known as the duration of load (DOL) effect (Köhler 2007). Another aspect that is related to the DOL effect is time-dependent creep deformation, where the material gradually loses strength and deforms over time under a constant load, leading to failure, or *creep-rupture*. Experimental tests regarding static fatigue introduces a variety of challenging research problems, and are thus kept relatively simple. Typically, either a constant (static) load or a ramp (increasing) load is applied, and the duration until failure is recorded. In general, three types of DOL-tests are used to illustrate stress history; short-term tests, long-term tests and impact load tests. A graphical illustration of these tests are shown in Figure 14.

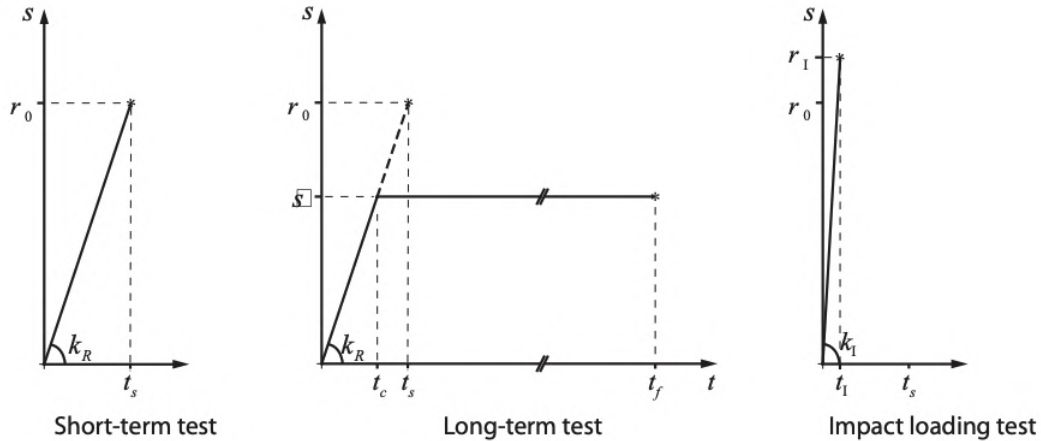


Figure 14: Stress history of short-term test, long-term test and impact loading test (Köhler 2007).

Over the years, various models have been proposed to describe the phenomenon of DOL and its effect on material behaviour, and in the subsequent sub-chapters a selection of these models will be presented.

3.2.1 Empirical models - The Madison and Pearson Curve

The Madison curve was proposed by Wood (1951), which is based on the findings of his long-term loading test, a short-term test by Liska (1950) and an impact test by Elmendorf (1916). All results combined led to the finding of an approximated hyperbola, with the function presented in Equation 11. According to Wood, the rapid-loading and impact data points are situated above the extrapolation of the straight line that represents long-time loading data, suggesting that a curve that encompasses all the data points cannot be linear. The empirical curve represented the DOL of 0.015 seconds to 156 days (Köhler 2007).

$$SL = 18.3 + 108.4 \cdot t_f^{-0.0464} \quad (11)$$

Where SL is the stress level and t_f is the time to failure in seconds.

When evaluating the long-term DOL effect in clear wood and structural timber, the Pearson curve is a more precise predictor compared to the frequently used Madison curve. This is due to the fact that the Pearson (1972) equation is primarily based on longer load duration, making it more suitable for analysing long-term DOL effect. In contrast, the Madison curve displays a more conservative approach by a lower reduction in strength that contradicts data obtained from tests of long duration. The Pearson function is given in Equation 12, followed by a comparison of the two curves in Figure 15.

$$SL = 91.5 + 7 \cdot \log(t_f) \quad (12)$$

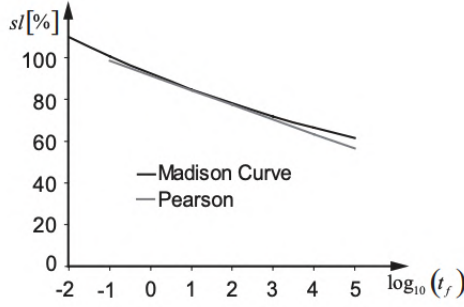


Figure 15: The Madison and the Pearson curve presented with t_f given in hours (Köhler 2007).

3.2.2 Theoretical models - The Nielsen and LEFM model

Models based on fracture mechanics, such as Nielsen and LEFM, introduces damage as the expansion of cracks within a viscoelastic solid (Köhler 2007). Nielsen (1979) introduced a model from theory of damaged viscoelastic material (DVM), where structural timber can be considered as primarily damaged with cracks representing the extent of the damage. A single crack under stress perpendicular to the crack plane is used to model the time-dependent behaviour of timber under load. Nielsen's model for a constant load intensity is given in Equation 13.

$$\frac{d\alpha_{\kappa}}{dt} = \frac{(\pi \cdot FL)^2}{8q_c\tau_c} \frac{\alpha_{\kappa} \cdot SL_{\kappa}^2}{\left((\alpha_{\kappa} \cdot SL_{\kappa}^2)^{-1} - 1\right)^{\frac{1}{b_c}}} \quad (13)$$

Where,

- α_{κ} is the damage defined by ratio between crack and initial crack length;
- SL_{κ} is the stress level;
- FL is the strength level;
- τ_c is a material parameter;
- b_c is a creep parameter;
- q_c is a parabolic function for progression of crack propagation.

The linear elastic fracture mechanics (LEFM) model is, like the Nielsen model, based on fracture mechanics. In the analysis by Hoffmeyer and Sørensen (2007), the LEFM model is derived from Sørensen and Svensson (2005). According to Hoffmeyer and Sørensen, there is a possibility that the creep behaviour observed at the microstructural level can be reflected in macrostructural creep behaviour. This behaviour can be converted into a material property that can be measured and verified through experiments. To calibrate the two models, Hoffmeyer and Sørensen (2007) utilized the experimental data obtained from creep tests and compared the models to the empirical models by Foschi and Yao (1986) and Gerhard (1979). The analysis concludes, among other things, that there is no experimental evidence supporting the existence of a strength threshold below which no damage accumulates.

Köhler and Svensson (2002) compared Gerhard's model, Nielsen's model and Foschi and Yao's model for constant load, resulting in marginal differences between the models. However, for greater \log hours, there is a slight deviation between the models. The end tail of Foschi and Yao's model and Gerhard's model overestimates the data, while Nielsen's model underestimates the data.

3.3 Tretten bridge

3.3.1 The bridge design

The older steel truss bridge over Gudbrandsdalslågen, shown in Figure 16, was decided to be replaced by a new one in September 2003. As the bridge was highly visible both from the highway and the city centre, aesthetics was an important factor in the planning phase. The consultancy utilized information and experience they gained from the rebuild of the new *Flisa* timber bridge, which opened for traffic in June 2003. The new *Flisa* timber bridge reused all existing foundations, and a similar truss system as the old one was designed. Despite similarities between the two bridges, the existing foundation on the eastern side of the river could not be reused at *Tretten*. This resulted in asymmetric foundations, which the architect also wanted to be visible in the superstructure. To utilize the existing foundations, it was necessary to prevent any increase in the weight of the truss system. As a result, timber was considered the preferred construction material. The final design of *Tretten* bridge with the asymmetry in both foundations and truss system is shown in Figure 17 (Hårstad-Evjen et al. 2013a).



Figure 16: The old *Tretten* bridge built in 1894 (Hårstad-Evjen et al. 2013b).



Figure 17: The new *Tretten* bridge opened for traffic in June 2012 (Hårstad-Evjen et al. 2013a).

Although the *Eurocodes* became the governing design codes for all new bridges in Norway in November 2010, the design of *Tretten* bridge had already begun before this date. As a result, it was decided to continue using the Norwegian material codes *NS 3470-1* (Standard Norge 1999), *NS 3472* (Standard Norge 2001) and *NS 3473* (Standard Norge 2003).

Tretten bridge consisted of dowel-type steel to timber connections with various amounts of dowels depending on attributing loads in the respective diagonals. The timber deck was composed of stress-

laminated beams, which were clamped together by high-strength pre-stressed steel rods. The main truss was completed in GLULAM, mainly GL32c. The highest tensile force in the chord was positioned above the newly constructed column foundation. Therefore, the timber in this area was changed to GL32h, as it possesses a higher tension capacity than GL32c. Additionally, to enhance lateral stability, it was decided to opt for stiffer cross beams close to the column foundation. As illustrated in Figure 17, the eastern end of the bridge also needed to be strengthened. The lower chord was hence reinforced with extended steel components as well as a change to GL32h for the diagonal braces.

3.3.2 The current investigations

Tretten bridge collapsed on August 15th 2022 and has since been a case of investigation. Norwegian safety investigation authority (NSIA) leads the ongoing investigation which seeks to clarify how and why the bridge collapsed, as well as identify safety problems and underlying factors of the incident.



Figure 18: A truck with a trailer and a car were on the bridge at the time of the collapse (Statens havarikommisjon 2022a).

SINTEF examined 21 half bolts found in the area around the column support, and the result from this is summarized in NSIA's first preliminary report (Statens havarikommisjon 2022a). Neither of the analyzed bolts showed any indication of prior damages or ongoing fatigue. The ductile fractures observed indicated that the bolts failed due to overload during the bridge collapse. Furthermore, SINTEF stated that the inspected steel parts had no signs of flaking corrosion products or increased corrosion rates. At the time when the first preliminary report was written, the remaining parts of the bridge were still in the river, and for that reason, the increased rate of corrosion could not be ruled out.

NSIA's second preliminary report (Statens havarikommisjon 2022b) stated that the initial cause of damage was due to a fracture in one of the diagonal braces in the main span over the old foundation, on the western side of the bridge. The fracture was identified as block shear failure. Figure 19 illustrates this failure mode and the expected location of the fracture. Block shear failure will be an important subject of interest for subsequent experiments in Section 4.



Figure 19: Red rings marks the upper nodes, while images represent the nodes that were under water. These nodes connected the diagonals in the main span (Statens havarikommisjon 2022b).

Tretten bridge was designed according to *NS 3470-1* (Standard Norge 1999), which did not specify a design check for block shear failure. Today, block shear failure is controlled according to *EC5*, Annex A (CEN 2010). Based on the calculation method, the relevant diagonal connections exhibited a utility ratio of 200 % (Statens havarikommisjon 2022b). This implies that the ULS capacity in the connections was only half of its intended capacity. It remains unclear if repeated loads has led to a reduction in the wood's capacity.

3.4 Capacity of dowel connections

3.4.1 Design guidelines in *EC5*

For dowel-type steel-timber connections with more than one row counted perpendicular to the grain, requirements of block failure provided in Annex A in *EC5* have to be taken into account (CEN 2010). The failure mechanism illustrates a rather complex load situation influenced by multiple factors with various degrees of impact. Empirical data over the last years indicates that demonstrating the block failure resistance from the code's equations is difficult (Stapf et al. 2012) and based on current investigations, possibly in need of adjustment. In bridges such as *Tretten*, block failure is of particular interest.

The design rules in the current European codes are established based on Johansen's theory (Johansen 1949). Johansen's theory considers failure related to the yielding of dowels and embedment failure in timber. Furthermore, the theory provides design guidelines for block and row failure illustrated in Figure 20.

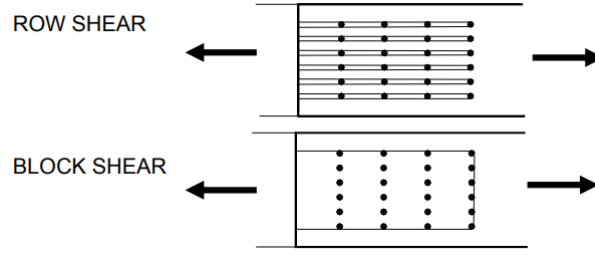


Figure 20: Block failure and row failure in EC5.

The row shear capacity is defined by reducing the effective amount of dowels in the row according to Equation 14. In the latter equation, F_{Sk} denotes the characteristic load-carrying capacity of splitting as defined in EC5 (assuming $n_d \neq n_{ef}$) and F_{Rk} denotes the capacity from Johansen's theory. Lastly, the effective amount of dowels for capacity calculation is found by using Equation 15.

$$F_{Sk} = \frac{n_{ef}}{n_d} \cdot F_{Rk} \quad (14)$$

$$n_{ef} = \min \left(n_d ; n_d^{0.9} \left(\frac{a_1}{13d} \right)^{0.25} \right) \quad (15)$$

Where,

- F_{Sk} is the characteristic load-carrying capacity of splitting;
- F_{Rk} is the capacity from Johansen's theory;
- n_d is the total amount of dowels;
- n_{ef} is the effective number of dowels;
- d is the dowel diameter;
- a_1 is the distance between dowels in a row.

The load-carrying capacity in the case of block shear in Annex A of EC5 is a more complicated issue that takes account of limitations set by the product of shear and tensile strength and corresponding net areas. Equation 16 defines the characteristic block shear capacity according to Annex A in EC5 (CEN 2010).

$$F_{bs,Rk} = \max \begin{cases} 1.5A_{net,t} \cdot f_{t,0,k} \\ 0.7A_{net,v} \cdot f_{v,k} \end{cases} \quad (16)$$

Where $A_{net,t}$ and $A_{net,v}$ denote the tensile and shear net area as defined by Equation 17 and Equation 18 respectively.

$$A_{net,t} = L_{net,t} \cdot t_1 \quad (17)$$

$$A_{net,v} = \begin{cases} L_{net,v} \cdot t_1 & \text{failure modes c, f, j/l, k, m} \\ \frac{L_{net,v}}{2} \cdot (L_{net,t} + 2t_{ef}) & \text{all other failure modes} \end{cases} \quad (18)$$

$L_{net,t}$ is the net width of the cross-section perpendicular to the grain, and $L_{net,v}$ denotes the net length of the shear fracture area. t_1 is the penetration depth of the timber member, while t_{ef} is the effective depth depending of the failure mode (CEN 2010). Failure modes for calculating the net areas are illustrated in Figure 21.

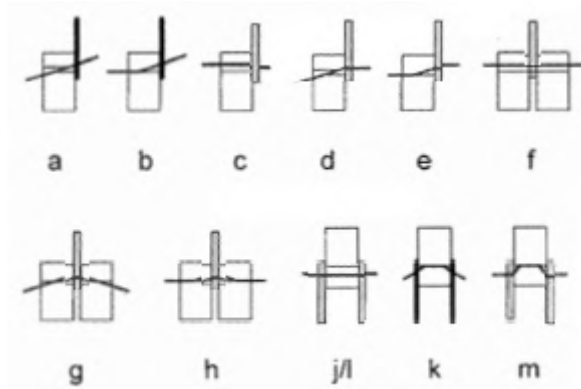


Figure 21: Failure modes defined in *EC5* (CEN 2010).

3.4.2 Correlation of block shear and tension in American standards

For the aforementioned Equation 16, European codes provide empirical factors $k_{bs,t} = 1.5$ and $k_{bs,v} = 0.7$ for designing load-capacity of block failure. In contrast, national design specification (NDS) used in the USA (American Wood Council 2012) and the Canadian standards association (CSA) (Canadian Wood Council 2014) provide more conservative reduction factors of $k_{bs,v} = 0.5$ and $k_{bs,v} = 0.6$, respectively. As for *EC5*, the factor in the Canadian standard *CSA-086* is derived from test results. In the case of the timber specifications given in *NDS-2005*, the reduction factor is defined by accounting for the uneven load distribution by the dowels in the grain direction (Stapf et al. 2012). In contrast to the European codes, *CSA-086* provides a range of tensile multiplication factor $k_{bs,t}$ between 1.26 to 1.34, whereas *NDS-2005* does not allow for increasing the tensile load-carrying capacity parallel to the grain.

Both of the latter North American design codes define the block failure resistance by adding the net tensile resistance, $F_{bs,t}$, with the net shear resistance, $F_{bs,v}$, in a manner described by Equation 19.

$$F_{bs,Rk} = F_{bs,t} + F_{bs,v} \quad (19)$$

Whereas the European codes specify the resistance as the max value of them as described in Equation 16. Figure 22 illustrates the correlation between block shear and tension in an arbitrary beam.

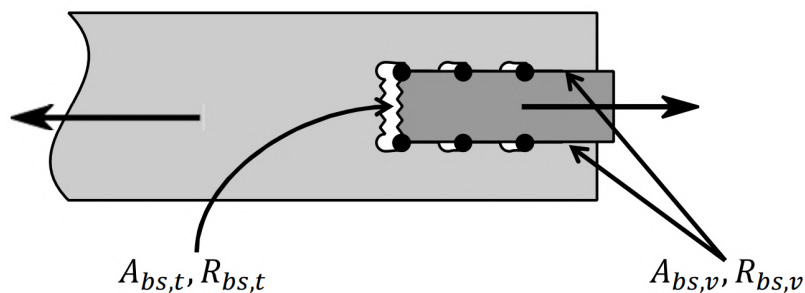


Figure 22: Resistance to tensile loads for dowel connections (Stapf et al. 2012).

4 Experimental test of Tretten bridge elements

Prior to the collapse of the *Tretten* bridge in 2022, it was claimed to have a 100-year life expectancy utilizing an innovative yet unconventional combination of timber and steel truss work (Hårstad-Evjen et al. 2013a). Completed in 2012, this bridge was constructed to replace its predecessor, a steel truss bridge that had been in place since 1895, though only saw 10 years of service before the collapse.

The objective of this report is to contribute to finding deviations in material properties for GL32c used in *Tretten* from specified ones in *EN14080*. By conducting tests in the laboratory on *T14.5* lamellas from downstream diagonal element number 13 (13B), the goal is to determine important strength parameters and compare them to projected values. The experiment includes four tension tests, three tests related to block failure, four four-point bending tests and, an additional ten compression tests. From the latter, the objective is to determine the tensile strength, compressive strength and find decisive failure surfaces that may be relevant in our understanding of the failure of the *Tretten* bridge. In addition to the latter, an analysis of MC and density of the material will be done in order to establish the state of the timber during experimental testing.

This chapter serves as a brief overview of a comprehensive analysis performed on the timber elements from the *Tretten* bridge. The complete report is available in Section J and is recommended for supplementary information.

4.1 Introduction to experiments

4.1.1 Background analysis of *Tretten* bridge

The *Tretten* bridge was a three-spanned truss bridge consisting of components of steel and timber. The diagonal elements of the bridge consisted of GL32c identically angled with respect to the horizontal plane. The vertical steel components were connected to the timber with dowel connections. *Tretten* bridge measured a total of 148 metres with a main span of 70.2 metres. Figure 23 illustrates the design of the bridge.

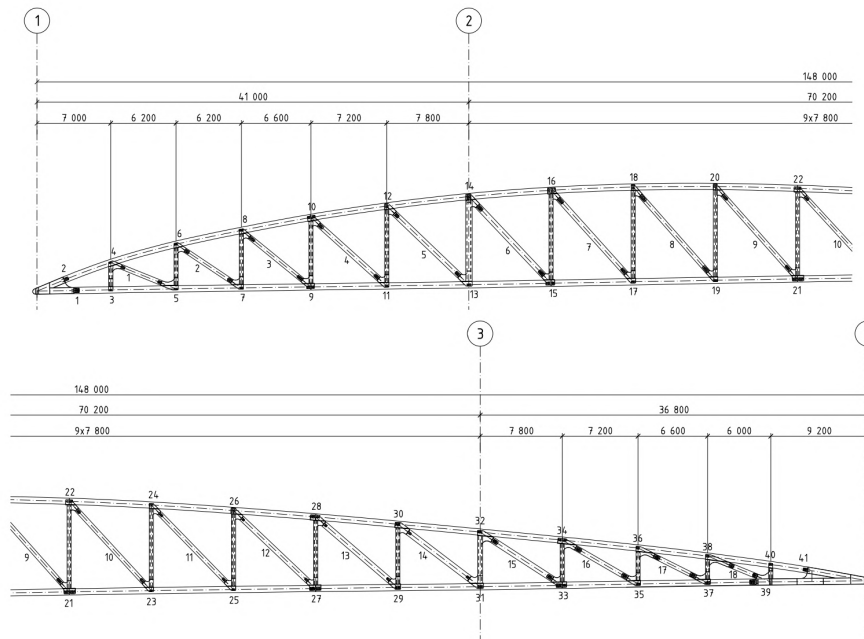


Figure 23: Details of *Tretten* bridge in drawing K300, see Section I.1.

The dimensions of the various components in the bridge depend on the loads they are subjected to. The top and lower chord in the truss have a constant cross-section of 700×600 and 650×600 denoted in millimetres, respectively. Both the vertical steel components and diagonal timber elements have dimensions according to attributing loads. The GLULAM elements varies between 500×450 millimetres to 600×600 millimetres where the largest cross-sections are situated in the main span (Qvist and Soland 2022). The dimensions of the experimental test pieces do not coincide with the latter measurements, which will be elaborated in Section 4.1.2. The dowel connections in the bridge consist of 8 millimetres wide steel plates with a total of 32 dowels for elements subjected to the largest loads.

4.1.2 Diagonal element of *Tretten* used for experiments

A total of seven specimens were sent to the Department of Structural Engineering at NTNU for conducting experiments related to the failure of the *Tretten* bridge. All specimens consisted of *T14.5* lamellas with origin from downstream diagonal element number 13, referred to 13B, where B denotes the downstream axis. Some diagonal elements were reportedly lifted out of the river of Grudbrandsdalslågen, hence likely containing various moisture content (MC). Before arrival to Trondheim, all the elements were shaped by *Moelven Limtre* according to the dimensions required for experimental test-

ing. At arrival in the laboratory, all specimens were placed in an environmentally controlled room with $RH = 65\%$ and $20\text{ }^{\circ}\text{C}$.

Milling machines were used to shape the specimens for tension and block failure tests, hereafter respectively referred to as *S-tests* and *B-tests*. Due to the specimens being cut from a larger element from the bridge diagonals, all the test pieces suffered from varying effects of swelling and shrinkage. For instance, a specimen with surfaces being directly exposed to water will contain vastly more water than a corresponding sample from the center due to the hygroscopic properties of timber. The latter induced minor deviations in dimension provided measurements by *Moelven Limtre*. The imposed alterations in the specimen length are assumed to have neglectable consequences for the sake of the tests, in opposition to the deviating width. The width is decisive for both tension and block failure hence needs to be accounted for. Nevertheless, provided specimen dimensions for tension (and later the bending test) and block tests are illustrated in Figure 24 and Figure 25, respectively. The uncertainties of the widths are measured to be ± 4 centimetres. All figures are drawn in millimetres.

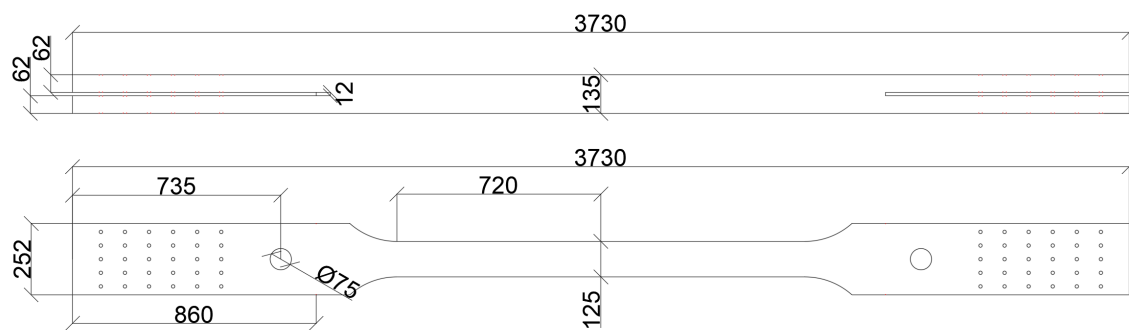


Figure 24: Dimensions of the 4 *S-tests* (used later for bending tests).

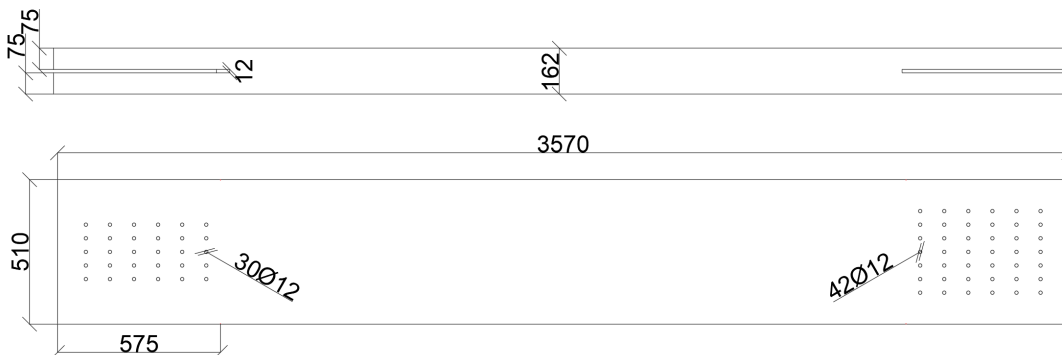


Figure 25: Dimensions of the 3 *B-tests*.

4.1.3 Details of dowel connections

The end details of the dowel connection are illustrated in Figure 26 and Figure 27 in millimetres. Note that the *B-test* specimens are longitudinally asymmetric in order to obtain block failure in the weakest end, from now referred to as the "weak"-end. The *S-tests* are however symmetric, hence both ends corresponds to the illustration in Figure 26.

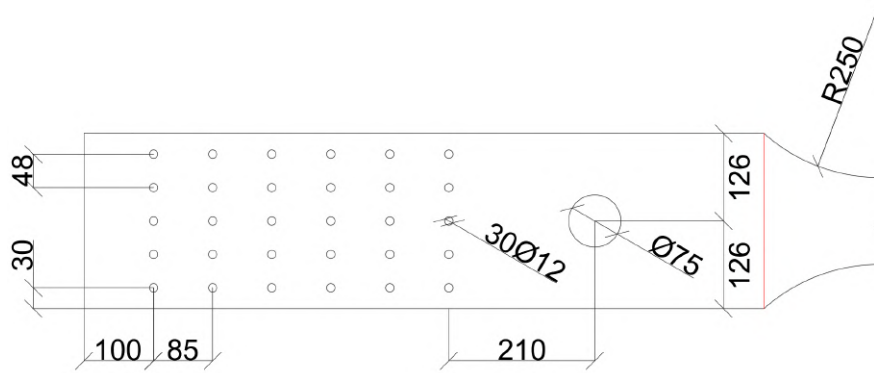


Figure 26: Dimensions of the 4 *S-test*.

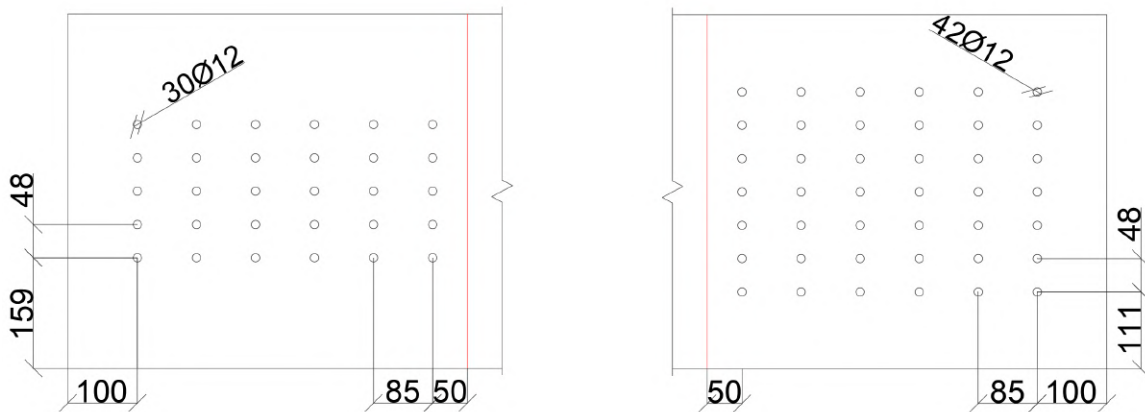


Figure 27: Dimensions of the 3 *B-test*.

The lengths of the dowels are defined according to the widths of each respective cross-section. The *S-test* and "weak"-end of the *B-test* will have connections with 30 Ø12 dowels, while the remaining "strong"-end of the *B-test* will have connections of 42 Ø12 dowels. The dimensions of the steel plates used for the experiments are defined according to Figure 28. Five of *Plate B* will be used for the strongest end of the block failure experiment. The connections are mounted with two outer plates on each side, and one in the center. The corresponding configuration with *Plate A* will be used for the "weak"-end of the block shear experiment. For the tension tests, three of *Plate A* will be used on each side.

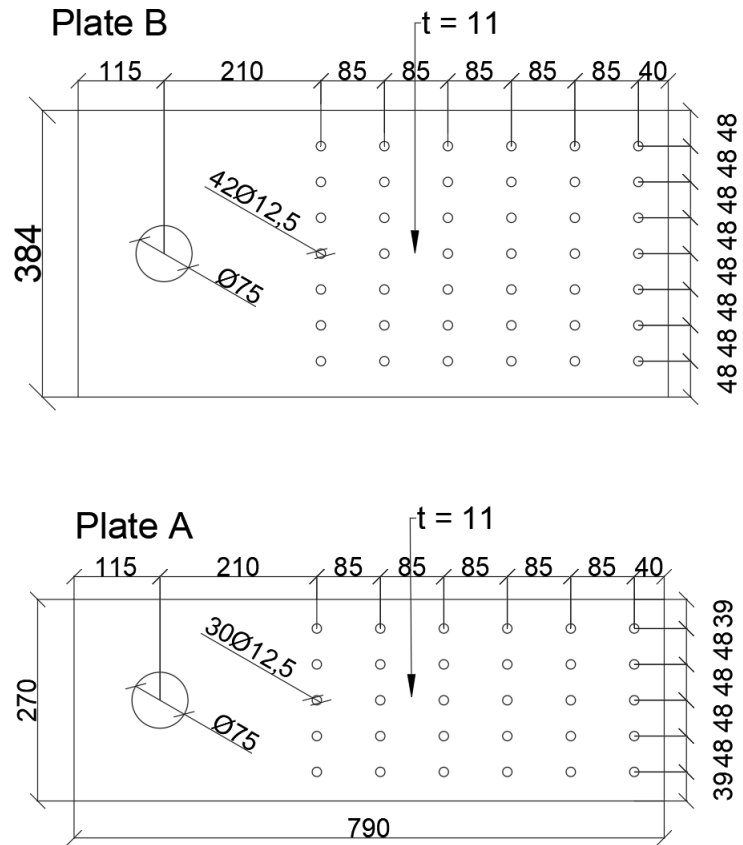


Figure 28: Dimensions of steel *Plate A* and steel *Plate B* in millimetres.

4.2 Tension test of timber elements

The objective of this experiment is to determine the tensile strength of the diagonal GLULAM elements, previously elaborated in Section 4.1.2. This chapter presents an experiment that examines the principles of tension testing for timber elements, including testing equipment, sample preparation, and post-data analysis. Moreover, discussions of various factors that may significantly impact the experimental outcomes are visited to ensure an accurate interpretation of the results.

4.2.1 Preparation for *S*-tests

The 4 specimens for the tension test are annotated *S1*, *S2*, *S3* and, *S4* and are hence referred to as *S*-tests. Each specimen was composed of a different configuration of lamellas accompanied by a variation of impurities such as knots illustrated by Figure 29. Note that *S4* had a large crack parallel to grain prior to testing which had to be glued. This process is elaborated in the full report in Section J.



Figure 29: Annotation of specimens prior to tests.

Prior to failure, cross-sectional areas were measured with calipers in intervals of 360 millimetres in order to obtain relevant parameters for later calculations. The areas are denoted $A_1 - A_5$ and are divided symmetrically along the gauge length of $l_0 = 1440$ millimetres. Figure 30 describes the variation in corresponding areas. Exact measurements are provided in Section E in the appendix.

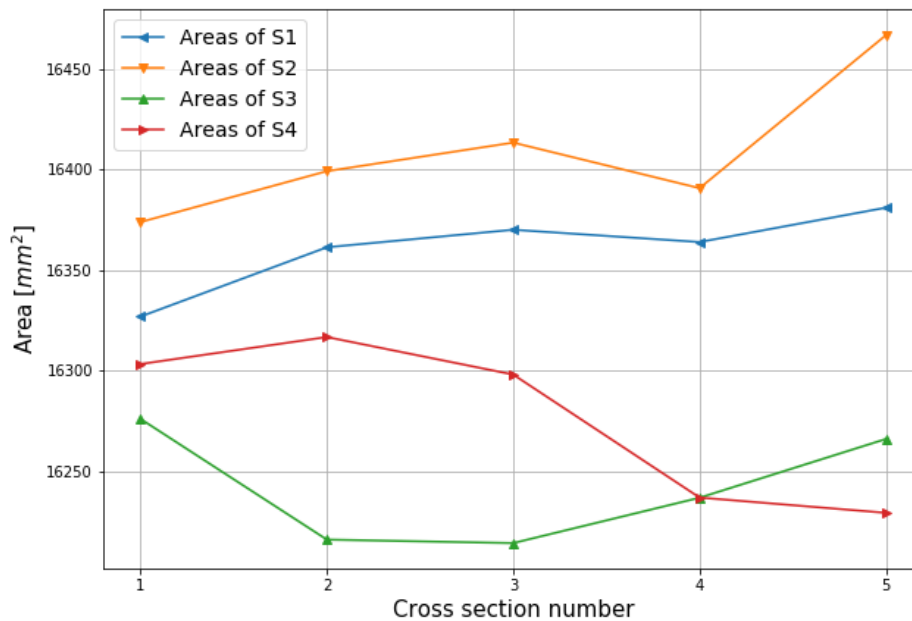


Figure 30: cross-section areas of tension-test elements from *Tretten* bridge.

To account for unforeseen and unwanted failure modes of the timber elements, given that the objective is to define the tensile strength of the material, reinforcement of the assumed weakest cross-sections is necessary. A total of 28 self-tapping screws were used to reinforce each of the specimens as illustrated in Figure 31. This process is elaborated in the full report in Section J in the appendix.

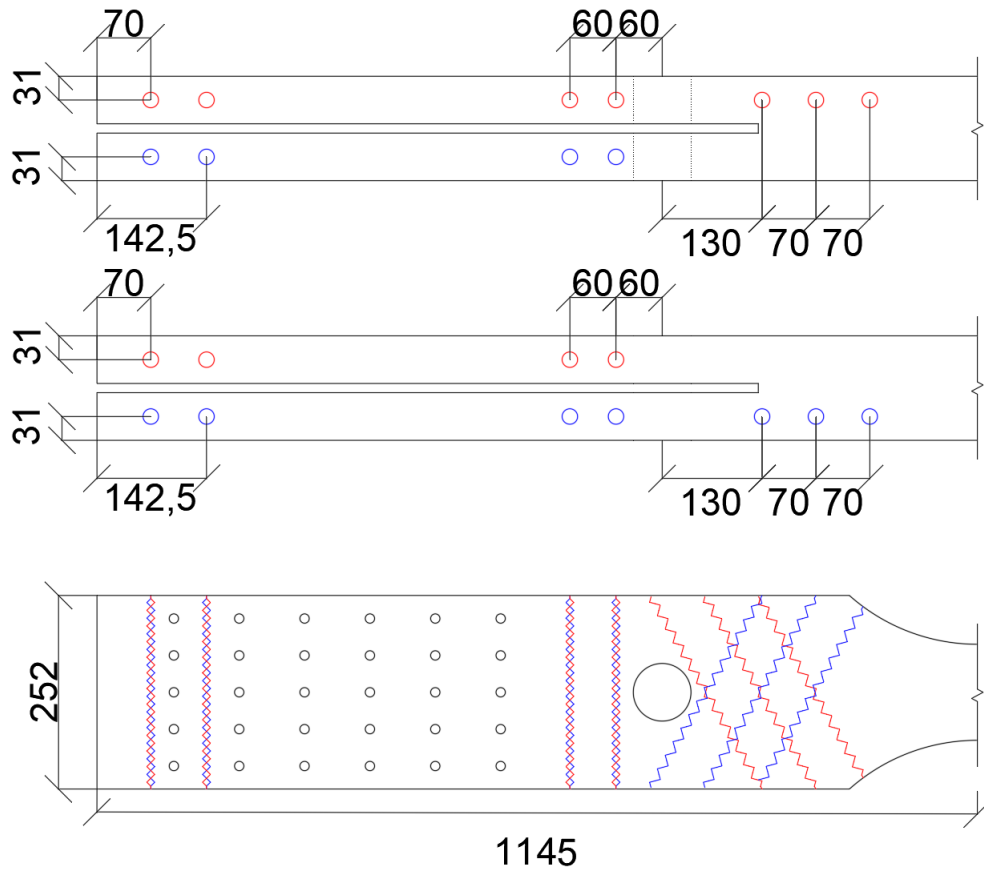


Figure 31: Reinforcement of *S-test*.

4.2.2 Equipment and method of *S-tests*

The four tension tests were carried out using a horizontal configuration of an Instron machine. The specimens were fastened to the machine by a dowel connection and three steel plates of type *Plate A* (see Figure 28). Two sets of bolts were used to connect two additional thicker steel plates to the Instron as described in Figure 32. Furthermore, rolling boundaries were used beneath the specimens to elevate them in order to reduce friction and avoid asymmetrical loading due to the chain effect.

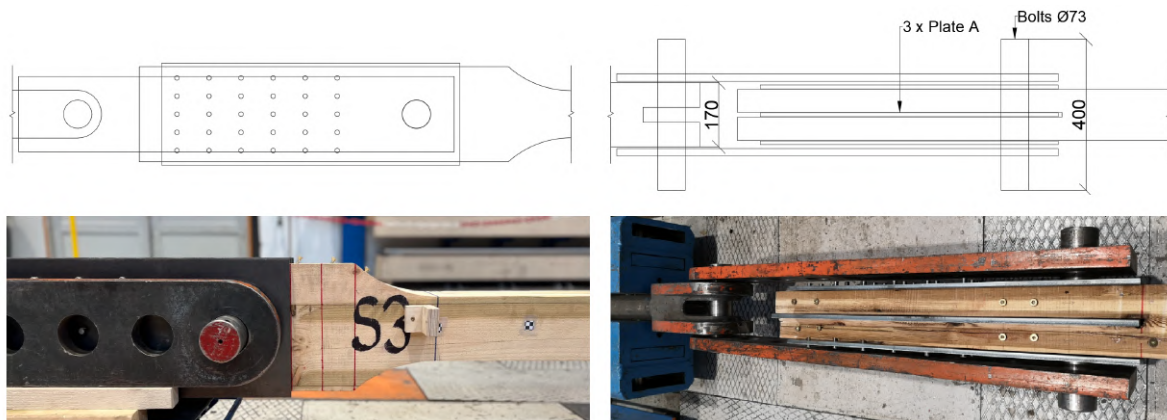


Figure 32: Mount of *S-tests*.

Longitudinal laser sensors were used for *S-tests* in order to evaluate the global displacement and compare it to the output from Instron. Lasers and non-reflective surfaces were mounted on both sides of the specimens at the location of $A1$ and $A5$, hence $\pm \frac{l_0}{2}$ or ± 720 millimetres from the specimen centre, where l_0 denotes the gauge length.

Additionally, a camera was used to track the relative position of markers to obtain any local displacement variations. 8 markers were evenly distributed with a distance of 180 millimetres along the longitudinal axes of the element where the tension failure was assumed to occur, hence where the height of the specimen is 125 millimetres. Figure 33 illustrates *S3* mounted with lasers along with the non-reflective surfaces. Four out of eight markers for tracking displacement with a camera are also visible in the figure.



Figure 33: Laser and non-reflective surface for measuring global displacement.

The testing procedure for this experiment is specified by *NS-ISO 6891* (ISO 1991). To find the estimated max load certain material properties had to be assumed. The mean tensile strength of GLULAM for the elements, $f_{t,0}$, was set equal to 15 MPa . Furthermore, the mean Young's modulus of the material, E_m was assumed to be 11000 MPa . The cross-sectional area, A_{cs} , was chosen conservatively from Figure 30 as 16250 millimetres squared. Equation 20 calculates the estimated maximum load of the *S-tests* which was needed to define the loading sequence.

$$F_{max,est} = A_{cs} \cdot f_{t,0} = 243.8 \text{ kN} \approx 250 \text{ kN} \quad (20)$$

This implies the following load parameters according to *NS-EN 408* (CEN 2012).

$$\begin{aligned} 0.4F_{max,est} &= 100 \text{ kN} \\ 0.1F_{max,est} &= 25 \text{ kN} \end{aligned} \quad (21)$$

Both loads from Equation 21 were to be held for 30 seconds during the experiment and occurs respectively at the first local maxima and minimum for the load cycle. Hence the last unknown parameter is the linear load inclination. The latter can be approximated using Hooke's formula, with a bold assumption that timber is linearly elastic, and the proportional relationship between displacement, strains and specimen length. Conservatively, the total change of length can be found by multiplying the result from Equation 22 with the ratio between the total and sectional length, assuming that displacements are constant over l . Thus, Equation 23 can be used as an approximation of total changes in displacement.

$$\Delta l_0 = \frac{0.4F_{max,est} \cdot l_0}{A_{cs} \cdot E_m} = \frac{100 \text{ kN} \cdot 1440 \text{ mm}}{16250 \text{ mm}^2 \cdot 11000 \text{ MPa}} = 0.8056 \text{ mm} \quad (22)$$

$$\Delta l = \Delta l_0 \cdot \frac{l}{l_0} = 2.086 \text{ mm} \quad (23)$$

Where,

Δl	is the total change in length;
Δl_0	is the change in gauge length;
l	is the total specimen length;
l_0	is the gauge length;
A_{cs}	is the cross-sectional area;
E_m	is the Young's modulus;
$F_{max,est}$	is the estimated max load.

Finally, the inclination of load or inclination of displacement is found by dividing the changes in load or displacement at the first local maxima, over the inclination of load duration. Based on *NS-EN 408*, the duration of inclination was set to 120 seconds. The results of Equation 24 imply a load configuration for the *S-tests* with an inclination of displacement of $0.018 \frac{mm}{s}$. The same value will be used for the declination of displacement after $0.4F_{max,est}$ is held for 30 seconds. Figure 34 summarises the calculated load configuration for *S-tests* plotted with force against time.

$$\begin{aligned} \frac{\Delta F}{s} &= \frac{100 \text{ kN}}{120 \text{ s}} = 0.833 \frac{\text{kN}}{\text{s}} \\ \frac{\Delta l}{s} &= \frac{2.086 \text{ mm}}{120 \text{ s}} = 0.018 \frac{\text{mm}}{\text{s}} \end{aligned} \quad (24)$$

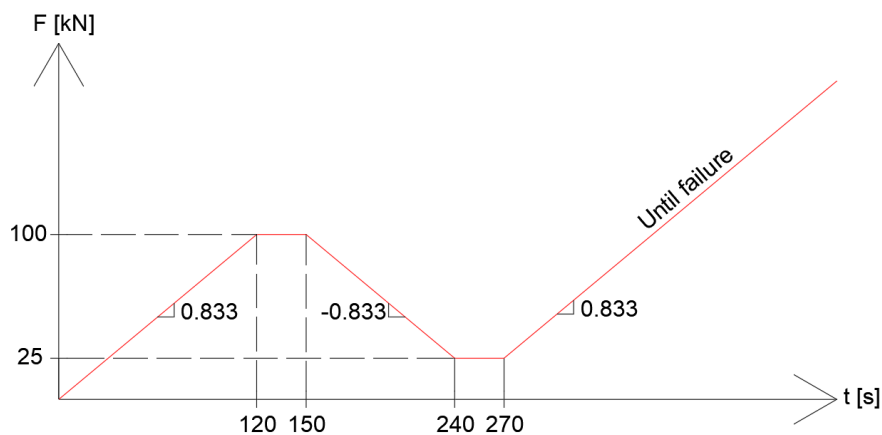


Figure 34: Load configuration for *S-tests* according to *NS-EN 408*.

4.2.3 Results of *S-tests*

All four *S-tests* tests produced similar failure patterns unrelated to tension failure, and hence the tension strength was difficult to obtain from this particular experiment. The results indicate that shear failure was more critical than tension, as illustrated in Figure 35. Regarding data acquired from the experiments, the laser sensors did not provide any useful information concerning displacement, thus not included in the results. The following results are based on displacement and force data acquired from the test machine.



Figure 35: Failure of S4.

By analysing the acquired data it is possible to see similar tendencies in specimen behaviour. The equivalent failure modes imply that the element capacity is equally similar. Note that $S4$ was used as a test for instrumental and load configuration calibration and is hence excluded from further calculations. Nevertheless, Figure 36 illustrates all experimental results plotted with force against time and displacement. The data from the experiments contained multiple minutes with irrelevant data prior to the loading sequence, thus normalized with respect to time to reduce post-processing computational costs. Figure 37 illustrates average values from acquired data from the experiments. Table 2 includes force and displacement values at failure.

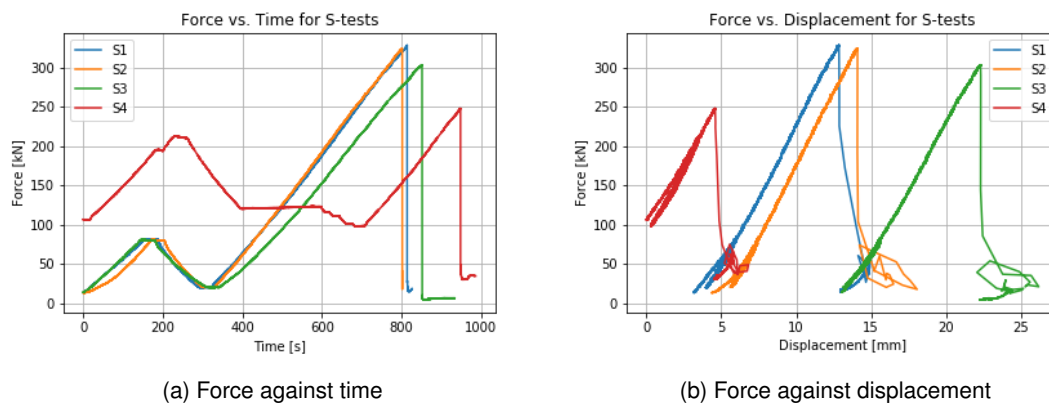


Figure 36: Data from all the S -tests.

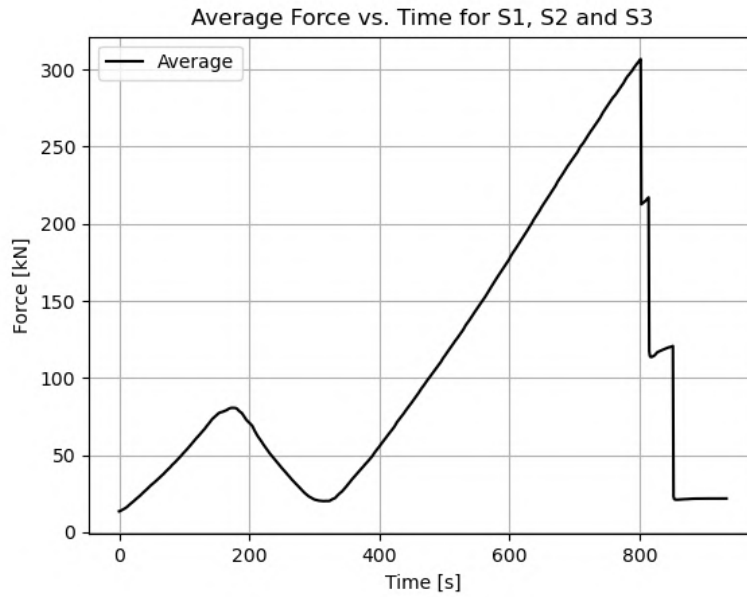


Figure 37: Average data of $S1$, $S2$ and $S3$.

Table 2: Force and displacement at failure for S -tests.

Specimen	δ_{tot} [mm]	F_{max} [kN]	$A_{cs,min}$ [mm ²]	$f_{t,0}$ [MPa]
$S1$	12.888	328.29	16326.96	20.11
$S2$	14.106	323.98	16373.91	19.79
$S3$	22.320	303.31	16214.41	18.71
Average values	16.438	318.53	16305.09	19.54

From the test data, it is possible to define the expected axial capacity for the specimen. Consequently, a bottom limit on mean tensile strength can be established. One could conservatively estimate the tensile strength by dividing the resisted axial force per respective smallest area according to Equation 25. The bottom limit of $f_{t,0}$ will be used as an estimated tensile capacity for calculations in Section 4.3. Let $F_{max,i}$ and $A_{cs,min,i}$ denote max resisted force and minimum cross-section area with subscript referring to respective specimen number. The expected lower limit of $\bar{f}_{t,0}$ can hence be defined independent of cross-sectional area.

$$\bar{f}_{t,0} \geq \frac{1}{3} \sum_{i=1}^3 \frac{F_{max,i}}{A_{cs,min,i}} = 19.54 \text{ MPa} \quad (25)$$

4.2.4 Discussion of tensile tests and concluding remarks

The S -tests did unfortunately not experience the desired failure mode, hence deemed unsuccessful for the sake of defining $f_{t,0}$. The specimens' load resistance along with the angled screws used to reinforce the specimens did not provide enough resistance to shear loads. Based on the failure surfaces of the elements, it is likely that the hole for the bolt contributed to forming a weak point for crack propagation along the fibres. Furthermore, sequences of knots caused a reduction of capacity. This is emphasized by cracks patterns forming along the knots indicating their contribution to a path of least resistance.

This is demonstrated in Figure 35.

On a better note, information acquired from the tests and failure patterns illustrates similar material tendencies for the specimens. This implies that the capacity for the specimens is predictable to a certain extent and not solely dominated by unknown variables. If additional tests were to be conducted on similar specimens, the data would likely give a smaller standard deviation of capacity and more precisely define the expected value, in other words, strengthen the tendency. Further testing is however not desirable, as the produced failure pattern is unrelated to tensile capacity.

To summarise the results of the *S-tests*, the specimens resisted a larger axial force than anticipated. The estimated tensile capacity of the elements was calculated to 250 *kN*, though *S1*, *S2* and, *S3* resisted on average 318.5 *kN*. It is therefore possible to conclude that the mean tensile strength of the timber must be at least 19.5 *MPa*. The latter value will be used for capacity estimation for block failure tests.

4.3 Block failure test

The objective of this experiment is to demonstrate a possible critical failure mechanism of *Tretten* bridge. Based on ongoing research, samples sent from the accident site and lack of restrictive guidance in *EC5* at the time of construction, block failure is likely a decisive cause of the structural collapse of *Tretten* bridge and hence an important topic of interest. By obtaining relevant parameters such as tensile and shear strength from other tests, corresponding sectional net areas from the fracture surfaces can be used to calculate the load-carrying capacity of elements.

4.3.1 Preparation for *B-tests*

The 3 specimens for block failure testing are annotated *B1*, *B2* and, *B3* and are hence referred to as *B-tests*. As for the tension tests, the *B-tests* needed to be reinforced prior to the application of load. Even though the "strong"-end with 42 dowels is considerably stronger than the "weak"-end, the existence of defects can cause a capacity reduction. The "strong"-end was hence reinforced with screws perpendicular to the global longitudinal axis as illustrated in Figure 38. More details of reinforcement can be found in the full report in Section J in the appendix.

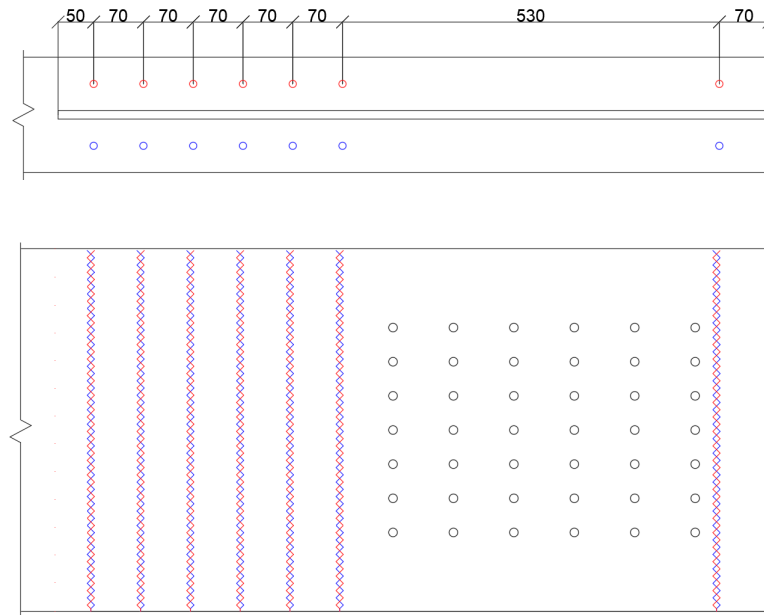


Figure 38: Reinforcement of *B-test*.

4.3.2 Equipment and method of *B-tests*

The three block failure tests were carried out using the same Instron machine as for the tension test. The "strong"-end and the "weak"-end were respectively fastened with five of *Plate B*, and five of *Plate A*. Additionally, bolts were used to fasten the plates to the test machine. Rolling boundaries were used under the specimens to reduce the impact of undesirable external forces on the system such as friction and rope effect. Figure 39 illustrates how the ends were fastened to the machine.

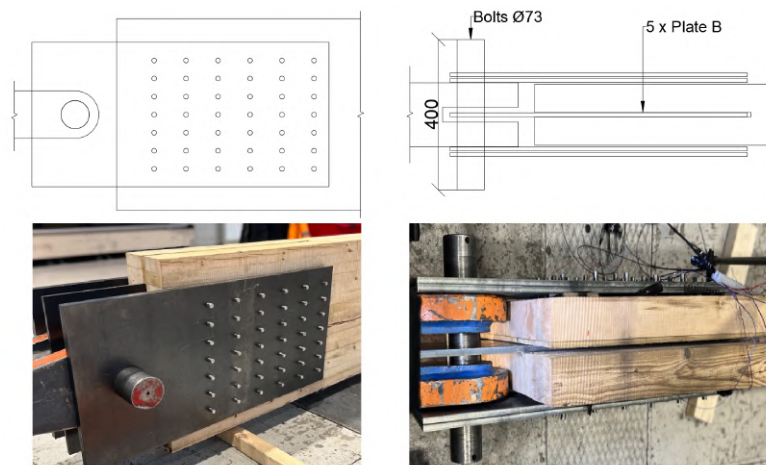


Figure 39: Mount of *B-tests* "strong"-end.

The *B-tests* were equipped with strain gauges and a pair of linear variable differential transformers (LVDT). *B3*, being the first specimen that was tested, was only equipped with strain gauges. The strain gauges were placed to detect the order of failure in the net tensile and shear area. LVDTs were mounted on each side to detect local displacements. The transformers are referred to as *LVDT1-LVDT4* in exported data, whereas *LVDT1* and *LVDT2*, and *LVDT3* and *LVDT4* were mounted pairwise on each side of the specimen. For the sake of clarification, all sensors were mounted on the "weak"-end. Table 3

and Figure 40 provides a picture and details of the location of the sensors. Details revolving around the mounting of the sensors are elaborated in Section J.

Table 3: Distances between LVDTs.

<i>B1</i>	Distance [mm]
$l_{LVDT,12}$	401
$l_{LVDT,34}$	432
<i>B2</i>	Distance [mm]
$l_{LVDT,12}$	399
$l_{LVDT,34}$	387

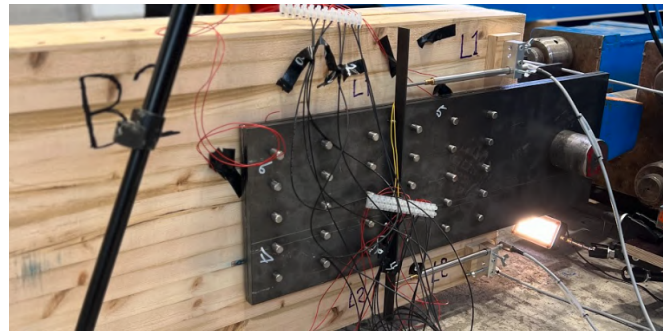


Figure 40: Configuration of strain gauges and LVDTs on *B2*.

The method of testing of *B-tests* is based on the same standards as for the tension test. The lower limit of $f_{t,0}$ was previously estimated in Section 4.2.3 to approximately 20 MPa . Furthermore, the mean shear strength of the material, $f_{v,m}$, was assumed to be 5 MPa . To find the estimated capacity of the block failure specimens, net tensile and net shear areas had to be calculated based on the connections' geometry according to Annex A in *EC5*. The aforementioned parameters are defined by summations of net vertical and horizontal fracture planes according to Figure 41. Finally, estimated load capacity can be found by multiplying respective net areas and mean strengths according to Equation 28. For the sake of simplicity, multiplication factors $k_{bs,v} = 0.7$ and $k_{bs,t} = 1.5$ are assumed to be equal to unity.

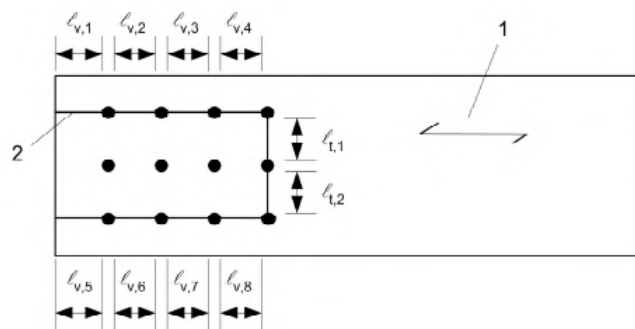


Figure 41: Parameters for calculating net area according to *EC5* (CEN 2010).

$$\sum_i l_{v,i} = 2 \cdot (100 \text{ mm} + 5 \cdot 85 \text{ mm} - 5.5 \cdot 12) = 918 \text{ mm}$$

$$\sum_i l_{t,i} = (4 \cdot 48 \text{ mm} - 4 \cdot 12 \text{ mm}) = 144 \text{ mm} \quad (26)$$

$$A_{net,v} = t L_{net,v} = t \sum_i l_{v,i} = (2 \cdot 75 \text{ mm}) \cdot 918 \text{ mm} = 137700 \text{ mm}^2$$

$$A_{net,t} = t L_{net,t} = t \sum_i l_{t,i} = (2 \cdot 75 \text{ mm}) \cdot 144 \text{ mm} = 21600 \text{ mm}^2$$
(27)

$$F_{bs} = \max \begin{cases} A_{net,t} \cdot f_{t,0} \\ A_{net,v} \cdot f_v \end{cases} = \max \begin{cases} 576.0 \text{ kN} \\ 688.5 \text{ kN} \end{cases}$$
(28)

Where,

- t is the specimen thickness;
- $L_{net,t}$ is the total net length of the tensile fracture area;
- $L_{net,v}$ is the total net length of the shear fracture area;
- $A_{net,t}$ is the net cross-sectional area perpendicular to the grain;
- $A_{net,v}$ is the net shear area in the parallel to grain direction;
- F_{bs} is the block shear capacity.

$F_{max,est}$ was chosen conservatively as 600 kN, rather than the max value of the values according to EC5. Consequently, $0.4F_{max,est} = 240 \text{ kN}$ and $0.1F_{max,est} = 60 \text{ kN}$. Equation 29 calculates the changes in specimen length in order to find the required inclination of load. Variable notations are the same as provided for tensile test estimations. Finally, the inclination of displacement and load could be defined according to Equation 30.

$$\Delta l = \frac{0.4F_{max,est} \cdot l}{A_{cs} \cdot E_m} = \frac{240 \text{ kN} \cdot 3700 \text{ mm}}{162 \text{ mm} \cdot 510 \text{ mm} \cdot 11000 \text{ MPa}} = 0.98 \text{ mm}$$
(29)

$$\frac{\Delta F}{s} = \frac{240 \text{ kN}}{2 \text{ min}} = 120 \frac{\text{kN}}{\text{min}}$$

$$\frac{\Delta l}{s} = \frac{0.98 \text{ mm}}{2 \text{ min}} = 0.5 \frac{\text{mm}}{\text{min}}$$
(30)

Note that for *B1* and *B2*, the inclination of displacement and value of rest load deviates from calculated values. Latter alterations to the method were decided after noticing that $F_{max,est}$ was calculated conservatively low. Figure 42 illustrates the load configuration for *B-tests*.

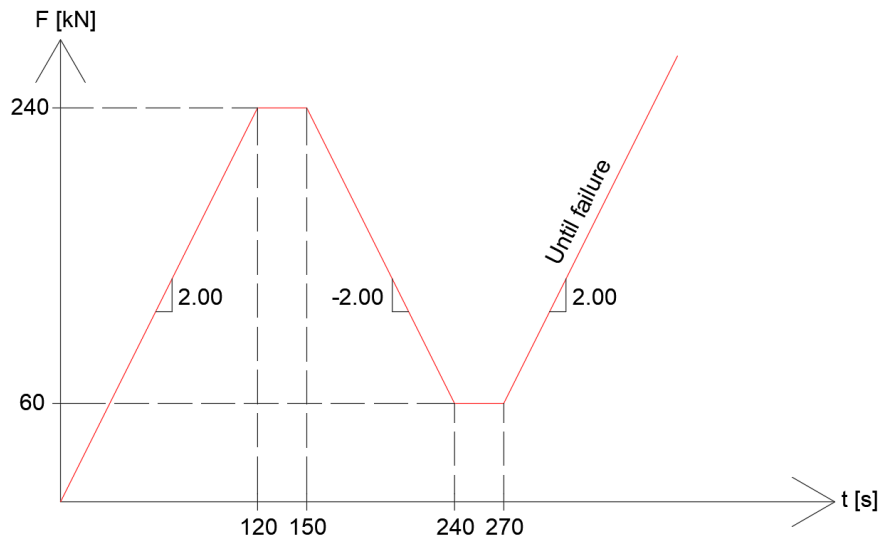


Figure 42: Load configuration for *B*-tests according to *NS-EN 408*.

4.3.3 Result of *B*-tests

All three *B*-tests yielded hypothetical failure patterns as illustrated in Figure 43, indicating successful testing outcomes. Failure surfaces of net tensile area are however highly dominated outside of the dowel zone, which equivalates to a larger net area than provided for calculation of block failure capacity in *EC5*. The results suggest that yield surfaces exhibit a tendency to follow the path of least resistance, which is reflected in the slight deviation of fracture surfaces on the net tension area from the theoretically calculated minimum area. This observation is further supported by the knots' contribution to crack propagation in the longitudinal mid-span of the element. Block failure is dependent upon the interplay between both shear and tension capacity, such that the failure of one of the latter may result in the failure of the other, and vice versa.



Figure 43: Visualization of block failure surfaces.

Data lists acquired from the Instron of displacement, force and, time were used to make graphs of all specimens as illustrated in Figure 44. Note that the load inclination for *B3* was half of the corresponding inclination of *B1* and *B2*. Furthermore, the data acquired by the sensors were used to make multiple additional graphs. Data from the four LVDTs mounted on *B1* and *B2* were used to calculate average local displacement and rotations. The average displacement of the LVDTs is found by adding all measurements and dividing by the number of sensors. Rotation around the middle point between the sensors, R_O , is calculated according to Equation 31. The result is in radians. Let $d_j - d_i$ be the difference in displacement readings of the lower and upper transformers. Furthermore, $l_{LVDT,ij}$ denotes the distance between the transformers. Lastly, subscripts i and j refer to the numerations of sensors.

$$R_O = \frac{d_j - d_i}{l_{LVDT,ij}} \quad (31)$$

The data collected from the LVDTs are illustrated in Figure 45 and Figure 46. The graphs illustrate similar behaviour of local displacements from *LVDT* readings as for the presented total displacements in Figure 44, naturally with a smaller magnitude. Note that both specimens seems to experience drastic changes in displacement and rotation at a timestamp of around 1200 seconds. Indicators such as sudden dynamic changes for displacements or rotations can be relevant in the sake of the establishment of unsymmetrical failure mechanisms.

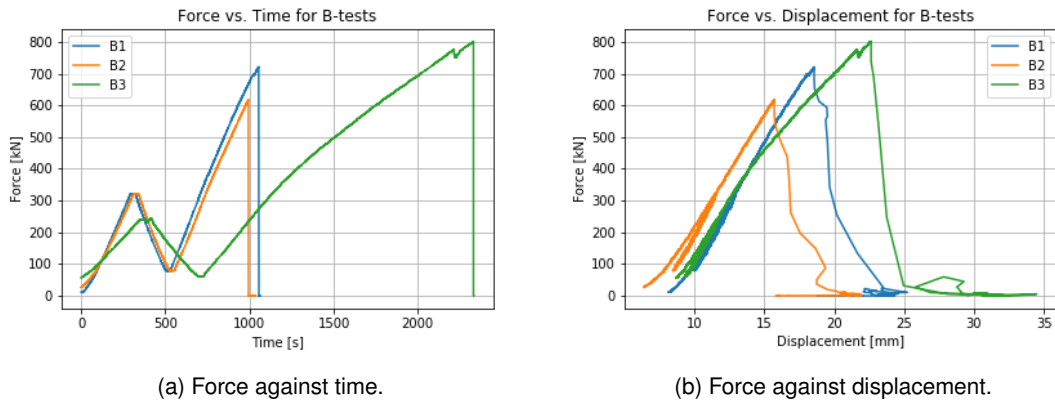


Figure 44: Data from all the *B*-tests.



Figure 45: Data from LVDTs on *B1*.



Figure 46: Data from LVDTs on B2.

Pictures taken from the cameras used in the block failure tests can provide valuable visual analysis of the failure modes, and possibly contribute to a deeper understanding of the specimen behaviour for block failure. Figure 47, Figure 48 and, Figure 49 describes the changes of respective specimen B1, B2, and, B3 experiences from the start of the loading sequence, before, and after block failure has occurred. By analysing the angle of the steel plate, it is noticeable from the pictures that the test pieces experience rotations before failure. Additionally, Figure 49 of B3 provides information of great significance. Illustrated by the picture before failure, the specimen experiences an asymmetrical initial failure that eventually leads to block failure. An asymmetrical failure implies that the last resisting side has to carry a much larger load than originally intended.

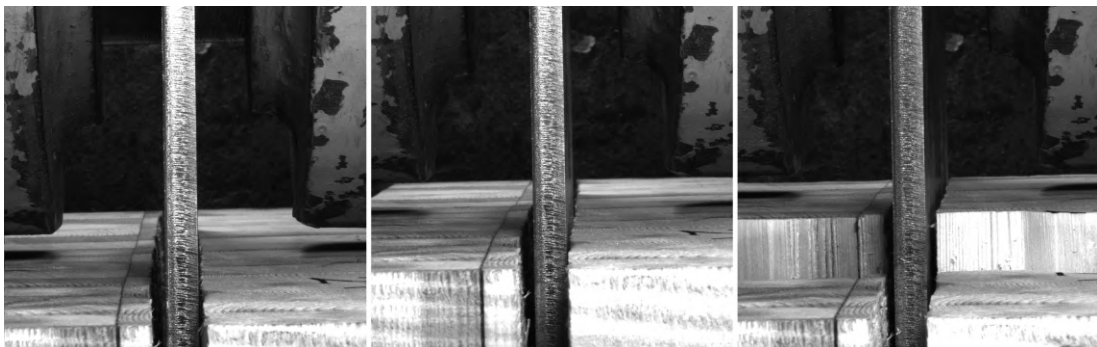


Figure 47: Camera pictures at the start, before, and after block failure of B1.

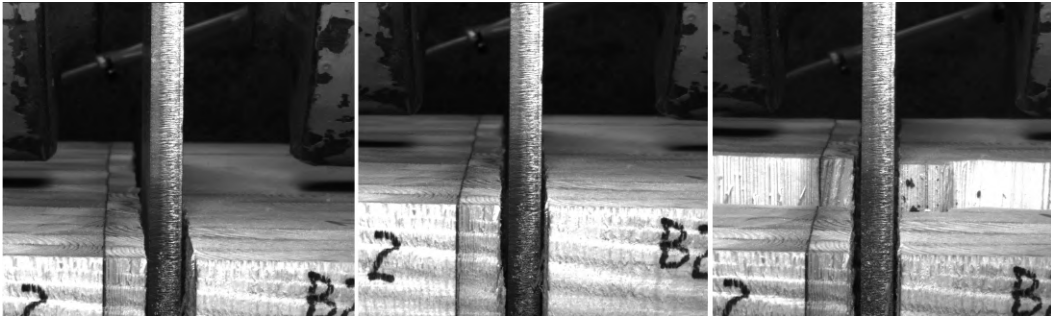


Figure 48: Camera pictures at the start, before, and after block failure of *B2*.

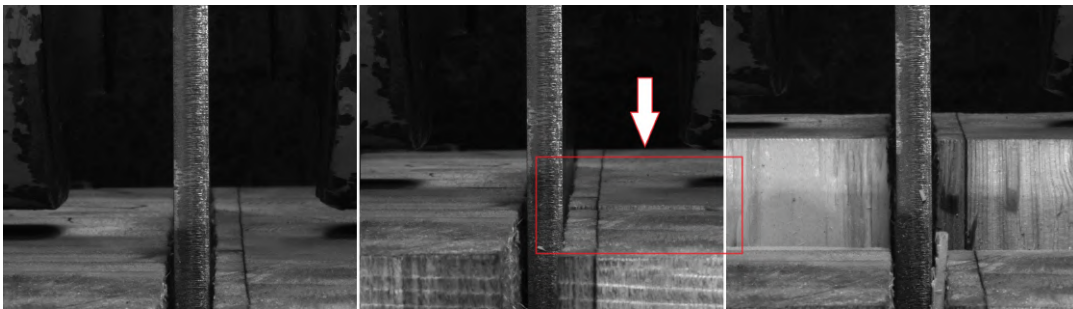


Figure 49: Camera pictures at the start, before, and after block failure of *B3*.

Table 4 includes all values acquired for time of failure, which is defined at the time F_{max} occurs. The latter can be used to estimate the tensile strength by division of calculated $A_{net,t}$ according to Equation 28. The total displacements are denoted by δ_{tot} . Furthermore, displacements from the LVDTs are presented as the average of four outputs and is hence denoted as $\bar{\delta}_{LVDT}$. Values of rotations are correspondingly the average of the values presented in Figure 45b and Figure 46b at failure. The true orientation of displacements and rotations is illustrated in Figure 50.

Table 4: Values at failure for *B-tests*.

Specimen	F_{max} [kN]	$f_{t,0}$ [MPa]	δ_{tot} [mm]	$\bar{\delta}_{LVDT}$ [mm]	\bar{R}_0 [rad]
<i>B1</i>	720.62	33.26	18.567	2.2970	0.002599
<i>B2</i>	617.30	28.58	15.718	1.5877	0.001048
<i>B3</i>	801.95	37.13	22.638	NA	NA
Average values	713.29	33.02	18.974	1.9424	0.001824

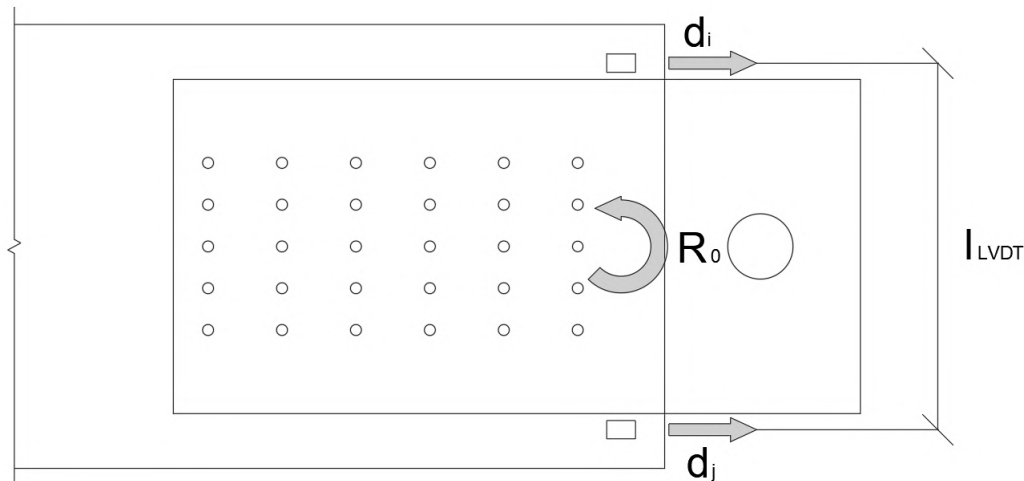


Figure 50: True direction of rotation for upper and lower LVDT displacement.

On a final note, strain measurements are excluded from this report due to their lack of credibility. The significant disparity in magnitude of the readings from the strain gauges posed challenges in the post-analysis of the results. Additionally, a majority of the strain gauges did not exhibit any displacements, resulting in zero strain measurements during the experiment.

4.3.4 Discussion of block failure tests and concluding remarks

The results of the experiments indicates that all the test specimens experiences similar tendencies before failure. All tests experienced hypothetical yielding patterns that, as anticipated, deviate slightly from theory due to the existence of defects in the timber material. It is, however, important to stress that all results are solely based on three tests, hence any conclusion potentially includes large uncertainties.

The maximum axial load capacity of the beam was defined conservatively as 600 kN based on $f_{t,0}$ obtained from the tension test. Oppositely, the specimens resisted an average force of 713.3 kN that equalates to around 120 % of the estimated capacity. The average resisted force divided per $A_{net,t}$ indicates that the mean tensile strength is approximately 33 MPa . In line with this finding, an ongoing separate investigation conducted by professor Kjell Arne Malo suggests similar values of the tensile strength as 33.5 MPa (K. A. Malo 2023), which complements the credibility of this result.

A comparison of *B1* and *B2* to *B3* sheds light on timber's dependency on DOL. Being subjected to half the load inclination over a longer duration, *B3* behaves differently than the other aforementioned specimens. Consequently, based on the characteristic behaviour of timber in regard to creep, *B3* experiences larger displacement and hence also energy absorbance before failure. This implies more ductile behaviour for increased DOL. Oppositely, *B1* and *B2* experienced relatively more brittle failure modes. Furthermore, the average total displacement observed during the block shear tests was measured as 19.0 millimetres at the point of failure. Analysis of the average values obtained from the LVDTs mounted on *B1* and *B2* revealed that 1.94 millimetres of this displacement were attributed to local displacements in close proximity to the point where block failure occurred. This corresponds to approximately 10% of the total displacement observed during the tests.

The rotations of the LVDTs were averagely calculated to be approximately -0.002 radians for both specimens. The graphs collected from the LVDTs additionally indicate (at approximately 1250 seconds) that *B1* and *B2* experience spikes in rotations around the horizontal axis. The calculated net average

rotation, excluding the dynamic spike, indicates instantaneous changes of approximately 0.0004 and 0.0005 radians, respectively. This corresponds to 20% and 50% of the total observed rotations prior to failure for the respective specimens. Notably, the majority of the rotation was observed along the 3 – 4 LVDT axis. Dynamic responses such as the latter on symmetrically tensile-loaded specimens indicate segmented brittle behaviour with possible initial failure of the weakest net areas based on the true direction of rotation.

Equivalently as for the rotations, the time correlation of the rotation graphs with Figure 45c and Figure 46c reveals a consistent pattern of failure. The displacements recorded by the LVDTs during the same time period exhibit a similar dynamic trend as observed in the rotations. Dominated by the 3 – 4 LVDT axis, the specimens experiences sudden unsymmetrical jumps in displacement moments before failure, indicating a partial weakening of the cross-section. Subsequently, the inclination of the displacement and rotation is increased, and block failure is imminent for further load increment.

Visual analysis of the pictures from the *B-tests* provides information of great significance that supports the statement from the rotation analysis that there is a great likelihood that the specimens experience an unsymmetrical initial failure in one of the net areas. Though it is inaccurate to conclude this for all specimens, it is almost certain that *B3* experiences an initial failure of the right section demonstrated by Figure 49 prior to ultimate failure. Based on the similar tendencies of rotation and displacement for the other specimens, it is not unlikely that they experience similar failure modes.

Calculations on block failure capacity according to *EC5* are based on the mean behaviour of the complex composition of tensile and shear strength around the dowel group. The experimental results have underscored the importance of incorporating the presence of defects or uneven cross-sectional areas that may result in an unsymmetrical reduction of cross-sectional capacity in capacity calculations. The occurrence of partial or complete failure of one side of the dowel plane implies a non-favorable load transfer such that the remaining side is subjected to a significantly higher axial load than anticipated. It is hence imperative, based on the results, that the ultimate bearing capacity is restricted by the weakest section, making it somewhat inaccurate to define block failure capacity based on a mean approach of evenly distributed tensile and shear strengths along the respective net areas.

4.4 Compression tests

The objective of this experiment is to determine both the compressive modulus of elasticity and the compressive strength parallel to grain of the diagonal GLULAM elements in *Tretten*. In addition, the compressive strain data will be used to estimate the tensile strain since the tension tests resulted in a shear fracture rather than a tensile fracture. This chapter delves into important topics such as the fundamentals of compression testing for timber elements, testing equipment, sample preparation, and post-analysis of data from the results.

4.4.1 Equipment and method of *C-tests*

The specimens in the compression test are identified as *C-tests*, referring to the ten individual specimens labeled as *C1* to *C10* shown in Figure 51. All of the specimens were obtained from *S4* and *S3*, with *C1* and *C2* being taken from *S4* and the remaining from *S3*.



Figure 51: Annotation of *C-test* specimens prior to tests.

The *C-tests* were carried out using Instron 5982, with a maximum load of 100 kN. The testing machine was equipped with smooth steel plates that were securely fastened to make a flat and frictionless surface. This configuration ensured that the testing machine could transfer force without introducing unwanted frictional effects, thereby enhancing the accuracy of the experimental measurements. However, it is inevitable that some friction will be present during the testing process. To minimize the influence of such frictional effects and ensure the accuracy of experimental measurements, the extensometer was attached at the center of the specimen's longitudinal axis where failure was most likely to occur. As the specimen undergoes compressive stress, the distance between the two contact points changes, and this variation was accurately detected and recorded by the extensometer. Figure 52 illustrates the test setup, wherein the extensometer is attached to the right of the specimen.

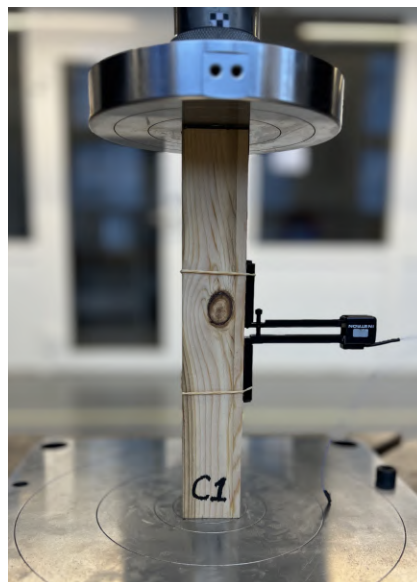


Figure 52: Mount of *C-tests*

The method used in the *C-tests* follows the standard *NS-EN 408*. The estimated load capacity was found according to Equation 32 and based on the characteristic compressive strength of the material equal to 30 MPa. The maximum load of 100 kN was set as the predetermined stopping point for the machine, hence A_{cs} was chosen as 50 × 50 millimetres squared. Equation 32 calculates the estimated

maximum load for the compressive tests.

$$F_{max,est} = A_{cs} \cdot f_{c,0,k} = 2500 \text{ mm}^2 \cdot 30 \text{ MPa} = 75 \text{ kN} \quad (32)$$

Unfortunately for the experiment, the Instron was incapable of inducing failure of the test pieces, hence specimen dimensions had to be reduced. Consequently, the dimensions of the compressive tests were decided as $l = 240$ millimetres and $A_{cs} = 40 \times 40 \text{ mm}^2$. Finally, the mean modulus of elasticity, E_m was assumed to be 11000 MPa . In order to determine the required inclination of load, Equation 34 was used to calculate the changes in sectional length. The final adjustments resulted in the load configuration and inclination of displacement as shown in Equation 35. The load configuration is illustrated in Figure 53.

$$\begin{aligned} 0.4F_{max,est} &= 30 \text{ kN} \\ 0.1F_{max,est} &= 7.5 \text{ kN} \end{aligned} \quad (33)$$

$$\Delta l = \frac{0.4F_{max,est} \cdot l}{A_{cs} \cdot E_m} = \frac{30 \text{ kN} \cdot 240 \text{ mm}}{1600 \text{ mm}^2 \cdot 11000 \text{ MPa}} = 0.0004 \text{ mm} \quad (34)$$

$$\begin{aligned} \frac{\Delta F}{s} &= \frac{30 \text{ kN}}{120 \text{ s}} = 0.25 \frac{\text{kN}}{\text{s}} \\ \frac{\Delta l}{s} &= \frac{0.0004 \text{ mm}}{120 \text{ s}} = 3.33 \cdot 10^{-6} \frac{\text{mm}}{\text{s}} \end{aligned} \quad (35)$$

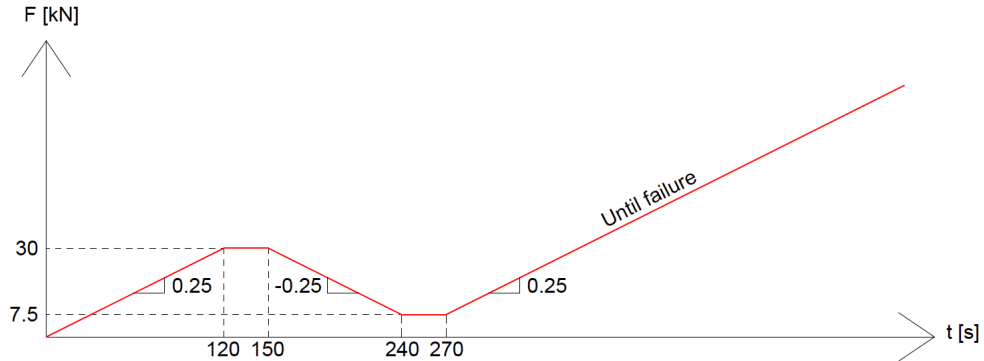
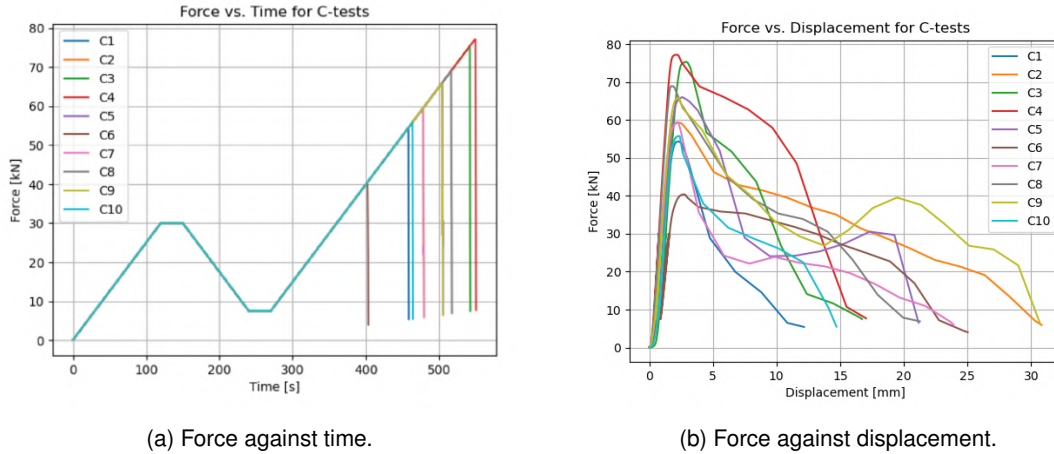


Figure 53: Load configuration for the *C*-tests.

4.4.2 Results of *C*-tests

All ten tests were performed with successful outcomes, meaning that failure was reached during the load sequence without unwanted failure mechanisms such as buckling. A plot of the loading procedure for all *C*-tests is shown in Figure 54, as well as the displacement of the hydraulic head. The obtained test results are summarised in Table 5. In Section C individual graphs are shown, as well as graphs used to calculate the compressive modulus of elasticity in Table 6. Table 5 consists of data obtained from the *C*-tests and the calculated compressive strength. The total displacements are denoted by δ_{tot} , and the maximum strain reached is denoted as ϵ_{max} . The average compressive strength was found as 38.9 MPa .



(a) Force against time.

(b) Force against displacement.

Figure 54: Data from all the *C*-tests.

Table 5: Results of the *C*-tests.

Specimen	F_{max} [kN]	A_{cs} [mm ²]	δ_{tot} [mm]	ε_{max} [%]	$f_{c,0}$ [MPa]
<i>C1</i>	54.313	1598	12.159	1.529	33.988
<i>C2</i>	59.359	1601	30.830	0.450	37.076
<i>C3</i>	75.339	1604	16.715	0.341	46.969
<i>C4</i>	77.180	1602	17.026	0.986	48.177
<i>C5</i>	66.000	1597	21.157	0.399	41.327
<i>C6</i>	40.388	1596	25.021	0.292	25.306
<i>C7</i>	59.396	1601	23.918	0.468	37.099
<i>C8</i>	68.940	1598	21.262	0.384	43.141
<i>C9</i>	65.753	1599	30.694	0.342	41.121
<i>C10</i>	55.782	1602	14.709	0.277	34.820
Average	62.246	1600	21.349	0.547	38.902

Based on the regression analysis, the objective was to determine two important properties, the compressive modulus of elasticity and the elastic compressive strength. In particular, the average value of the elastic compressive strength obtained from the regression analysis was found to be 35.7 MPa , as given in Table 6. This value will be used in the subsequent calculation of the tensile strength, further discussed in Section 4.5. In accordance with *NS-EN 14080*, it is specified that the *T14.5* strength class has a mean characteristic modulus of elasticity of 11000 MPa . The result obtained from the test was found to be an average value of 11420 MPa , which indicates that the stiffness was in the expected range.

Table 6: Results obtained from regression analysis, see Section C.

Specimen	K_c [kN/mm]	$F_{c,0,el}$ [MPa]	$f_{c,0,el}$ [MPa]	$E_{c,0}$ [MPa]
<i>C1</i>	137.29	40.55	25.34	7365.8
<i>C2</i>	64.74	55.08	34.43	9710.9
<i>C3</i>	212.80	69.14	43.21	11638
<i>C4</i>	226.86	69.66	43.54	12407
<i>C5</i>	292.60	59.18	36.99	16002
<i>C6</i>	161.51	38.87	24.30	8832.6
<i>C7</i>	164.16	55.62	34.76	8977.6
<i>C8</i>	218.91	66.07	41.29	11972
<i>C9</i>	219.34	65.38	40.86	11995
<i>C10</i>	279.82	50.89	31.81	15303
Average	197.80	57.04	35.65	11420.4

4.5 Four-point bending test

As the *S-tests* failed to produce a single tension failure, the specimens still have the capacity to be tested differently. The objective of conducting this pure bending test is to obtain strength parameters that could not be derived from the tension test. By analysing the data from this experiment, moment, curvature, and strain distribution can be used together with the compression strength to derive the tension strength of the elements. Using results from previous tests and post-data analysis of pure bending tests, it is anticipated that the last decisive strength parameters for the timber elements can be derived. This chapter will hence cover the test preparations, methods, and present the obtained results.

4.5.1 Equipment and method of bending test

The bending tests were conducted on the same specimens for the tension test, hence equally referred to as *S1 – S4*. All four 4-point bending specimens were mounted on an Instron machine capable of producing 100 *kN* of axial load. The load was transferred to the specimen using a horizontal steel beam. The beam symmetrically divided the force into two point loads that induced a constant moment in the beam. Steel clamps were used to prevent lateral displacements of the specimen under the experiment in order to obtain valid test data from sensors. The *Instron* machine was capable of tracing both force, time and displacement of the hydraulic press head. Additional equipment such as camera trackers were mounted, though not used in the results. Information of these are elaborated in Section J.

The 4-point bending tests were carried out according to the method provided in the standard *NS-EN 408*. The experiment was conducted with a load configuration provided *NS-EN 408*, which specifies that the inclination of displacement shall not exceed 0.003*h* millimetres per second. Thus, the inclination was chosen as 10 millimetres per minute, which corresponds to 0.167 millimetres per second. The latter configuration implies a linear relationship between displacement and time throughout the DOL. Additional information on the requirements for this experiment is elaborated in the full report in Section J.

The beam displacement induced a curvature that was measured using three lasers, two located directly under the point loads, and one in the middle at $\frac{l}{2}$. Theoretically, the lasers were placed such that an interpolation through the measured points would provide displacement as a second-degree polynomial. Figure 55 illustrates the laser placements for the bending test of *S4*.



Figure 55: Placement of lasers for curvature measurement.

4.5.2 Result of bending tests

The four test was carried out successfully with failure occurring within the gauge length of the specimens. All sensor data, except for *S1*, which regrettably suffered from file corruption, was acquired without any impediments. All the specimens showed similar tendencies during the loading phase, a linear relationship between force and displacement, followed by minor slips resulting in a "stairway" shaped declination of load. Figure 56 illustrates the values and averaged values from the files that were not corrupted.

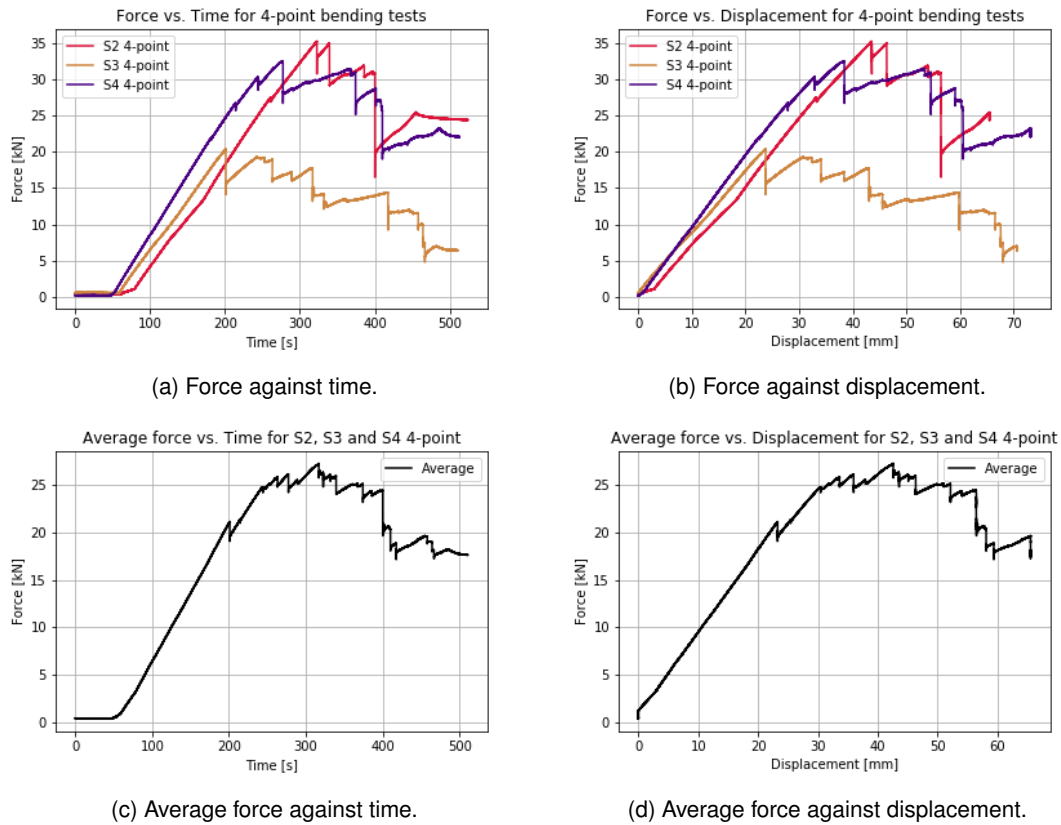


Figure 56: Data from 4-point bending tests.

A four-point bending experiment induces a constant moment distribution between the two point loads, hence a failure is anticipated in the gauge length. Furthermore, symmetry and moment equilibrium can be used to calculate bending moment and cross-sectional strength parameters. Figure 57 illustrates how the moment distribution can be derived with l_s and l_0 denoting the distance between supports and gauge length respectively. Note that the force output from the acquired data is equal to the sum of the two point loads, which are hence denoted as $\frac{F}{2}$.

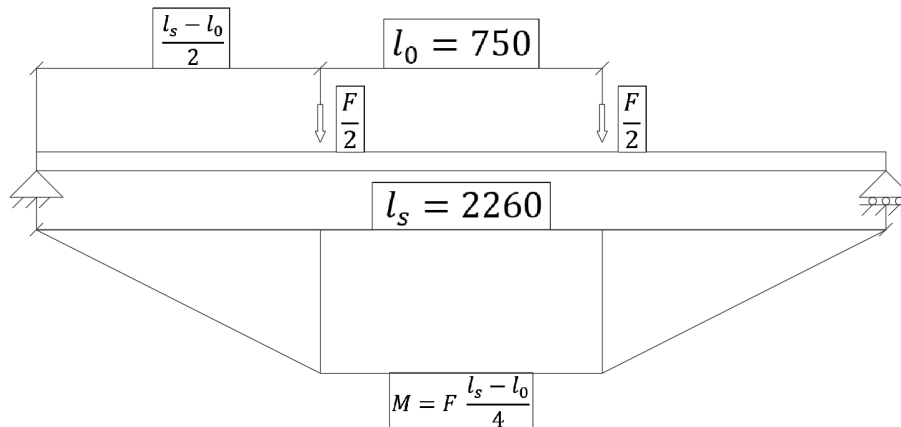


Figure 57: Moment distribution for 4-point test.

Equation 36 is obtained by moment equilibrium of the diagram in Figure 57. Based on previous

gathered information from the compression tests, the material is expected to behave elastically for such tests. As the elastic compression strength, $f_{c,0,el}$, is greater than the tensile strength, failure will occur before the compression zone behaves non-linearly. Thus, the stress distribution in the cross-section is linear with a zero stress point at the centroid.

Additionally, the tension strength is calculated according to Equation 37, which is the same equation used to calculate bending strength in *NS-EN 384* (CEN 2022). The latter equations are used to obtain the relevant parameters when failure occurs in Table 7. To obtain the cross-sectional dimensions, w and h from *A3* is used as the reference point, which represents the cross-sectional area at the midpoint of the *S-test*, as defined in Section E. a_d denotes the distance between the loading position and the nearest support, visualized as $\frac{l_s - l_0}{2}$ in Figure 57.

$$M = F \cdot \frac{l_s - l_0}{4} \quad (36)$$

$$f_m = \frac{3 \cdot F \cdot a_d}{w \cdot h^2} \quad (37)$$

Table 7: Values at failure for 4-point bending tests.

Specimen	F_{max} [kN]	δ_{tot} [mm]	M [kNm]	$f_{t,0}$ [MPa]
<i>S2</i>	35.224	45.965	13.297	38.53
<i>S3</i>	20.352	25.676	7.683	22.66
<i>S4</i>	32.526	38.402	12.279	35.97
Average	29.367	36.681	11.086	32.39

It is important to note that the average bending strength obtained from the tests is lower than the bending strength obtained for both *S2* and *S4*. This is mainly due to *S3*, which has significantly weaker bending strength and is exerting a disproportionate influence on the overall average, as shown in Table 7. Additionally, the average compression strength calculated in Table 6 is lower than both *S2* and *S4*, which suggests that there is a significant degree of uncertainty in determining the appropriate stress analysis approach, i.e., linear or non-linear. However, there was no indication of exceeding the elastic compressive capacity in the bending tests.

The determination of the global modulus of elasticity follows the method described in *NS-EN 408* (CEN 2012). Based on the experimental results, it was found that Laser 3 provided the most accurate deformation measurements compared to Laser 1 and Laser 2. This was evident from the graphs included in the appendix in Section D, which showed the relationship between force and the deformation measured by each laser. The slope of the curve obtained from Laser 3 was found to be roughly constant, which allowed for a more accurate determination of the modulus of elasticity.

For the purpose of this analysis, the deformation measurements were taken at the center of the tension edge, which is located at the centre of the span. To ensure the highest possible correlation coefficient, the entire linear portion of the deformation curve was included in the analysis, as shown in the graphs presented in Section D for the stiffness regressions. The graphs were created using Excel and the *trendline* function, which yielded a correlation coefficient of approximately 0.99.

According to *NS-EN 408*, the shear modulus is taken as infinity. However, coniferous wood species have a shear modulus of 650 MPa. Both results with and without the shear deformation correction were calculated, as prescribed by the standard. In line with *NS-EN 384*, when the shear modulus is taken as infinity, softwood specimens must be adjusted to the modulus of elasticity parallel to the grain, as described by Equation 38.

$$E_0 = E_{m,g} \cdot 1.3 - 2690 \quad (38)$$

Table 8 contains the stiffness and the computed global modulus of elasticity for two scenarios: when the shear modulus, G is set to a value of 650 MPa , and when it is set to infinity. In the latter case, the global modulus of elasticity is adjusted using the formula presented in Equation 38.

Table 8: Stiffness and global modulus of elasticity from 4-point bending tests.

Specimen	K_b [kN/mm]	$E_{m,g}(G = 650)$ [MPa]	$E_{m,g}(G = \infty)$ [MPa]
S2	0.901	8830.76	8350.74
S3	0.914	9181.47	8776.85
S4	0.966	9637.20	9320.85
Average	0.927	9216.47	8816.15

Wood exhibits a considerably lower shear modulus compared to its modulus of elasticity. This characteristic, combined with the typically large cross-sectional height of GLULAM components in relation to their span, can result in significant shear deformations in wooden constructions. To obtain precise results without incurring any extra computational costs or numerical issues, it is highly recommended to always consider shear deformations in calculations (Bell and Liven 2018). The observed failure patterns in the bending specimen indicate the presence of shear stresses. This is clear from the horizontal lines in Figure 58. In Figure 59, the strain is calculated from Hooke's law, using the average modulus of elasticity with a value of $G = 650 \text{ MPa}$, which indicates the presence of shear stresses. The value for σ_m at the extreme fibres is equal to $f_{t,0}$ in Table 7.



Figure 58: Failure in tension zone with secondary shear failure.

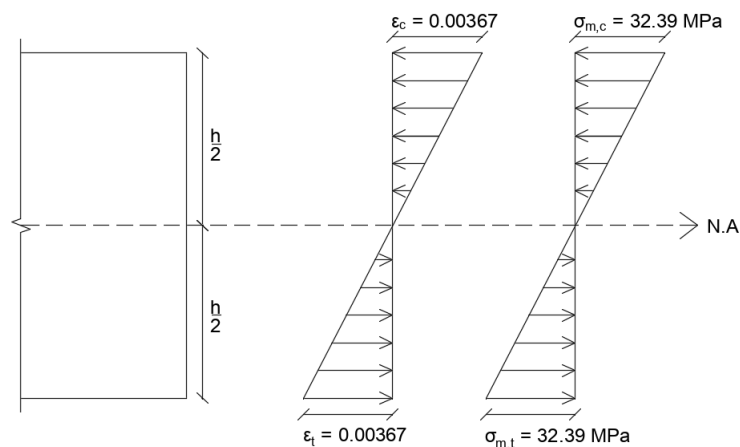


Figure 59: Stress-strain distribution across the cross-section of the beam.

4.6 Specimen moisture and density calculations

As previously discussed in Section 2, the structural behaviour of timber is largely dependent on MC and hence also density. In order to clarify the background of which all strength parameters in the previous tests are defined, it is necessary to determine the MC and density of the tested specimens based on standardized methods. The ten specimens for both MC and density determination are identified as *MC-tests*. All specimens have origin from tension specimen *S4* and are labelled as *MC1-MC10* as illustrated in Figure 60.



Figure 60: Annotation of specimens from *MCs*.

4.6.1 Density

In *ISO 13061-2*, the procedure for the determination of density is described (ISO 2014b). The dimensions of the test specimens were measured to the nearest 0.1 millimetre or a precision of $\pm 0.3\%$, according to the standard. To ensure consistency between the *MC-tests*, measurements of the dimensions were taken from the same sides on each specimen, and the values can be found in Table 9. Following this, the density values were arranged in ascending order and presented in Table 10.

As all ten specimens were cut from the same sub-sample of *S4*, it can be concluded that $\rho_{05,i}$ is equivalent to $\rho_{05,i,min}$. Furthermore, the rank and the resulting 5-percentile density were calculated by interpolation, according to Equation 39.

Table 9: Values for density in partially dry state.

Specimen	$m_W [g]$	$b_W [mm]$	$d_w [mm]$	$h_W [mm]$	$V_W [mm^3]$	$\rho_W [kg/m^3]$
MC1	33.1	55.2	34.0	30.8	57805.4	572.6
MC2	29.5	55.3	32.8	28.1	50968.9	578.8
MC3	28.5	55.5	33.0	27.2	49816.8	572.1
MC4	28.6	55.9	32.0	27.5	49192.0	581.4
MC5	28.3	57.0	31.5	26.9	48299.0	585.9
MC6	27.8	55.9	32.0	26.7	47761.0	582.1
MC7	29.4	55.3	31.8	28.1	49415.0	595.0
MC8	27.6	57.1	31.2	26.2	46675.8	591.3
MC9	28.8	56.5	31.6	27.5	49099.0	586.6
MC10	28.8	55.2	33.5	32.0	59174.4	486.7
Average values	29.0	55.9	32.3	28.1	50820.7	573.3

Table 10: Values for density in ascending order and the corresponding ranks.

Rank	1	2	3	4	5	6	7	8	9	10
ρ_W	486.7	572.1	572.6	578.8	581.4	582.1	585.9	586.6	591.3	595

$$Rank = \frac{p}{100} \cdot (n - 1) + 1 = \frac{5}{100} \cdot (10 - 1) + 1 = 1.45 \quad (39)$$

$$\rho_{05,i} = 486.7 + 0.45 \cdot (572.1 - 486.7) = 525.1 \frac{kg}{m^3}$$

The final calculation for the characteristic density is shown in Equation 40, where factor k_n set to be 0.88.

$$\rho_k = \min \left(1.1 \cdot 525.1 ; \frac{\sum_{i=1}^1 10 \cdot 525.1}{10} \right) \cdot 0.88 = 462.1 \frac{kg}{m^3} \quad (40)$$

4.6.2 Moisture content

The procedure for the determination of moisture content is described in *ISO 13061-1* (ISO 2014a). The initial step of this procedure was to measure the weight and dimensions of the specimens. Once this was done, the specimens were placed in an oven set at a temperature of $(103 \pm 2)^\circ C$ for a period of 48 hours to completely dry them out. However, to ensure the accuracy of the measurements, the specimens were weighed thrice, with an interval of 8 hours in between, to confirm that there was a weight difference of less than 0.2 %. This step was crucial to ensure that the specimens were completely dried out and the weight remained constant. The moisture content results, including the initial mass, oven-dry mass, and moisture content for each specimen, are summarised in Table 11. m_{init} and m_{od} denote the initial mass and oven-dried mass with subscript referring to the steps in the drying cycle.

Table 11: Values for MC.

Specimen	m_{init} [g]	m_{od_1} [g]	m_{od_2} [g]	m_{od_3} [g]	MC [%]
MC1	33.1	29.4	29.3	29.3	13.0
MC2	29.5	26.3	26.2	26.1	12.6
MC3	28.5	25.4	25.3	25.2	12.6
MC4	28.6	25.3	25.3	25.2	13.0
MC5	28.3	25.1	25.1	25.0	13.2
MC6	27.8	24.7	24.7	24.6	13.0
MC7	29.4	26.2	26.1	26.0	13.1
MC8	27.6	23.5	24.5	24.4	13.1
MC9	28.8	25.6	25.6	25.5	13.0
MC10	28.8	25.6	25.6	25.5	13.0
Average values	29.0	25.8	25.8	25.7	13.0

5 Fatigue life determination based on static strength

Determining the fatigue life of timber bridges holds significant importance in safeguarding their durability and ensuring their safety and reliability over time. As highlighted in the preliminary report, there is a high possibility that the structural collapse of *Tretten* bridge can be attributed to block failure, but it is not unlikely that fatigue loads also played a role in the collapse. The evaluation of fatigue life in combination with block failure capacity for critical sections of *Tretten* bridge is hence considered a crucial subject in our understanding of the accident.

Based on the current investigation, diagonals 6 and 7 are deemed of special interest regarding the latter. These diagonals are illustrated in Figure 61. The objective of this chapter is to assess the capacity of the latter diagonals regarding block failure and fatigue loads. The load-carrying capacity of the critical connections will be evaluated by resistance to axial loads with increasing eccentricity. S-N curves will be constructed in an attempt of defining the most critical diagonal, and thus also the point of failure for *Tretten* bridge.

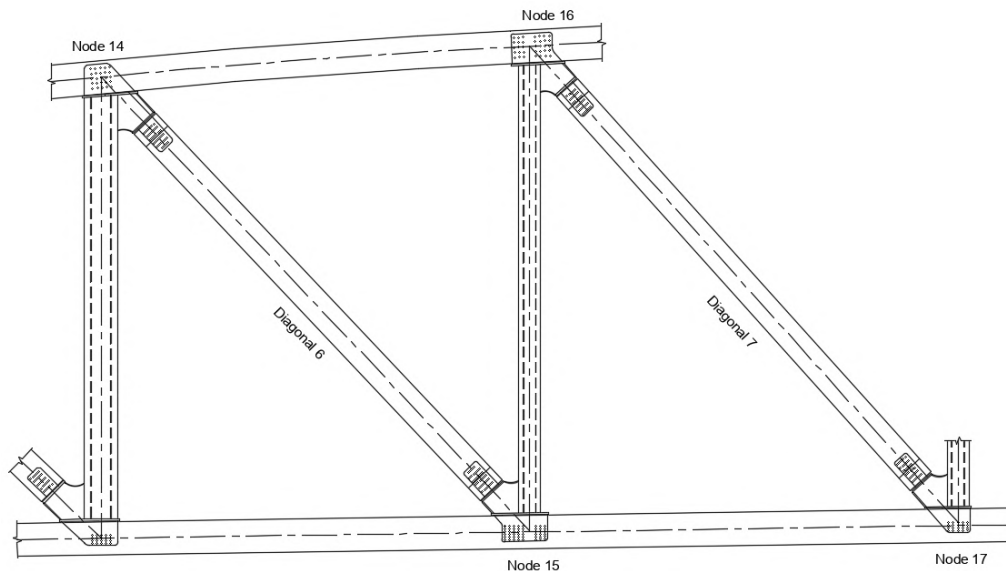


Figure 61: Diagonals and nodes of interest.

5.1 Analysis of critical connections

The connection's capacity of resisting moments is based upon the magnitude of its second moment of inertia. Let z denote the vertical axis, then the second moment of inertia is defined by the integral over the area as denoted in Equation 41.

$$I_y = \int_A z^2 dA \quad (41)$$

In order to define the second moment of inertia in dowel connections, it is necessary to exclude cross-sectional areas that encompass dowels. The net second moment of inertia will therefore include multiple regions that are not positioned along the neutral axis, where each of their contributions can be accounted for by the use of the parallel axis theorem. Let d denote the distance between the main axis, x , and the parallel axis x' as illustrated in Figure 62.

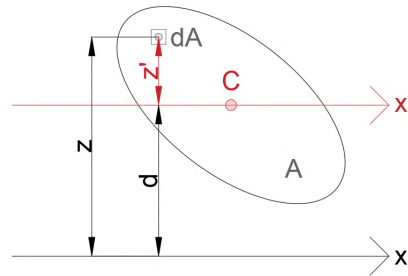


Figure 62: Contribution to second moment of inertia.

Substituting $z = z' + d$ in the equation for the second moment inertia will give Equation 42. Note that the resulting three integrals are familiar. The first is simply the second moment of inertia with respect to the neutral axis, and the third is the distance between the axes multiplied by the area. The second integral denotes the first moment of inertia with respect to the centroidal axis, thus cancels out.

$$\begin{aligned} I_{y'} &= \int_A (z' + d)^2 dA \\ &= \int_A [(z')^2 + 2z'd + d^2] dA \\ &= \int_A (z')^2 dA + 2d \int_A z' dA + d^2 \int_A dA \\ &= I_y + wh \cdot d^2 \end{aligned} \quad (42)$$

Where I_y for a square beam with constant cross-sections can be reduced as described in Equation 43.

$$I_y = \int \int_R z^2 dA = \int_{-w/2}^{w/2} \int_{-h/2}^{h/2} z^2 dy dz = \frac{wh^3}{12} \quad (43)$$

Based on current investigations, block failure samples from the bridge and experiments conducted in the laboratory, it is likely that block failure was decisive for a critical section limited by the net shear planes denoted as A_{net} in Figure 65 and Figure 66. Evidence suggests consequently that net area and net second moment of inertia should be limited by the outermost dowel rows for capacity calculations. A finite element analysis (FEA) of the experimental specimens conducted by a fellow doctoral

student Wefag Alawd justifies chosen critical cross-section by stress analysis. For a given axial displacement, stresses parallel to the grain accumulate in the critical section as illustrated in Figure 63 and Figure 64 (Alawd 2023). Excluding the outermost lamellas is deemed more accurate for further capacity calculations, and thus the critical section has parameters denoted A_{net} and I_{net} .

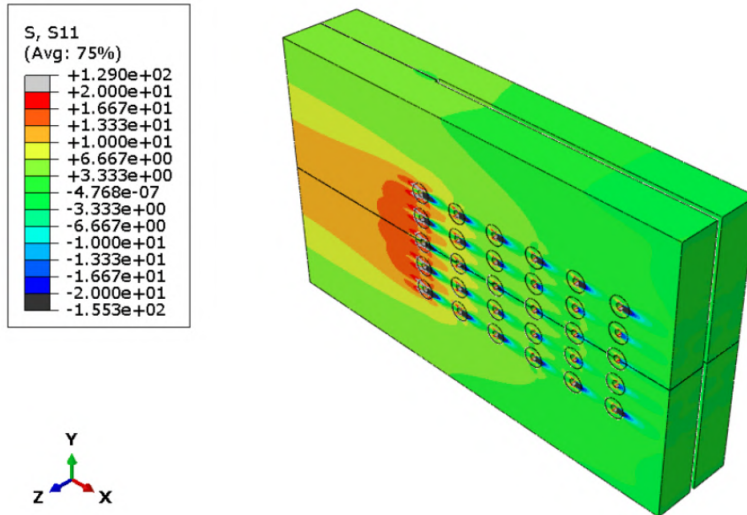


Figure 63: Stress distribution parallel to grain (Alawd 2023).

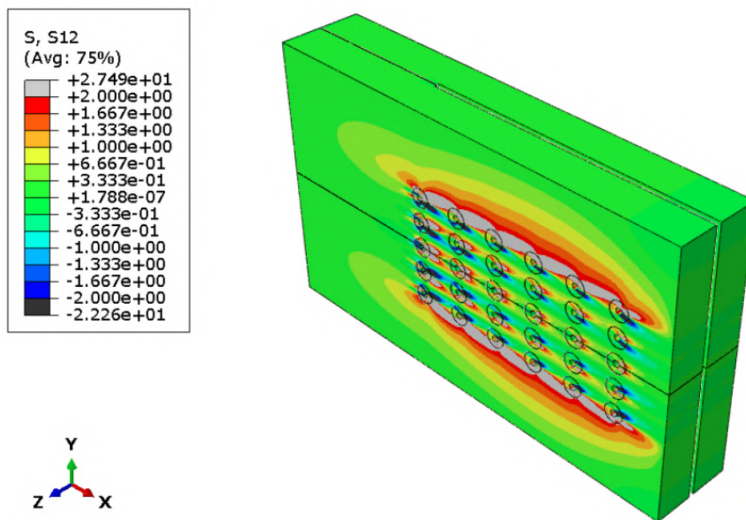


Figure 64: Stress distribution perpendicular to grain (Alawd 2023).

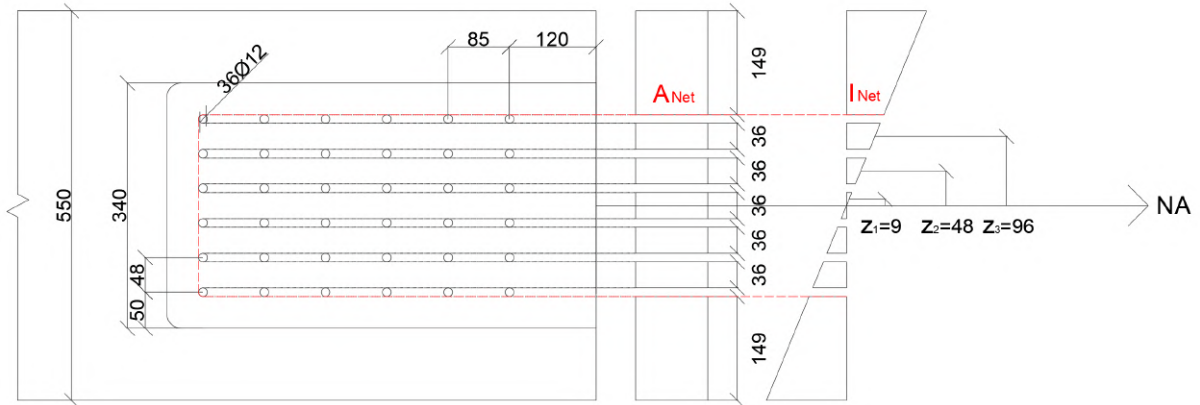


Figure 65: Details of node 14 and 15.

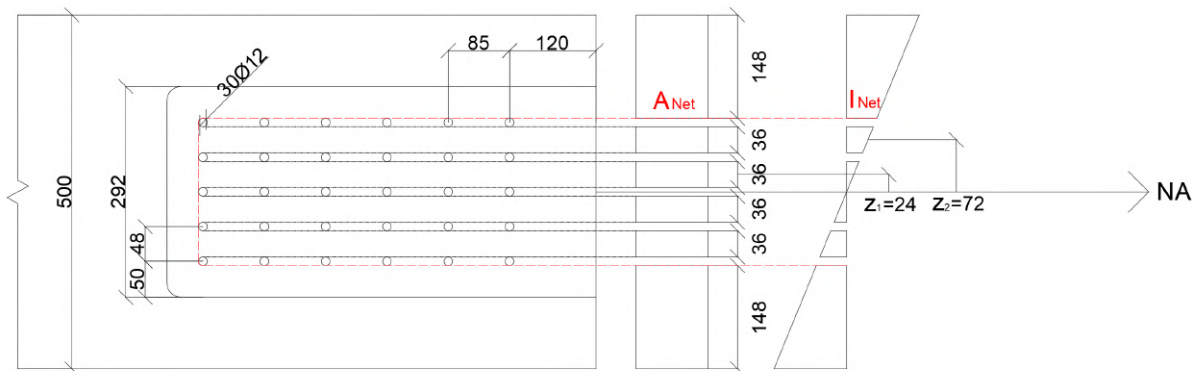


Figure 66: Details of node 16 and 17.

Table 12 includes parameters used for calculating the net second moment of inertia and net area for the connections of interest with respect to the drawings in Figure 65 and Figure 66. z_i denotes the distance between the parallel axes, substituted for d in the aforementioned equations. The effective width of the cross-sections equals the total width subtracted by six steel plate slots of 11 millimetres.

Table 12: Node geometry in *Tretten* bridge diagonal 6 and 7.

Parameter	Node 14 and 15	Node 16 and 17
w [mm]	550	500
w_{ef} [mm]	484	434
h [mm]	550	500
h_{ef} [mm]	478	440
$z_{max,net}$ [mm]	126	102
z_1 [mm]	9	24
z_2 [mm]	48	72
z_3 [mm]	96	—

Table 13: Net cross-sectional parameters in *Tretten*.

Nodes	A_{net} [$10^3 \cdot mm^2$]	I_{net} [$10^6 \cdot mm^4$]
14 and 15	87.120	410.858
16 and 17	62.496	186.738

5.2 Fatigue verification according to EC5-2

EC5-2 provides a simplified design method for fatigue verification of bridges. This method is based on constant amplitude equivalent fatigue loading, which represents the fatigue effects of the full range of loading events (CEN 2004). A fatigue verification must be conducted when the ratio κ exceeds the specified limit value in EC5-2. The ratio is given in Equation 44, where $\sigma_{d,max}$ and $\sigma_{d,min}$ are the numerically maximum and minimum design stresses, respectively. f_k is characteristic strength and $\gamma_{M,fat}$ is the material partial factor for fatigue loading.

$$\kappa = \frac{|\sigma_{d,max} - \sigma_{d,min}|}{\frac{f_k}{\gamma_{M,fat}}} \quad (44)$$

The fatigue verification is given in Equation 45, wherein $f_{fat,d}$ denotes the design fatigue strength, as described by Equation 46.

$$\sigma_{d,max} \leq f_{fat,d} \quad (45)$$

$$f_{fat,d} = k_{fat} \frac{f_k}{\gamma_{M,fat}} \quad (46)$$

The strength reduction factor k_{fat} incorporates the reduction in strength due to the number of loading cycles and the influence of the stress ratio R . k_{fat} is a dimensionless parameter that establishes the relationship between fatigue strength and the corresponding static strength. The expression for k_{fat} is given in Equation 47.

$$k_{fat} = 1 - \frac{1 - R}{a \cdot (b - R)} \cdot \log(\beta \cdot N_{obs} \cdot t_L) \geq 0 \quad (47)$$

Where stress ratio R and the slope of the curve, A , are defined in Equation 48 and Equation 49.

$$R = \frac{\sigma_{d,min}}{\sigma_{d,max}} \quad -1 \leq R \leq 1 \quad (48)$$

$$A = \frac{1 - R}{a \cdot (b - R)} \quad (49)$$

The determination of the fatigue strength reduction factor, k_{fat} , per the EC5-2 standard, involves the use of a logarithmic function that is dependent on the total number of stress cycles. The latter is defined by Equation 50. The calculation of k_{fat} includes adjusting for the consequences of damage through the incorporation of a factor β , as well as accounting for the service life of the structure as described by EC0, represented by t_L . Additionally, the calculation takes into consideration the number of stress cycles with constant amplitude, N_{obs} .

$$N = \beta \cdot N_{obs} \cdot t_L \quad (50)$$

5.3 S-N curves for Tretten bridge diagonals

A truss system is a structural composition that consists of two-force members only, which implies that external forces and reactions are only assumed to act at the nodes. The nodes are typically assumed pin-connected, hence the connections do not experience any moments. In reality, node forces are not necessarily inflicted through the COG of the members, and thus the product of axial force and eccentricity will induce moments. These moment forces are small in the diagonals, hence often ignored in the design process because the dominant force acting on the members is axial forces.

In order to evaluate the fatigue capacity of diagonals 6 and 7, it is possible to utilize S-N curves. S-N curves can be constructed by analyzing the stress state in the connection, whereas the effects of eccentric loading must be accounted for. By assuming that there are no pre-existing moments in the connections, the moment can be defined out of axial load and eccentricity according to Equation 51. Furthermore, it is possible to define eccentricity as a dimensionless variable by dividing it per cross-section height. The eccentricity in millimetres can hence be determined by the percentage offset of the height from the origin of the loaded surface end, as described in Equation 52. Further capacity calculations will include eccentricities of 5 – 20 % as included in Table 14.

$$M = M_0 + N_x \cdot e_N \quad (51)$$

$$e = \frac{e_N}{h} [-] \quad (52)$$

Where,

- M_0 is the constant moment;
- N_x is the axial load;
- e_N is the true eccentricity;
- e is the eccentricity as a dimensionless variable;
- h is the cross-section height.

Table 14: Values for eccentricities in millimetres.

	Diagonal 6	Diagonal 7
e [%]	$e_{N,6}$ [mm]	$e_{N,7}$ [mm]
5	27.5	25.0
10	55.0	50.0
15	82.5	75.0
20	110.0	100.0

The diagonals of *Tretten* are assumed to be dominated by tensile loads parallel to the grain, thus Equation 53 will always be satisfied. By incorporating insights from professor Kjell Arne Malo, a part-taker in the investigation of *Tretten* bridge, the load picture can be defined more accurately. The loads described in Table 15 represent a loading situation that resembles the conditions leading to the collapse of the bridge. These loads are attributed to a single lorry.

$$R = \frac{\sigma_{d,min}}{\sigma_{d,max}} \geq 0 \quad (53)$$

Table 15: Load picture used for calculations.

Load	Self-weight [kN]	Lorry, min [kN]	Lorry, max [kN]	R
Diagonal 6	1398	-31	+378	0.77
Diagonal 7	1121	-32	+332	0.75

The slope of the curve used to analyse fatigue stress is dependent on the specific type of stress being experienced and the stress ratio. In the case of fatigue stress in tensile-loaded elements, *EC5-2* provides necessary constants as previously visited in Table 1. For this particular case, the values of the parameters a and b are 9.5 and 1.1, respectively. By substituting the stress ratio in Equation 54 with the R values in Table 15, the slope of the S-N curves can be found.

$$A = \frac{1 - R}{9.5 \cdot (1.1 - R)} \quad (54)$$

The effective tensile strength of the timber samples from diagonal 13B was previously, based on two separate experiments, determined as slightly above 30 MPa . Due to the inadequacy in sample size from the previously conducted experiment, 29 MPa will be used for further calculations. The latter value is based on standardized sorting procedures with large sampling size, and thus have a better statistical background (K. A. Malo 2023). In order to define the maximum axial resistance of the diagonals, Navier's formula in Equation 55 can be utilised. Substituting 29 MPa as σ_{max} in addition to previously defined variables for the connection makes it possible to solve for the diagonals' resistance to axial loads $N_{x,R}$.

$$\begin{aligned} \sigma_{max} &= \frac{N_x}{A_{net}} + \frac{N_R \cdot e_N}{I_{net}} \\ \Rightarrow N_{x,R} &= \sigma_{max} \cdot \left(\frac{1}{A_{net}} + \frac{e_N \cdot z_{max}}{I_{net}} \right)^{-1} \end{aligned} \quad (55)$$

Table 16: Axial capacity of diagonals calculated defined by eccentricities.

	Diagonal 6	Diagonal 7
e [%]	$N_{x,R}$ [kN]	$N_{x,R}$ [kN]
0	2526	1812
5	1456	978
10	1023	670
15	788	509
20	641	411

In the standard *EC5-2*, the parameter k_{fat} is employed to adjust the design fatigue strength, while serving as an indicator of the design stress level. The determination of k_{fat} , is initially presented in a simplified expression in Equation 56. However, to solve for NOC, N , the equation is subsequently rearranged as demonstrated in Equation 57.

$$k_{fat} = 1 - A \cdot \log(N) \quad (56)$$

$$N = 10^{\frac{1 - k_{fat}}{A}} \quad (57)$$

Calculations are further utilized to create the S-N curves in Figure 67. The curves provide a comparative analysis between the calculated parameters for the two diagonals, which reveals subtle variations that arise from the influence of R values on the slope parameter A . Notably, diagonal 7 exhibits a slightly steeper S-N curve compared to diagonal 6. This observation suggests that diagonal 7 is more prone to failure under similar stress conditions when compared to diagonal 6.

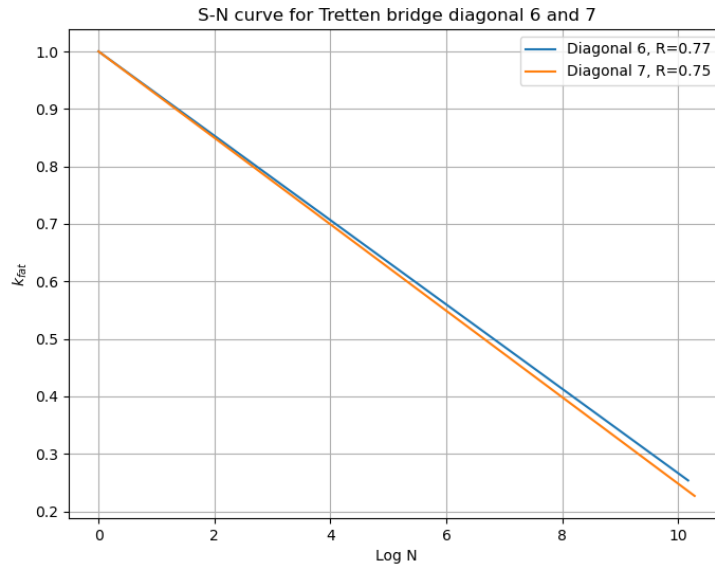


Figure 67: S-N curves for diagonal 6 and 7.

Equation 57 evaluates the number of cycles to failure, whereas k_{fat} is found according to Equation 58. The latter equation estimates the maximum design stress level, where F_{max} represents the maximum load exerted by the lorry and the self-weight. The NOC to failure, denoted N , is presented in Table 17. The loading scenario considered in these calculations identifies diagonal 7 as the critical diagonal, experiencing a stress level of 0.80, which leads to a failure after 432 cycles.

$$k_{fat} = \frac{F_{max}}{N_{x,R}} \quad (58)$$

Table 17: The number of cycles at maximum design stress level.

	Diagonal 6	Diagonal 7
k_{fat}	0.70	0.80
N	11144	432

The results presented in Table 17 clearly indicate a significantly low expected NOC to failure at the fatigue stress level for both diagonals, particularly diagonal 7. This observation raises the question of the underlying explanation, which could potentially be attributed to the slope parameter A . In the framework of *EC5-2*, the determination of this parameter relies on the coefficients a and b as previously described. However, the origin and rationale behind these coefficient values and their implications for the slope of the curves remain unknown.

Bonfield and Ansell conducted experimental testing on tensile fatigue loading with $R = 0.1$ (Bonfield and Ansell 1991). Although their experimental tests did not involve GL32c, comparing the results

is still valuable due to the potential discrepancies that may arise between theoretical predictions and experimental outcomes. Their experimental findings revealed that the slope of the S-N curve was found to be 0.05. Notably, the S-N curve for diagonal 7 in the present case study exhibited a steeper slope of 0.075. This discrepancy suggests a more rapid decline in fatigue life with increasing stress cycles for diagonal 7 compared to the observations made by Bonfield and Ansell. Traditionally, it is well-known that lower stress ratios lead to a higher rate of fatigue damage. This is clearly not the case in this comparison. The experimental results by Bonfield and Ansell with $R = 0.1$ did not exhibit a steeper slope as would be expected. If the value of $R = 0.1$ is utilized in the formula for calculating the slope parameter A in EC5-2, the resulting slope for diagonal 7 would be 0.095. This observation suggests that the S-N curve obtained from EC5-2 exhibits a steeper slope than the curve derived by Bonfield and Ansell. Consequently, the S-N curve obtained from EC5-2 is notably conservative, leading to a lower capacity, as evidenced by the discrepancy in the slope parameter.

5.4 Discussion on case study for diagonal 6 and 7

The conducted case study on diagonal 6 and 7 encompasses various amounts of assumptions of which their consequences must be discussed. Certain assumptions are deemed quite accurate, while others have been done due to the lack of information existing on the topic so far in the investigation of the collapse of *Tretten* bridge. Certain topics in this case study have been less prioritised, hence substituted with simpler assumptions. Nevertheless, the presumptions have been debated and advised prior to application.

The resistance-defined parameters are based on drawings provided by the consultancy *Norconsult*. Capacity calculations in this chapter are based on net sections and areas limited by the outermost dowel row. After conducting an analysis in which the whole section was taken into consideration, it was deemed more structurally accurate to only include the critical sections in the resistance parameter based on the ongoing investigation regarding the reason for the collapse. An FEA was used to illustrate the stress distributions in the critical connection as a supplementary statement for the assumption. However, if the whole section were to resist subjected forces, one would see an increase in load-carrying capacity. Considering the latter in the calculations for fatigue life would however still not give a result that would be satisfactory to ensure the safety of a bridge.

Furthermore, an assumption was made stating $\sigma_{min} \geq 0$ based on the given load scenario. This would imply that the diagonal would not in any circumstance experience compressive loads. Consequently, R is defined as equally larger or equal to zero. As previously discussed in Section 3, alternating stresses are decisive for fatigue loads but are not taken into consideration for the S-N curves. There is little information that indicates that the diagonals would experience negative stresses, hence the assumption is deemed accurate for this calculation.

The calculated values of k_{fat} for both diagonal 6 and 7 are relatively high, with values of 0.7 and 0.8, respectively. These values indicate that the applied stress levels are quite significant, which would naturally result in a lower number of cycles to failure compared to lower stress levels. While high-stress levels themselves are not necessarily incorrect, it is important to consider the specific load scenario described. The k_{fat} values are obtained from the load scenario of a single lorry crossing the bridge. For this specific load, the stress levels should be considerably lower than what the calculated k_{fat} values implies. It is also worth noting the significance of slope parameter A in fatigue analysis, which is demonstrated by the experiments conducted by Bonfield and Ansell and the theoretical results obtained in this case study based on EC5-2. The experimental results obtained do not align with the expectations from the standard.

6 Conclusion

As for all the tests on diagonal element 13B, it is imperative to stress the fact that all conclusions drawn are based on limited data obtained from a small number of tests. This inadequacy in sample size hampers the ability to accurately establish trends with minimal uncertainties. There is a sparse amount of material resources to conduct experimental tests, hence all collected data is considered valuable and significant. Additional uncertainties of MC and density were neither accounted for in calculations regarding estimated specimen capacity. On a final note, irregularities such as knots, differential swelling, and existing cracks contributed to diverse specimen quality. The latter is arguably a beneficial factor, as it more accurately describes the real situation in events such as the collapse of *Tretten* bridge.

Four tensile tests were conducted on the specimens sent to *NTNU* from the *Tretten* bridge. All four failed to produce failure modes related to tension, hence the tensile strength parallel to grain ($f_{t,0}$) could not be determined. The three specimens that exhibited the most consistent material behavior resisted on average a max tensile force of 318.5 kN . Divided by their respective areas, suggested that the timber used at *Tretten* had a mean tensile strength of at least 19.5 MPa . This value was later more accurately determined by conducting additional tests.

All three block failure tests experienced successful test results. In light of these, specimens mounted with LVDTs experienced sudden unsymmetrical rotation and dynamic displacement responses prior to failure. The latter in addition to visual analysis, suggests that the limitation of block failure capacity is highly influenced by unsymmetrical effects due to defects or uneven cross-sectional areas. Nevertheless, results indicate that the mean tensile capacity of the material ($f_{t,0}$) is approximately 33 MPa .

A total of ten compressive tests were conducted to determine compressive strength parallel to grain ($f_{c,0}$) and the stiffness (K_c) of the timber material. On average, the respective parameters were determined as 38.9 MPa and 197.8 kN/mm for the ten tests. The latter was used to find the corresponding elastic compressive strength $f_{c,0,el}$. As there were no indications of exceeding the elastic compressive capacity in the bending test, the possibility of non-linear compressive behavior was dismissed. Subsequently, a moment equilibrium analysis of the bending test results was utilized to ascertain the value of the tensile strength parallel to the grain ($f_{t,0}$) of the timber as 32.4 MPa . This value closely matches the one calculated from the block failure tests and the separate investigation carried out by K. A. Malo (2023), confirming its accuracy based on the experiments.

The static strength determined for the experiments was then later used for conducting a case study on the critical diagonals of *Tretten* bridge. Based on current investigations, it is likely that resistance to block failure is critical for a cross-section limited by the outermost dowel row. Consequently, resistance parameters such as net cross-section area (A_{net}) and net second moment of inertia (I_{net}) were determined accordingly. This assumption is supported by FEA, block failure samples from the bridge, and experiments conducted in the lab.

A simplified fatigue analysis related to block failure was then carried out according to procedures in *EC5-2*. The axial capacity of diagonals was calculated based on Navier's formula with increasing eccentricity. The stress ratio (R) is determined from a simple load scenario of a lorry crossing the bridge, of which the diagonals were only to be experiencing tensile loads, hence $R \geq 0$. S-N curves were utilized to determine that diagonal 7 is the critical diagonal with a stress level (k_{fat}) equal to 0.8. This result indicates 432 NOC until failure for diagonal 7. On the contrary, calculations for diagonal 6 imply 11144 NOC until failure with a stress level equal to 0.7.

On a final note, the result indicates that the material quality of the lamellas *T14.5* used in diagonal 13B satisfies the qualities provided for GL32c in *EN14080*. The similarity between retrieved values from the bending tests and block failure test indicates accurate results for the experiment. Block failure is

regarded as the failure mechanism that provides the least capacity against tensile loads, considerably lower than the capacity of the dowel group.

Bibliography

- Alawd, W. (2023). 'Numerical and Experimental Investigation into Fracture Mechanisms in Timber Connections'. Ongoing PhD for NTNU.
- American Wood Council (2012). 'National Design Specification for Wood Construction'. In: URL: <https://awc.org/publications/archive/>.
- Ansell, M.P. and I.P. Bond (1998). 'Fatigue properties of jointed wood composites: Part I Statistical analysis, fatigue master curves and constant life diagrams'. In: *Journal Of Materials Science* 33, pp. 2751–2762. DOI: <https://doi.org/10.1023/A:1017565215274>.
- Basquin, O.H. (1910). 'The exponential law of endurance tests'. In: 10, pp. 625–630.
- Bell, K. and H. Liven (2018). *Limtreboka - Bergeningsseksempler*. Trondheim/Moelv: Norske Limtreprodusenters Forening.
- Bonfield, P.W. and M.P. Ansell (1991). 'Fatigue properties of wood in tension, compression and shear'. In: URL: <https://link.springer.com/content/pdf/10.1007/BF00612416.pdf>.
- Booker, R.E. and J. Sell (1998). 'The nanostructure of the cell wall of softwoods and its functions in a living tree'. In: DOI: <https://doi.org/10.1007/s001070050255>.
- Canadian Wood Council (2014). 'CSA 068: Engineering design in wood'. In: URL: <https://cwc.ca/en/how-to-build-with-wood/codes-standards/wood-standards/csa-o86-engineering-design-in-wood/>.
- CEN (2004). *Eurocode 5: Design of timber structures - Part 2: Bridges*. CEN.
- (2010). *Eurocode 5: Design of timber structures - Part 1-1: General - Common rules and rules for buildings*. CEN.
- (2012). *NS-EN 408:2010+A1:2012 Timber structures - Structural timber and glued laminated timber - Determination of some physical and mechanical properties*. CEN.
- (2022). *NS-EN 384:2016+A2 Structural timber — Determination of characteristic values of mechanical properties and density*. CEN.
- Elmendorf, A. (1916). 'Stresses in impact'. In: *Journal of the Franklin Institute* 182.6, pp. 771–790. DOI: [https://doi.org/10.1016/S0016-0032\(16\)90063-2](https://doi.org/10.1016/S0016-0032(16)90063-2).
- Foschi, R.O. and Z.C. Yao (1986). 'Another look at three duration of load models'. In: URL: <https://cib-w18.com/proceedings>.
- Fragkia, V. and I.W. Isak Foged (2020). 'Energy-Based Responsive Building Composites'. In: URL: https://www.researchgate.net/publication/344151597_Exergy-Based_Responsive_Building_Composites_For_Thermal_Control_Stimuli_of_an_Adaptive_Envelope.
- Gerhard, C.C. (1979). 'Time-related effects of loading on wood strength: a linear cumulative damage theory'. In: *Wood Science* 11.3, pp. 139–144. URL: <https://agris.fao.org/agris-search/search.do?recordID=US19790438090>.
- Harris, Bryan (2003). *Fatigue in composites: Science and Technology of the Fatigue Response of Fibre Reinforced Plastics*. 1st. Cambridge CB22 3HJ, United Kingdom: Woodhead Publishing Limited.
- Hårstad-Evjen et al. (2013a). 'Tretten Bridge – Timber and Steel in Harmony'. In: URL: https://intrans.iastate.edu/app/uploads/sites/12/2019/03/ID_100_Harstad-Evjen.pdf.
- (2013b). 'Tretten Bridge – Timber and Steel in Harmony'. In: URL: https://intrans.iastate.edu/app/uploads/sites/12/2019/03/9_5_ID100_Tretten-Bridge-Timber-and-Steel-in-Harmony_rev.pdf.
- Hoffmeyer, P. and J.D. Sørensen (2007). 'Duration on load revisited'. In: *Wood Sci Technol* 41, pp. 687–711. DOI: <https://doi.org/10.1007/s00226-007-0154-5>.
- ISO (1991). *NS-ISO 6891:1991 Timber structures - Joints made with mechanical fasteners - General principles for the determination of strength and deformation characteristics*. ISO.
- (2014a). *ISO 13061-1 Physical and mechanical properties of wood — Test methods for small clear wood specimens — Part 1: Determination of moisture content for physical and mechanical tests*. ISO.

- ISO (2014b). *ISO 13061-2 Physical and mechanical properties of wood — Test methods for small clear wood specimens — Part 2: Determination of density for physical and mechanical tests*. ISO.
- Jenssen, C.G. and E.D. Vetter (2022). 'Introduction of fatigue behaviour of timber and processing experimental data'. Project thesis. NTNU.
- Jockwer, R. et al. (2017). 'Impact of knots on the fracture propagating along grain in timber beams'. In: DOI: <https://doi.org/10.1080/20426445.2016.1275093>.
- Johansen, K. W. (1949). 'Theory of timber connections'. In: URL: <http://doi.org/10.5169/seals-9703>.
- Koehler, Arthur (1917). 'Guidebook for the identification of woods used for ties and timbers'. In: URL: <https://www.rta.org/assets/docs/basicieinfo/commonly%20used%20crosstie%20species.pdf>.
- Köhler, J. (2007). 'Reliability of timber structures'. In: DOI: <https://doi.org/10.3929/ethz-a-005454370>.
- Köhler, J. and S. Svensson (2002). 'Probabilistic Modeling of Duration of Load Effects in Timber Structures'. In: URL: https://www.researchgate.net/publication/242218167_Probabilistic_Modeling_of_Duration_of_Load_Effects_in_Timber_Structures.
- Liska, J.A. (1950). 'Effect of rapid loading on the compressive and flexural strength of wood'. In: URL: <https://ir.library.oregonstate.edu/concern/defaults/tq57nw50m?locale=en>.
- Malo, K.A., F.M. Massaro and Stamatopoulos H. (2022). 'Exploring fatigue rules for timber structures in Eurocode 5'. In: DOI: <https://doi.org/10.24451/ggxx-h219>.
- Malo, Kjell Arne (2023). 'Eksperimentelle undersøkelser av trematerialer fra Tretten bru'. Ongoing investigation for Havarikommisjonen.
- Mårtensson, Annika (1994). *Wood Science and Technology*. Springer-Verlag, pp. 437–449.
- Miner, M.A. (1945). 'Cumulative Damage in Fatigue'. In: *Journal of Applied Mechanics* 12.3, A159–A164. DOI: <https://doi.org/10.1115/1.4009458>.
- Nielsen, L.F. (1979). 'Crack failure of dead-, ramp-and combined loaded viscoelastic materials'. In: First International Conference on Wood Fracture, Banff, Alberta, Canada.
- Nygaard, K. (2020). 'Fatigue in Timber: A State of the Art Review, Modeling Investigations, and Fatigue Tests of Glued Laminated Timber in Shear'. Master's thesis. NTNU.
- Palmgren, A. (1924). 'The fatigue life of ball-bearings'. German. In: *ZVDI* 68, pp. 339–341.
- Pearson, R.G. (1972). 'The effect of duration of load on bending strength of wood'. In: *Holzforschung* 26.4, pp. 153–158. DOI: <https://doi.org/10.1515/hfsg.1972.26.4.153>.
- Porteous, J. and A. Kermani (2008). *Structural Timber Design to Eurocode 5*. Blackwell Science Ltd, 9600 Garsington Road, Oxford OX4 2DQ, UK: Blackwell Science Ltd, p. 9.
- Qvist, S. and C. Soland (2022). 'Parameterstudie av Tretten bru'. Project thesis. NTNU.
- Schijve, J. (2009). *Fatigue of structures and materials*. 2nd ed. Springer Dordrecht, p. 561. DOI: <https://doi.org/10.1007/978-1-4020-6808-9>.
- Schütz, Walter (1996). 'A history of fatigue'. In: *Engineering Fracture Mechanics* 54.2, pp. 263–300. DOI: [https://doi.org/10.1016/0013-7944\(95\)00178-6](https://doi.org/10.1016/0013-7944(95)00178-6).
- Sørensen, J.D. and S. Svensson (2005). 'Reliability-based modeling of moisture and load duration effects'. In: pp. 79–86. URL: <https://vbn.aau.dk/en/publications/reliability-based-modeling-of-moisture-and-load-duration-effects>.
- Standard Norge (1999). *NS 3470-1:1999*. Standard Norge.
- (2001). *NS 3472:2001*. Standard Norge.
- (2003). *NS 3473:2003*. Standard Norge.
- (2013). *NS-EN 14080:2013+NA:2016*. Standard Norge.
- Stapf, G., S. Aicher and N Zisi (2012). 'Block shear failure of wooden connections'. In: URL: https://www.researchgate.net/publication/261878137_Block_shear_failure_of_wooden_dowel_connections.
- Statens havarikommisjon (2022a). 'Informasjonsskriv nr.1: Foreløpige undersøkelser av brukollapsen ved Tretten 15. august 2022'. In: URL: <https://havarikommisjonen.no/Vei/Undersokelser/22-441?iid=35531&pid=SHT-Report-Attachments.Native-InnerFile-File&attach=1>.

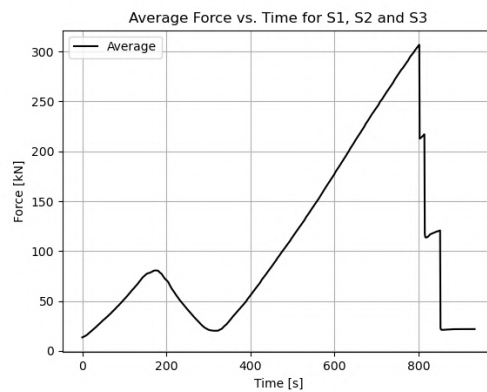
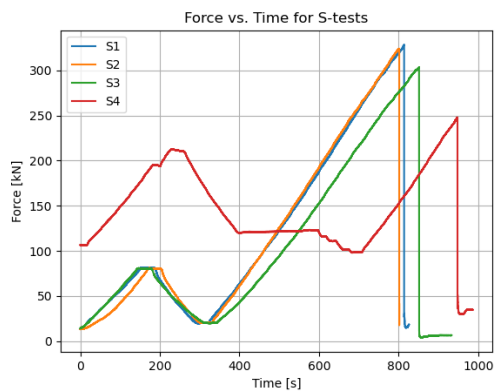
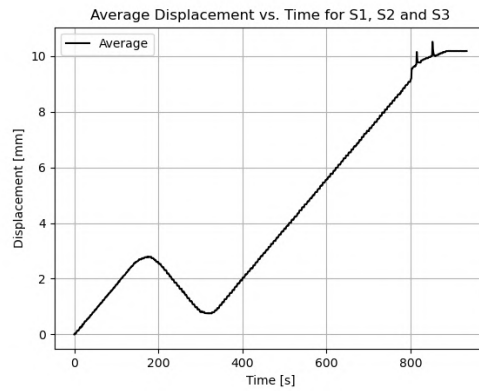
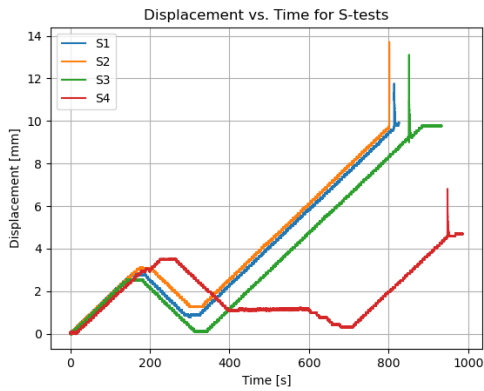
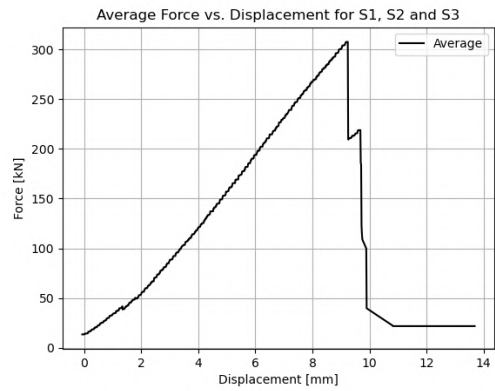
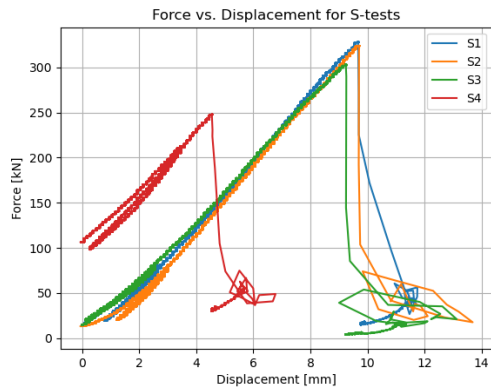
- (2022b). 'Informasjonsskriv nr.2: Foreløpige undersøkelser av brukollapsen ved Tretten 15. august 2022'. In: URL: <https://havarikommisjonen.no/Vei/Undersokelser/22-441?iid=35880&pid=SHT-Report-Attachments.Native-InnerFile-File&attach=1>.
- Swedish wood (2018). *Limträhandbok del 1*. 102 04 Stockholm: Svenskt Trä, p. 15.
- (2022). *Design of timber structures Volume 1*. 3rd ed. ISBN: 978-91-980304-8-8, pp. 28–60.
- Thue, Jan Vincent (2016). *Bygningsfysikk*. 1st. Kanalveien 51, 5068 Bergen, Norway: Fagbokforlaget, pp. 314–323.
- Tronstad, S. (2000). 'Trefuktighet - tørking'. In: URL: <https://www.treteknisk.no/publikasjoner/fokus-pa-tre/fokus-38--trefuktighet--torking>.
- Wood, L.W. (1951). 'Relation of Strength of Wood to Duration of Load'. In: URL: https://books.google.no/books?hl=no&lr=&id=SJLbTeiz7V8C&oi=fnd&pg=PA3&ots=ZNjuNI6LDj&sig=5mUGJI_fuqIQngAMKYKKvEWyBSs&redir_esc=y#v=onepage&q&f=false.

Appendix

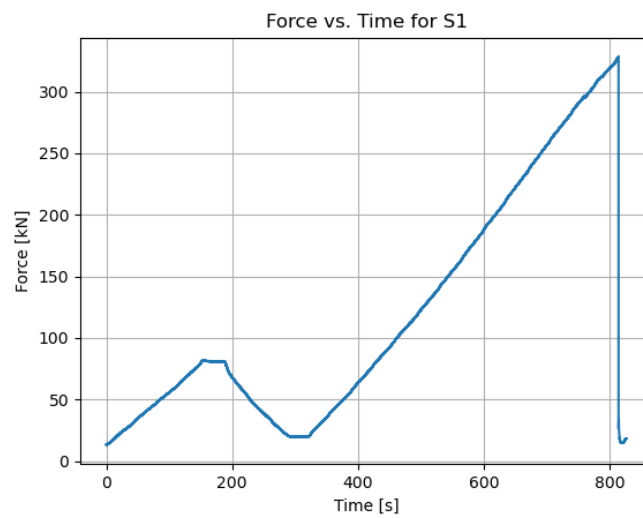
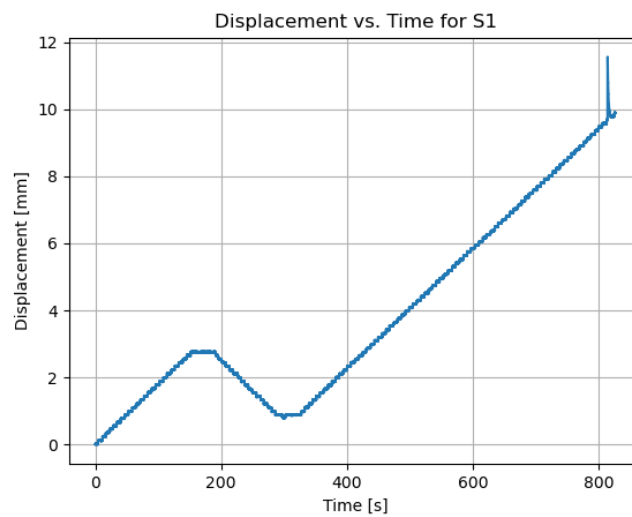
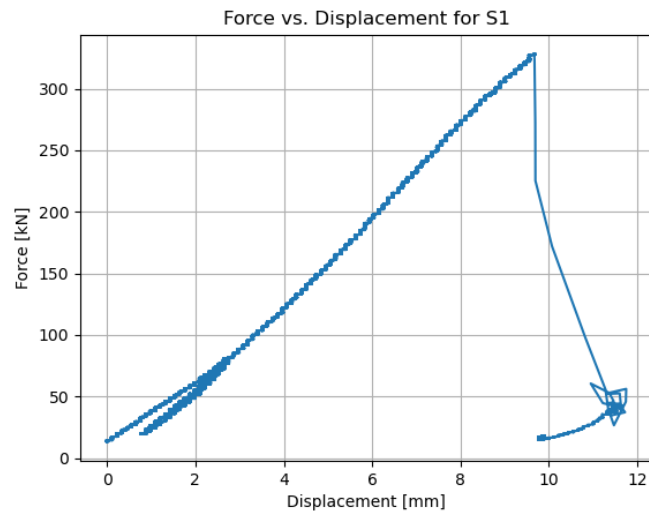
A Tension test

The following graphs are based on data acquired from the experimental tensile tests. *S1-S4* are notations referring to the specimen numbering as explained in the report. The graphs including multiple specimens and average calculations is based on the codes provided in Section F.1. The codes regarding the individual graphs are found in their respective section; Section F.2 - Section F.5.

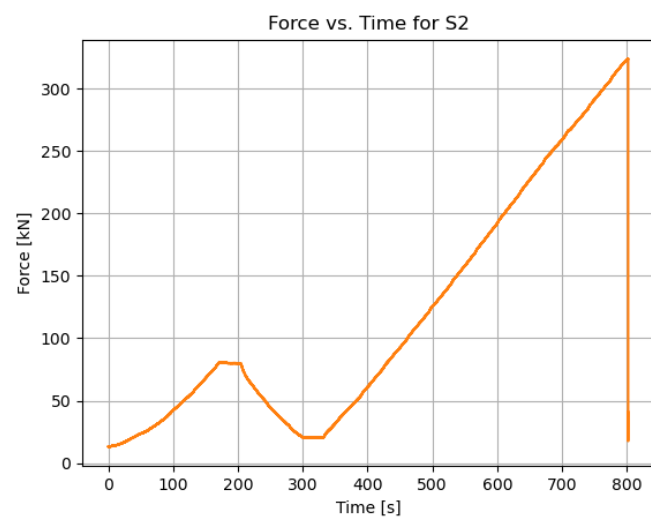
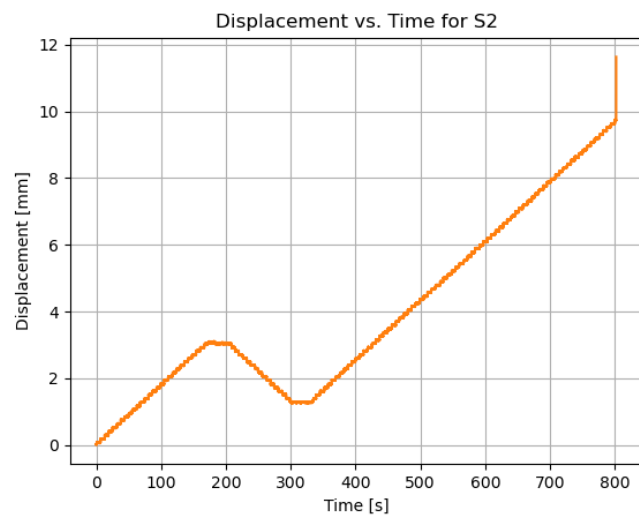
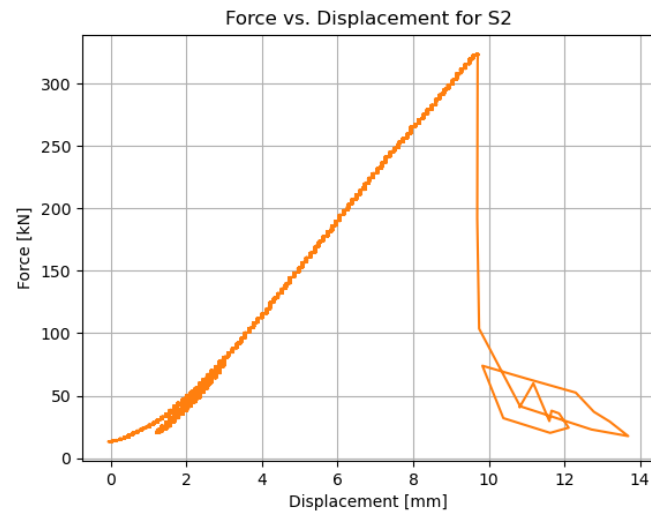
All specimens from S-test



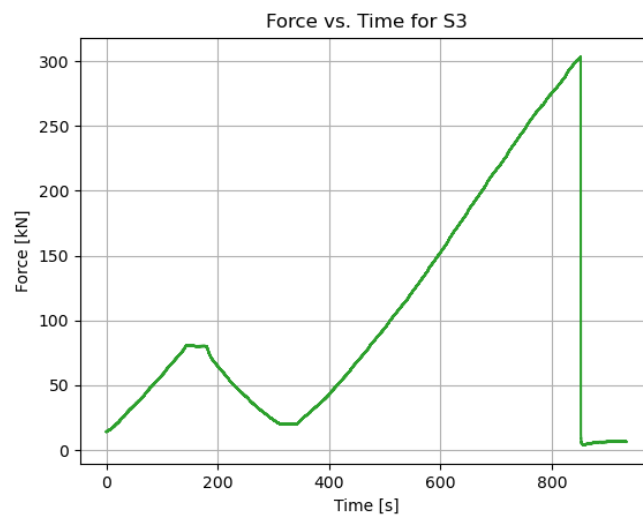
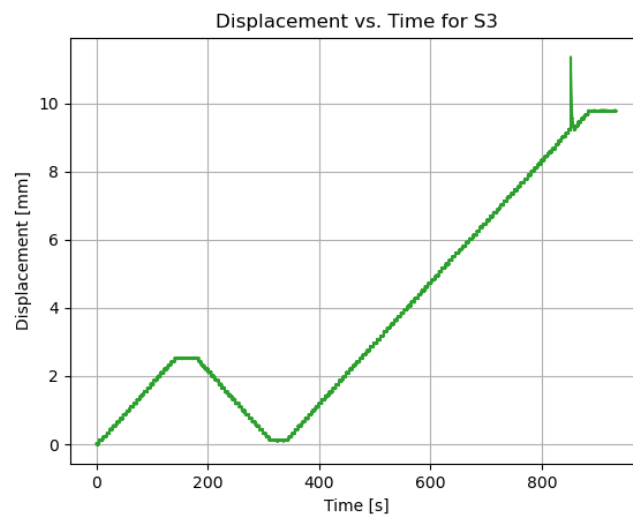
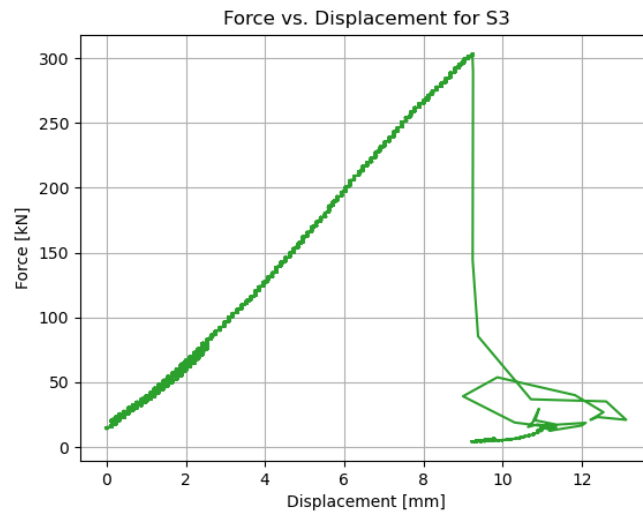
A.1 Specimen S1



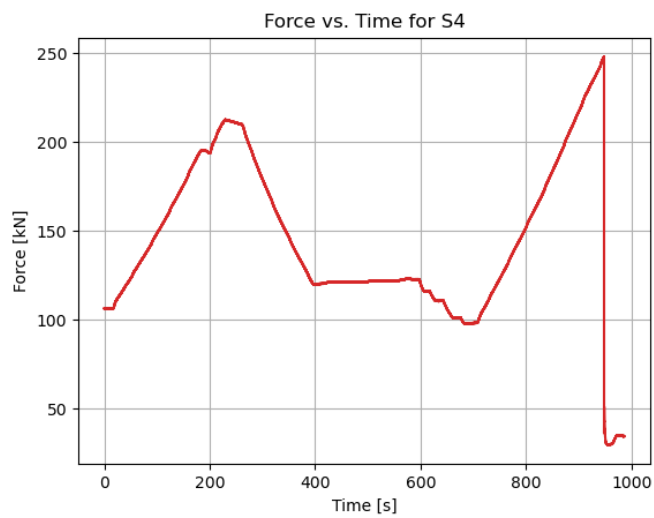
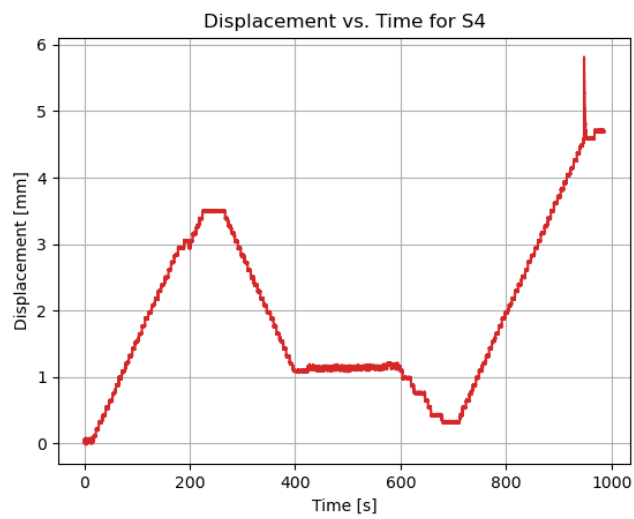
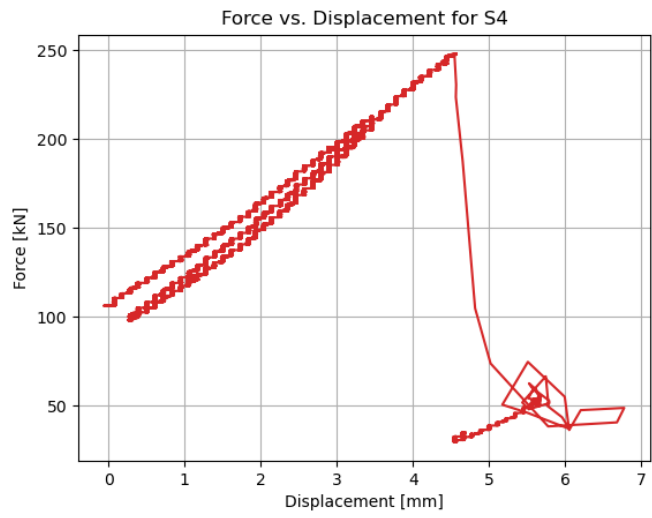
A.2 Specimen S2



A.3 Specimen S3



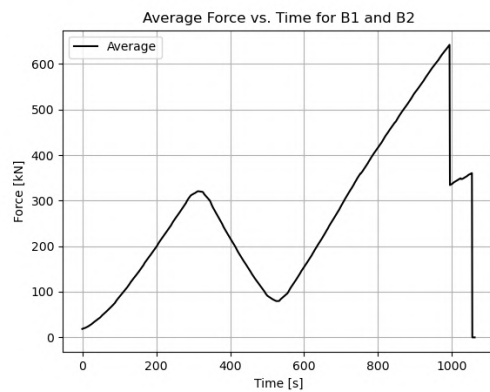
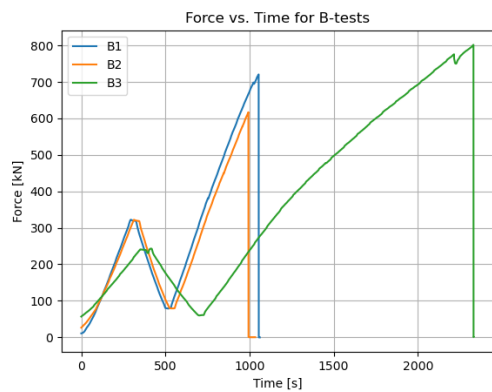
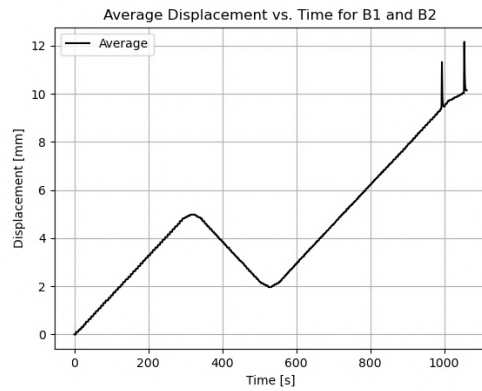
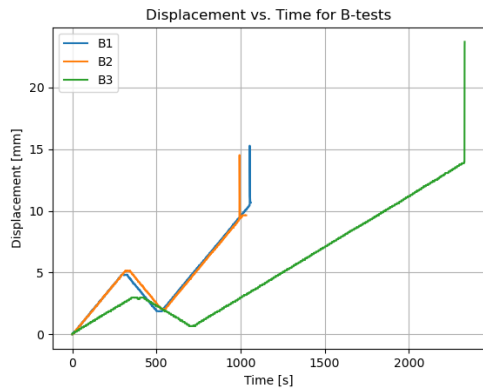
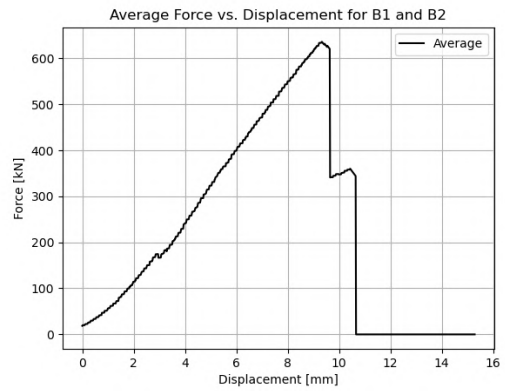
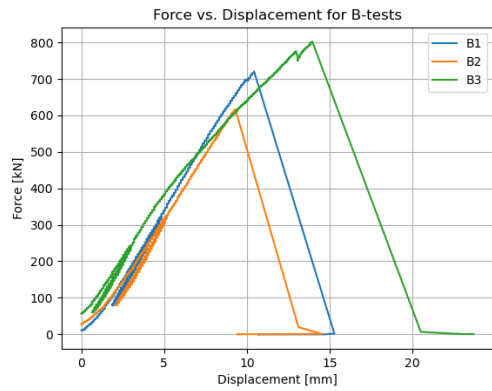
A.4 Specimen S4



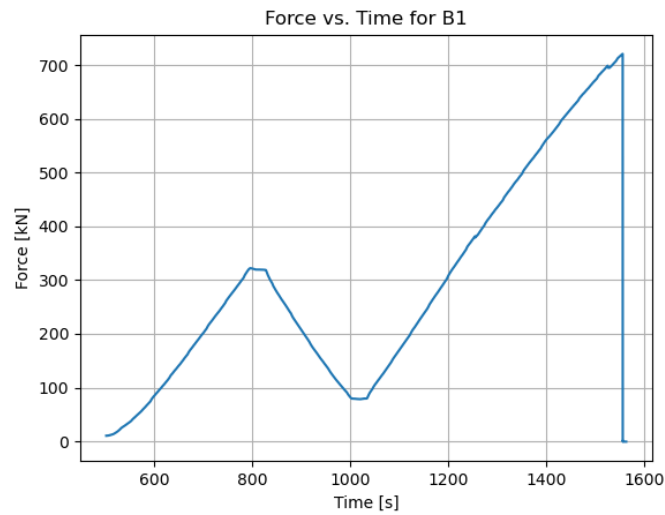
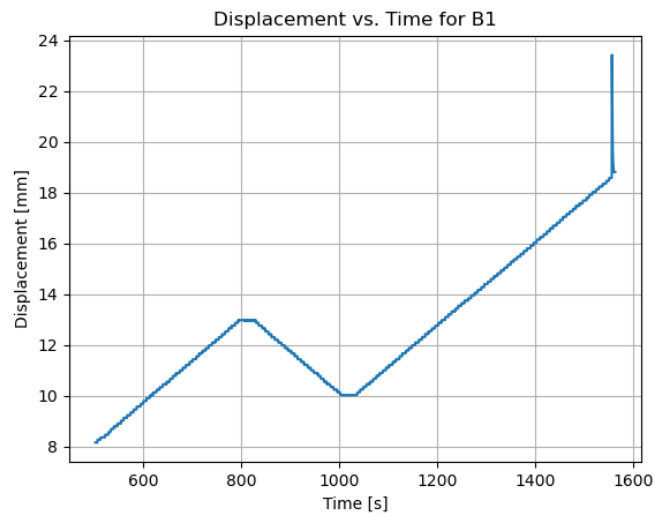
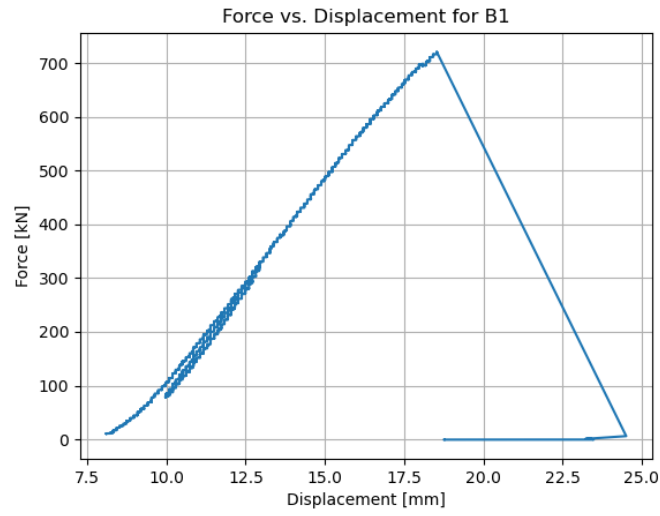
B Block shear test

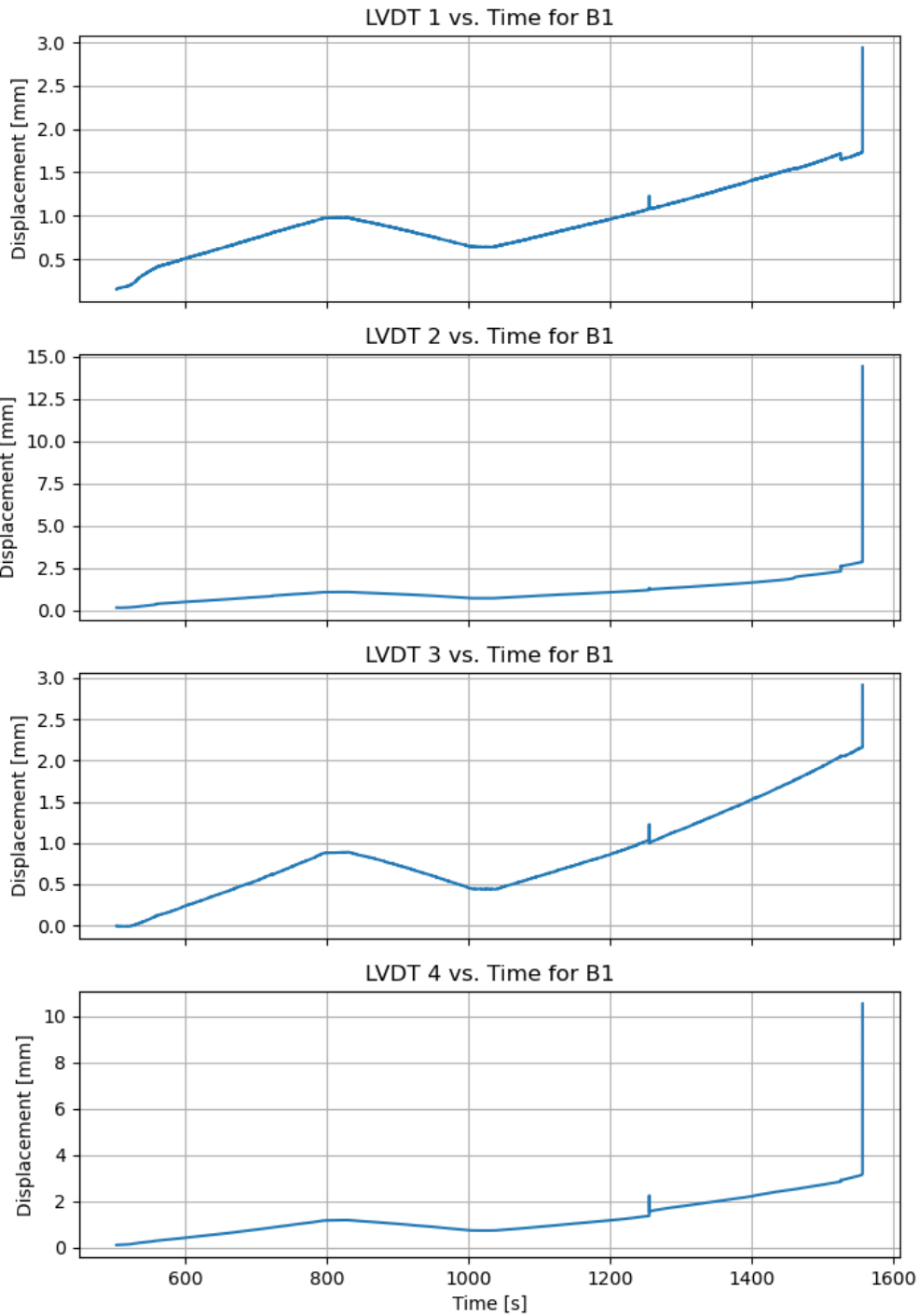
The following graphs are based on data acquired from the experimental block failure tests. *B1-B3* are notations referring to the specimen numbering as explained in the report. Graphs includes data from *LVDTs*, force-displacement analysis and rotations. The interval of time steps are defined by the machine. The graphs including multiple specimens and average calculations is based on the codes provided in Section F.6. The codes regarding the individual graphs are found in their respective code numbering Section F.7 - Section F.9.

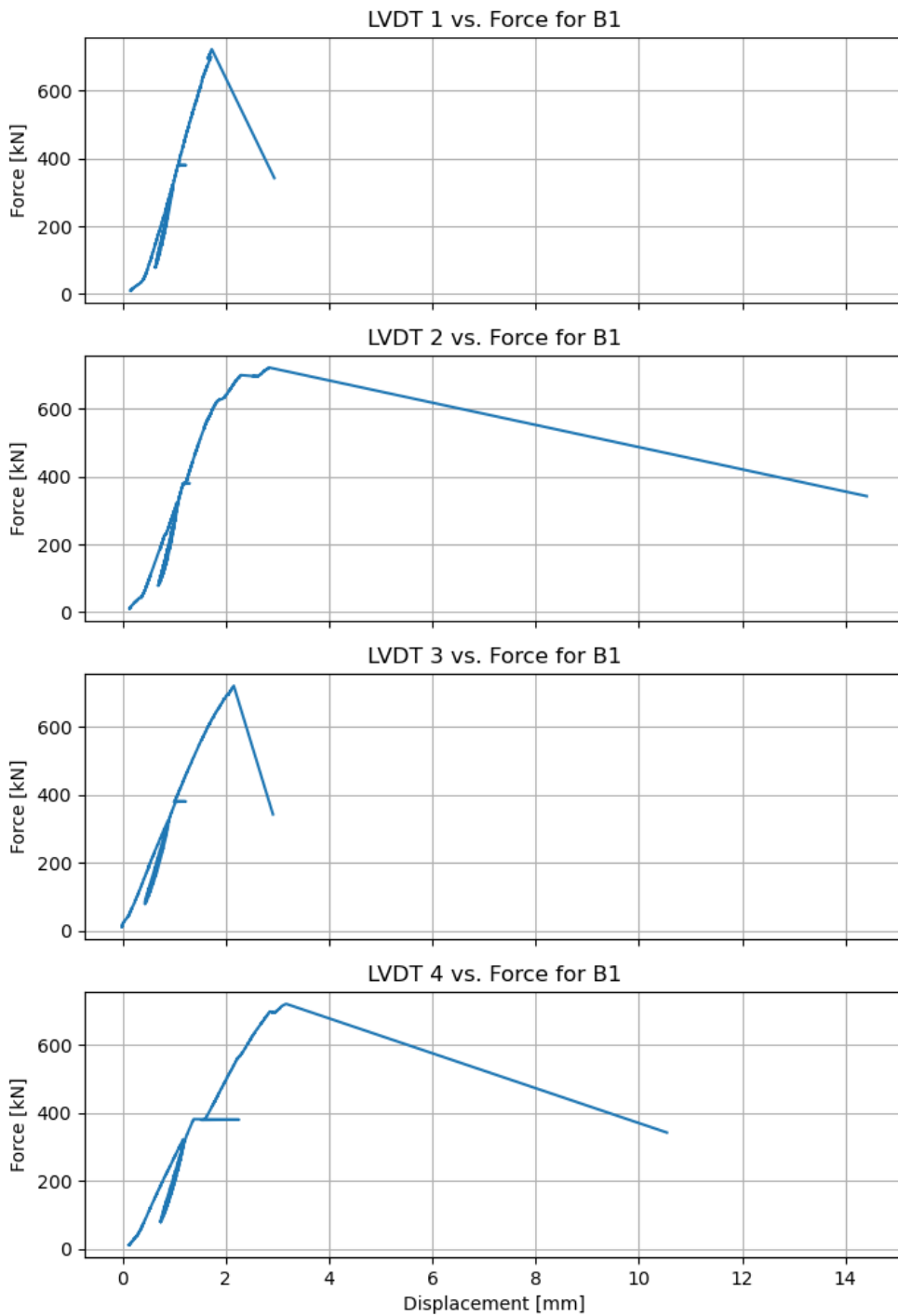
All specimens from *B*-test

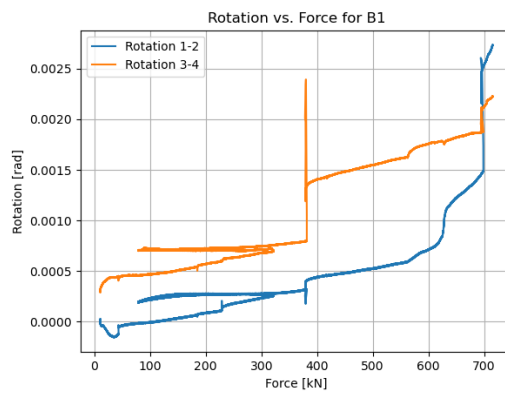
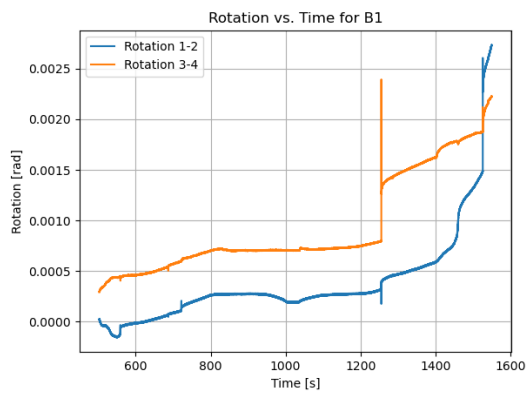
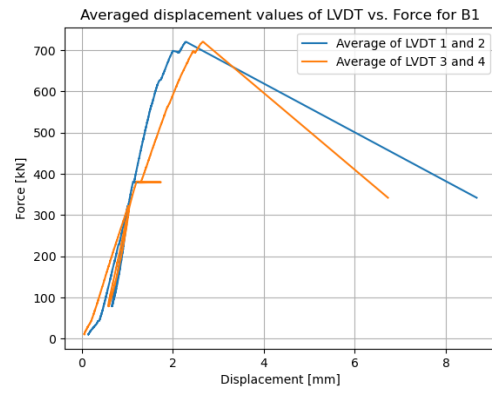
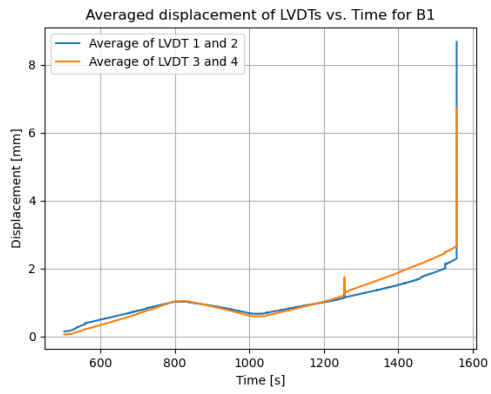


B.1 Specimen B1

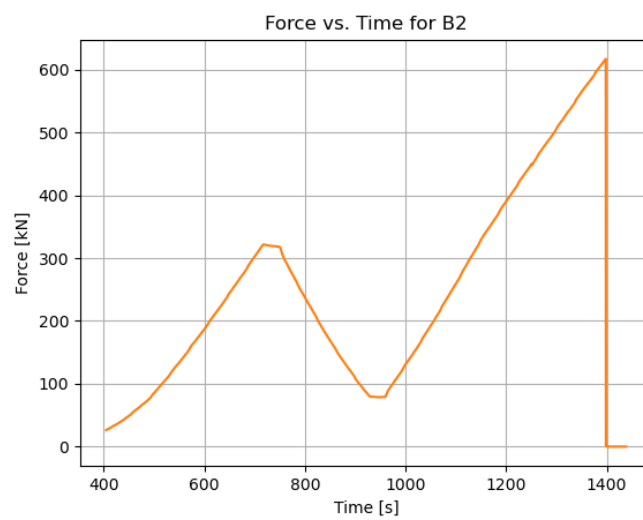
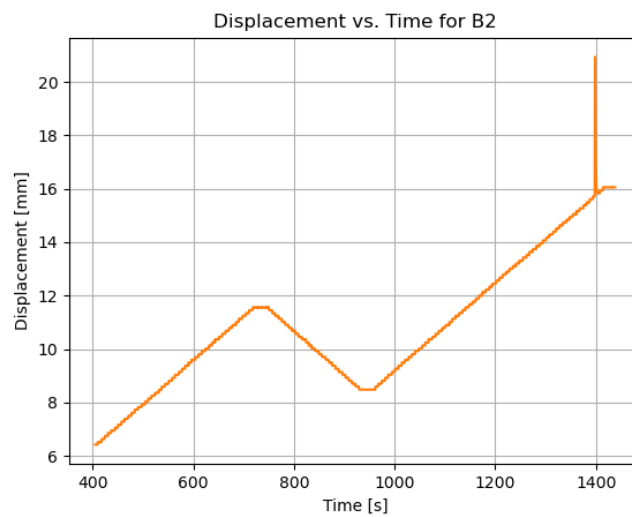
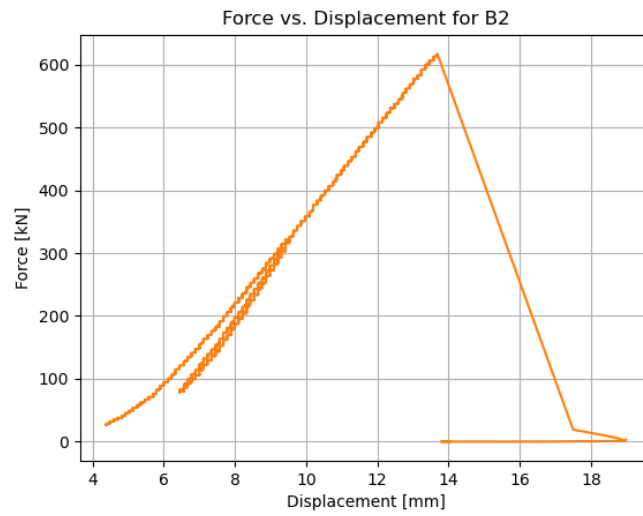


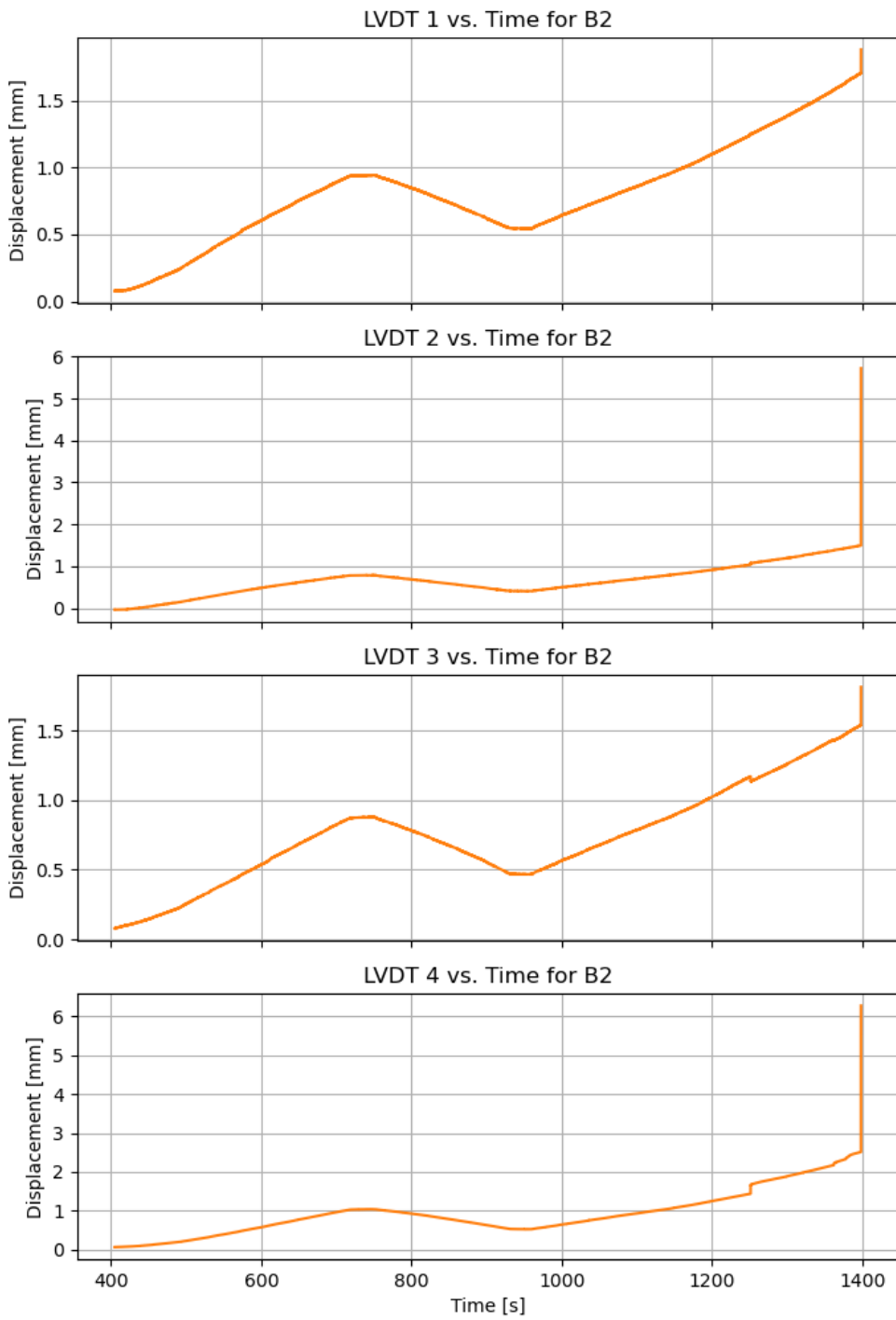


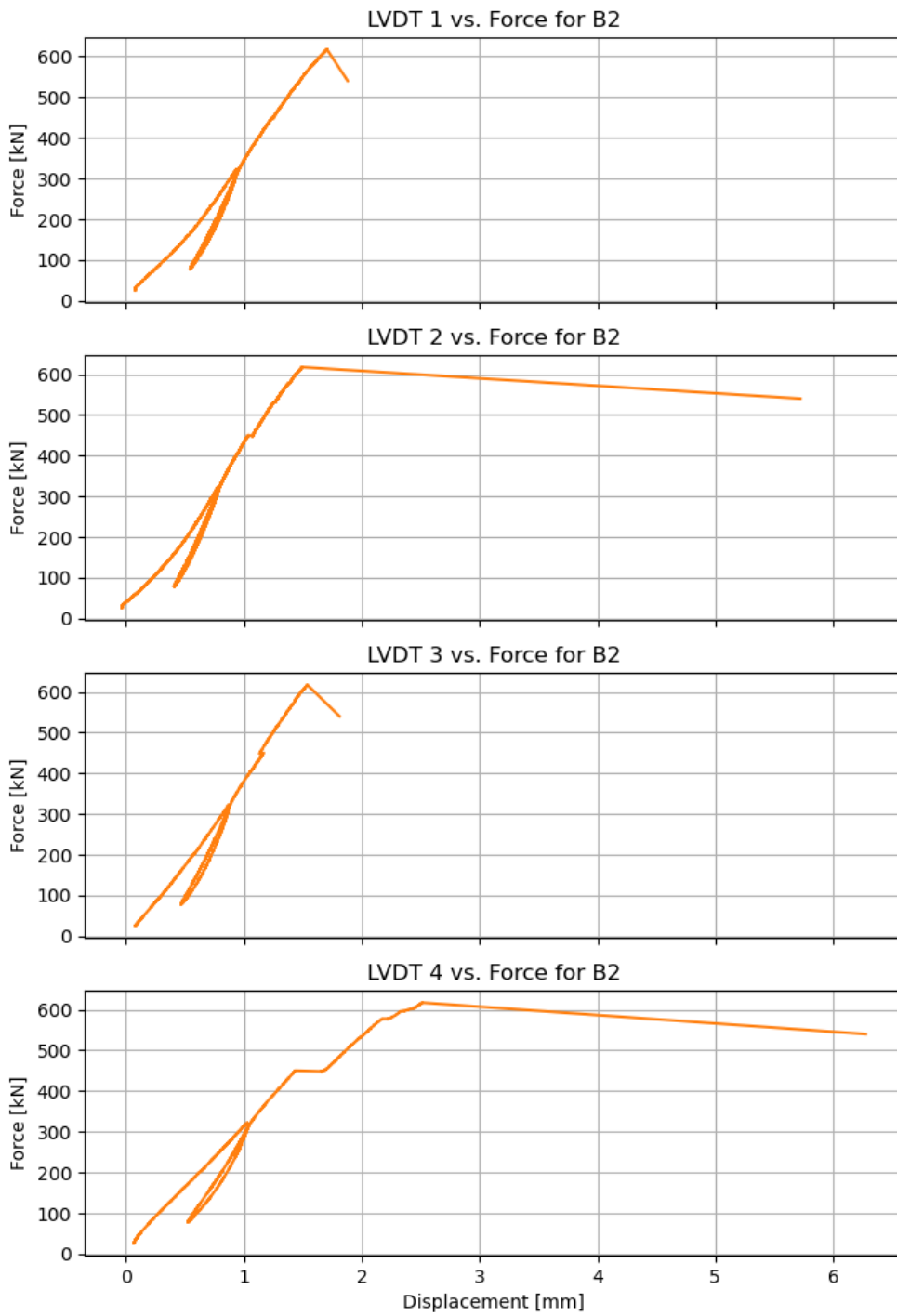


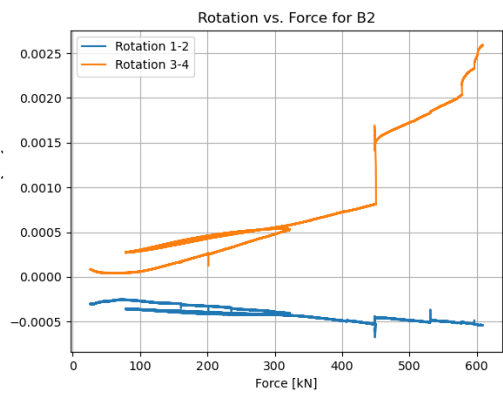
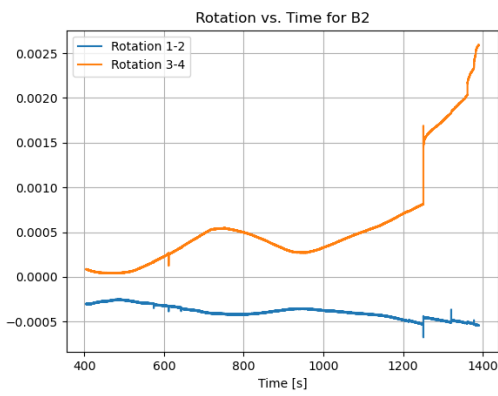
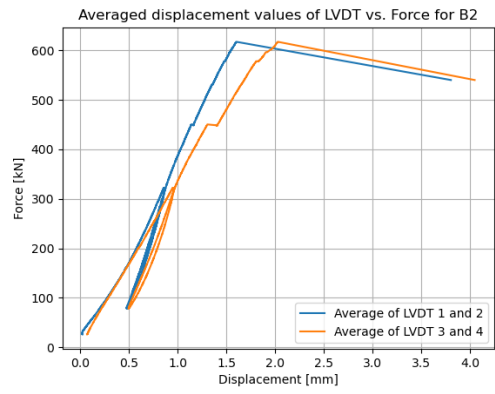
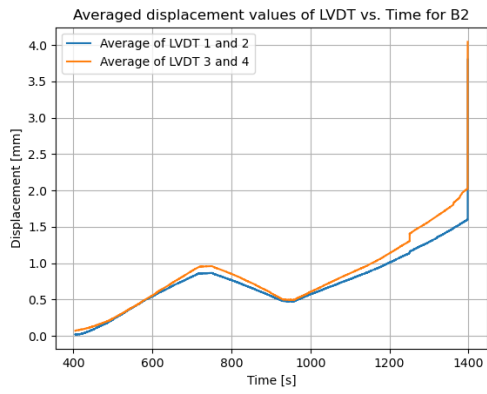


B.2 Specimen B2

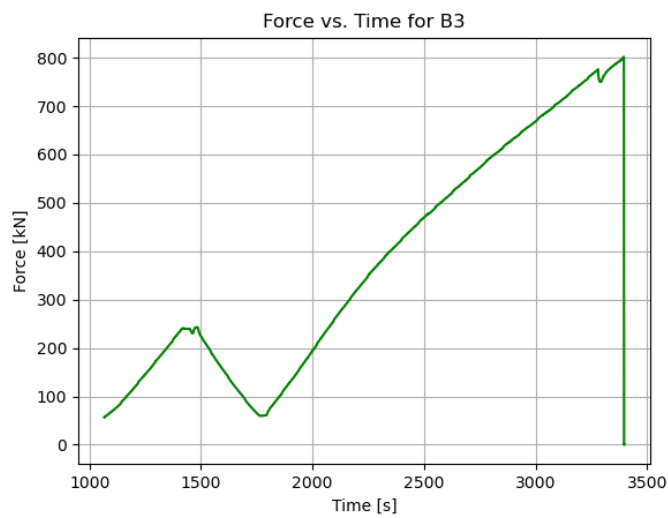
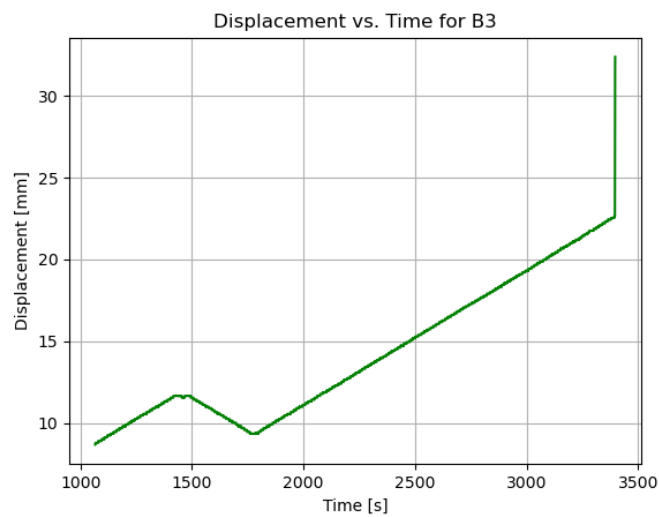
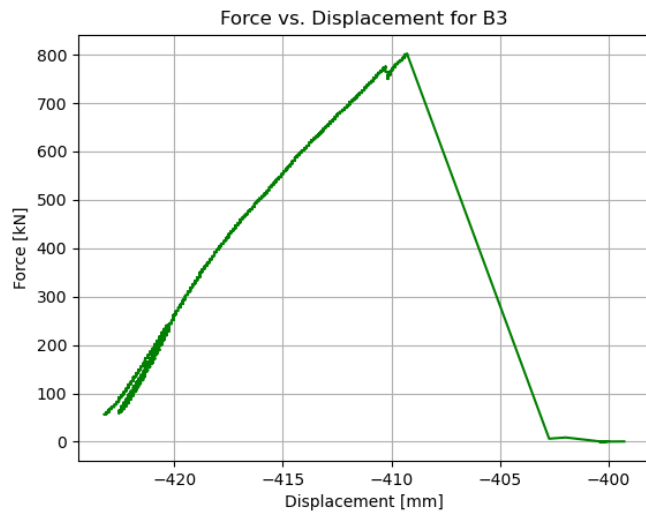








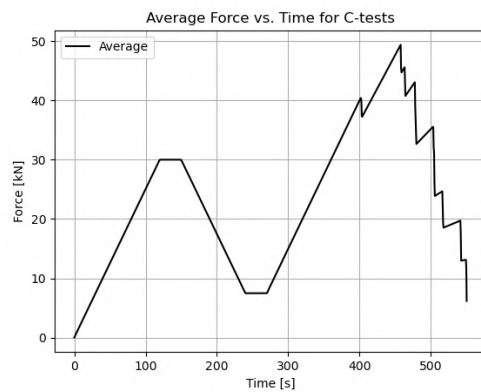
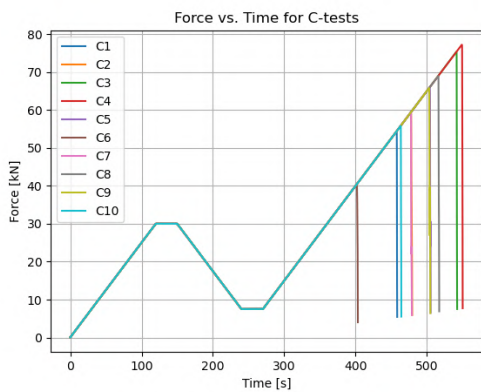
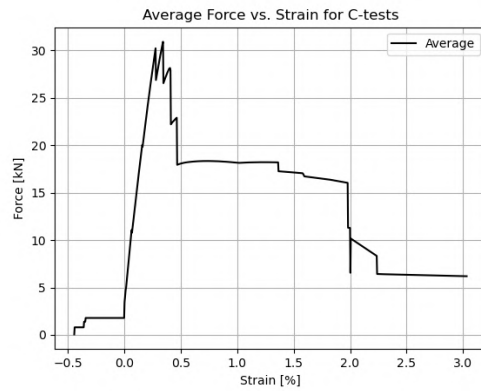
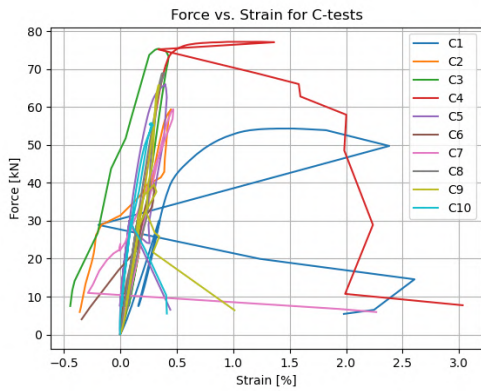
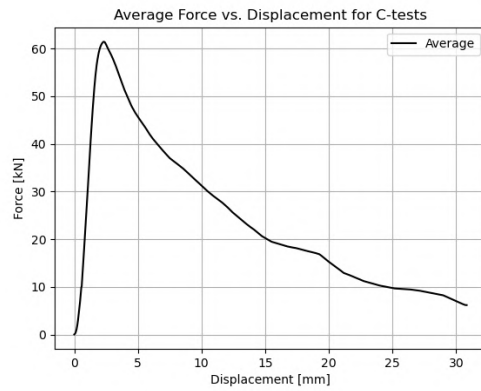
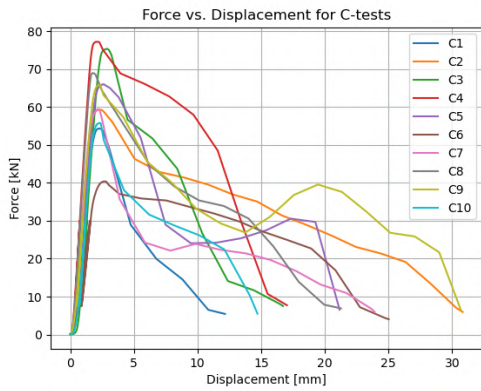
B.3 Specimen B3



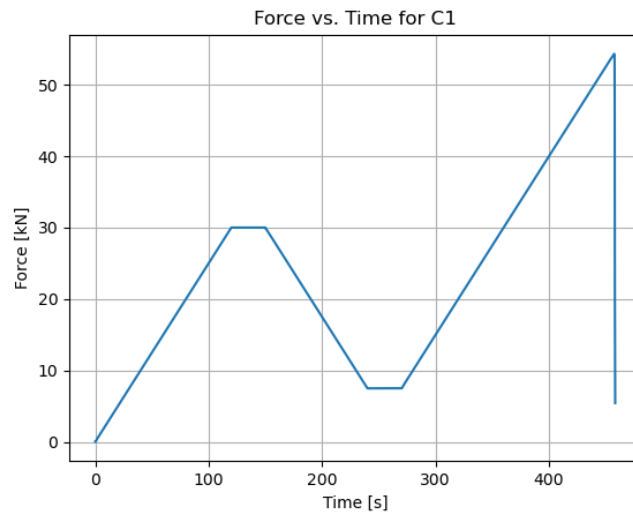
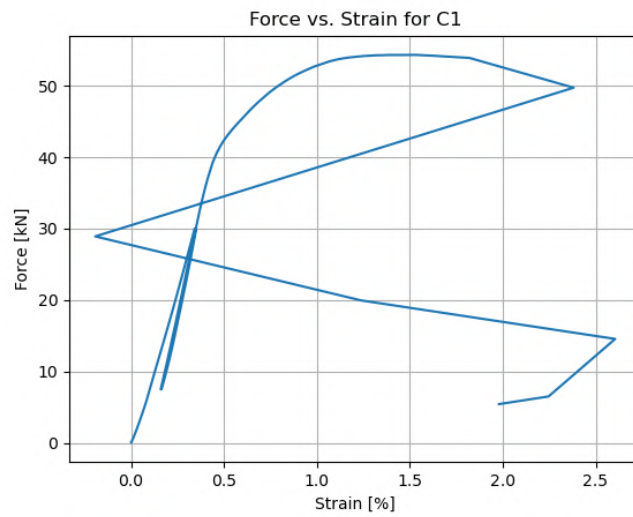
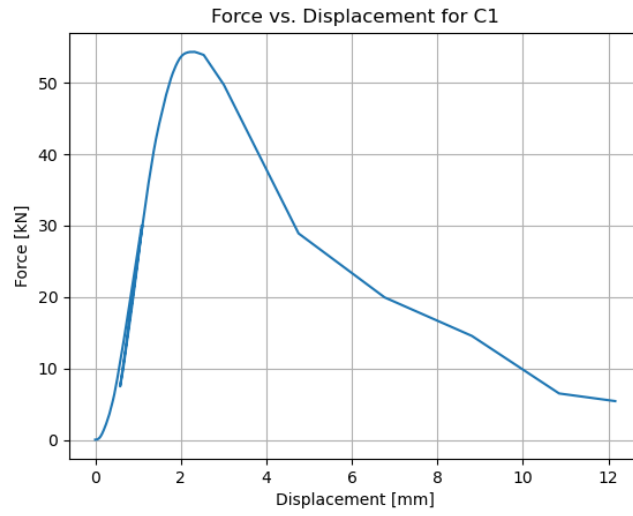
C Compression test

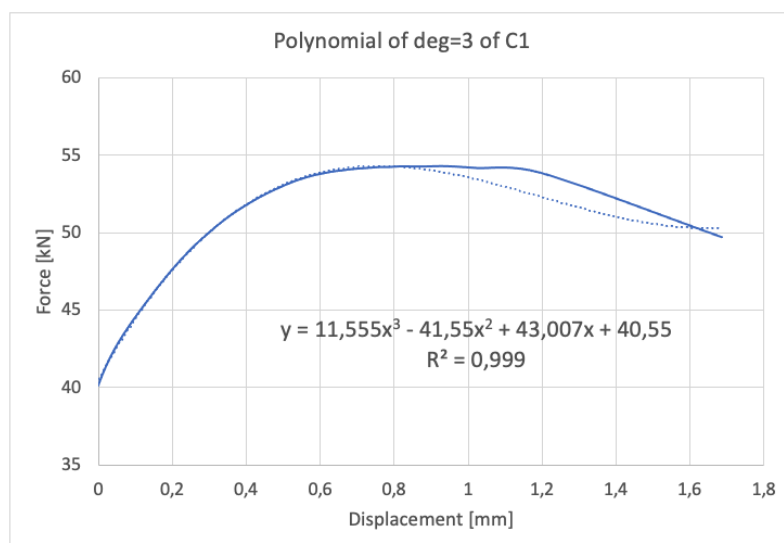
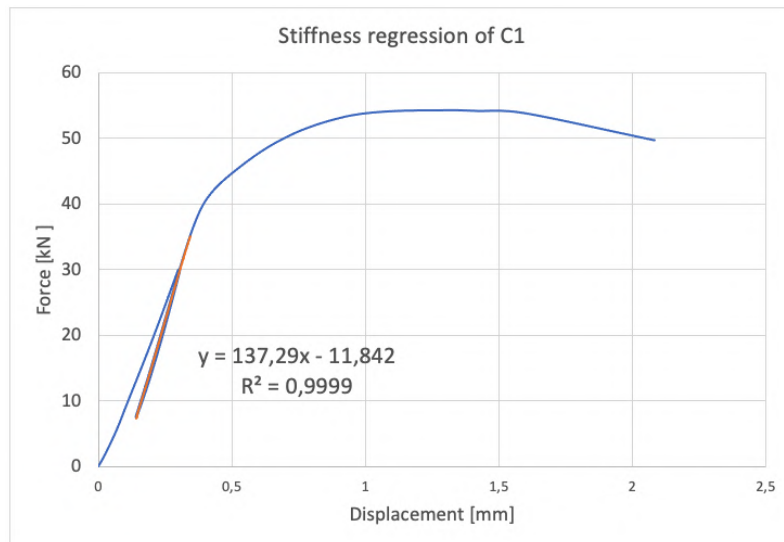
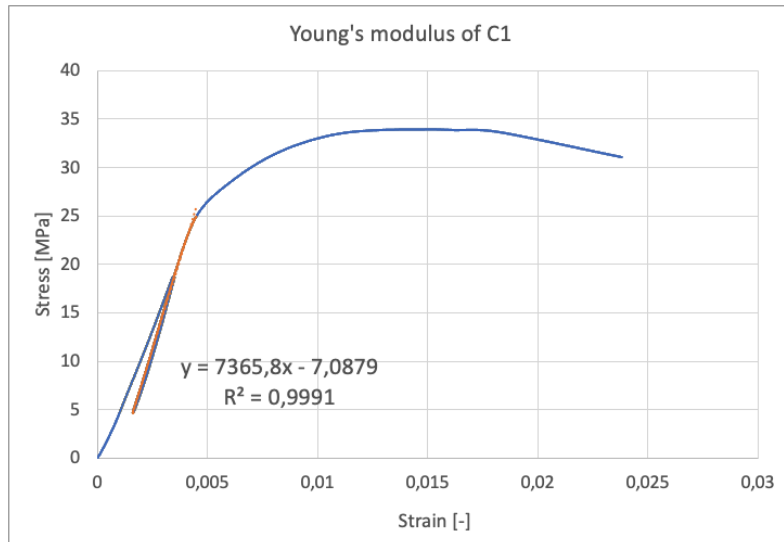
The following graphs are based on data acquired from the experimental compression tests. *C1-C10* are notations referring to the specimen numbering as explained in the report. The graphs includes data from strain, displacement, and force measurement from mounted sensors. The interval of time steps are defined by the machine. The codes from these graphs are included in Section F.10. Regression analysis are carried out in Excel.

All specimens from C-test

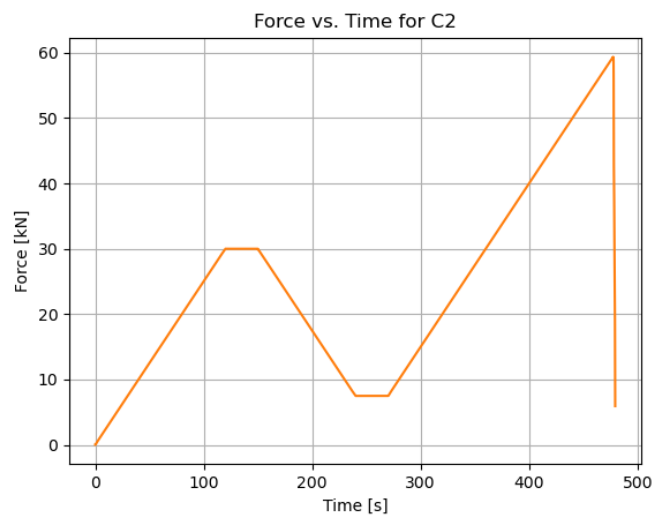
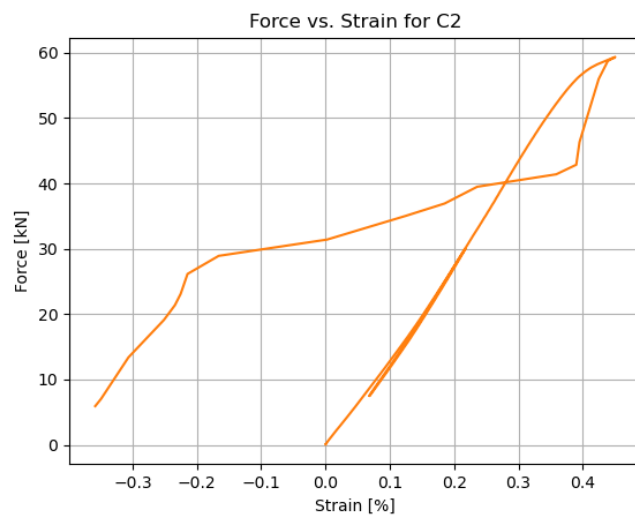
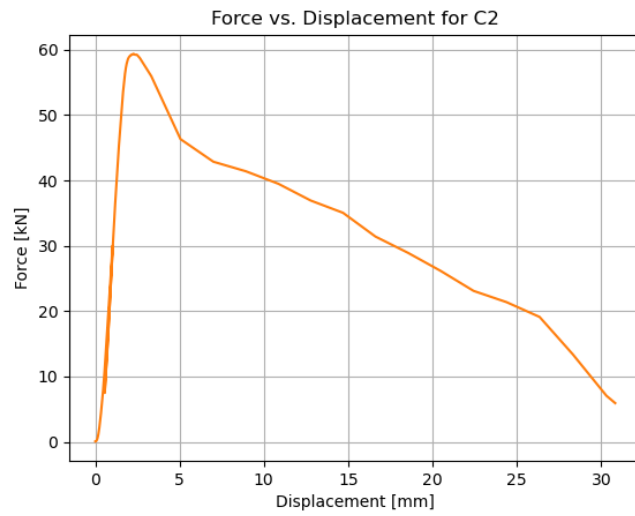


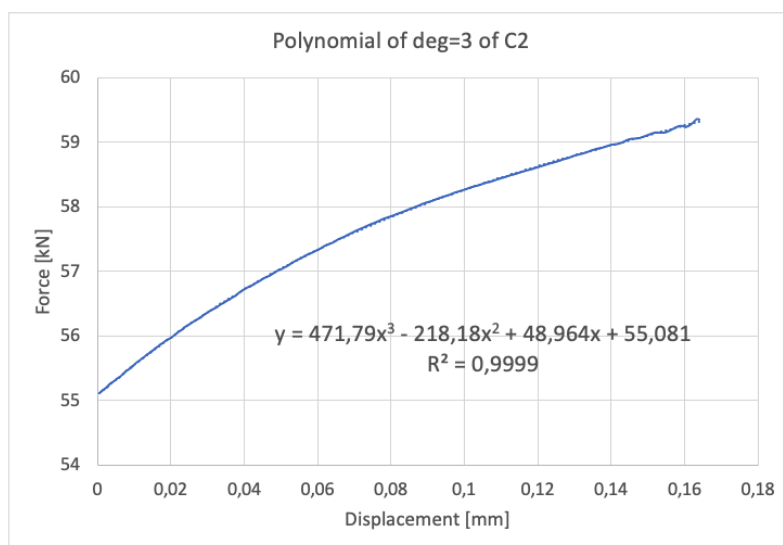
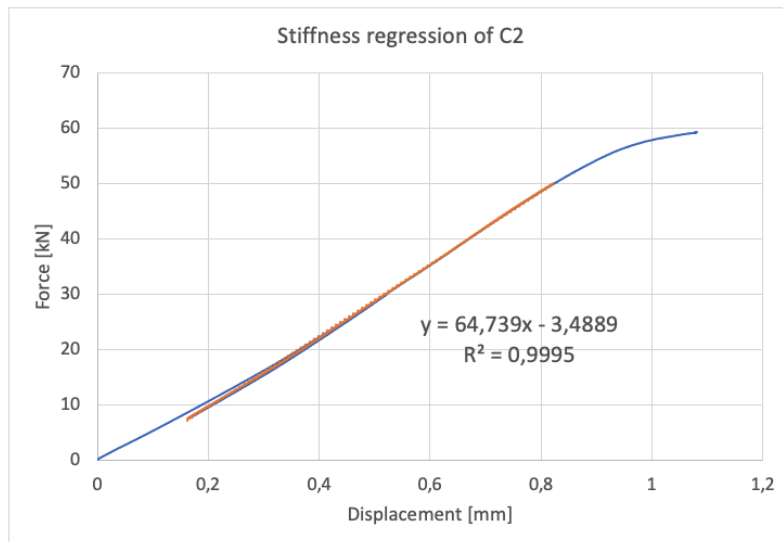
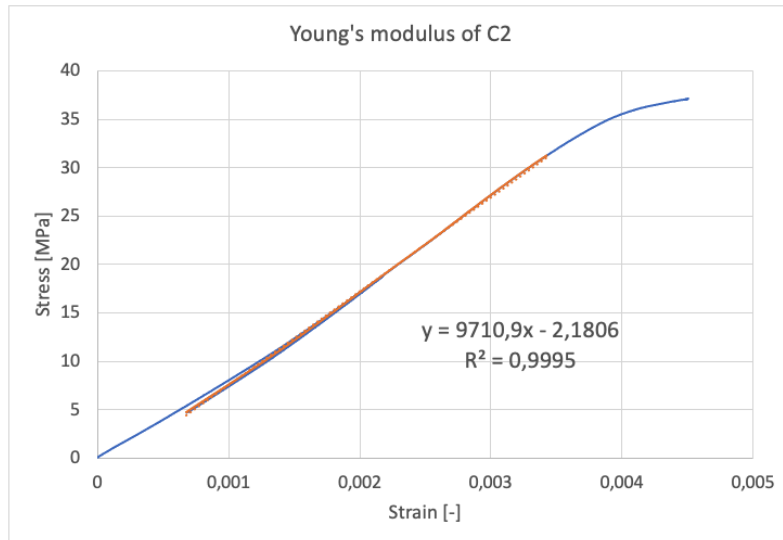
C.1 Specimen C1



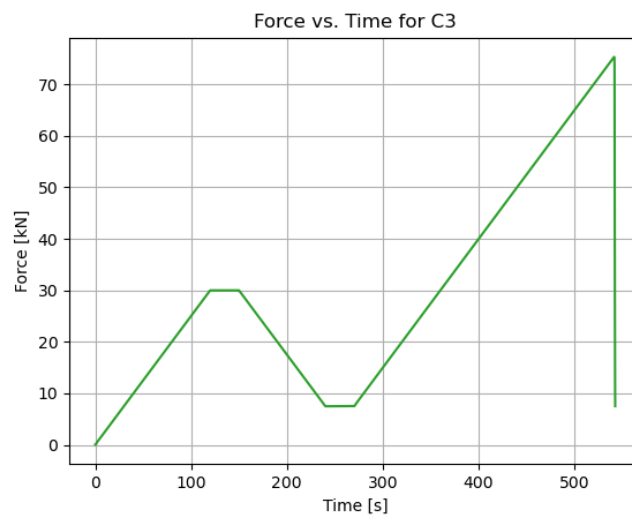
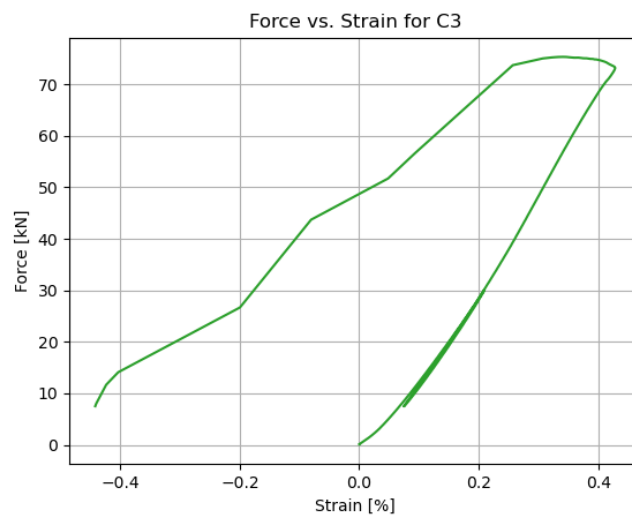
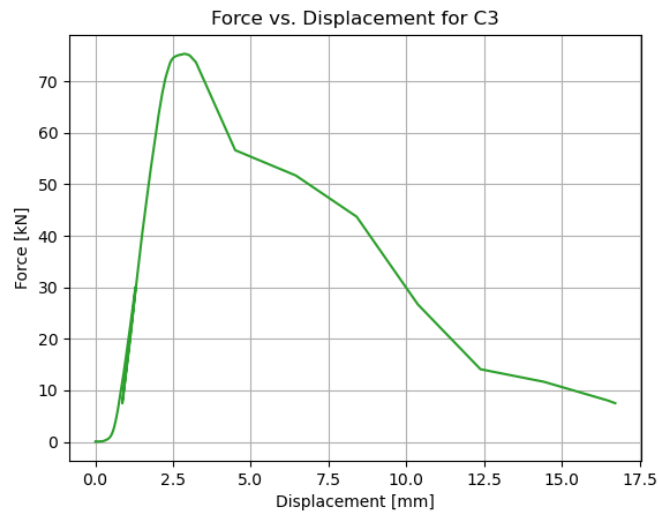


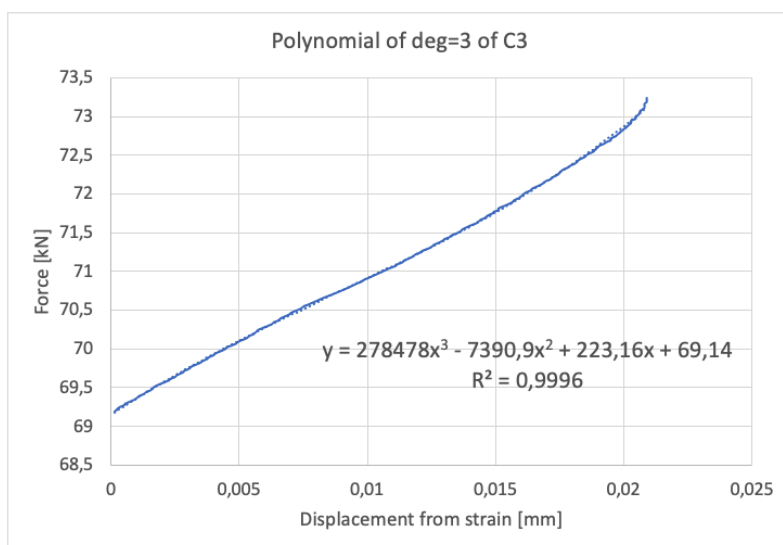
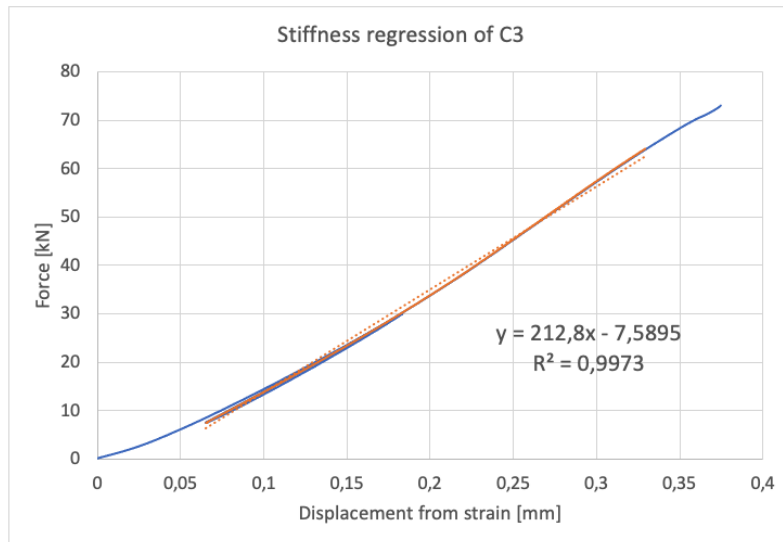
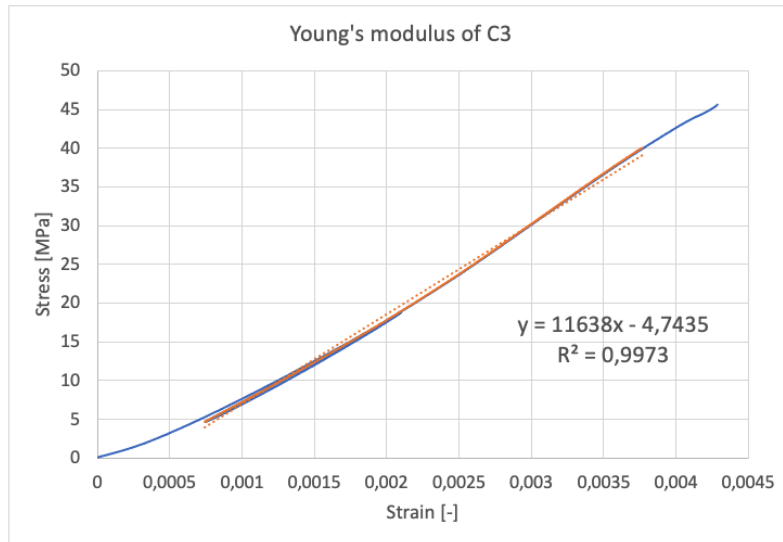
C.2 Specimen C2



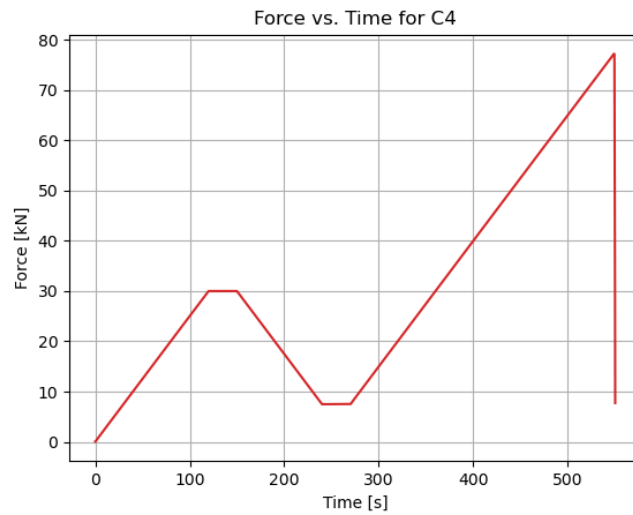
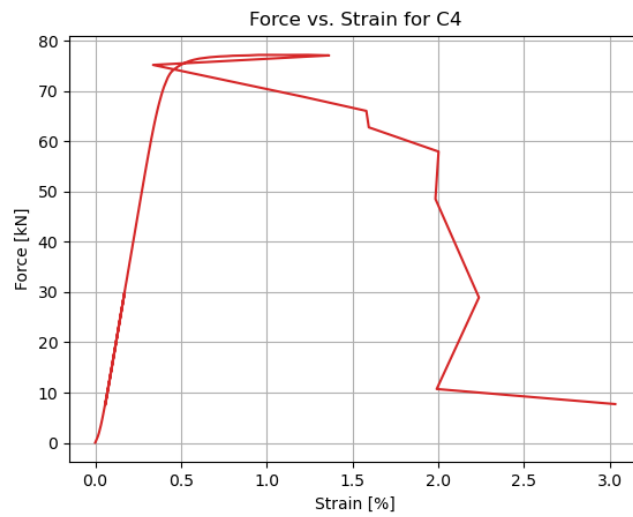
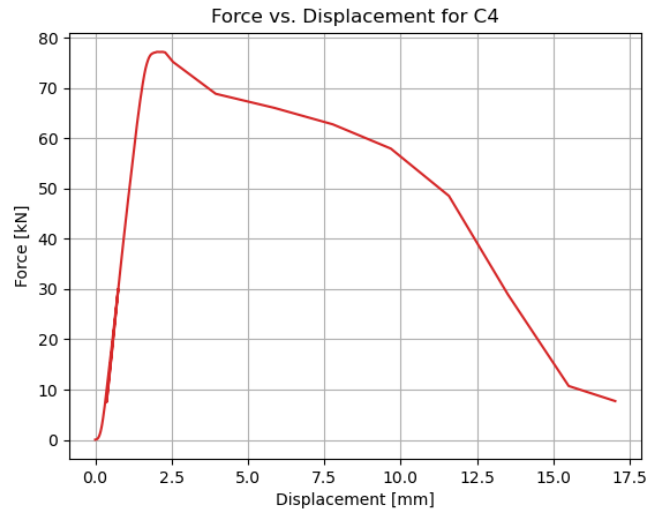


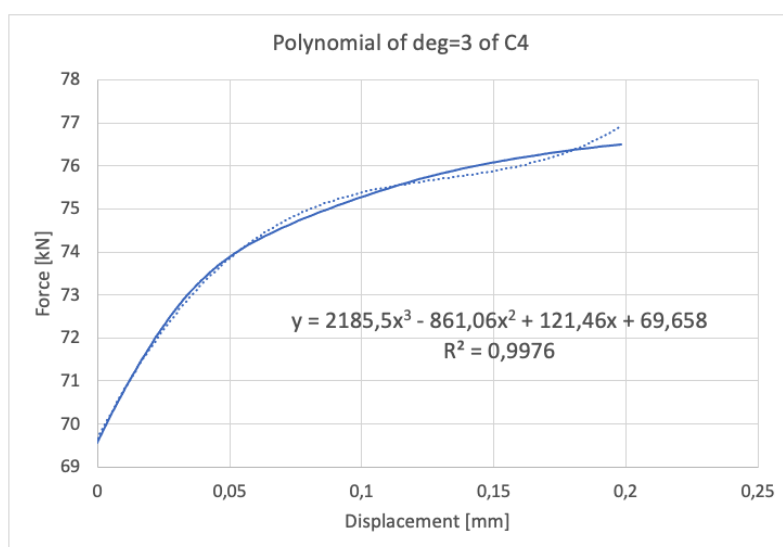
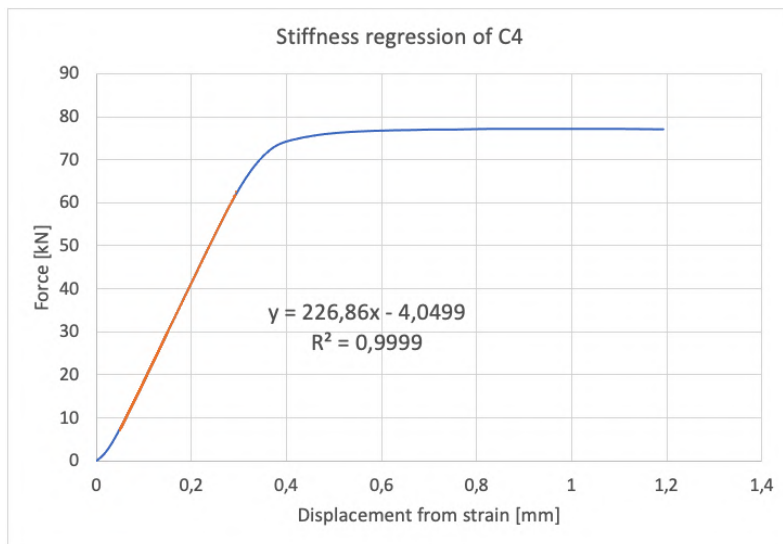
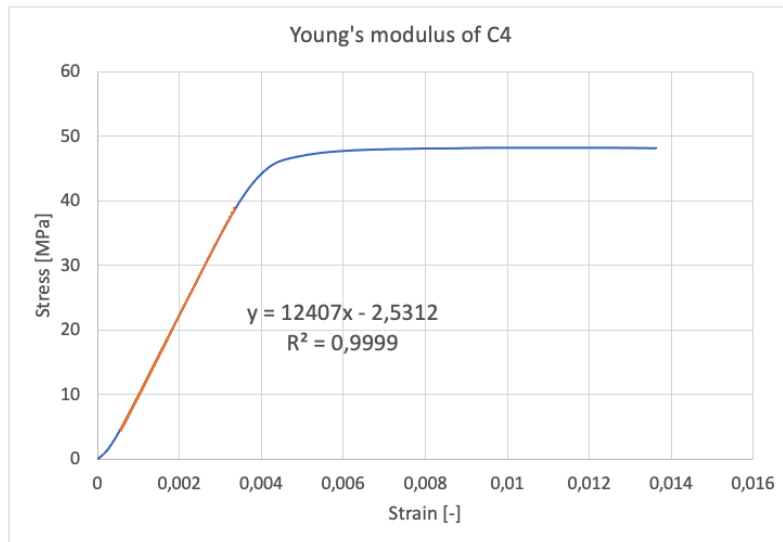
C.3 Specimen C3



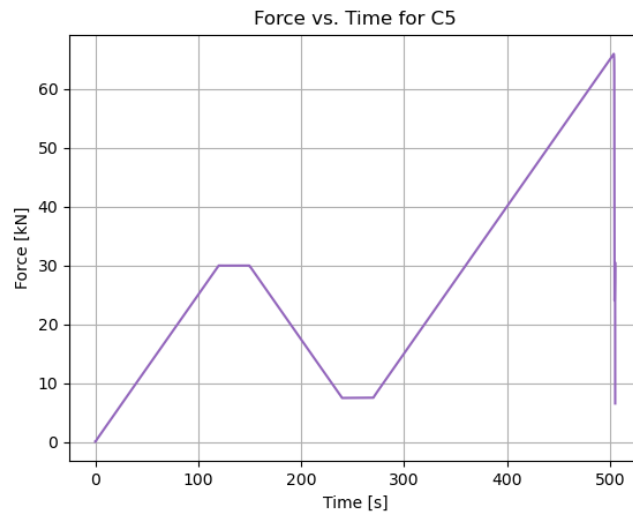
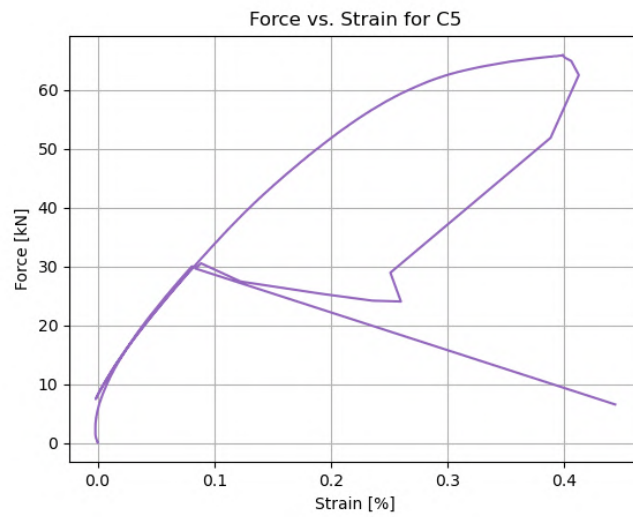
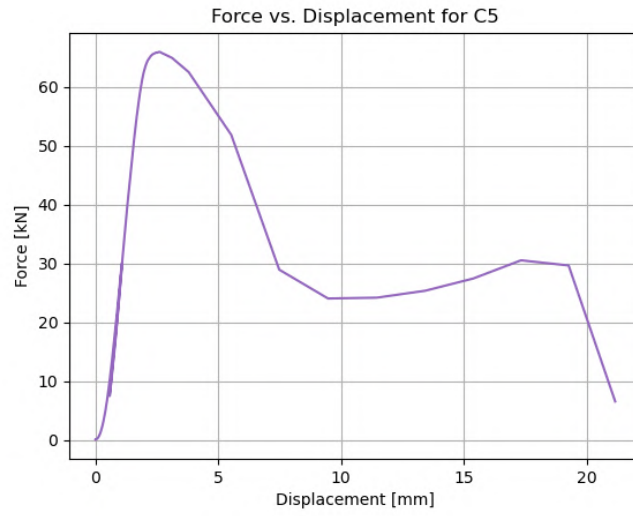


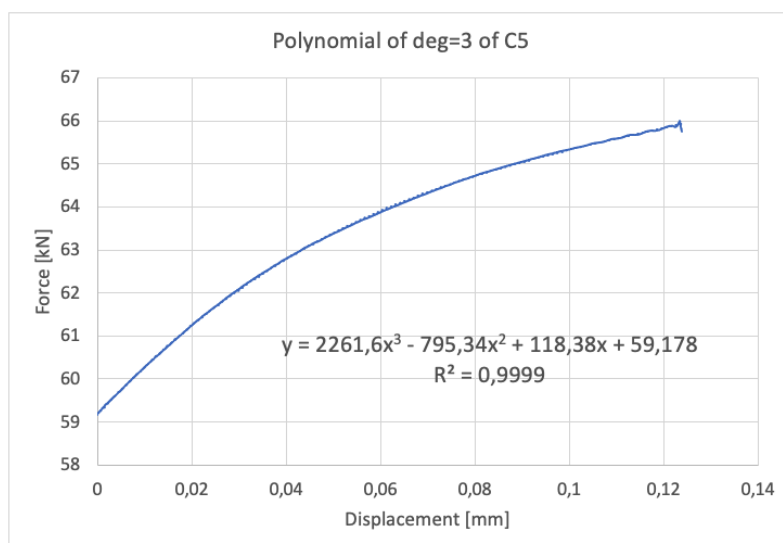
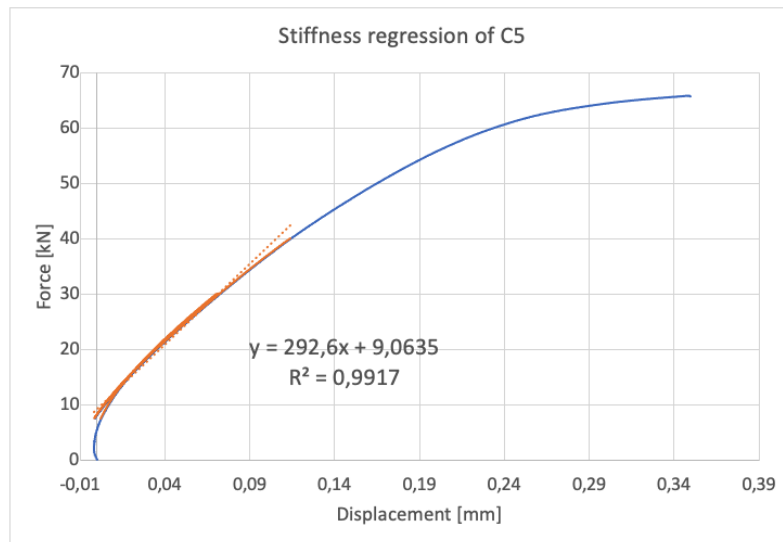
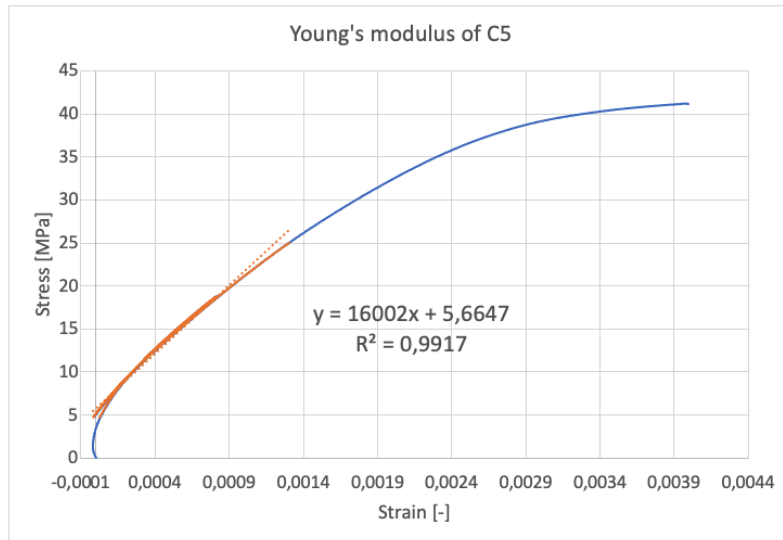
C.4 Specimen C4



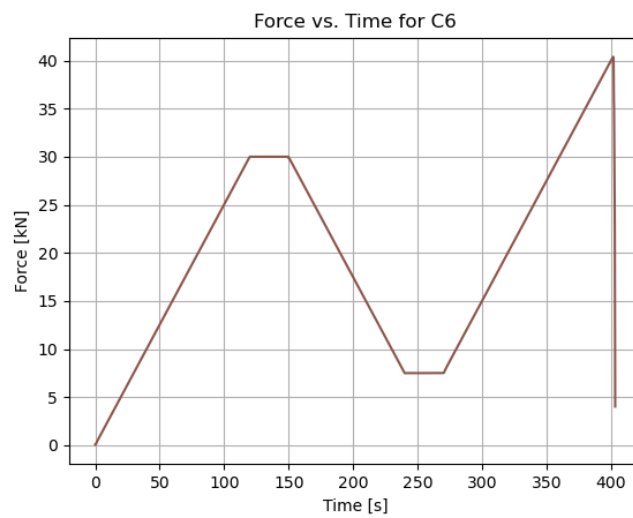
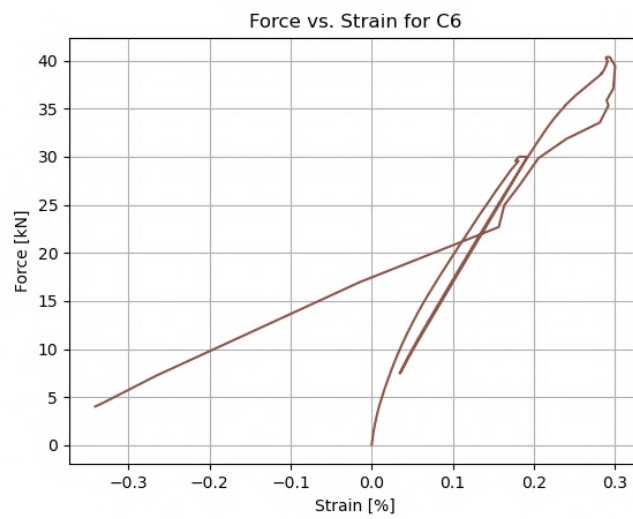
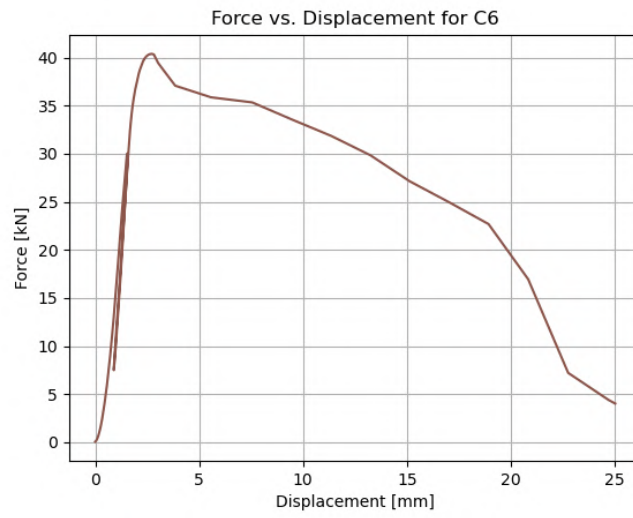


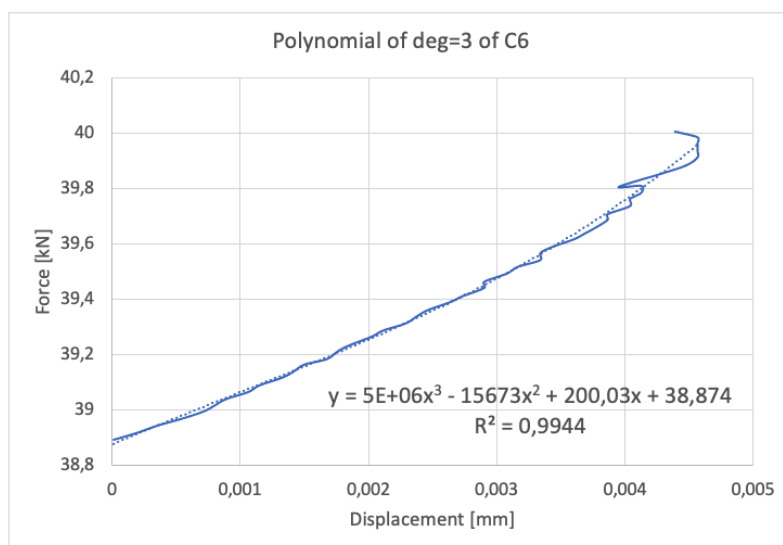
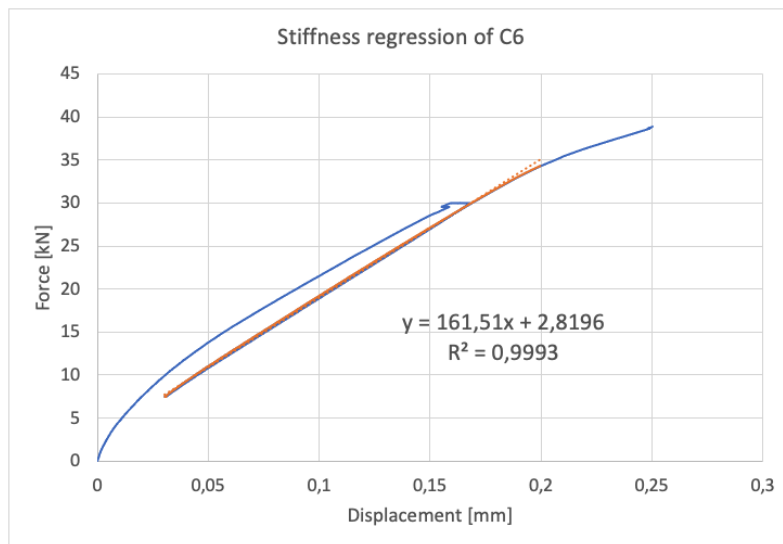
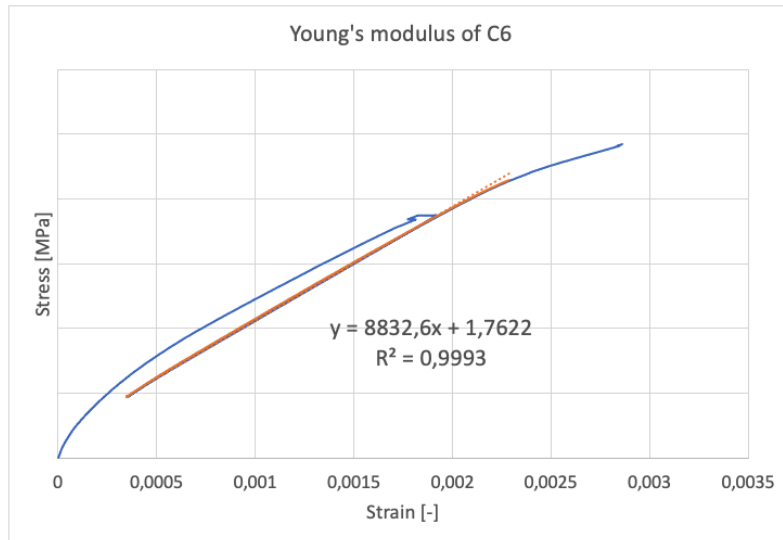
C.5 Specimen C5



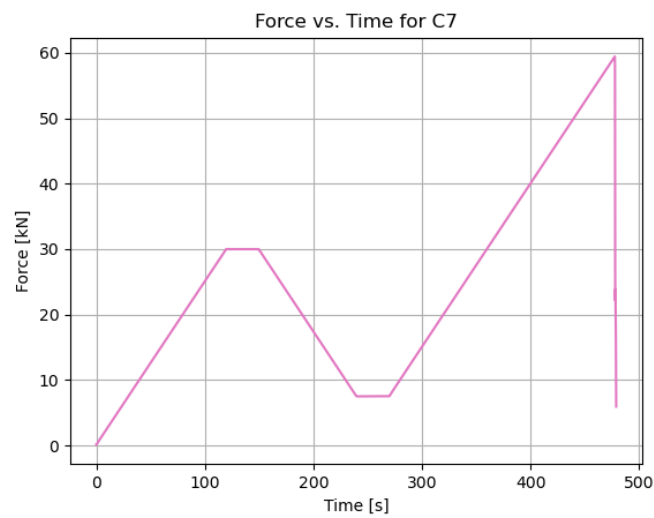
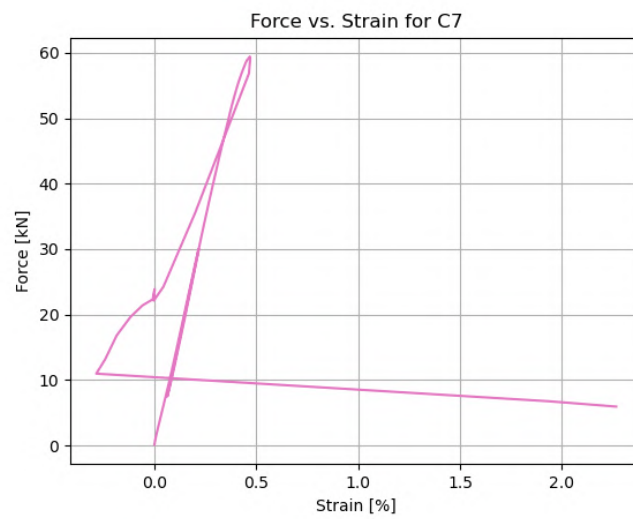
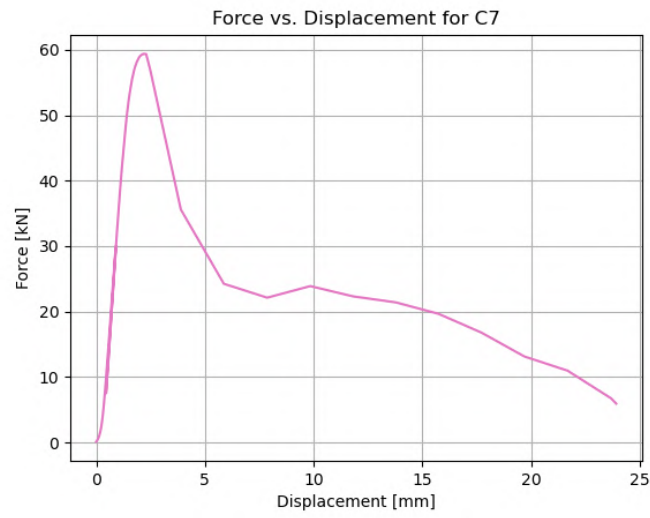


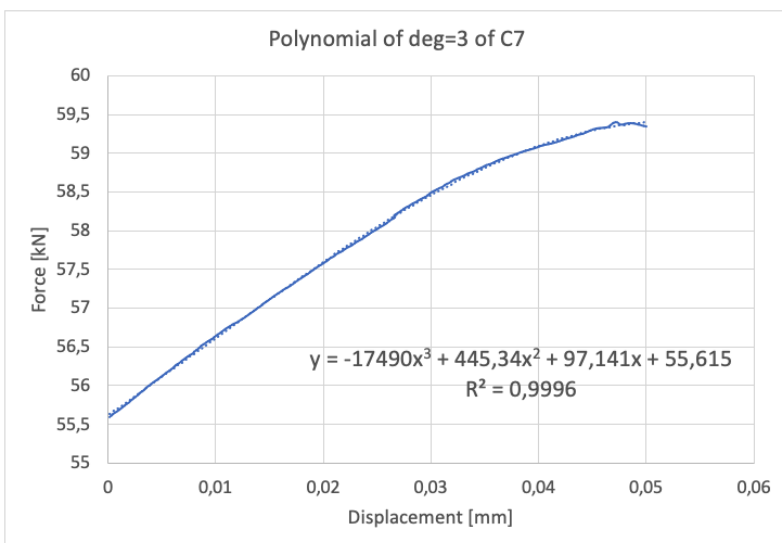
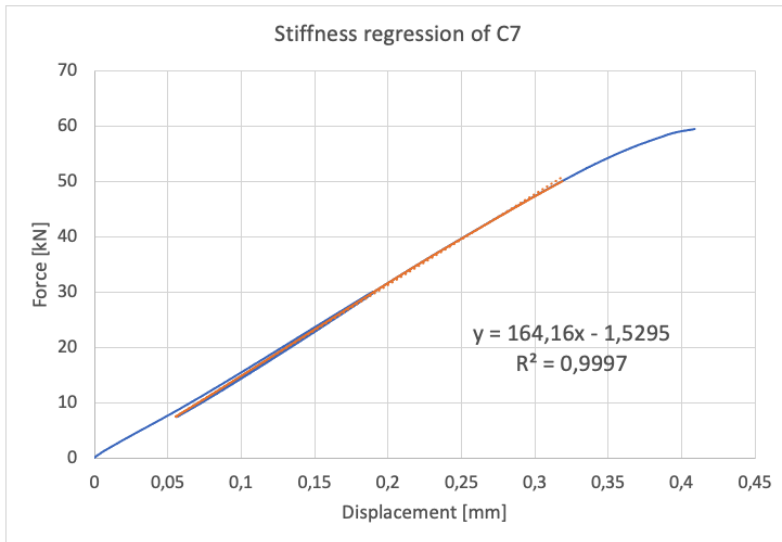
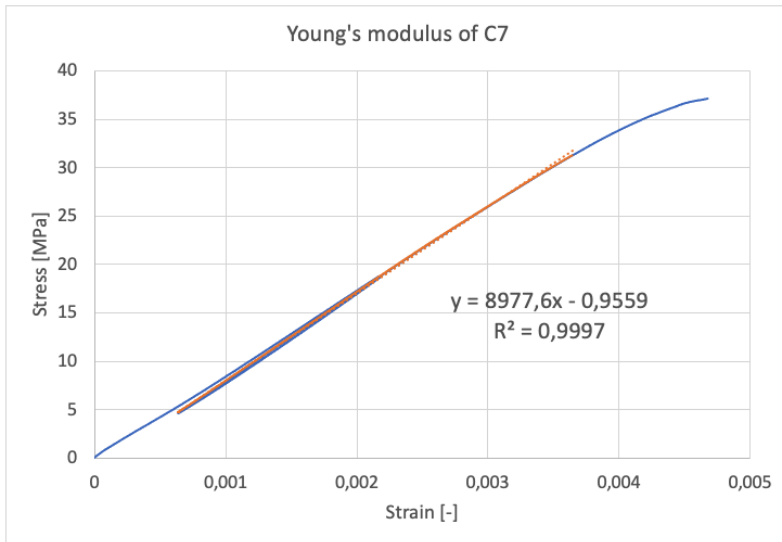
C.6 Specimen C6



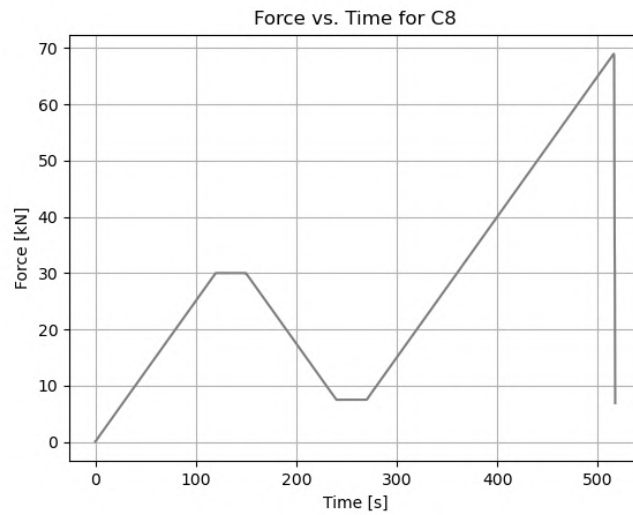
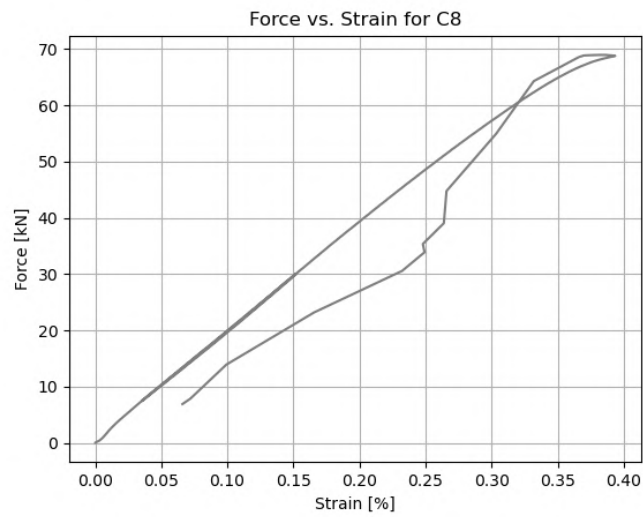
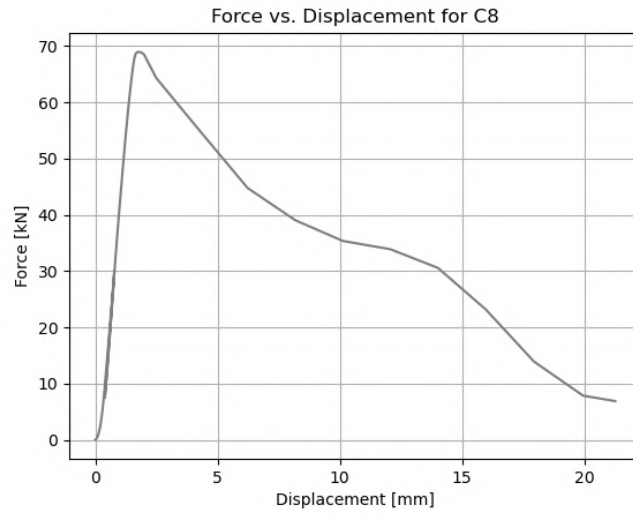


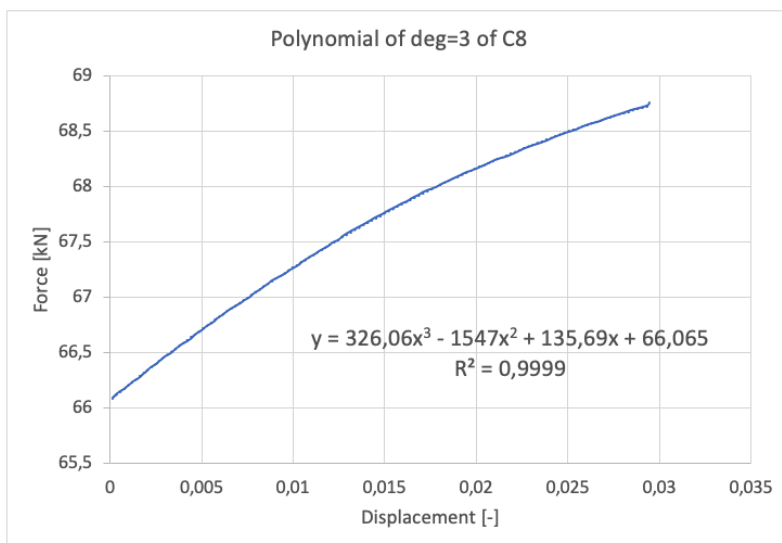
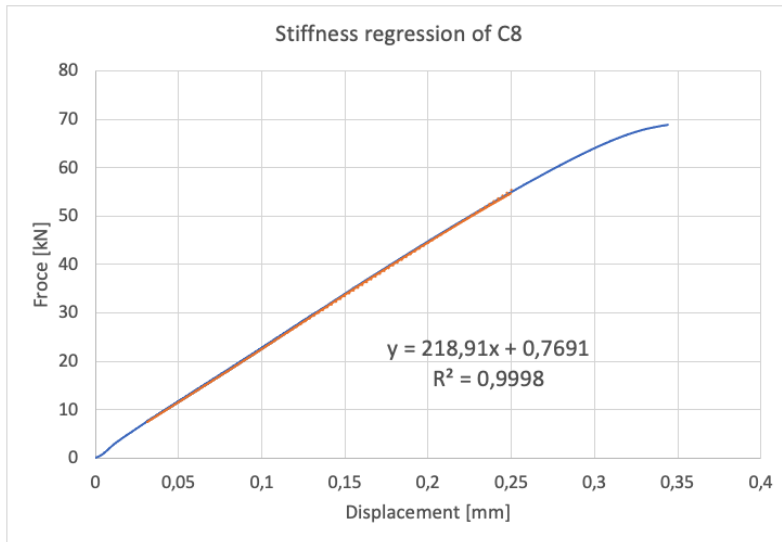
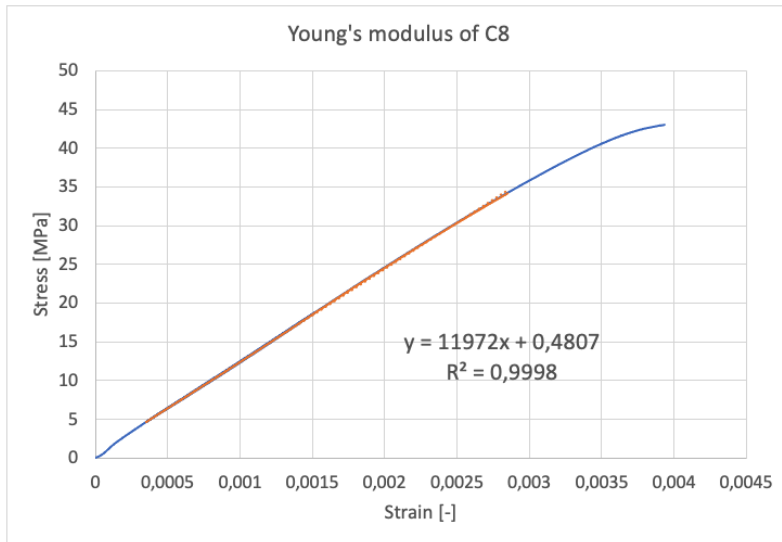
C.7 Specimen C7



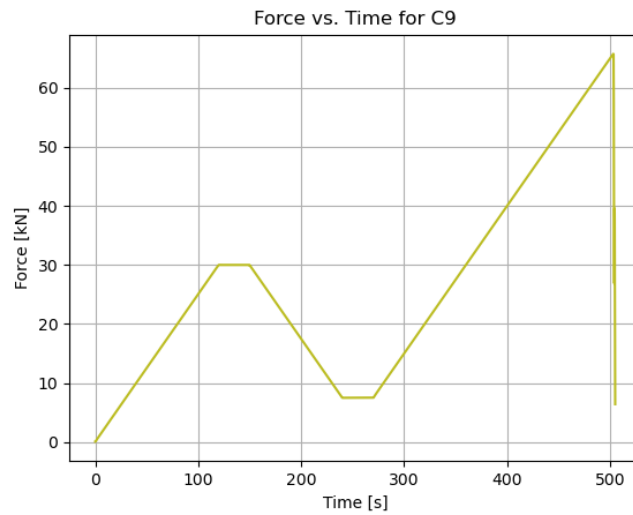
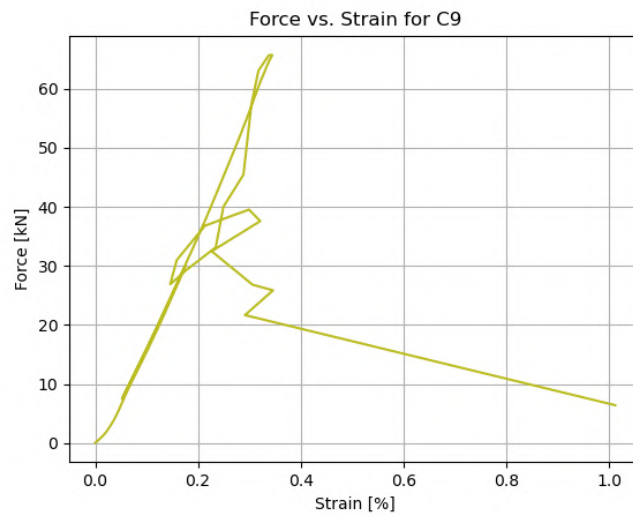
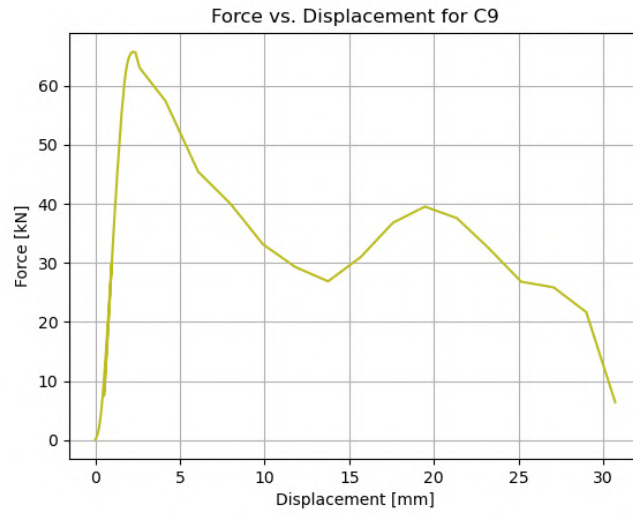


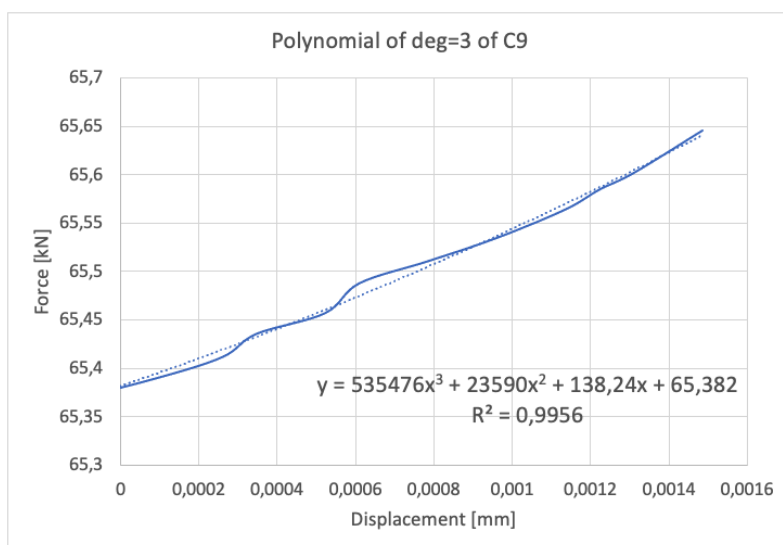
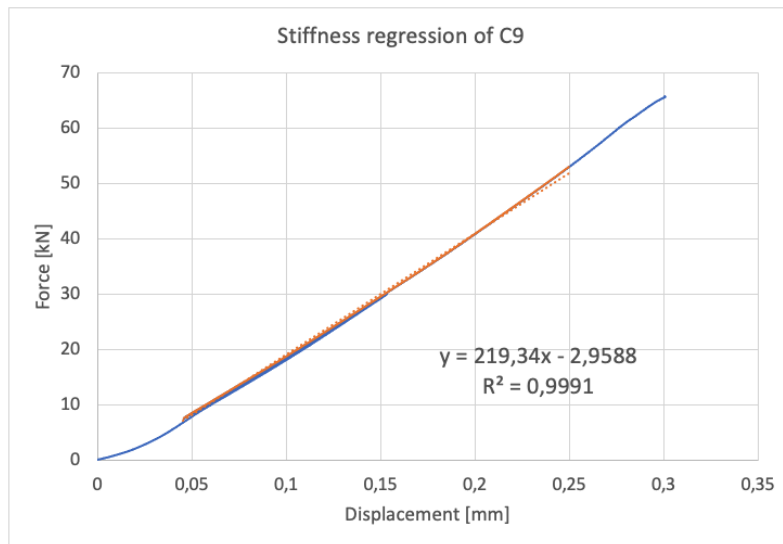
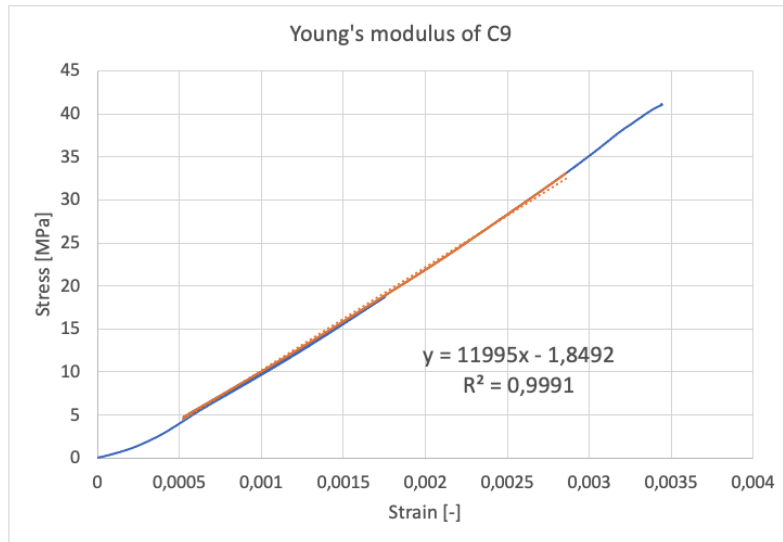
C.8 Specimen C8



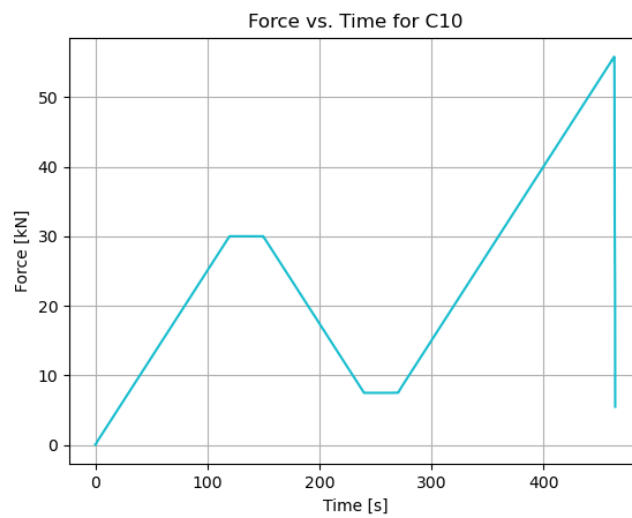
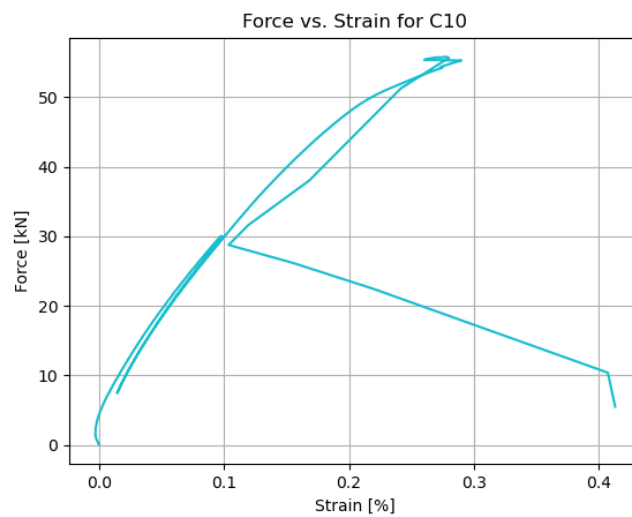
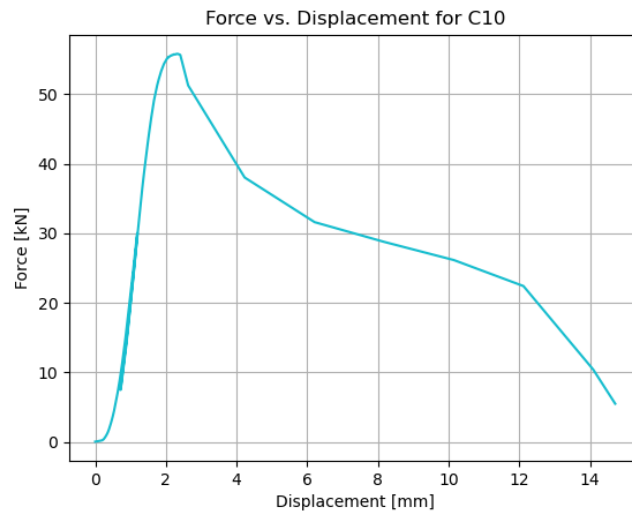


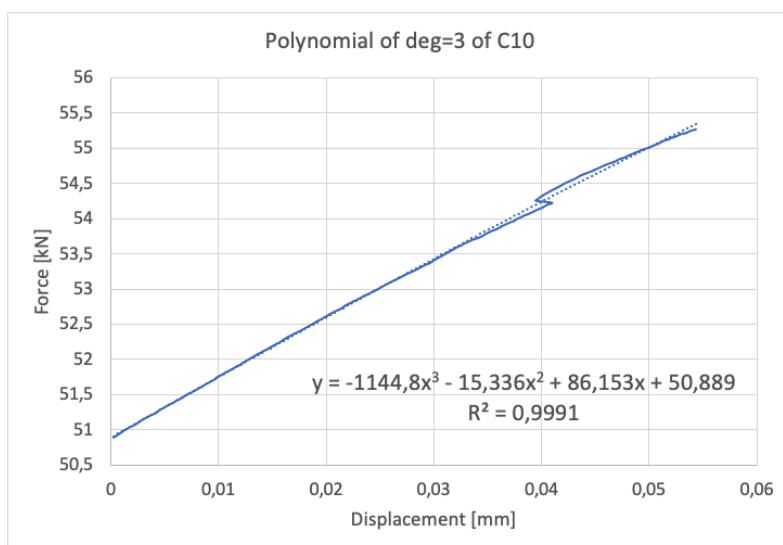
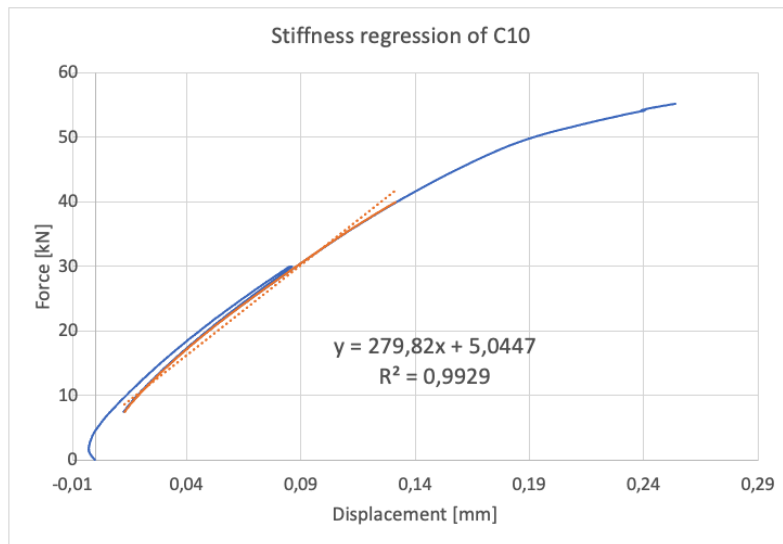
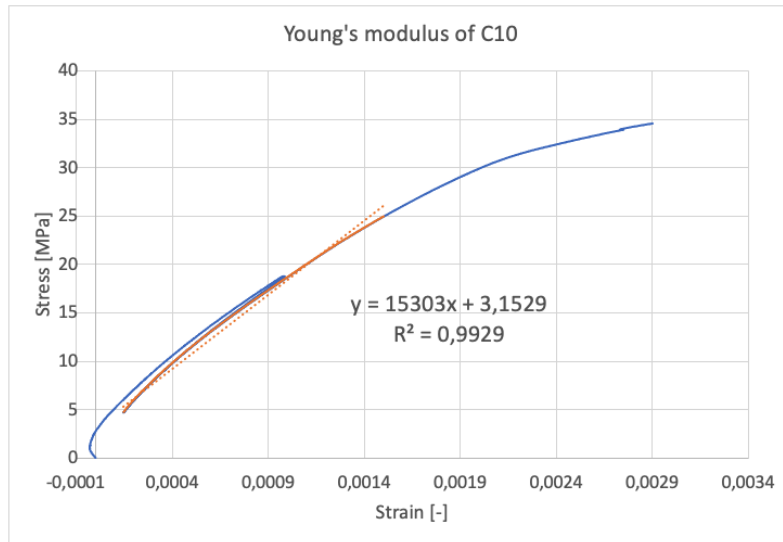
C.9 Specimen C9





C.10 Specimen C10

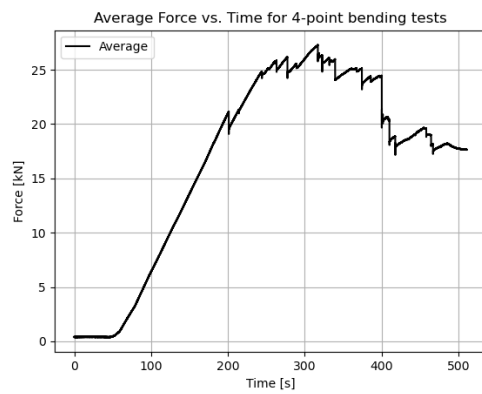
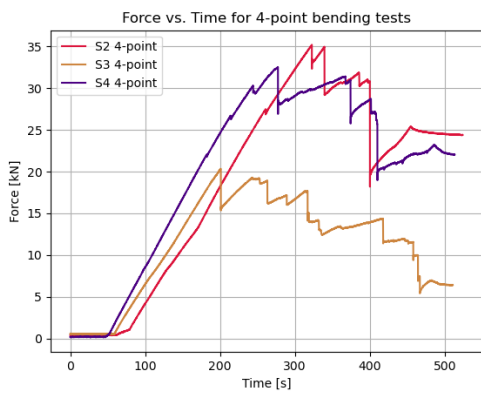
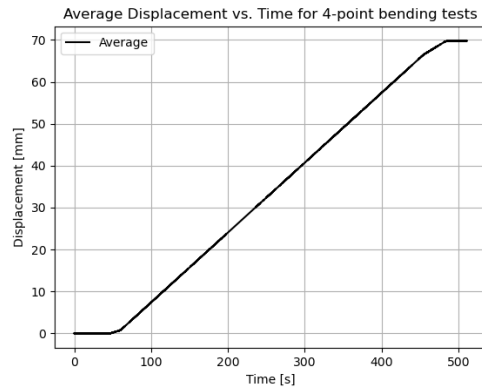
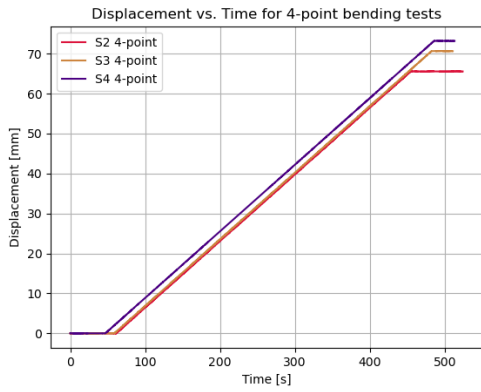
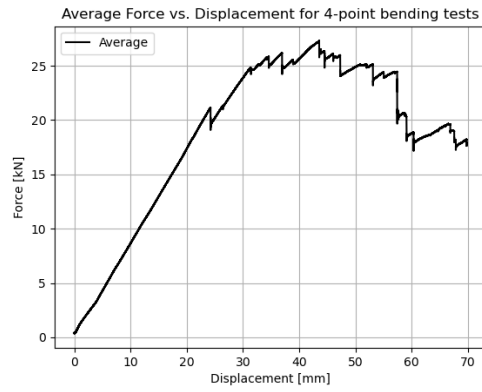
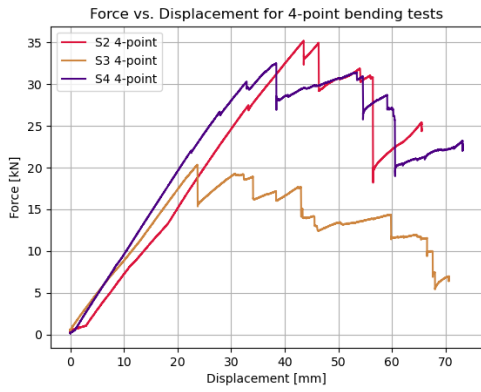




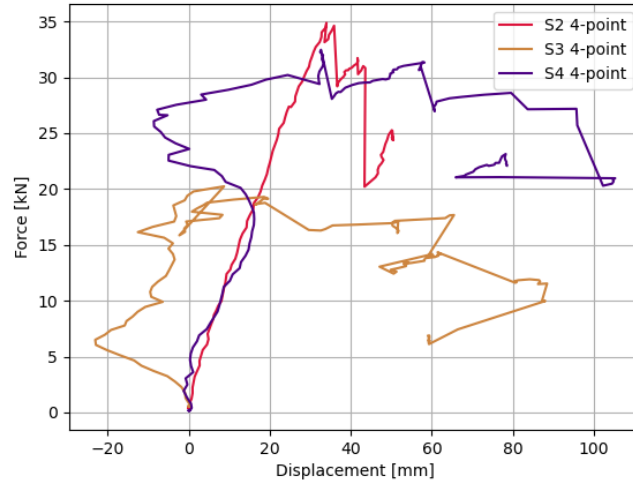
D 4-point bending test

The following graphs are based on data acquired from experimental four-point bending tests. *S2-S4* are notations referring to the specimen numbering as explained in the report. The graphs includes data from force, time and displacement obtained by the load cell and three individual lasers. The interval of time steps are defined by the machine. The codes from these graphs are included in Section F.11. Regression analysis are carried out in Excel.

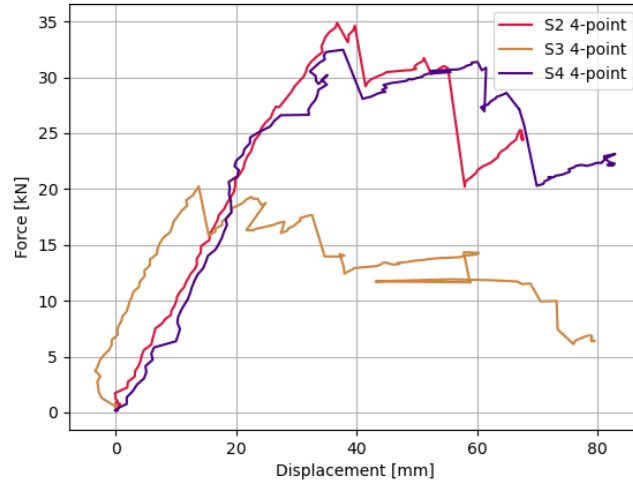
All specimens from 4-point bending test



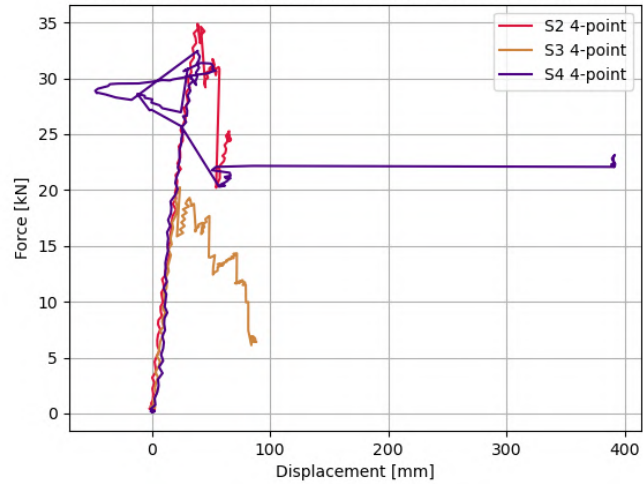
Force vs. Laser 1 Displacement for 4-point bending tests



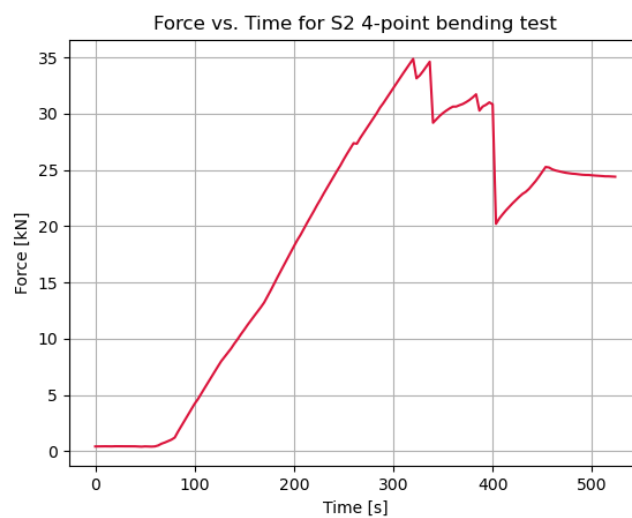
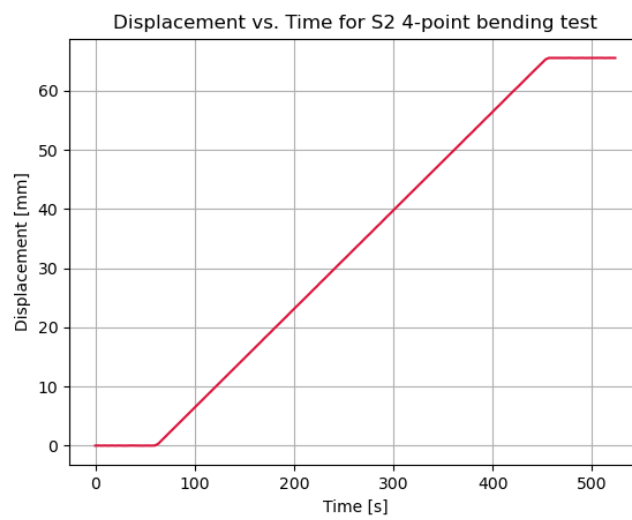
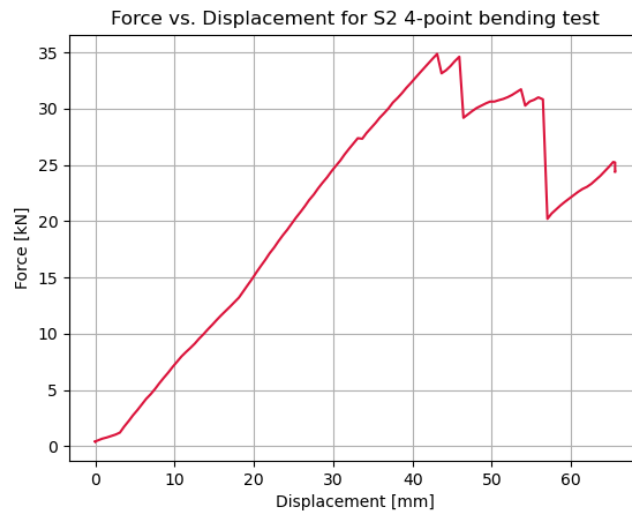
Force vs. Laser 2 Displacement for 4-point bending tests

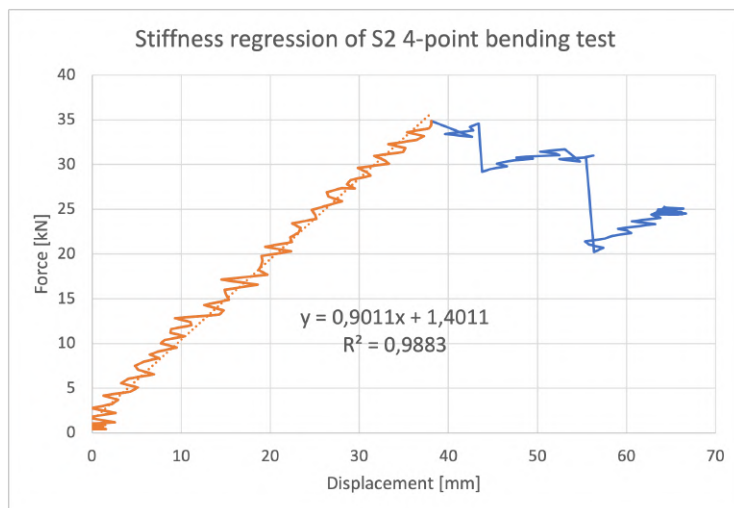
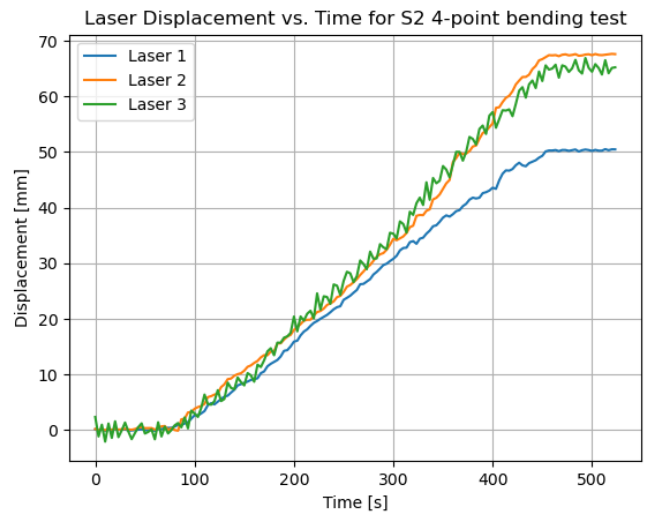
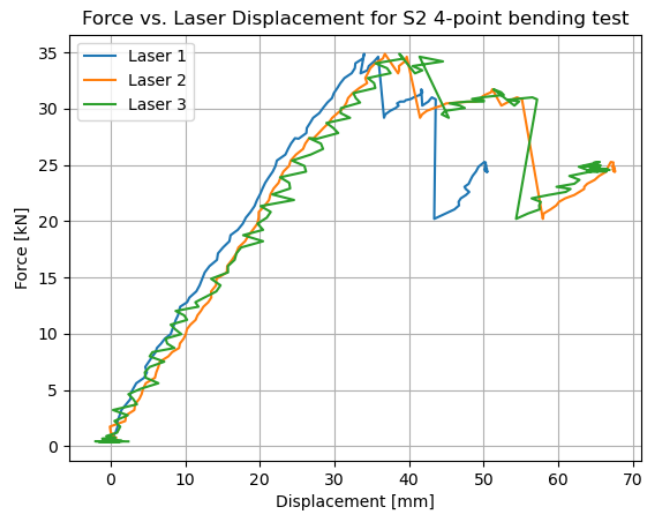


Force vs. Laser 3 Displacement for 4-point bending tests

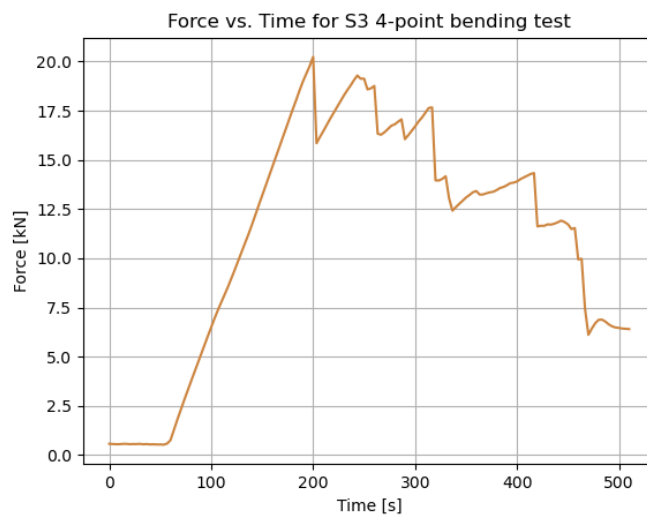
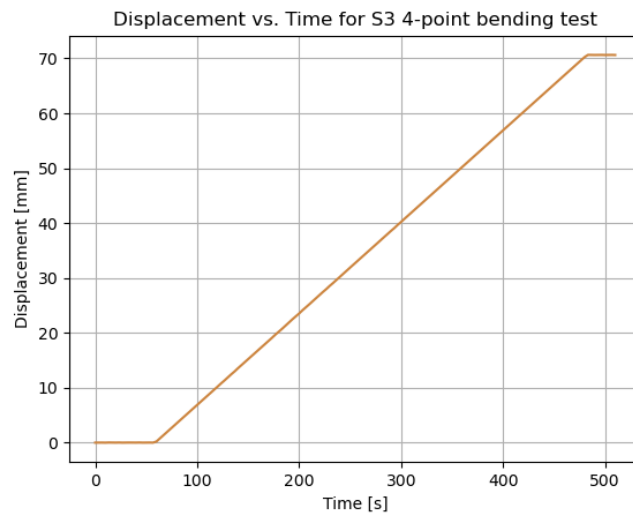
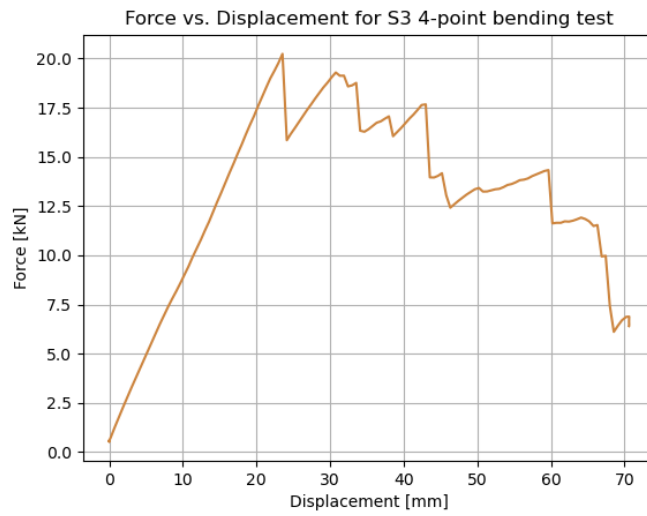


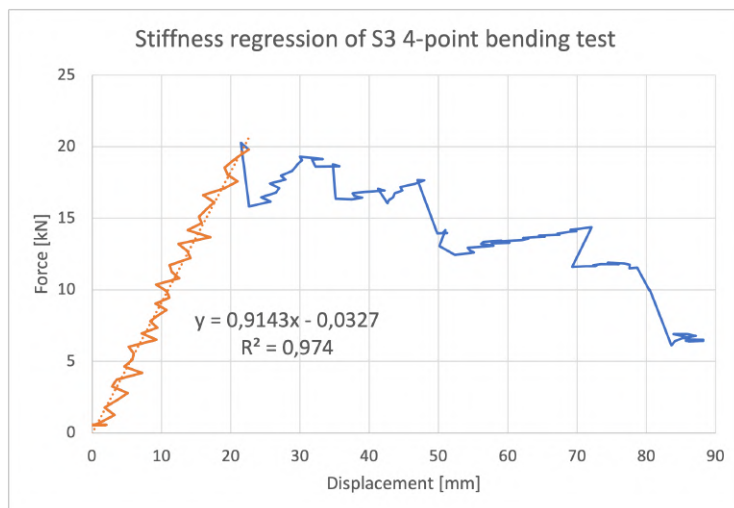
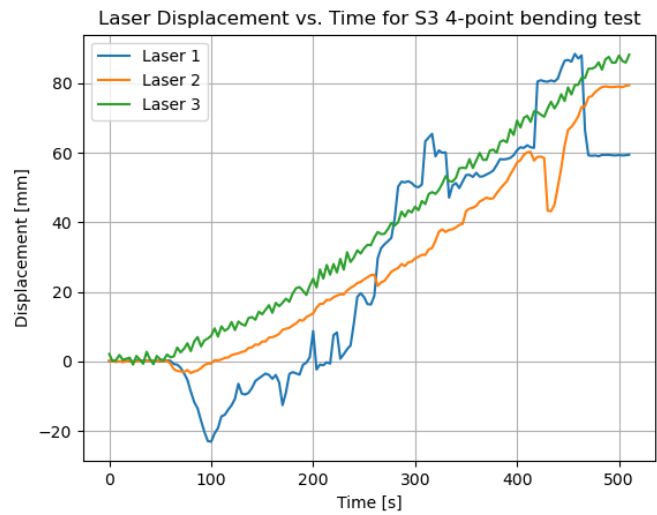
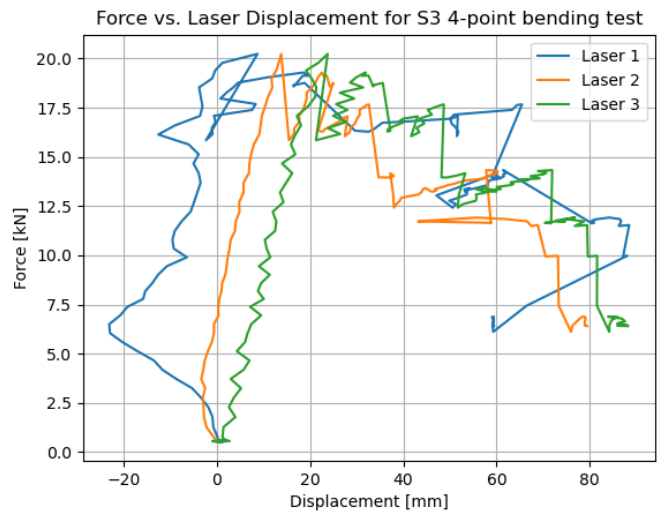
D.1 Specimen S2



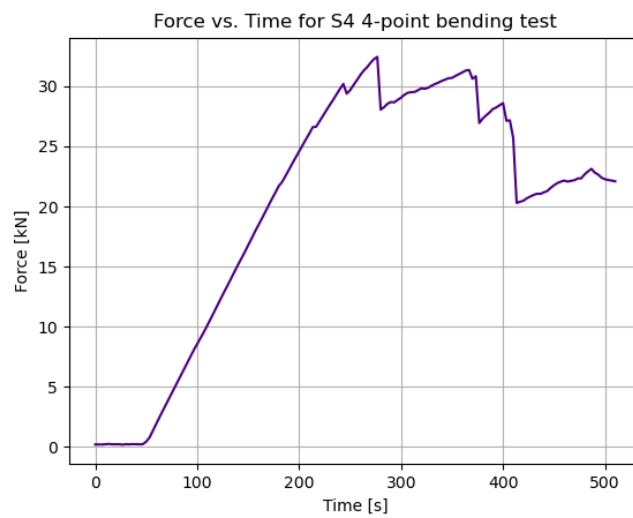
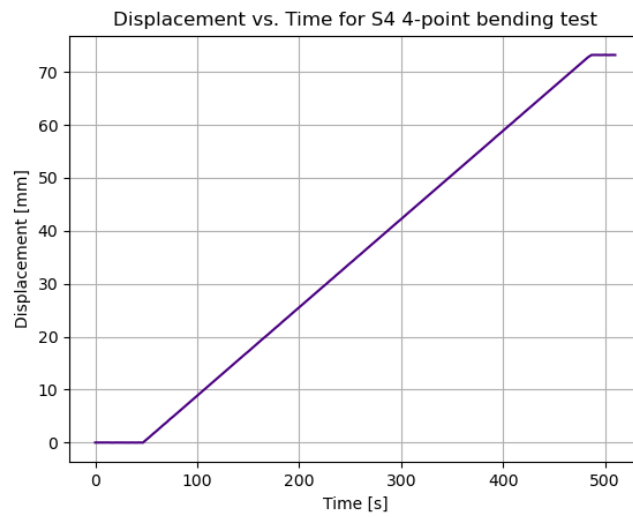
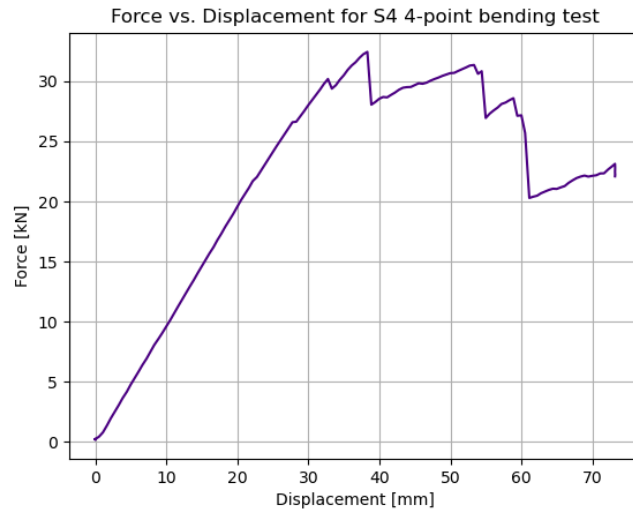


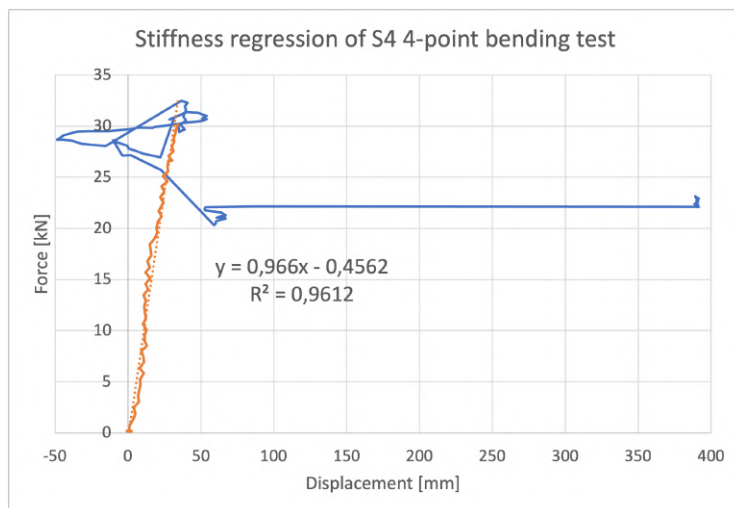
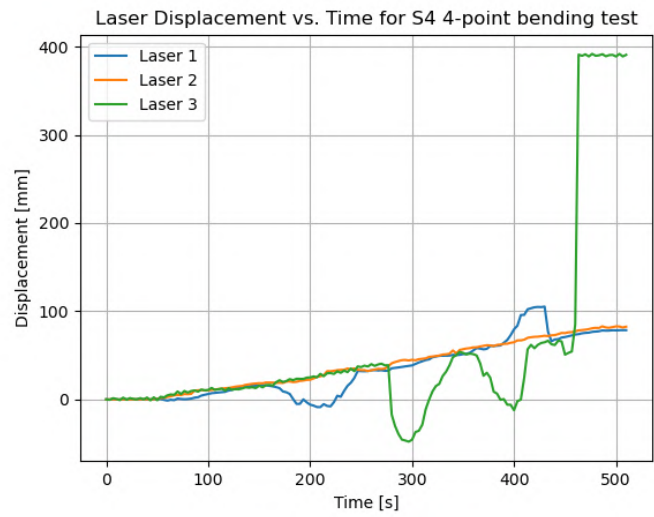
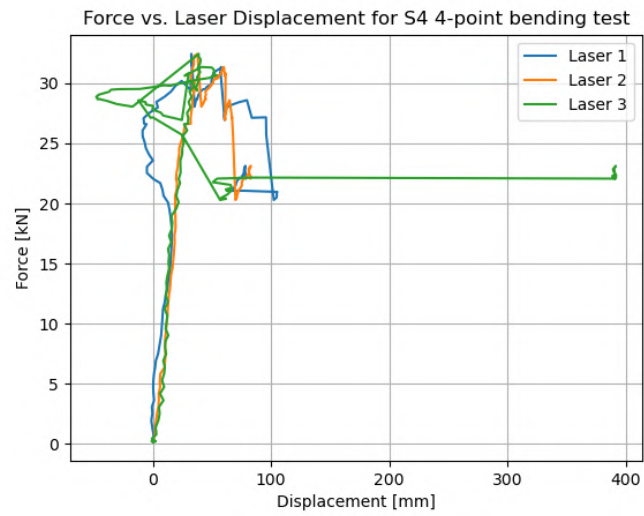
D.2 Specimen S3





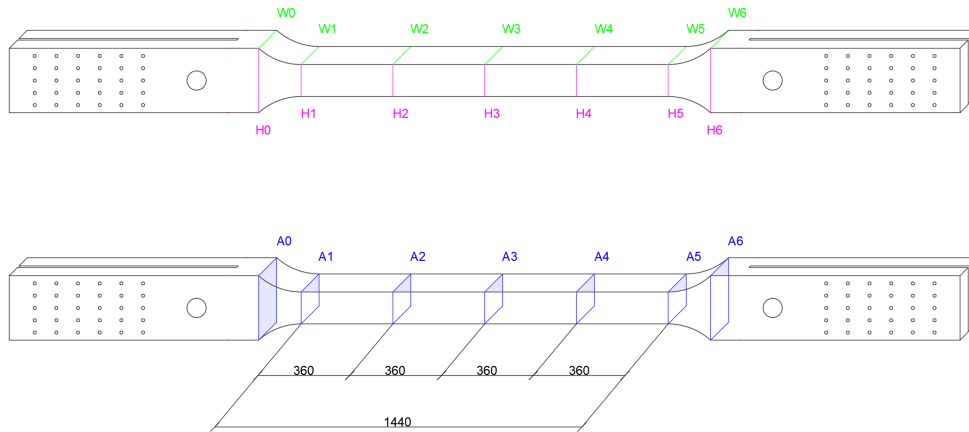
D.3 Specimen S4





E cross-section areas of specimens for S-tests

The following tables and figure includes cross-section dimensions from the tensile test specimens measured by calipers, and the location of respective measurement. Parameter i in the tables refers to the area numbering on the figure.



i	h_i [mm]	w_i [mm]	A_i [mm ²]
0	250.30	129.74	32473.92
1	125.65	129.94	16326.96
2	125.76	130.10	16361.34
3	125.74	130.19	16370.10
4	125.78	130.10	16363.98
5	125.95	130.06	16381.06
6	249.20	129.70	32321.24

cross-section parameters of element specimen S1

i	h_i [mm]	w_i [mm]	A_i [mm ²]
0	253.36	130.67	33106.55
1	125.75	130.21	16373.91
2	126.07	130.08	16399.19
3	126.15	130.11	16413.38
4	126.17	129.91	16390.74
5	126.24	130.44	16466.75
6	251.97	130.70	32932.48

cross-section parameters of element specimen S2

i	h_i [mm]	w_i [mm]	A_i [mm ²]
0	251.67	128.88	32435.23
1	125.83	129.35	16216.15
2	125.58	129.13	16216.15
3	125.45	129.25	16214.41
4	125.44	129.44	16236.95
5	125.52	129.59	16266.14
6	253.25	129.63	32828.80

cross-section parameters of element specimen S3

i	h_i [mm]	w_i [mm]	A_i [mm ²]
0	251.02	129.56	32522.15
1	125.72	129.68	16303.37
2	125.94	129.56	16316.79
3	125.67	129.69	16298.14
4	125.81	130.06	16237.04
5	125.15	130.68	16229.45
6	251.20	130.86	32872.03

cross-section parameters of element specimen S4

F *Python codes*

The following *Python* codes are used for representing results from excel-files acquired by experiments and fatigue related calculations. For the sake of clarity, all of the files are included in an individual manner. Note that all the data from the experiments have different initial displacements and time spans, hence all files can not be ran simultaneously. Nevertheless, each sub-chapter contain following information:

S-tests	contains average calculations of data from S-tests;
S1-test	contains individual graphs of data from S1;
S2-test	contains individual graphs of data from S2;
S3-test	contains individual graphs of data from S3;
S4-test	contains individual graphs of data from S4;
B-tests	contains average calculations of data from B-tests;
B1-test	contains individual graphs of data from B1;
B2-test	contains individual graphs of data from B2;
B3-test	contains individual graphs of data from B3;
C-tests	contains graphs of data from compression tests;
4-point tests	contains graphs of data from four-point bending tests;
S-N curves	contains plots and calculations for S-N curves.

F.1 S-tests

```

import pandas as pd
import matplotlib.pyplot as plt

## Plotting Displacement vs. Force and Time vs. Displacement
# Define a function to read in data from a file and shift the time values
def read_data(filename, label):
    df = pd.read_excel(filename, skiprows=2, usecols='A:C', header=None,
        ↪ names=['Time', 'Force', 'Displacement'])
    df['Time'] = df['Time'] - df['Time'][0]
    return df
# Call the function for each Excel file and plot the data
df1 = read_data('S1_data.xlsx', 'S1')
df2 = read_data('S2_data.xlsx', 'S2')
df3 = read_data('S3_data.xlsx', 'S3')
df4 = read_data('S4_data.xlsx', 'S4')
# Plot time vs. force
plt.plot(df1['Time'], df1['Force'], label='S1')
plt.plot(df2['Time'], df2['Force'], label='S2')
plt.plot(df3['Time'], df3['Force'], label='S3')
plt.plot(df4['Time'], df4['Force'], label='S4')
plt.xlabel('Time [s]')
plt.ylabel('Force [kN]')
plt.title('Force vs. Time for S-tests')
plt.grid()
plt.legend()
plt.savefig('Force_Time_S-tests')
plt.show()
# Subtracting initial displacement of sensors
initial_displacements = [0.00951131153851748, -0.00199953746050596,
    ↪ 0.0029427211266011, -430.875732421875]
df1['Displacement'] = df1['Displacement'] - initial_displacements[0]
df2['Displacement'] = df2['Displacement'] - initial_displacements[1]
df3['Displacement'] = df3['Displacement'] - initial_displacements[2]
df4['Displacement'] = df4['Displacement'] - initial_displacements[3]
# Plot displacement vs. force
plt.plot(df1['Displacement'], df1['Force'], label='S1')
plt.plot(df2['Displacement'], df2['Force'], label='S2')
plt.plot(df3['Displacement'], df3['Force'], label='S3')
plt.plot(df4['Displacement'], df4['Force'], label='S4')
plt.xlabel('Displacement [mm]')
plt.ylabel('Force [kN]')
plt.title('Force vs. Displacement for S-tests')
plt.grid()
plt.legend()
plt.savefig('Displacement_Time_S-tests')
plt.show()
## Plotting average force vs. time for S1-S3

```

```

df1 = pd.read_excel('S1_data.xlsx', skiprows=2, usecols='A,B', header=None,
    ↪ names=['Time', 'Force'])
df3 = pd.read_excel('S2_data.xlsx', skiprows=2, usecols='A,B', header=None,
    ↪ names=['Time', 'Force'])
df3 = pd.read_excel('S3_data.xlsx', skiprows=2, usecols='A,B', header=None,
    ↪ names=['Time', 'Force'])
# Calculating the average force values of S1, S2 and S3
df_avg = pd.DataFrame({'Time': df1['Time'], 'Force': (df1['Force'] + df2['Force']
    ↪ + df3['Force']) / 3})
# Plot the time and force data from Excel files
plt.plot(df_avg['Time'], df_avg['Force'], label='Average', color='black')
# Add axis labels and a legend
plt.xlabel('Time [s]')
plt.ylabel('Force [kN]')
plt.title('Average force vs. Time for S1, S2 and S3')
plt.grid()
plt.legend()
plt.savefig('Average_Force_Time_S-tests')
# Show the plot
plt.show()

## Plotting average force vs. displacement for S1-S3
df1 = pd.read_excel('S1_data.xlsx', skiprows=2, usecols='B,C', header=None,
    ↪ names=['Force', 'Displacement'])
df2 = pd.read_excel('S2_data.xlsx', skiprows=2, usecols='B,C', header=None,
    ↪ names=['Force', 'Displacement'])
df3 = pd.read_excel('S3_data.xlsx', skiprows=2, usecols='B,C', header=None,
    ↪ names=['Force', 'Displacement'])
# Subtracting initial displacement of sensors
initial_displacements = [0.00951131153851748, -0.00199953746050596,
    ↪ 0.0029427211266011]
df1['Displacement'] = df1['Displacement'] - initial_displacements[0]
df2['Displacement'] = df2['Displacement'] - initial_displacements[1]
df3['Displacement'] = df3['Displacement'] - initial_displacements[2]
# Calculating the average displacement values of S1, S2 and S3
df_avg = pd.DataFrame({'Displacement': df1['Displacement'], 'Force':
    ↪ (df1['Force'] + df2['Force'] + df3['Force']) / 3})
# Plot the time and force data from Excel files
plt.plot(df_avg['Displacement'], df_avg['Force'], label='Average', color='black')
# Add axis labels and a legend
plt.xlabel('Displacement [mm]')
plt.ylabel('Force [kN]')
plt.title('Average force vs. Displacement for S1, S2 and S3')
plt.grid()
plt.legend()
plt.savefig('Average_Force_Displacement_S-tests')
# Show the plot
plt.show()

```

F.2 S1-test

*# S1_data.xlsx is shortened to load exposure and contains 5 columns (A:E) and
→ 247853 rows (1:247853).*

```
import pandas as pd
import matplotlib.pyplot as plt
```

```
## Plotting Force vs. Time for S1
```

```
df = pd.read_excel('S1_data.xlsx', skiprows=2, usecols='A:B', header=None,
→ names=['Time', 'Force'])
```

```
# Skip every 20th value
```

```
df = df.iloc[2::20, :]
```

```
# Extract the time and force columns as NumPy arrays
```

```
time = df['Time'].values
```

```
force = df['Force'].values
```

```
# Create a line plot of force vs. time
```

```
plt.plot(time, force)
```

```
plt.xlabel('Time [s]')
```

```
plt.ylabel('Force [kN]')
```

```
plt.title('Force vs. Time for S1')
```

```
plt.grid()
```

```
plt.savefig('Force_Time_S1')
```

```
# Show plot
```

```
plt.show()
```

```
## Plotting Force vs. Displacement for S1
```

```
df = pd.read_excel('S1_data.xlsx', skiprows=2, usecols='B:C', header=None,
→ names=['Force', 'Displacement'])
```

```
# Skip every 20th value
```

```
df = df.iloc[2::20, :]
```

```
# Extract the time and force columns as NumPy arrays
```

```
force = df['Force'].values
```

```
displacement = df['Displacement'].values
```

```
# Create a line plot of force vs. time
```

```
plt.plot(displacement, force)
```

```
plt.xlabel('Displacement [mm]')
```

```
plt.ylabel('Force [kN]')
```

```
plt.title('Force vs. Displacement for S1')
```

```
plt.grid()
```

```
plt.savefig('Force_Displacement_S1')
```

```
# Show plot
```

```
plt.show()
```

```
## Plotting Displacement vs. Time for S1
```

```
df = pd.read_excel('S1_data.xlsx', skiprows=2, usecols='A,C', header=None,
→ names=['Time', 'Displacement'])
```

```
# Set initial displacement
```

```
initial_displacement = 0.00951131153851748
```

```

# Skip every 100th value
df = df.iloc[2::100, :]
# Extract the time and force columns as NumPy arrays
time = df['Time'].values
displacement = df['Displacement'].values - initial_displacement
# Create a line plot of force vs. time
plt.plot(time, displacement)
plt.xlabel('Time [s]')
plt.ylabel('Displacement [mm]')
plt.title('Displacement vs. Time for S1')
plt.grid()
plt.savefig('Displacement_Time_S1')
# Show plot
plt.show()

## Plotting Laser 1 and 2 displacement vs. time for S1
df = pd.read_excel('S1_data.xlsx', skiprows=2, usecols='A,D', header=None,
    ↪ names=['Time', 'Displacement'])
# Set initial displacement
L1_initial_displacement = -0.44361087679863
# Skip every 1000th value
df = df.iloc[2::1000, :]
# Extract the time and force columns as NumPy arrays
time = df['Time'].values
displacement = df['Displacement'].values - L1_initial_displacement
# Create a line plot of force vs. time
plt.plot(time, displacement)
plt.xlabel('Time [s]')
plt.ylabel('Displacement [mm]')
plt.title('Laser 1 displacement vs. Time for S1')
plt.grid()
plt.savefig('L1Displacement_Time_S1')
# Show plot
plt.show()

df = pd.read_excel('S1_data.xlsx', skiprows=2, usecols='A,E', header=None,
    ↪ names=['Time', 'Displacement'])
# Set initial displacement
L2_initial_displacement = -0.0889168754220009
# Skip every 1000th value
df = df.iloc[2::1000, :]
# Extract the time and force columns as NumPy arrays
time = df['Time'].values
displacement = df['Displacement'].values - L2_initial_displacement
# Create a line plot of force vs. time
plt.plot(time, displacement)
plt.xlabel('Time [s]')
plt.ylabel('Displacement [mm]')
plt.title('Laser 2 displacement vs. Time for S1')
plt.grid()

```



```
plt.savefig('L2Displacement_Time_S1')  
# Show plot  
plt.show()
```

F.3 S2-test

*# S2_data.xlsx is shortened to load exposure and contains 5 columns (A:E) and
 → 240547 rows (1:240547).*

```
import pandas as pd
import matplotlib.pyplot as plt
```

Plotting Force vs. Time for S2

```
df = pd.read_excel('S2_data.xlsx', skiprows=2, usecols='A:B', header=None,
  → names=['Time', 'Force'])
```

Skip every 20th value

```
df = df.iloc[2::20, :]
```

Extract the time and force columns as NumPy arrays

```
time = df['Time'].values
```

```
force = df['Force'].values
```

Create a line plot of force vs. time

```
plt.plot(time, force, color='g')
```

```
plt.xlabel('Time [s]')
```

```
plt.ylabel('Force [kN]')
```

```
plt.title('Force vs. Time for S2')
```

```
plt.grid()
```

```
plt.savefig('Force_Time_S2')
```

Show plot

```
plt.show()
```

Plotting Force vs. Displacement for S2

```
df = pd.read_excel('S2_data.xlsx', skiprows=2, usecols='B:C', header=None,
  → names=['Force', 'Displacement'])
```

Skip every 20th value

```
df = df.iloc[2::20, :]
```

Extract the time and force columns as NumPy arrays

```
force = df['Force'].values
```

```
displacement = df['Displacement'].values
```

Create a line plot of force vs. time

```
plt.plot(displacement, force, color='g')
```

```
plt.xlabel('Displacement [mm]')
```

```
plt.ylabel('Force [kN]')
```

```
plt.title('Force vs. Displacement for S2')
```

```
plt.grid()
```

```
plt.savefig('Force_Displacement_S2')
```

Show plot

```
plt.show()
```

Plotting Displacement vs. time for S2

```
df = pd.read_excel('S2_data.xlsx', skiprows=2, usecols='A,C', header=None,
  → names=['Time', 'Displacement'])
```

Set initial displacement

```
initial_displacement = -0.00199953746050596
```

```

# Skip every 100th value
df = df.iloc[2::100, :]
# Extract the time and force columns as NumPy arrays
time = df['Time'].values
displacement = df['Displacement'].values - initial_displacement
# Create a line plot of force vs. time
plt.plot(time, displacement, color='g')
plt.xlabel('Time [s]')
plt.ylabel('Displacement [mm]')
plt.title('Displacement vs. Time for S2')
plt.grid()
plt.savefig('Displacement_Time_S2')
# Show plot
plt.show()

## Plotting Laser 1 and 2 displacement vs. time for S2
df = pd.read_excel('S2_data.xlsx', skiprows=2, usecols='A,D', header=None,
    ↪ names=['Time', 'Displacement'])
# Set initial displacement
L1_initial_displacement = 1.09977853298187
# Skip every 1000th value
df = df.iloc[2::1000, :]
# Extract the time and force columns as NumPy arrays
time = df['Time'].values
displacement = df['Displacement'].values - L1_initial_displacement
# Create a line plot of force vs. time
plt.plot(time, displacement, color='g')
plt.xlabel('Time [s]')
plt.ylabel('Displacement [mm]')
plt.title('Laser 1 displacement vs. Time for S2')
plt.grid()
plt.savefig('L1Displacement_Time_S2')
# Show plot
plt.show()

df = pd.read_excel('S2_data.xlsx', skiprows=2, usecols='A,E', header=None,
    ↪ names=['Time', 'Displacement'])
# Set initial displacement
L2_initial_displacement = 0.371244192123413
# Skip every 1000th value
df = df.iloc[2::1000, :]
# Extract the time and force columns as NumPy arrays
time = df['Time'].values
displacement = df['Displacement'].values - L2_initial_displacement
# Create a line plot of force vs. time
plt.plot(time, displacement, color='g')
plt.xlabel('Time [s]')
plt.ylabel('Displacement [mm]')
plt.title('Laser 2 displacement vs. Time for S2')
plt.grid()

```

```
plt.savefig('L2Displacement_Time_S2')  
# Show plot  
plt.show()
```

F.4 S3-test

*# S3_data.xlsx is shortened to load exposure and contains 5 columns (A:E) and
→ 279951 rows (1:279951).*

```
import pandas as pd
import matplotlib.pyplot as plt

## Plotting Displacement vs. Force for S3
df = pd.read_excel('S3_data.xlsx', skiprows=2, usecols='A:B', header=None,
→ names=['Time', 'Force'])
# Skip every 20th value
df = df.iloc[2::20, :]
# Extract the time and force columns as NumPy arrays
time = df['Time'].values
force = df['Force'].values
# Create a line plot of force vs. time
plt.plot(time, force, color='orange')
plt.xlabel('Time [s]')
plt.ylabel('Force [kN]')
plt.title('Force vs. Time for S3')
plt.grid()
plt.savefig('Force_Time_S3')
# Show plot
plt.show()

## Plotting Force vs. Displacement for S3
df = pd.read_excel('S3_data.xlsx', skiprows=2, usecols='B:C', header=None,
→ names=['Force', 'Displacement'])
# Skip every 20th value
df = df.iloc[2::20, :]
# Extract the time and force columns as NumPy arrays
force = df['Force'].values
displacement = df['Displacement'].values
# Create a line plot of force vs. time
plt.plot(displacement, force, color='orange')
plt.xlabel('Displacement [mm]')
plt.ylabel('Force [kN]')
plt.title('Force vs. Displacement for S3')
plt.grid()
plt.savefig('Force_Displacement_S3')
# Show plot
plt.show()

## Plotting Displacement vs. Time for S3
df = pd.read_excel('S3_data.xlsx', skiprows=2, usecols='A,C', header=None,
→ names=['Time', 'Displacement'])
# Set initial displacement
initial_displacement = 0.376945406198502
```

```

# Skip every 100th value
df = df.iloc[2::100, :]
# Extract the time and force columns as NumPy arrays
time = df['Time'].values
displacement = df['Displacement'].values - initial_displacement
# Create a line plot of force vs. time
plt.plot(time, displacement, color='orange')
plt.xlabel('Time [s]')
plt.ylabel('Displacement [mm]')
plt.title('Displacement vs. Time for S3')
plt.grid()
plt.savefig('Displacement_Time_S3')
# Show plot
plt.show()

## Plotting Laser 1 and 2 displacement vs. Time for S3
df = pd.read_excel('S3_data.xlsx', skiprows=2, usecols='A,D', header=None,
    ↪ names=['Time', 'Displacement'])
# Set initial displacement
L1_initial_displacement = -0.304718762636185
# Skip every 1000th value
df = df.iloc[2::1000, :]
# Extract the time and force columns as NumPy arrays
time = df['Time'].values
displacement = df['Displacement'].values - L1_initial_displacement
# Create a line plot of force vs. time
plt.plot(time, displacement, color='orange')
plt.xlabel('Time [s]')
plt.ylabel('Displacement [mm]')
plt.title('Laser 1 displacement vs. Time for S3')
plt.grid()
plt.savefig('L1Displacement_Time_S3')
# Show plot
plt.show()

df = pd.read_excel('S3_data.xlsx', skiprows=2, usecols='A,E', header=None,
    ↪ names=['Time', 'Displacement'])
# Set initial displacement
L2_initial_displacement = -1.34839904308319
# Skip every 1000th value
df = df.iloc[2::1000, :]
# Extract the time and force columns as NumPy arrays
time = df['Time'].values
displacement = df['Displacement'].values - L2_initial_displacement
# Create a line plot of force vs. time
plt.plot(time, displacement, color='orange')
plt.xlabel('Time [s]')
plt.ylabel('Displacement [mm]')
plt.title('Laser 2 displacement vs. Time for S3')
plt.grid()

```

```
plt.savefig('L2Displacement_Time_S3')  
# Show plot  
plt.show()
```

F.5 S4-test

*# S4_data.xlsx is shortened to load exposure and contains 5 columns (A:E) and
 → 295877 rows (1:295877).*

```
import pandas as pd
import matplotlib.pyplot as plt

## Plotting Force vs. Time for S4
df = pd.read_excel('S4_data.xlsx', skiprows=2, usecols='A:B', header=None,
  → names=['Time', 'Force'])
# Skip every 20th value
df = df.iloc[2::20, :]
# Extract the time and force columns as NumPy arrays
time = df['Time'].values
force = df['Force'].values
# Create a line plot of force vs. time
plt.plot(time, force, color='purple')
plt.xlabel('Time [s]')
plt.ylabel('Force [kN]')
plt.title('Force vs. Time for S4')
plt.grid()
plt.savefig('Force_Time_S4')
# Show plot
plt.show()

## Plotting Force vs. Displacement for S4
df = pd.read_excel('S4_data.xlsx', skiprows=2, usecols='B:C', header=None,
  → names=['Force', 'Displacement'])
# Skip every 20th value
df = df.iloc[2::20, :]
# Extract the time and force columns as NumPy arrays
force = df['Force'].values
displacement = df['Displacement'].values
# Create a line plot of force vs. time
plt.plot(displacement, force, color='purple')
plt.xlabel('Displacement [mm]')
plt.ylabel('Force [kN]')
plt.title('Force vs. Displacement for S4')
plt.grid()
plt.savefig('Force_Displacement_S4')
# Show plot
plt.show()

## Plotting Displacement vs. Time for S4
df = pd.read_excel('S4_data.xlsx', skiprows=2, usecols='A,C', header=None,
  → names=['Time', 'Displacement'])
# Set initial displacement
initial_displacement = -430.875732421875
```



```

# Skip every 100th value
df = df.iloc[2::100, :]
# Extract the time and force columns as NumPy arrays
time = df['Time'].values
displacement = df['Displacement'].values - initial_displacement
# Create a line plot of force vs. time
plt.plot(time, displacement, color='purple')
plt.xlabel('Time [s]')
plt.ylabel('Displacement [mm]')
plt.title('Displacement vs. Time for S4')
plt.grid()
plt.savefig('Displacement_Time_S4')
# Show plot
plt.show()

## Plotting Laser 1 and 2 Displacement vs. Time for S4
df = pd.read_excel('S4_data.xlsx', skiprows=2, usecols='A,D', header=None,
→ names=['Time', 'Displacement'])
# Set initial displacement
L1_initial_displacement = 1488.79333496093
# Skip every 1000th value
df = df.iloc[2::1000, :]
# Extract the time and force columns as NumPy arrays
time = df['Time'].values
displacement = df['Displacement'].values - L1_initial_displacement
# Create a line plot of force vs. time
plt.plot(time, displacement, color='purple')
plt.xlabel('Time [s]')
plt.ylabel('Displacement [mm]')
plt.title('Laser 1 displacement vs. Time for S4')
plt.grid()
plt.savefig('L1Displacement_Time_S4')
# Show plot
plt.show()

df = pd.read_excel('S4_data.xlsx', skiprows=2, usecols='A,E', header=None,
→ names=['Time', 'Displacement'])
L2_initial_displacement = 1479.47033691406
# Skip every 1000th value
df = df.iloc[2::1000, :]
# Extract the time and force columns as NumPy arrays
time = df['Time'].values
displacement = df['Displacement'].values - L2_initial_displacement
# Create a line plot of force vs. time
plt.plot(time, displacement, color='purple')
plt.xlabel('Time [s]')
plt.ylabel('Displacement [mm]')
plt.title('Laser 2 displacement vs. Time for S4')
plt.grid()
plt.savefig('L2Displacement_Time_S4')

```

```
# Show plot  
plt.show()
```

F.6 B-tests

```

import pandas as pd
import matplotlib.pyplot as plt

## Plotting Force vs. Time and Force vs. Displacement for B-tests
# Set initial displacements
initial_displacements = [-0.0405851043760777, -2.03297615051269, -431.919982910156]
# Read in the data from the Excel files
df1 = pd.read_excel('B1_data.xlsx', skiprows=2, usecols='J,K,L', header=None,
    → names=['Time', 'Force', 'Displacement'])
df2 = pd.read_excel('B2_data.xlsx', skiprows=2, usecols='I,J,K', header=None,
    → names=['Time', 'Force', 'Displacement'])
df3 = pd.read_excel('B3_data.xlsx', skiprows=2, usecols='J,K,L', header=None,
    → names=['Time', 'Force', 'Displacement'])
# Normalizing time and displacement by subtracting initial values
df1['Time'] = df1['Time'] - df1['Time'][0]
df2['Time'] = df2['Time'] - df2['Time'][0]
df3['Time'] = df3['Time'] - df3['Time'][0]
df1['Displacement'] = df1['Displacement'] - initial_displacements[0]
df2['Displacement'] = df2['Displacement'] - initial_displacements[1]
df3['Displacement'] = df3['Displacement'] - initial_displacements[2]
# Plot the time and force data from all four Excel files on the same graph
plt.plot(df1['Time'], df1['Force'], label='B1')
plt.plot(df2['Time'], df2['Force'], label='B2')
plt.plot(df3['Time'], df3['Force'], label='B3')
plt.xlabel('Time [s]')
plt.ylabel('Force [kN]')
plt.title('Force vs. Time for B-tests')
plt.grid()
plt.legend()
plt.savefig('Force_Time_B-tests')
plt.show()
# Plot the time and force data from all four Excel files on the same graph
plt.plot(df1['Displacement'], df1['Force'], label='B1')
plt.plot(df2['Displacement'], df2['Force'], label='B2')
plt.plot(df3['Displacement'], df3['Force'], label='B3')
plt.xlabel('Displacement [mm]')
plt.ylabel('Force [kN]')
plt.title('Force vs. Displacement for B-tests')
plt.grid()
plt.legend()
plt.savefig('Force_Displacement_B-tests')
plt.show()

## Finding key values from data sets
# Find the index of the largest force value in each data frame
max_force_idx_1 = df1['Force'].idxmax()
max_force_idx_2 = df2['Force'].idxmax()

```

```
max_force_idx_3 = df3['Force'].idxmax()
max_force = []
max_displacement = []
max_force = [df1.loc[max_force_idx_1, 'Force'], df2.loc[max_force_idx_2,
→ 'Force'], df3.loc[max_force_idx_3, 'Force']]
max_displacement = [df1.loc[max_force_idx_1, 'Displacement'],
→ df2.loc[max_force_idx_2, 'Displacement'], df3.loc[max_force_idx_3,
→ 'Displacement']]
# Print the largest force values and corresponding displacement
print("Respective list of largest force values and their corresponding
→ displacement:")
print(max_force)
print(max_displacement)
```

F.7 B1-test

*# B1_data.xlsx is shortened to load exposure and contains 16 columns (A:P) and
 → 318374 rows (1:318374). Certain graphs only include measurements until
 → approximately 1560 seconds, when failure occur. Rotations are plotted until
 → 1550 seconds, due to unreadable results beyond this point.*

```
import pandas as pd
import matplotlib.pyplot as plt

## Plotting Force vs. Time for B1
df = pd.read_excel('B1_data.xlsx', skiprows=2, usecols='J,K', header=None,
  → names=['Time', 'Force'])
# Skip every 20th value
df = df.iloc[2::20, :]
# Extract the time and force columns as NumPy arrays
time = df['Time'].values
force = df['Force'].values
# Create a line plot of force vs. time
plt.plot(time, force)
plt.xlabel('Time [s]')
plt.ylabel('Force [kN]')
plt.title('Force vs. Time for B1')
plt.grid()
plt.savefig('Force_Time_B1')
# Show plot
plt.show()

## Plotting Force vs. Displacement for B1
df = pd.read_excel('B1_data.xlsx', skiprows=2, usecols='K,L', header=None,
  → names=['Force', 'Displacement'])
# Skip every 20th value
df = df.iloc[2::20, :]
# Extract the time and force columns as NumPy arrays
force = df['Force'].values
displacement = df['Displacement'].values
# Create a line plot of force vs. time
plt.plot(displacement, force)
plt.xlabel('Displacement [mm]')
plt.ylabel('Force [kN]')
plt.title('Force vs. Displacement for B1')
plt.grid()
plt.savefig('Force_Displacement_B1')
# Show plot
plt.show()

## Plotting Displacement vs. Time for B1
df = pd.read_excel('B1_data.xlsx', skiprows=2, usecols='J,L', header=None,
  → names=['Time', 'Displacement'])
```

```

# Set initial displacement
initial_displacement = -0.0405851043760777
# Skip every 100th value
df = df.iloc[2::100, :]
# Extract the time and force columns as NumPy arrays
time = df['Time'].values
displacement = df['Displacement'].values - initial_displacement
# Create a line plot of force vs. time
plt.plot(time, displacement)
plt.xlabel('Time [s]')
plt.ylabel('Displacement [mm]')
plt.title('Displacement vs. Time for B1')
plt.grid()
plt.savefig('Displacement_Time_B1')
# Show plot
plt.show()

## Plotting displacements LVDTs for B1 against time
# Read the Excel data into a pandas DataFrame
df = pd.read_excel('B1_data.xlsx', skiprows=2, usecols='J,M,N,O,P', header=None,
→ names=['Time', 'Disp1', 'Disp2', 'Disp3', 'Disp4'])
# Set initial displacement values for each column
initial_displacements = [-0.004628034, 0.0160224288702011, -0.00120963889639825,
→ 0.00191606185398996]
# Skip every 10th value
df = df.iloc[2::10, :]
# Subtract initial displacement value for each column of displacement data
for i in range(1, 5):
    df['Disp' + str(i)] = df['Disp' + str(i)].values - initial_displacements[i-1]
# Create a figure with four subplots for each column of displacement data
fig, axs = plt.subplots(4, 1, sharex=True, figsize=(8, 12))
# Plot each column of displacement data on a separate subplot only until time
→ reaches 1556.87 seconds
for i in range(4):
    axs[i].plot(df['Time'][df['Time']<=1556.87], df['Disp' +
→ str(i+1)][df['Time']<=1556.87])
    axs[i].set_ylabel('Displacement [mm]')
    axs[i].set_title('LVDT ' + str(i+1) + ' vs. Time for B1')
    axs[i].grid()
# Add x-axis label to the bottom subplot
axs[-1].set_xlabel('Time [s]')
# Save the figure
plt.savefig('LVDT1_Time_B1')
# Show the plot
plt.show()

## Plotting displacements of LVDTs for B1 against force
# Read the Excel data into a pandas DataFrame
df = pd.read_excel('B1_data.xlsx', skiprows=2, usecols='J,K,M,N,O,P',
→ header=None, names=['Time', 'Force', 'Disp1', 'Disp2', 'Disp3', 'Disp4'])

```

```

# Set initial displacement values for each column
initial_displacements = [-0.004628034, 0.0160224288702011, -0.00120963889639825,
    ↪ 0.00191606185398996]
# Skip every 10th value
df = df.iloc[2::10, :]
# Subtract initial displacement value for each column of displacement data
for i in range(1, 5):
    df['Disp' + str(i)] = df['Disp' + str(i)].values - initial_displacements[i-1]
# Create a figure with four subplots for each column of displacement data
fig, axs = plt.subplots(4, 1, sharex=True, figsize=(8, 12))
# Plot each column of displacement data on a separate subplot only until time
    ↪ reaches 1556.87 seconds
for i in range(4):
    axs[i].plot(df['Disp' + str(i+1)][df['Time']<=1556.87],
        ↪ df['Force'][df['Time']<=1556.87])
    axs[i].set_ylabel('Force [kN]')
    axs[i].set_title('LVDT ' + str(i+1) + ' vs. Force for B1')
    axs[i].grid()
# Add x-axis label to the bottom subplot
axs[-1].set_xlabel('Displacement [mm]')
# Save the figure
plt.savefig('LVDT2_Force_B1')
# Show the plot
plt.show()

## Plotting averaged displacement of LVDTs against time
# Read the Excel data into a pandas DataFrame
df = pd.read_excel('B1_data.xlsx', skiprows=2, usecols='J,M,N,O,P', header=None,
    ↪ names=['Time', 'Disp1', 'Disp2', 'Disp3', 'Disp4'])
# Set initial displacement values for each column
initial_displacements = [-0.004628034, 0.0160224288702011, -0.00120963889639825,
    ↪ 0.00191606185398996]
# Skip every 10th value
df = df.iloc[2::10, :]
# Subtract initial displacement value for each column of displacement data
for i in range(1, 5):
    df['Disp' + str(i)] = df['Disp' + str(i)].values - initial_displacements[i-1]
# Calculate the average of two and two displacement values, and plot the result
avg_disp1_2 = (df['Disp1'] + df['Disp2']) / 2
avg_disp3_4 = (df['Disp3'] + df['Disp4']) / 2
# Create a line plot of the averaged displacement values vs. time
plt.plot(df['Time'][df['Time']<=1556.87], avg_disp1_2[df['Time']<=1556.87],
    ↪ label='Average of LVDT 1 and 2')
plt.plot(df['Time'][df['Time']<=1556.87], avg_disp3_4[df['Time']<=1556.87],
    ↪ label='Average of LVDT 3 and 4')
plt.xlabel('Time [s]')
plt.ylabel('Displacement [mm]')
plt.title('Averaged displacement of LVDTs vs. Time for B1')
plt.grid()
plt.legend()

```

```

plt.savefig('Averaged_LVDT_Time_B1')
# Show plot
plt.show()

## Plotting averaged displacement of LVDTs against force
# Read the Excel data into a pandas DataFrame
df = pd.read_excel('B1_data.xlsx', skiprows=2, usecols='J,K,M,N,O,P',
    → header=None, names=['Time', 'Force', 'Disp1', 'Disp2', 'Disp3', 'Disp4'])
# Set initial displacement values for each column
initial_displacements = [-0.004628034, 0.0160224288702011, -0.00120963889639825,
    → 0.00191606185398996]
# Skip every 10th value
df = df.iloc[2::10, :]
# Subtract initial displacement value for each column of displacement data
for i in range(1, 5):
    df['Disp' + str(i)] = df['Disp' + str(i)].values - initial_displacements[i-1]
# Calculate the average of two and two displacement values, and plot the result
avg_disp1_2 = (df['Disp1'] + df['Disp2']) / 2
avg_disp3_4 = (df['Disp3'] + df['Disp4']) / 2
# Create a line plot of the averaged displacement values vs. time
plt.plot(avg_disp1_2[df['Time']<=1556.87], df['Force'][df['Time']<=1556.87],
    → label='Average of LVDT 1 and 2')
plt.plot(avg_disp3_4[df['Time']<=1556.87], df['Force'][df['Time']<=1556.87],
    → label='Average of LVDT 3 and 4')
plt.xlabel('Displacement [mm]')
plt.ylabel('Force [kN]')
plt.title('Averaged displacement values of LVDT vs. Force for B1')
plt.grid()
plt.legend()
plt.savefig('Averaged_LVDT_Force_B1')
# Show plot
plt.show()

## Plotting rotation between two sets of LVDTs vs. Time for B1
# Read the Excel data into a pandas DataFrame
df = pd.read_excel('B1_data.xlsx', skiprows=2, usecols='J,M,N,O,P', header=None,
    → names=['Time', 'Disp1', 'Disp2', 'Disp3', 'Disp4'])
# Set the distance between each pair of gauges
distance_12 = 401 # mm
distance_34 = 432 # mm
# Calculate the rotation between disp1 and disp2
rotation_12 = (df['Disp2'].values - df['Disp1'].values) / distance_12
# Calculate the rotation between disp3 and disp4
rotation_34 = (df['Disp4'].values - df['Disp3'].values) / distance_34
# Create a line plot of rotation vs. time only until time reaches 1550 seconds
plt.plot(df['Time'][df['Time']<=1550].values, rotation_12[df['Time']<=1550],
    → label='Rotation 1-2')
plt.plot(df['Time'][df['Time']<=1550].values, rotation_34[df['Time']<=1550],
    → label='Rotation 3-4')
plt.xlabel('Time [s]')

```



```

plt.ylabel('Rotation [rad]')
plt.title('Rotation vs. Time for B1')
plt.grid()
plt.legend()
plt.savefig('Rotation_Time_B1')
# Show plot
plt.show()

## Plotting rotation between two sets of LVDT vs. Force for B1
# Read the Excel data into a pandas DataFrame
df = pd.read_excel('B1_data.xlsx', skiprows=2, usecols='J,K,M,N,O,P',
    → header=None, names=['Time', 'Force', 'Disp1', 'Disp2', 'Disp3', 'Disp4'])
# Set the distance between each pair of gauges
distance_12 = 401 # mm
distance_34 = 432 # mm
# Calculate the rotation between disp1 and disp2
rotation_12 = (df['Disp2'].values - df['Disp1'].values) / distance_12

# Calculate the rotation between disp3 and disp4
rotation_34 = (df['Disp4'].values - df['Disp3'].values) / distance_34
# Create a line plot of rotation vs. time only until time reaches 1550 seconds
plt.plot(df['Force'][df['Time']<=1550].values, rotation_12[df['Time']<=1550],
    → label='Rotation 1-2')
plt.plot(df['Force'][df['Time']<=1550].values, rotation_34[df['Time']<=1550],
    → label='Rotation 3-4')
plt.xlabel('Force [kN]')
plt.ylabel('Rotation [rad]')
plt.title('Rotation vs. Force for B1')
plt.grid()
plt.legend()
plt.savefig('Rotation_Force_B1')
# Show plot
plt.show()

## Plotting average rotation of horizontal axis
# Read the Excel data into a pandas DataFrame
df = pd.read_excel('B1_data.xlsx', skiprows=2, usecols='J,K,M,N,O,P',
    → header=None, names=['Time', 'Force', 'Disp1', 'Disp2', 'Disp3', 'Disp4'])
# Set the distance between each pair of gauges
distance_12 = 401 # mm
distance_34 = 432 # mm
d_13 = (df['Disp1'].values + df['Disp3'].values) / 2 # Upper sensors
d_24 = (df['Disp2'].values + df['Disp4'].values) / 2 # Lower sensors
avg_distance = (distance_12 + distance_34) / 2 # Average distance
avg_rot = (d_13 - d_24) / avg_distance
# Create a line plot of rotation vs. time only until time reaches 1550 seconds
plt.plot(df['Time'][df['Time']<=1550].values, -avg_rot[df['Time']<=1550],
    → label='Average rotation')
plt.xlabel('Time [s]')
plt.ylabel('Rotation [rad]')

```

```

plt.title('Average rotation vs. Time for B1')
plt.grid()
plt.legend()
plt.savefig('avg_horizontal_rotation_B1')
# Show plot
plt.show()

## Finding relevant values from B1-test
# Read from dataframe
df = pd.read_excel('B1_data.xlsx', skiprows=2, usecols='J:P', header=None,
→ names=['Time', 'Force', 'Displacement', 'Disp1', 'Disp2', 'Disp3', 'Disp4'])
# Initial displacement
initial_displacement = -0.0405851043760777
# Set the distance between each pair of gauges
distance_12 = 401 # mm
distance_34 = 432 # mm
# Find the index of the largest force value
max_force_idx = df['Force'].idxmax()
max_force = df.loc[max_force_idx, 'Force']
max_displacement = df.loc[max_force_idx, 'Displacement'] - initial_displacement
max_LVDT = (df.loc[max_force_idx, 'Disp1'] + df.loc[max_force_idx, 'Disp2'])/2
max_rotation_12 = (df.loc[max_force_idx, 'Disp1'] - df.loc[max_force_idx,
→ 'Disp2'])/distance_12
max_rotation_34 = (df.loc[max_force_idx, 'Disp3'] - df.loc[max_force_idx,
→ 'Disp4'])/distance_34
avg_max_rotation = (max_rotation_12 + max_rotation_34)/2
# Print the largest values with same index as largest force
print("Respective list of largest force values and their corresponding
→ displacement:")
print(max_force)
print(max_displacement)
print(max_LVDT)
print(avg_max_rotation)

```

F.8 B2-test

*# B2_data.xlsx is shortened to load exposure and contains 16 columns (A:P) and
 → 310128 rows (1:310128). Certain graphs only include measurements until
 → approximately 1400 seconds, when failure occur. Rotations are plotted until
 → 1390 seconds, due to unreadable results beyond this point.*

```
import pandas as pd
import matplotlib.pyplot as plt

## Plotting Force vs. Time for B2
df = pd.read_excel('B2_data.xlsx', skiprows=2, usecols='I,J', header=None,
  → names=['Time', 'Force'])
# Skip every 20th value
df = df.iloc[2::20, :]
# Extract the time and force columns as NumPy arrays
time = df['Time'].values
force = df['Force'].values
# Create a line plot of force vs. time
plt.plot(time, force, color='tab:orange')
plt.xlabel('Time [s]')
plt.ylabel('Force [kN]')
plt.title('Force vs. Time for B2')
plt.grid()
plt.savefig('Force_Time_B2')
# Show plot
plt.show()

## Plotting Force vs. Displacement for B2
df = pd.read_excel('B2_data.xlsx', skiprows=2, usecols='J,K', header=None,
  → names=['Force', 'Displacement'])
# Skip every 20th value
df = df.iloc[2::20, :]
# Extract the time and force columns as NumPy arrays
force = df['Force'].values
displacement = df['Displacement'].values
# Create a line plot of force vs. time
plt.plot(displacement, force, color='tab:orange')
plt.xlabel('Displacement [mm]')
plt.ylabel('Force [kN]')
plt.title('Force vs. Displacement for B2')
plt.grid()
plt.savefig('Force_Displacement_B2')
# Show plot
plt.show()

## Plotting Displacement vs. Time for B2
df = pd.read_excel('B2_data.xlsx', skiprows=2, usecols='I,K', header=None,
  → names=['Time', 'Displacement'])
```

```

# Set initial displacement
initial_displacement = -2.03297615051269
# Skip every 100th value
df = df.iloc[2::100, :]
# Extract the time and force columns as NumPy arrays
time = df['Time'].values
displacement = df['Displacement'].values - initial_displacement
# Create a line plot of force vs. time
plt.plot(time, displacement, color='tab:orange')
plt.xlabel('Time [s]')
plt.ylabel('Displacement [mm]')
plt.title('Displacement vs. Time for B2')
plt.grid()
plt.savefig('Displacement_Time_B2')
# Show plot
plt.show()

## Plotting displacements of LVDTs for B2 against time
# Read the Excel data into a pandas DataFrame
df = pd.read_excel('B2_data.xlsx', skiprows=2, usecols='I,L,M,N,O', header=None,
→ names=['Time', 'Disp1', 'Disp2', 'Disp3', 'Disp4'])
# Set initial displacement values for each column
initial_displacements = [-0.0102987438440323, -0.0172233711928129,
→ -0.0444290079176426, 0.00270642968825996]
# Skip every 10th value
df = df.iloc[2::10, :]
# Subtract initial displacement value for each column of displacement data
for i in range(1, 5):
    df['Disp' + str(i)] = df['Disp' + str(i)].values - initial_displacements[i-1]
# Create a figure with four subplots for each column of displacement data
fig, axs = plt.subplots(4, 1, sharex=True, figsize=(8, 12))
# Plot each column of displacement data on a separate subplot only until time
→ reaches 1398.054 seconds
for i in range(4):
    axs[i].plot(df['Time'][df['Time']<=1398.054], df['Disp' +
→ str(i+1)][df['Time']<=1398.054], color='tab:orange')
    axs[i].set_ylabel('Displacement [mm]')
    axs[i].set_title('LVDT ' + str(i+1) + ' vs. Time for B2')
    axs[i].grid()
# Add x-axis label to the bottom subplot
axs[-1].set_xlabel('Time [s]')
# Save the figure
plt.savefig('LVDT1_Time_B2')
# Show the plot
plt.show()

## Plotting displacements of LVDTs for B2 against force
# Read the Excel data into a pandas DataFrame
df = pd.read_excel('B2_data.xlsx', skiprows=2, usecols='I,J,L,M,N,O',
→ header=None, names=['Time', 'Force', 'Disp1', 'Disp2', 'Disp3', 'Disp4'])

```

```

# Set initial displacement values for each column
initial_displacements = [-0.0102987438440323, -0.0172233711928129,
    ↪ -0.0444290079176426, 0.00270642968825996]
# Skip every 1000th value
df = df.iloc[2::10, :]
# Subtract initial displacement value for each column of displacement data
for i in range(1, 5):
    df['Disp' + str(i)] = df['Disp' + str(i)].values - initial_displacements[i-1]
# Create a figure with four subplots for each column of displacement data
fig, axs = plt.subplots(4, 1, sharex=True, figsize=(8, 12))
# Plot each column of displacement data on a separate subplot only until time
    ↪ reaches 1398.054 seconds
for i in range(4):
    axs[i].plot(df['Disp' + str(i+1)][df['Time']<=1398.054],
    ↪ df['Force'][df['Time']<=1398.054], color='tab:orange')
    axs[i].set_ylabel('Force [kN]')
    axs[i].set_title('LVDT ' + str(i+1) + ' vs. Force for B2')
    axs[i].grid()
# Add x-axis label to the bottom subplot
axs[-1].set_xlabel('Displacement [mm]')
# Save the figure
plt.savefig('LVDT2_Force_B2')
# Show the plot
plt.show()

## Plotting averaged displacement of LVDTs against time
# Read the Excel data into a pandas DataFrame
df = pd.read_excel('B2_data.xlsx', skiprows=2, usecols='I,L,M,N,O', header=None,
    ↪ names=['Time', 'Disp1', 'Disp2', 'Disp3', 'Disp4'])
# Set initial displacement values for each column
initial_displacements = [-0.0102987438440323, -0.0172233711928129,
    ↪ -0.0444290079176426, 0.00270642968825996]
# Skip every 10th value
df = df.iloc[2::10, :]
# Subtract initial displacement value for each column of displacement data
for i in range(1, 5):
    df['Disp' + str(i)] = df['Disp' + str(i)].values - initial_displacements[i-1]
# Calculate the average of two and two displacement values, and plot the result
avg_disp1_2 = (df['Disp1'] + df['Disp2']) / 2
avg_disp3_4 = (df['Disp3'] + df['Disp4']) / 2
# Create a line plot of the averaged displacement values vs. time
plt.plot(df['Time'][df['Time']<=1398.054], avg_disp1_2[df['Time']<=1398.054],
    ↪ label='Average of LVDT 1 and 2')
plt.plot(df['Time'][df['Time']<=1398.054], avg_disp3_4[df['Time']<=1398.054],
    ↪ label='Average of LVDT 3 and 4')
plt.xlabel('Time [s]')
plt.ylabel('Displacement [mm]')
plt.title('Averaged displacement values of LVDT vs. Time for B2')
plt.grid()
plt.legend()

```

```

plt.savefig('Averaged_LVDT_Time_B2')
# Show plot
plt.show()

## Plotting averaged displacement of LVDTs against force
# Read the Excel data into a pandas DataFrame
df = pd.read_excel('B2_data.xlsx', skiprows=2, usecols='I,J,L,M,N,O',
    → header=None, names=['Time', 'Force', 'Disp1', 'Disp2', 'Disp3', 'Disp4'])
# Set initial displacement values for each column
initial_displacements = [-0.0102987438440323, -0.0172233711928129,
    → -0.0444290079176426, 0.00270642968825996]
# Skip every 10th value
df = df.iloc[2::10, :]
# Subtract initial displacement value for each column of displacement data
for i in range(1, 5):
    df['Disp' + str(i)] = df['Disp' + str(i)].values - initial_displacements[i-1]
# Calculate the average of two and two displacement values, and plot the result
avg_disp1_2 = (df['Disp1'] + df['Disp2']) / 2
avg_disp3_4 = (df['Disp3'] + df['Disp4']) / 2
# Create a line plot of the averaged displacement values vs. time
plt.plot(avg_disp1_2[df['Time']<=1398.054], df['Force'][df['Time']<=1398.054],
    → label='Average of LVDT 1 and 2')
plt.plot(avg_disp3_4[df['Time']<=1398.054], df['Force'][df['Time']<=1398.054],
    → label='Average of LVDT 3 and 4')
plt.xlabel('Displacement [mm]')
plt.ylabel('Force [kN]')
plt.title('Averaged displacement values of LVDT vs. Force for B2')
plt.grid()
plt.legend()
plt.savefig('Averaged_LVDT_Force_B2')
# Show plot
plt.show()

## Plotting rotation between two sets of LVDTs against time for B2
# Read the Excel data into a pandas DataFrame
df = pd.read_excel('B2_data.xlsx', skiprows=2, usecols='I,L,M,N,O', header=None,
    → names=['Time', 'Disp1', 'Disp2', 'Disp3', 'Disp4'])
# Set the distance between each pair of gauges
distance_12 = 399 # mm
distance_34 = 387 # mm
# Calculate the rotation between disp1 and disp2
rotation_12 = (df['Disp2'].values - df['Disp1'].values) / distance_12
# Calculate the rotation between disp3 and disp4
rotation_34 = (df['Disp4'].values - df['Disp3'].values) / distance_34
# Create a line plot of rotation vs. time only until time reaches 1390 seconds
plt.plot(df['Time'][df['Time']<=1390].values, rotation_12[df['Time']<=1390],
    → label='Rotation 1-2')
plt.plot(df['Time'][df['Time']<=1390].values, rotation_34[df['Time']<=1390],
    → label='Rotation 3-4')
plt.xlabel('Time [s]')

```

```

plt.ylabel('Rotation [rad]')
plt.title('Rotation vs. Time for B2')
plt.grid()
plt.legend()
plt.savefig('Rotation_Time_B2')
# Show plot
plt.show()

## Plotting rotation between two sets of LVDTs against force for B2
# Read the Excel data into a pandas DataFrame
df = pd.read_excel('B2_data.xlsx', skiprows=2, usecols='I,J,L,M,N,O',
    ↪ header=None, names=['Time', 'Force', 'Disp1', 'Disp2', 'Disp3', 'Disp4'])
# Set the distance between each pair of gauges
distance_12 = 399 # mm
distance_34 = 387 # mm
# Calculate the rotation between disp1 and disp2
rotation_12 = (df['Disp2'].values - df['Disp1'].values) / distance_12
# Calculate the rotation between disp3 and disp4
rotation_34 = (df['Disp4'].values - df['Disp3'].values) / distance_34
# Create a line plot of rotation vs. time only until time reaches 1390 seconds
plt.plot(df['Force'][df['Time']<=1390].values, rotation_12[df['Time']<=1390],
    ↪ label='Rotation 1-2')
plt.plot(df['Force'][df['Time']<=1390].values, rotation_34[df['Time']<=1390],
    ↪ label='Rotation 3-4')
plt.xlabel('Force [kN]')
plt.ylabel('Rotation [rad]')
plt.title('Rotation vs. Force for B2')
plt.grid()
plt.legend()
plt.savefig('Rotation_Force_B2')
# Show plot
plt.show()

## Plotting average rotation of horizontal axis
# Read the Excel data into a pandas DataFrame
df = pd.read_excel('B2_data.xlsx', skiprows=2, usecols='I,J,L,M,N,O',
    ↪ header=None, names=['Time', 'Force', 'Disp1', 'Disp2', 'Disp3', 'Disp4'])
# Set the distance between each pair of gauges
distance_12 = 399 # mm
distance_34 = 387 # mm
d_13 = (df['Disp1'].values + df['Disp3'].values) / 2 # Upper sensors
d_24 = (df['Disp2'].values + df['Disp4'].values) / 2 # Lower sensors
avg_distance = (distance_12 + distance_34) / 2 # Average distance
avg_rot = (d_13 - d_24) / avg_distance
# Create a line plot of rotation vs. time only until time reaches 1390 seconds
plt.plot(df['Time'][df['Time']<=1390].values, -avg_rot[df['Time']<=1390],
    ↪ label='Average rotation', color='tab:orange')
plt.xlabel('Time [s]')
plt.ylabel('Rotation [rad]')
plt.title('Average rotation vs. Time for B2')

```

```

plt.grid()
plt.legend()
plt.savefig('avg_horizontal_rotation_B2')
# Show plot
plt.show()

## Finding relevant parameters from data of B2
# Read from dataframe
df = pd.read_excel('B2_data.xlsx', skiprows=2, usecols='I:O', header=None,
→ names=['Time', 'Force', 'Displacement', 'Disp1', 'Disp2', 'Disp3', 'Disp4'])
# Initial displacement
initial_displacement = -2.03297615051269
# Set the distance between each pair of gauges
distance_12 = 399 # mm
distance_34 = 387 # mm
# Find the index of the largest force value
max_force_idx = df['Force'].idxmax()
max_force = df.loc[max_force_idx, 'Force']
max_displacement = df.loc[max_force_idx, 'Displacement'] - initial_displacement
max_LVDT = (df.loc[max_force_idx, 'Disp1'] + df.loc[max_force_idx, 'Disp2'])/2
max_rotation_12 = (df.loc[max_force_idx, 'Disp1'] - df.loc[max_force_idx,
→ 'Disp2'])/distance_12
max_rotation_34 = (df.loc[max_force_idx, 'Disp3'] - df.loc[max_force_idx,
→ 'Disp4'])/distance_34
avg_max_rotation = (max_rotation_12 + max_rotation_34)/2
# Print the largest values with same index as largest force
print("Respective list of largest force values and their corresponding
→ displacement:")
print(max_force)
print(max_displacement)
print(max_LVDT)
print(avg_max_rotation)

```

F.9 B3-test

*# B3_data.xlsx is shortened to load exposure and contains 12 columns (A:L) and
→ 699492 rows (1:699492). This specimen is not mounted with displacement
→ gauges.*

```

import pandas as pd
import matplotlib.pyplot as plt

## Plotting Force vs. Time for B3
df = pd.read_excel('B3_data.xlsx', skiprows=2, usecols='J,K', header=None,
→ names=['Time', 'Force'])
# Skip every 20th value
df = df.iloc[2::20, :]
# Extract the time and force columns as NumPy arrays

```



```

time = df['Time'].values
force = df['Force'].values
# Create a line plot of force vs. time
plt.plot(time, force, color='green')
plt.xlabel('Time [s]')
plt.ylabel('Force [kN]')
plt.title('Force vs. Time for B3')
plt.grid()
plt.savefig('Force_Time_B3')
# Show plot
plt.show()

## Plotting Force vs. Displacement for B3
df = pd.read_excel('B3_data.xlsx', skiprows=2, usecols='K,L', header=None,
→ names=['Force', 'Displacement'])
# Skip every 20th value
df = df.iloc[2::20, :]
# Extract the time and force columns as NumPy arrays
force = df['Force'].values
displacement = df['Displacement'].values
# Create a line plot of force vs. time
plt.plot(displacement, force, color='green')
plt.xlabel('Displacement [mm]')
plt.ylabel('Force [kN]')
plt.title('Force vs. Displacement for B3')
plt.grid()
plt.savefig('Force_Displacement_B3')
# Show plot
plt.show()

## Plotting Displacement vs. Time for B3
df = pd.read_excel('B3_data.xlsx', skiprows=2, usecols='J,L', header=None,
→ names=['Time', 'Displacement'])
# Set initial displacement
initial_displacement = -431.919982910156
# Skip every 100th value
df = df.iloc[2::100, :]
# Extract the time and force columns as NumPy arrays
time = df['Time'].values
displacement = df['Displacement'].values - initial_displacement
# Create a line plot of force vs. time
plt.plot(time, displacement, color='green')
plt.xlabel('Time [s]')
plt.ylabel('Displacement [mm]')
plt.title('Displacement vs. Time for B3')
plt.grid()
plt.savefig('Displacement_Time_B3')
# Show plot
plt.show()

```

F.10 C-tests

```

import pandas as pd
import matplotlib.pyplot as plt
import numpy as np

# Define the file names and labels
file_names = ['C1.xlsx', 'C2.xlsx', 'C3.xlsx', 'C4.xlsx', 'C5.xlsx',
              'C6.xlsx', 'C7.xlsx', 'C8.xlsx', 'C9.xlsx', 'C10.xlsx']
labels = ['C1', 'C2', 'C3', 'C4', 'C5', 'C6', 'C7', 'C8', 'C9', 'C10']

## Time vs. Force
# Read in the data and plot it
for file_name, label in zip(file_names, labels):
    df = pd.read_excel(file_name, skiprows=7, usecols='A:D', header=None,
                      names=['Time', 'Disp', 'Force', 'Strain'])
    plt.plot(df['Time'], df['Force'], label=label)
# Add axis labels and a legend
plt.xlabel('Time [s]')
plt.ylabel('Force [kN]')
plt.title('Force vs. Time for C-tests')
plt.grid()
plt.legend()
# Save the plot to a file
plt.savefig('Force_Time_C-tests')
# Show the plot
plt.show()

## Force vs. Displacement
# Read in the data and plot it
for file_name, label in zip(file_names, labels):
    df = pd.read_excel(file_name, skiprows=7, usecols='A:D', header=None,
                      names=['Time', 'Disp', 'Force', 'Strain'])
    plt.plot(df['Disp'], df['Force'], label=label)
# Add axis labels and a legend
plt.xlabel('Displacement [mm]')
plt.ylabel('Force [kN]')
plt.title('Displacement vs. Time for C-tests')
plt.grid()
plt.legend()
# Save the plot to a file
plt.savefig('Force_Displacement_C-tests')
# Show the plot
plt.show()

## Strain vs. Force
# Read in the data and plot it
for file_name, label in zip(file_names, labels):
    df = pd.read_excel(file_name, skiprows=7, usecols='C,D', header=None,

```

```
        names=['Force', 'Strain'])
    plt.plot(df['Strain'], df['Force'], label=label)
# Add axis labels and a legend
plt.xlabel('Strain [%]')
plt.ylabel('Force [kN]')
plt.title('Force vs. Strain for C-tests')
plt.grid()
plt.legend()
# Save the plot to a file
plt.savefig('Force_Strain_C-tests')
# Show the plot
plt.show()
```

F.11 4-point bending test

```

import pandas as pd
import matplotlib.pyplot as plt
import numpy as np

# Define file names, labels and colors
file_names = ['S2_4point_data.xlsx', 'S3_4point_data.xlsx', 'S4_4point_data.xlsx']
labels = ['S2', 'S3', 'S4']
colors = ['crimson', 'peru', 'indigo']

## Force - Time (all curves)
# Read in the data and plot it
for i, (file_name, label) in enumerate(zip(file_names, labels)):
    df = pd.read_excel(file_name, skiprows=2, usecols='A,C', header=None,
        ↪ names=['Time', 'Force'])
    df['Time'] = df['Time'] - df['Time'][0]
    # Skip every 20th value
    df = df.iloc[2::20, :]
    plt.plot(df['Time'], -df['Force'], label = label + ' 4-point',
        ↪ color=colors[i%len(colors)])
# Add axis labels, legend and save figure
plt.xlabel('Time [s]')
plt.ylabel('Force [kN]')
plt.title('Force vs. Time for 4-point bending tests')
plt.legend(loc='upper left')
plt.grid()
plt.savefig('Bend_All_Force_Time')
# Show the plot
plt.show()

## Force - Displacement (all curves)
# Read in the data and plot it
for i, (file_name, label) in enumerate(zip(file_names, labels)):
    df = pd.read_excel(file_name, skiprows=2, usecols='B,C', header=None,
        ↪ names=['Displacement', 'Force'])
    df['Displacement'] = df['Displacement'] - df['Displacement'][0]
    # Skip every 20th value
    df = df.iloc[2::20, :]
    plt.plot(-df['Displacement'], -df['Force'], label = label+ ' 4-point',
        ↪ color=colors[i%len(colors)])

# Add axis labels, legend and save figure
plt.xlabel('Displacement [mm]')
plt.ylabel('Force [kN]')
plt.title('Force vs. Displacement for 4-point bending tests')
plt.legend()
plt.grid()
plt.savefig('Bend_All_Force_Displ')

```

```

# Show the plot
plt.show()

## Displacement - Time (all curves)
# Read in the data and plot it
for i, (file_name, label) in enumerate(zip(file_names, labels)):
    df = pd.read_excel(file_name, skiprows=2, usecols='A,B', header=None,
        ↪ names=['Time', 'Displacement'])
    df['Time'] = df['Time'] - df['Time'][0]
    df['Displacement'] = df['Displacement'] - df['Displacement'][0]
    # Skip every 20th value
    df = df.iloc[2::20, :]
    plt.plot(df['Time'], -df['Displacement'], label = label+ ' 4-point',
        ↪ color=colors[i%len(colors)])

# Add axis labels, legend and save figure
plt.xlabel('Time [s]')
plt.ylabel('Displacement [mm]')
plt.title('Displacement vs. Time for 4-point bending tests')
plt.legend(loc='upper left')
plt.grid()
plt.savefig('Bend_All_Displacement_Time')
# Show the plot
plt.show()

## Force - Laser 1 Displacement (all curves)
# Read in the data and plot it
for i, (file_name, label) in enumerate(zip(file_names, labels)):
    df = pd.read_excel(file_name, skiprows=2, usecols='C,D', header=None,
        ↪ names=['Force', 'L1'])
    df['L1'] = df['L1'] - df['L1'][0]
    # Skip every 1000th value
    df = df.iloc[2::1000, :]
    plt.plot(-df['L1'], -df['Force'], label = label+ ' 4-point',
        ↪ color=colors[i%len(colors)])

# Add axis labels, legend and save figure
plt.xlabel('Displacement [mm]')
plt.ylabel('Force [kN]')
plt.title('Force vs. Laser 1 Displacement for 4-point bending tests')
plt.legend()
plt.grid()
plt.savefig('Bend_All_Force_L1Disp')
# Show the plot
plt.show()

## Force - Laser 2 Displacement (all curves)
# Read in the data and plot it
for i, (file_name, label) in enumerate(zip(file_names, labels)):

```

```

df = pd.read_excel(file_name, skiprows=2, usecols='C,E', header=None,
↳ names=['Force', 'L2'])
df['L2'] = df['L2'] - df['L2'][0]
# Skip every 1000th value
df = df.iloc[2::1000, :]
plt.plot(-df['L2'], -df['Force'], label = label+ ' 4-point',
↳ color=colors[i%len(colors)])

# Add axis labels, legend and save figure
plt.xlabel('Displacement [mm]')
plt.ylabel('Force [kN]')
plt.title('Force vs. Laser 2 Displacement for 4-point bending tests')
plt.legend()
plt.grid()
plt.savefig('Bend_All_Force_L2Disp')
# Show the plot
plt.show()

## Force - Laser 3 Displacement (all curves)
# Read in the data and plot it
for i, (file_name, label) in enumerate(zip(file_names, labels)):
    df = pd.read_excel(file_name, skiprows=2, usecols='C,F', header=None,
↳ names=['Force', 'L3'])
    df['L3'] = df['L3'] - df['L3'][0]
    # Skip every 1000th value
    df = df.iloc[2::1000, :]
    plt.plot(-df['L3'], -df['Force'], label = label+ ' 4-point',
↳ color=colors[i%len(colors)])

# Add axis labels, legend and save figure
plt.xlabel('Displacement [mm]')
plt.ylabel('Force [kN]')
plt.title('Force vs. Laser 3 Displacement for 4-point bending tests')
plt.legend()
plt.grid()
plt.savefig('Bend_All_Force_L3Disp')
# Show the plot
plt.show()

## Force - Time (average)
curves = []
for file_name, label in zip(file_names, labels):
    df = pd.read_excel(file_name, skiprows=2, usecols='A,C', header=None,
↳ names=['Time', 'Force'])
    df['Time'] = df['Time'] - df['Time'][0]
    # store data for each curve in a list
    curves.append((df['Time'], -df['Force']))

# Compute average curve
avg_time = np.mean([curve[0] for curve in curves], axis=0)

```

```

avg_force = np.mean([curve[1] for curve in curves], axis=0)

# Plot average curve
plt.plot(avg_time, avg_force, label='Average', color='black')
# Add axis labels, legend and save figure
plt.xlabel('Time [s]')
plt.ylabel('Force [kN]')
plt.title('Average Force vs. Time for 4-point bending tests')
plt.legend(loc='upper left')
plt.grid()
plt.savefig('Bend_Average_Force_Time')
# Show the plot
plt.show()

## Force - Displacement (average)
curves = []
for file_name, label in zip(file_names, labels):
    df = pd.read_excel(file_name, skiprows=2, usecols='B,C', header=None,
        ↪ names=['Displacement', 'Force'])
    df['Displacement'] = df['Displacement'] - df['Displacement'][0]
    # store data for each curve in a list
    curves.append((-df['Displacement'], -df['Force']))

# Compute average curve
avg_displacement = np.mean([curve[0] for curve in curves], axis=0)
avg_force = np.mean([curve[1] for curve in curves], axis=0)

# Plot average curve
plt.plot(avg_displacement, avg_force, label='Average', color='black')
# Add axis labels, legend and save figure
plt.xlabel('Displacement [mm]')
plt.ylabel('Force [kN]')
plt.title('Average Force vs. Displacement for 4-point bending tests')
plt.legend(loc='upper left')
plt.grid()
plt.savefig('Bend_Average_Force_Displ')
# Show the plot
plt.show()

## Displacement - Time (average)
curves = []
for file_name, label in zip(file_names, labels):
    df = pd.read_excel(file_name, skiprows=2, usecols='A,B', header=None,
        ↪ names=['Time', 'Displacement'])
    df['Displacement'] = df['Displacement'] - df['Displacement'][0]
    # store data for each curve in a list
    curves.append((df['Time'], -df['Displacement']))

# Compute average curve
avg_time = np.mean([curve[0] for curve in curves], axis=0)

```

```

avg_disp = np.mean([curve[1] for curve in curves], axis=0)

# Plot average curve
plt.plot(avg_time, avg_disp, label='Average', color='black')
# Add axis labels, legend and save figure
plt.xlabel('Time [s]')
plt.ylabel('Displacement [mm]')
plt.title('Average Displacement vs. Time for 4-point bending tests')
plt.legend(loc='upper left')
plt.grid()
plt.savefig('Bend_Average_Displacement_Time')
# Show the plot
plt.show()

### Individual plots for each bending test
# Read in the data and plot it
for i, (file_name, label) in enumerate(zip(file_names, labels)):
    df = pd.read_excel(file_name, skiprows=2, usecols='A,B,C', header=None,
        ↪ names=['Time', 'Displacement', 'Force'])
    df['Time'] = df['Time'] - df['Time'][0]
    df['Displacement'] = df['Displacement'] - df['Displacement'][0]
    # Skip every 20th value
    df = df.iloc[2::20, :]

## Force - Time
plt.plot(df['Time'], -df['Force'], color=colors[i%len(colors)])
# Add axis labels
plt.xlabel('Time [s]')
plt.ylabel('Force [kN]')
plt.title('Force vs. Time for '+ label + ' 4-point bending test')
plt.grid()
# Show the plots and save the figures
plt.savefig('Bend_Force_Time_'+label)
plt.show()

## Force - Displacement
plt.plot(-df['Displacement'], -df['Force'], color=colors[i%len(colors)])
# Add axis labels
plt.xlabel('Displacement [mm]')
plt.ylabel('Force [kN]')
plt.title('Force vs. Displacement for '+ label + ' 4-point bending test')
plt.grid()
# Show the plots and save the figures
plt.savefig('Bend_Force_Displacement_'+label)
plt.show()

## Displacement - Time
plt.plot(df['Time'], -df['Displacement'], color=colors[i%len(colors)])
# Add axis labels
plt.xlabel('Time [s]')

```



```

plt.ylabel('Displacement [mm]')
plt.title('Displacement vs. Time for '+ label +' 4-point bending test')
plt.grid()
# Show the plots and save the figures
plt.savefig('Bend_Displ_Time_'+label)
plt.show()

## Force - Laser Displacements
# Read in the data and plot it
for i, (file_name, label) in enumerate(zip(file_names, labels)):
    df = pd.read_excel(file_name, skiprows=2, usecols='C,D,E,F', header=None,
        ↪ names=['Force', 'L1', 'L2', 'L3'])

    df['L1'] = df['L1'] - df['L1'][0]
    df['L2'] = df['L2'] - df['L2'][0]
    df['L3'] = df['L3'] - df['L3'][0]

    # Skip every 1000th value
    df = df.iloc[2::1000, :]

    # Plot Force vs. Laser Displacements
    plt.plot(-df['L1'], -df['Force'], color='tab:blue', label='Laser 1')
    plt.plot(-df['L2'], -df['Force'], color='tab:orange', label='Laser 2')
    plt.plot(-df['L3'], -df['Force'], color='tab:green', label='Laser 3')
    # Add axis labels
    plt.xlabel('Displacement [mm]')
    plt.ylabel('Force [kN]')
    plt.title('Force vs. Laser Displacement for '+ label +' 4-point bending
        ↪ test')
    plt.legend()
    plt.grid()
    # Show the plots and save the figures
    plt.savefig('Bend_Force_LaserDisp_'+label)
    plt.show()

## Laser Displacements - Time
# Read in the data and plot it
for i, (file_name, label) in enumerate(zip(file_names, labels)):
    df = pd.read_excel(file_name, skiprows=2, usecols='A,D,E,F', header=None,
        ↪ names=['Time', 'L1', 'L2', 'L3'])

    df['Time'] = df['Time'] - df['Time'][0]
    df['L1'] = df['L1'] - df['L1'][0]
    df['L2'] = df['L2'] - df['L2'][0]
    df['L3'] = df['L3'] - df['L3'][0]

    # Skip every 1000th value
    df = df.iloc[2::1000, :]

    # Plot Laser Displacements vs. Time

```

```
plt.plot(df['Time'], -df['L1'], color='tab:blue', label='Laser 1')
plt.plot(df['Time'], -df['L2'], color='tab:orange', label='Laser 2')
plt.plot(df['Time'], -df['L3'], color='tab:green', label='Laser 3')
# Add axis labels
plt.xlabel('Time [s]')
plt.ylabel('Displacement [mm]')
plt.title('Laser Displacement vs. Time for '+ label +' 4-point bending test')
plt.legend()
plt.grid()
# Show the plots and save the figures
plt.savefig('Bend_Time_LaserDisp_'+label)
plt.show()
```

F.12 S-N curves

```

import numpy as np
import matplotlib.pyplot as plt

def sn_curve(a, b, R, kfat):
    A = (1 - R) / (a * (b - R))
    N = 10 ** ((1 - kfat) / A)
    return N

# Maximum strength tolerated
max_strength_6 = 2526
max_strength_7 = 1812
# Critical strengths for diagonal 6 and 7
strength_6 = [2526, 1456, 1023, 788, 641]
strength_7 = [1812, 978, 670, 509, 411]
# Parameters for S-N curve
a = 9.5
b = 1.1
R_6 = 0.77
R_7 = 0.75
# Generate kfat values
kfat_6 = [strength / max_strength_6 for strength in strength_6]
kfat_7 = [strength / max_strength_7 for strength in strength_7]
# Calculate number of cycles for kfat_6 and kfat_7
cycles_6 = [sn_curve(a, b, R_6, kfat) for kfat in kfat_6]
cycles_7 = [sn_curve(a, b, R_7, kfat) for kfat in kfat_7]

fig, ax = plt.subplots(figsize=(8, 6))
# Plotting the S-N curves with log scale for N
ax.plot(np.log10(cycles_6), kfat_6, label='Diagonal 6, R=0.77')
ax.plot(np.log10(cycles_7), kfat_7, label='Diagonal 7, R=0.75')
ax.set_xlabel('Log N')
ax.set_ylabel('$k_{fat}$')
ax.set_title('S-N curve for Tretten bridge diagonal 6 and 7')
ax.grid(True)
ax.legend()
# Save figure and display the plot
fig.savefig('SN_curves.png')
plt.show()

```

G Pictures from *Tretten* bridge elements

G.1 Tension test specimens

The appendix contains a diverse range of pictures related to the tension tests, depicting various stages of preparation and setup, such as the gluing of specimen S_4 , reinforcement with screws, and placement of steel plates, dowels, and lasers. Additionally, it includes pictures that capture the distinct fracture lines observed in each specimen, with black markings highlighting them for easy identification of the experimental results.

Gluing of specimen S4



Longitudinal cracks

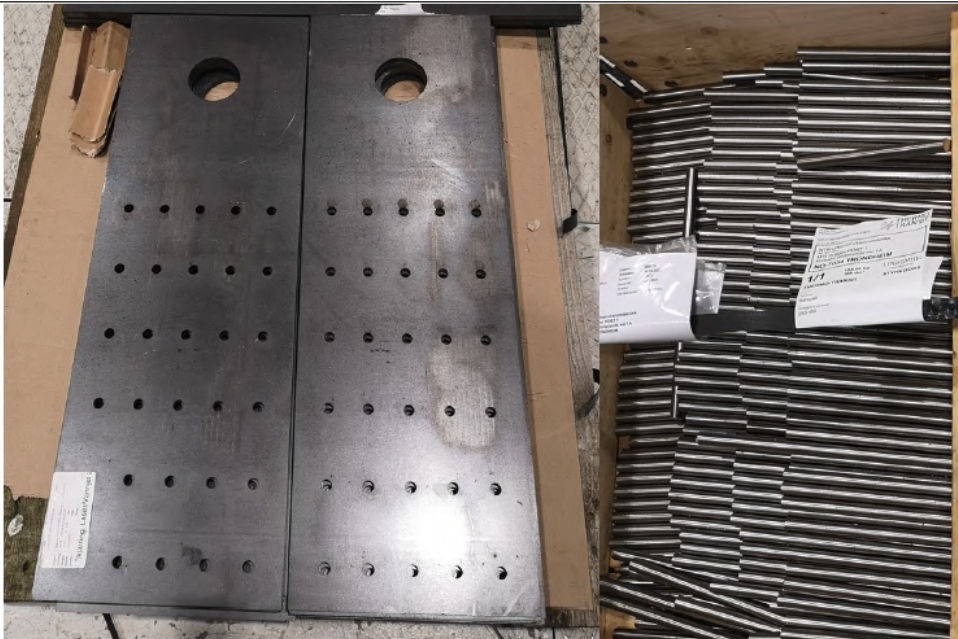


Glued with wood glue

Steel components

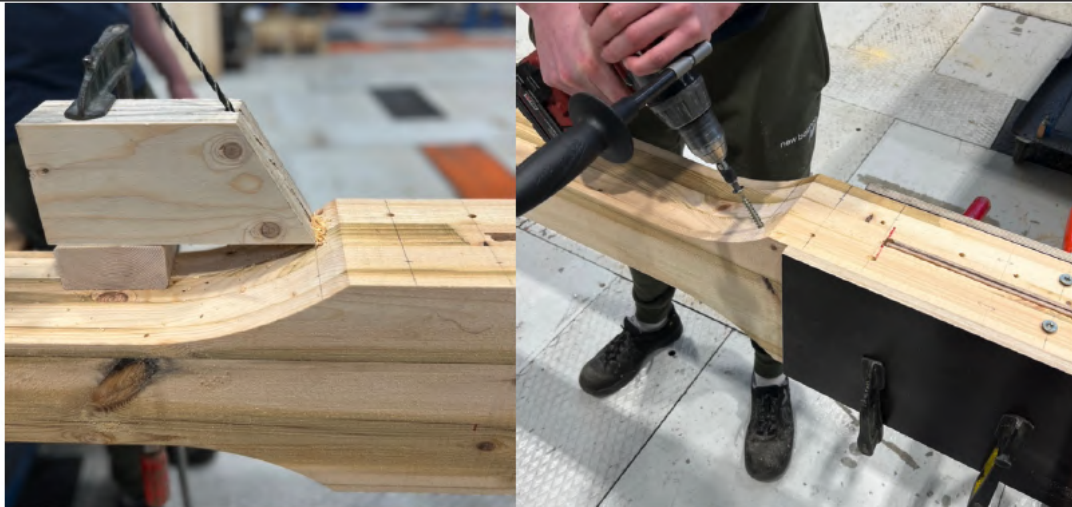


Screws and drill bit



Steel plates and dowels

Reinforcement with screws and mounting of steel plates and dowels



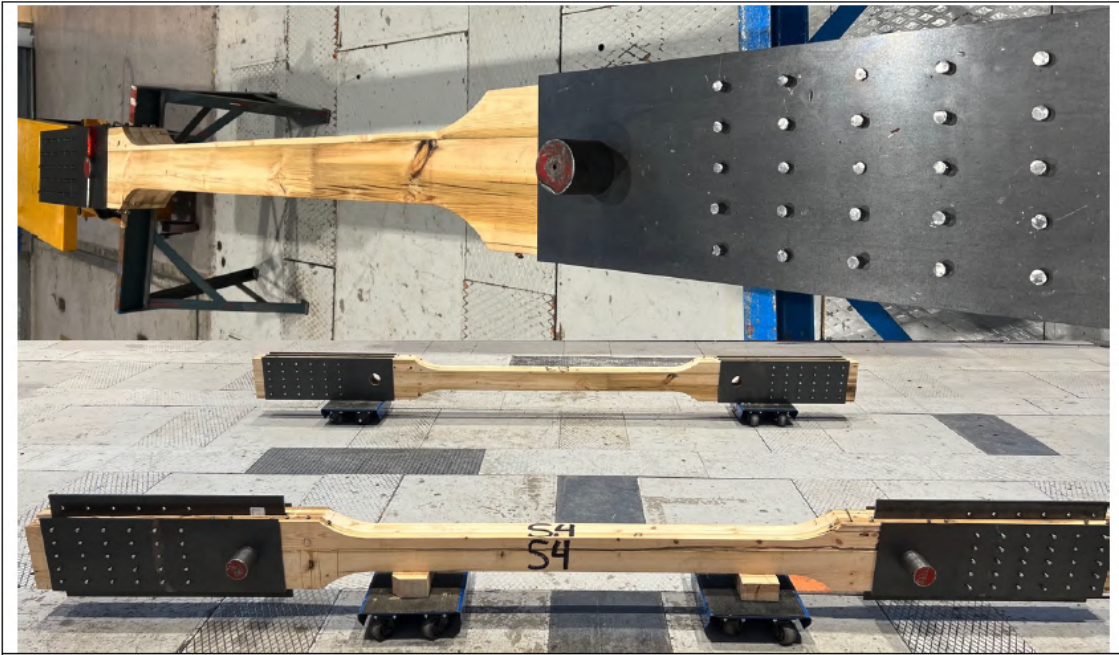
Predrilling and screwing of inclined screws



Cuts off screw tips for safety reasons

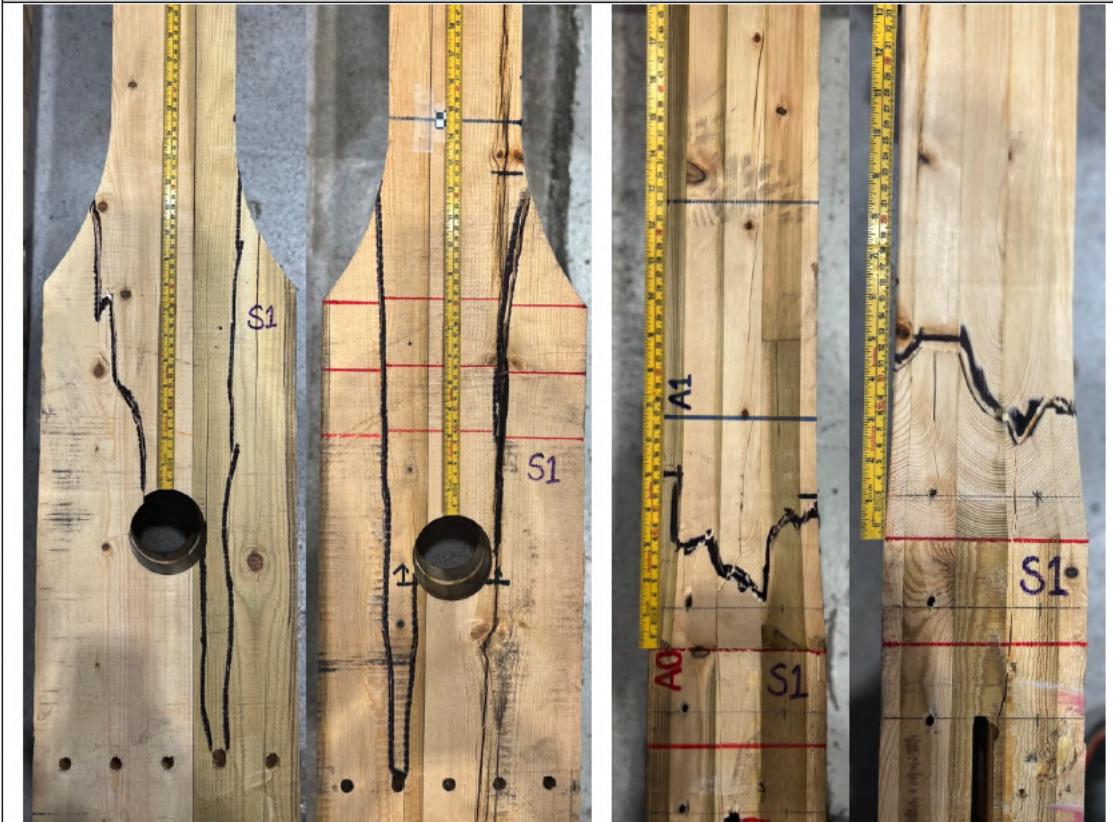


Crooked holes in S3 posed challenges for plate alignment, requiring pre-drilled dowel holes



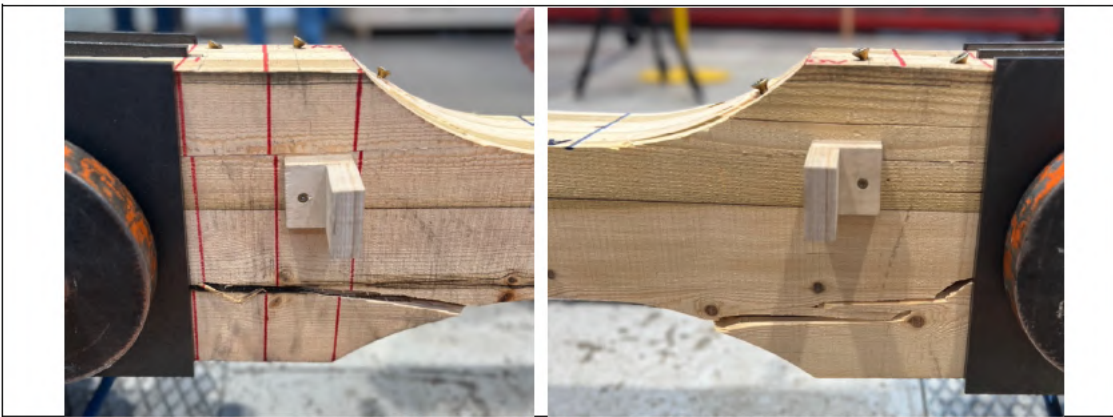
Complete mounting of steel plates and dowels

S1



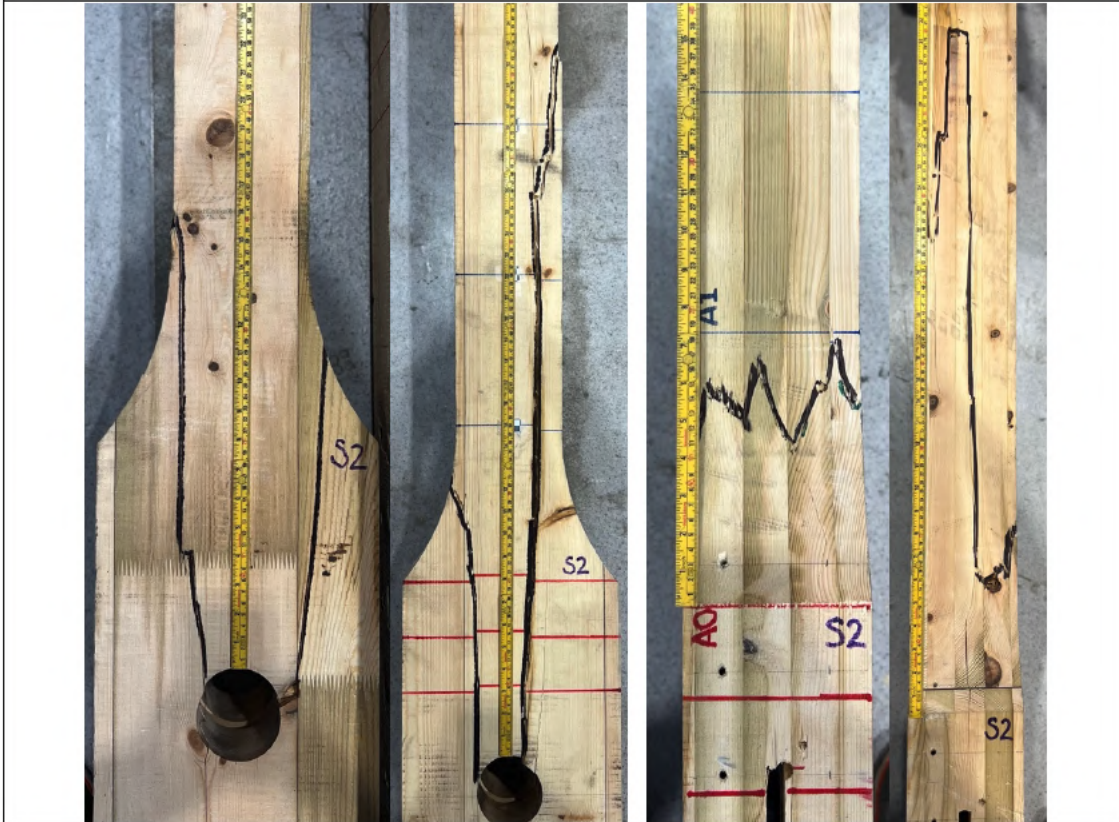
Side view

Top and bottom view



Side view (without marking)

S2



Side view

Top and bottom view



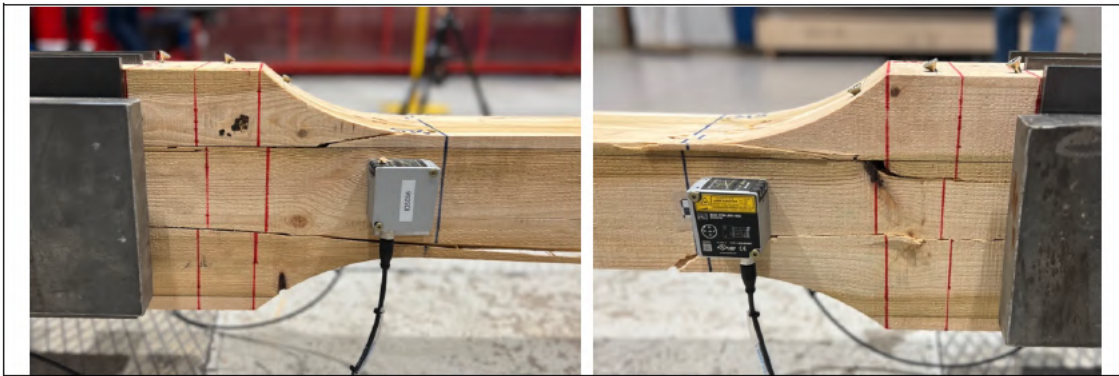
Side view (without marking)

S3



Side view

Top and bottom view



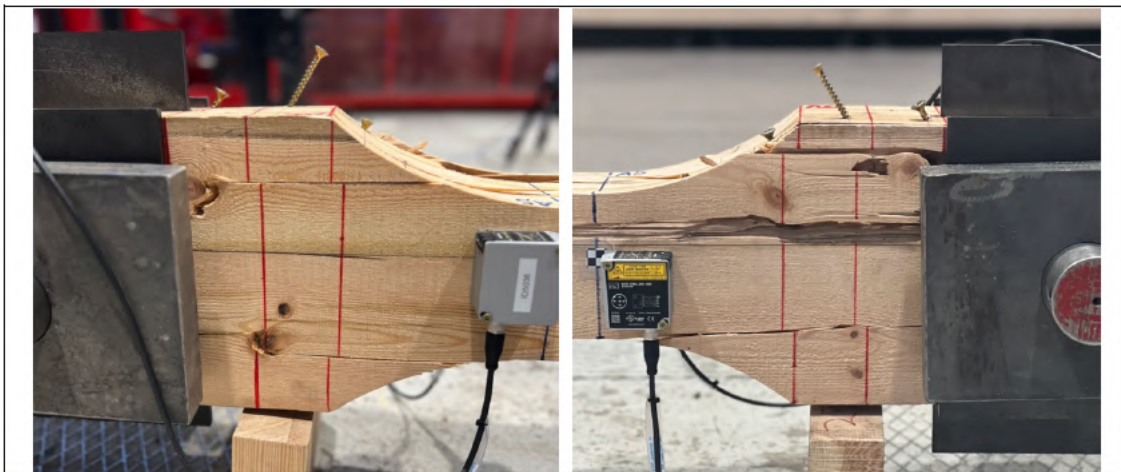
Side view (without marking)

S4



Side view

Top and bottom view



Side view (without marking)

G.2 Block failure test specimens

The appendix contains a diverse range of pictures pertaining to the block failure tests. These pictures depict the stages of preparation and setup for the tests, including the reinforcement with screws and the placement of strain gauges, steel plates, dowels, and LVDTs. Additionally, there are pictures capturing the distinct fracture modes observed in each specimen. Furthermore, the appendix features pictures of the fracture lines present in each specimen, along with visuals from a camera monitoring the weak end during the tests.

Strain gauges and mounting equipment



Sanding paper and alcoholic anti-bacterial sanitiser

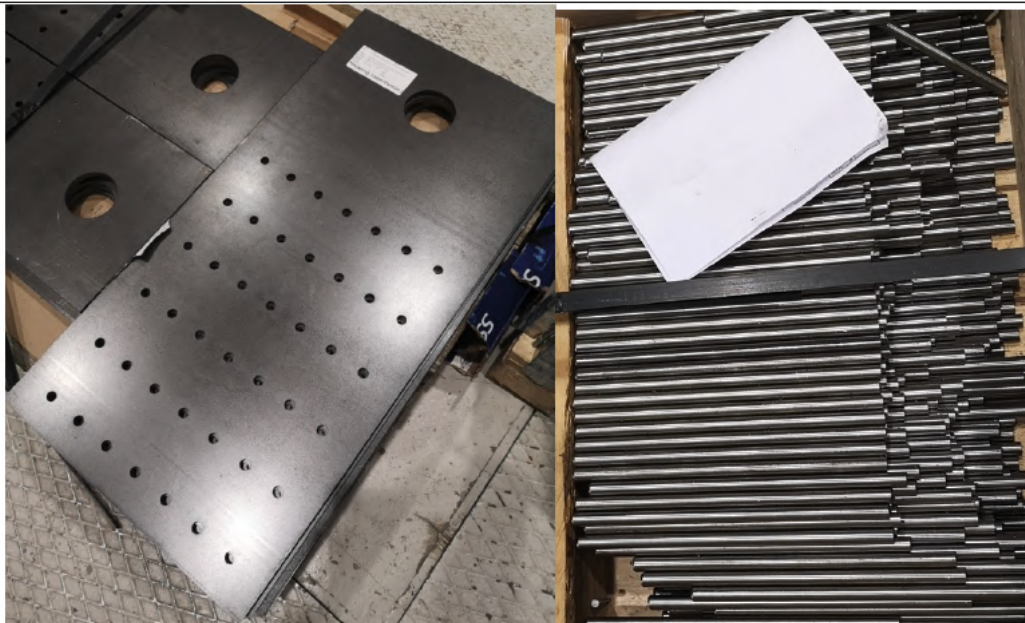


Adhesive and two types of strain gauges with different gauge factor

Steel components

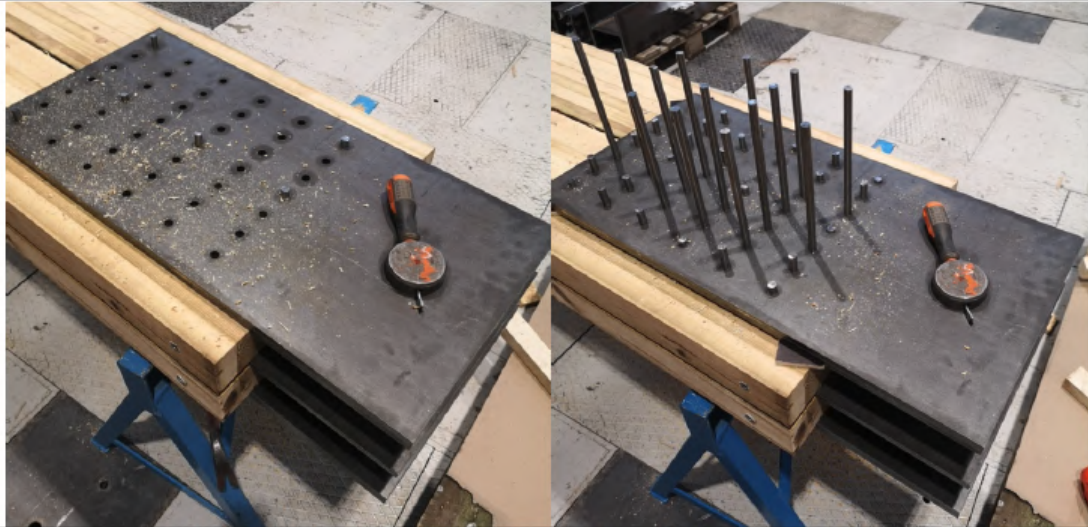


Screws and drill bit



Steel plates and dowels

Mounting of steel plates and dowels



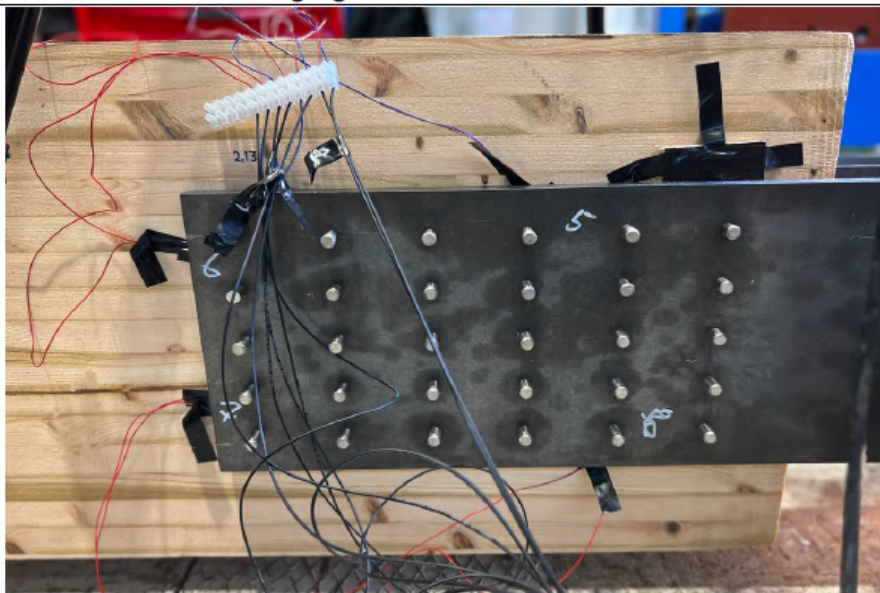
Predrilling of dowel holes before mounting steel plates on strong end



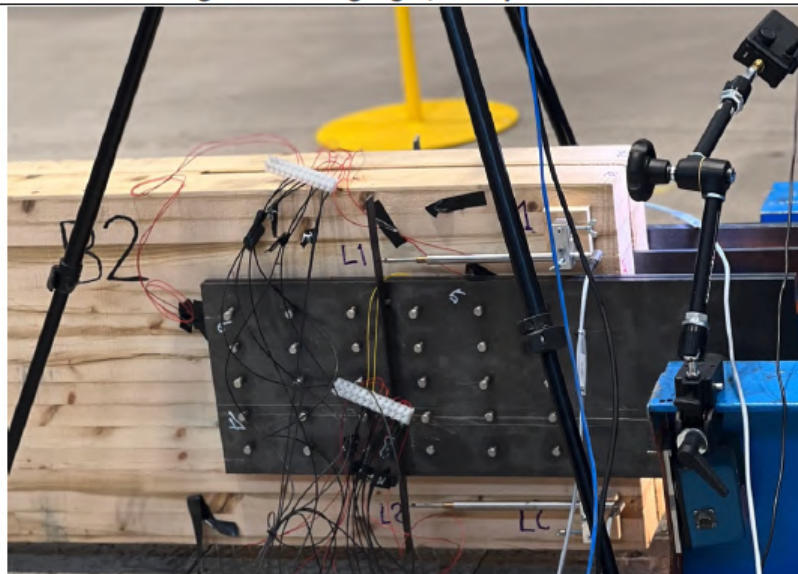
Before attaching the strain gauges to the weak end, the surface was sanded and cleaned



Strain gauges with different orientation



Mounting with strain gauges, steel plates and dowels



Complete mounting with LVDTs

B1



Side view



Side view without steel plates and dowels

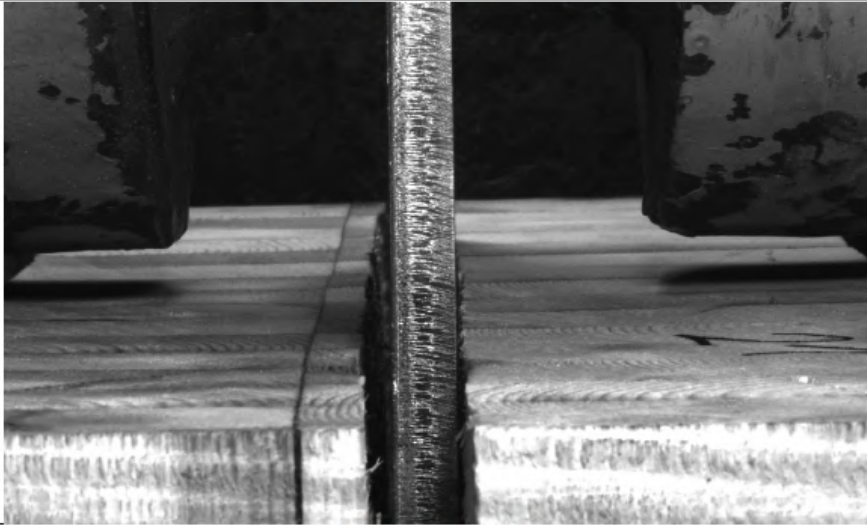




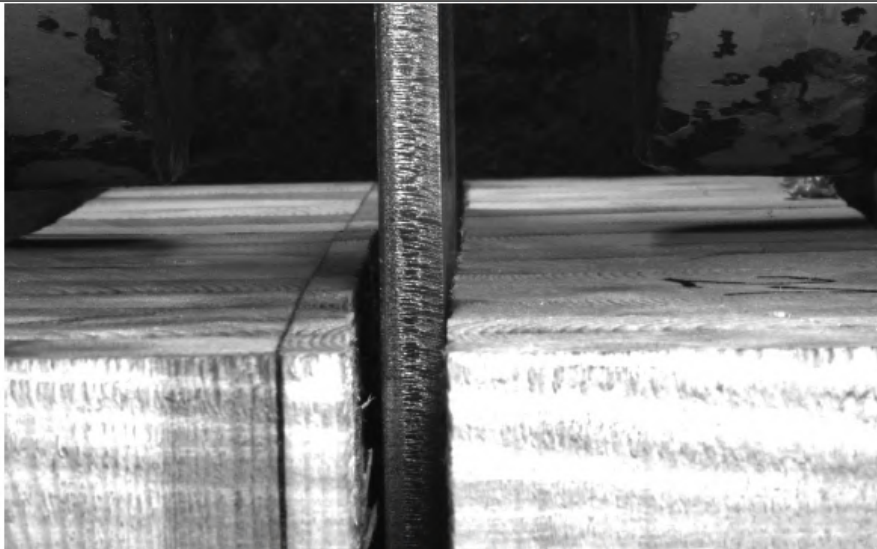
Weak end

Strong end

B1 – pictures from test



Start (picture 1)

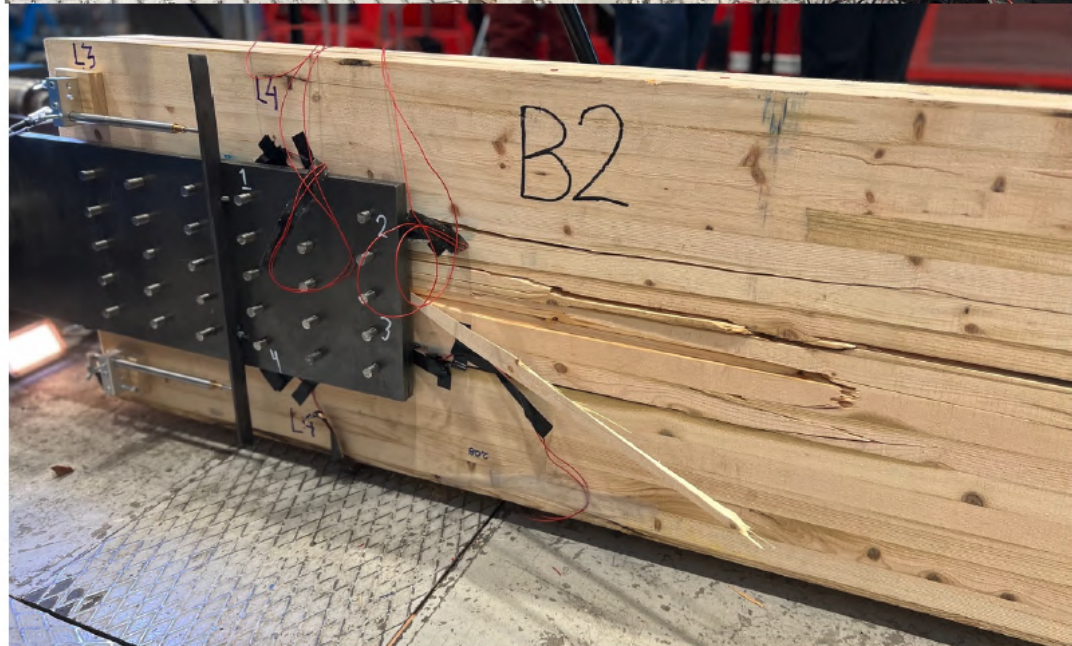
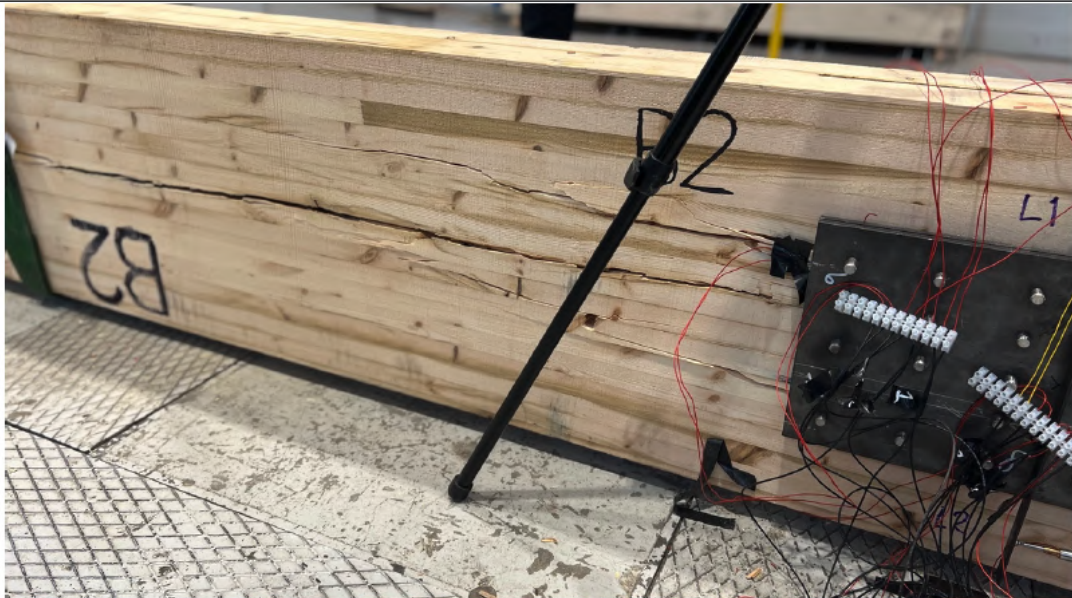


Before block failure (picture 1547)

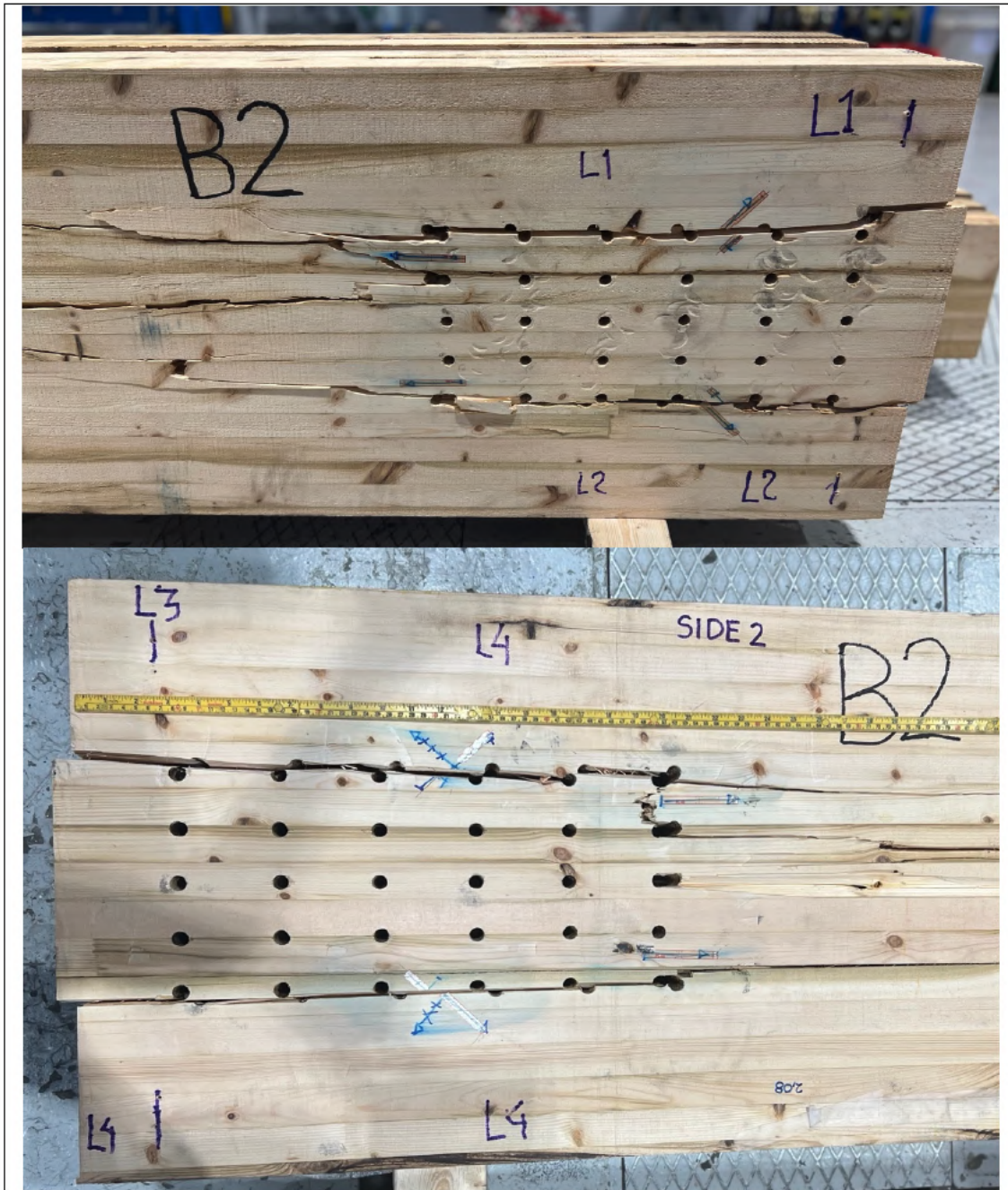


Block failure (picture 1549)

B2



Side view

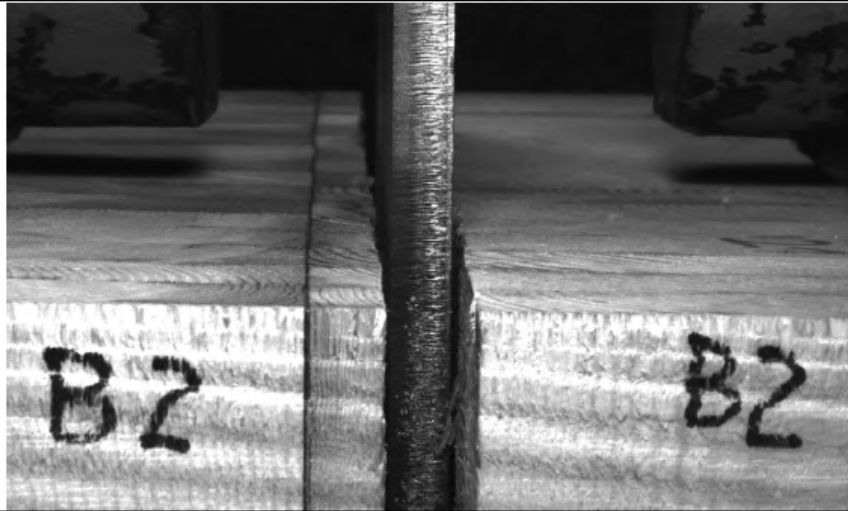


Side view without steel plates and dowels

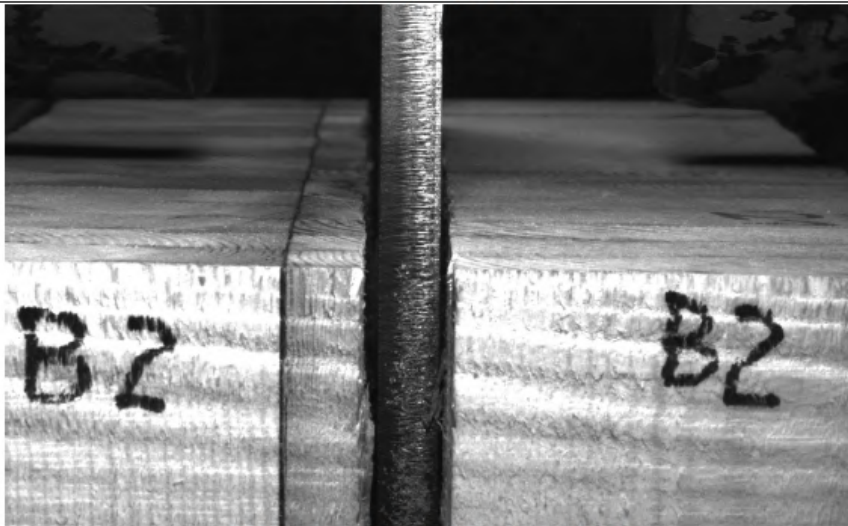


End view

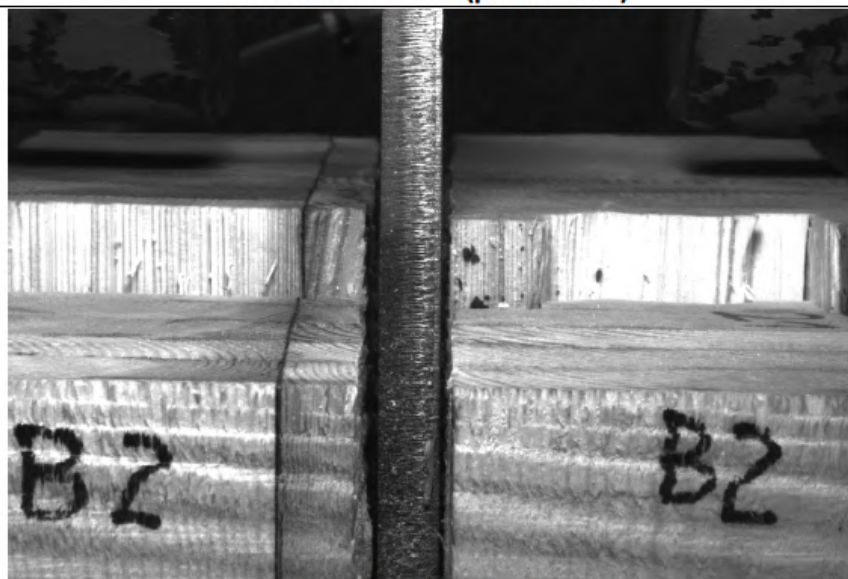
B2 – pictures from test



Start (picture 1)

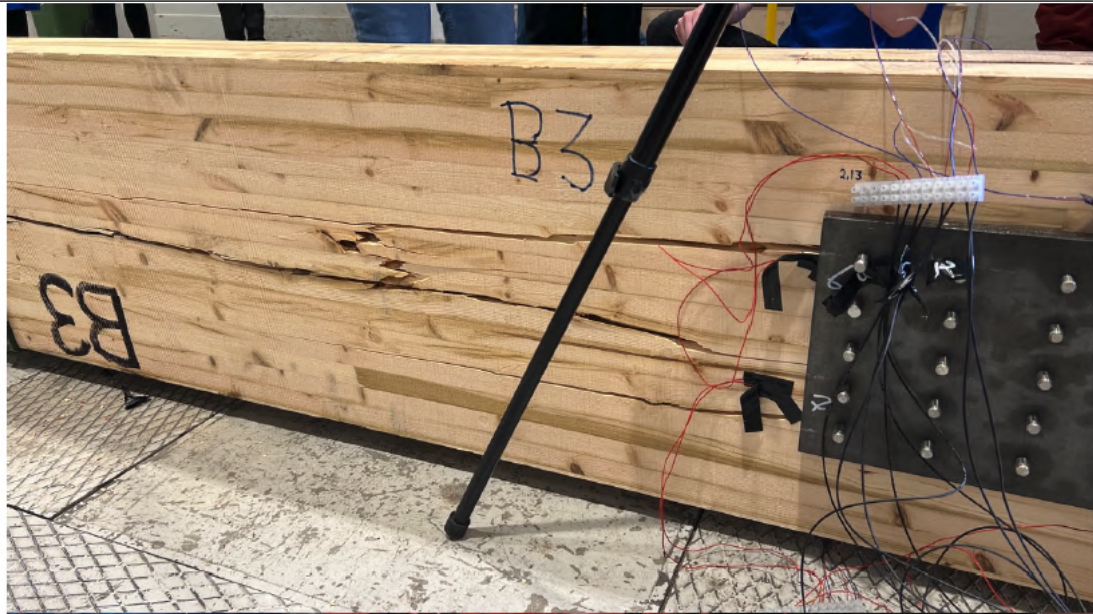


Before block failure (picture 1387)



Block failure (picture 1389)

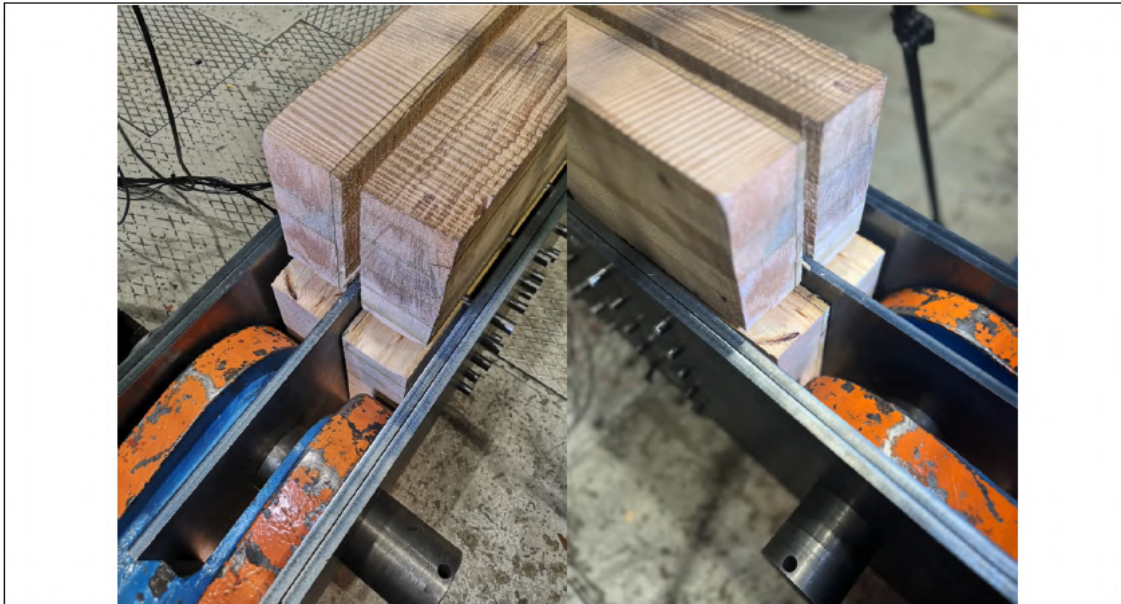
B3



Side view

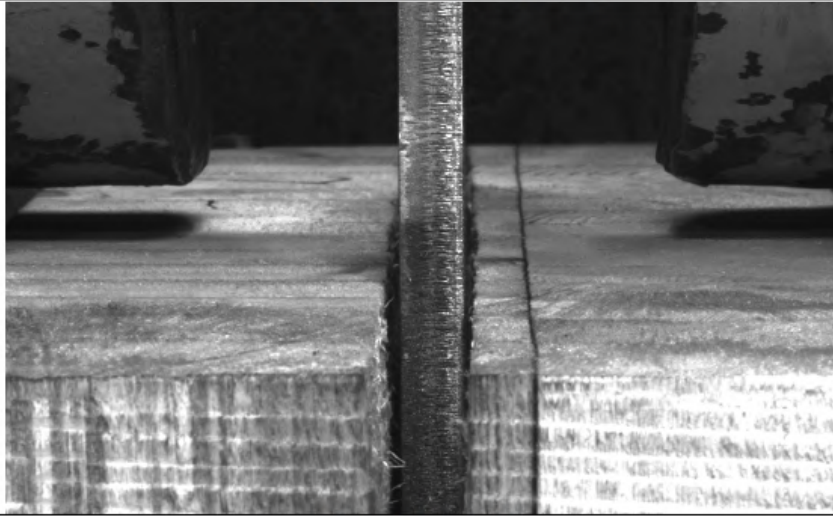


Side view without steel plates

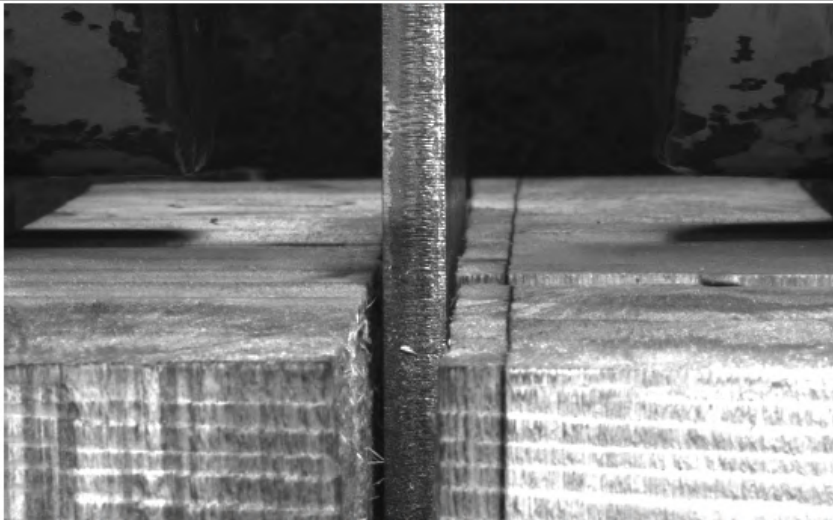


End view

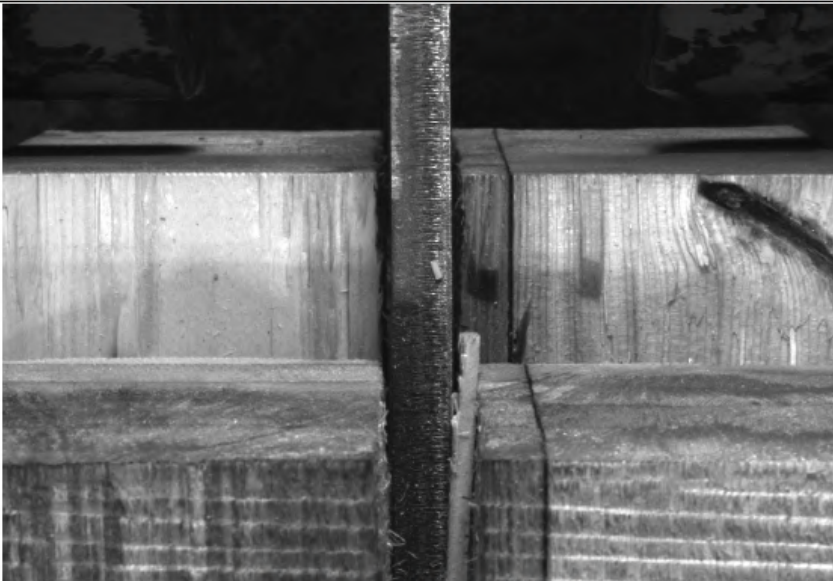
B3 – pictures from test



Start (picture 1)



Before block failure, in picture 3263 a crack occurs in the right part (picture 3377)



Block failure (picture 3379)

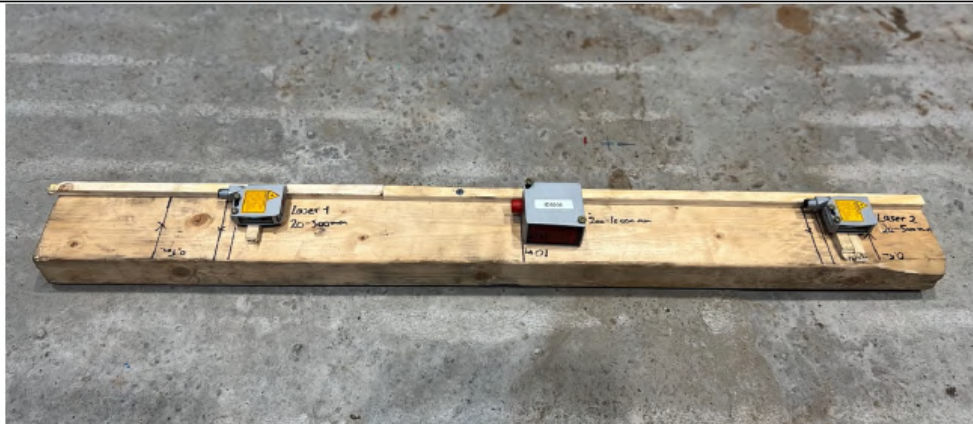
G.3 4-point bending specimens

The appendix features a variety of pictures related to the 4-point bending tests, including pictures of preparation and test setup, as well as pictures of the different fracture modes observed in each specimen. This include placement of supporting and loading pins, lasers and reinforcement of fractured part from tension test. Additionally, the appendix features pictures that capture the distinct fracture lines observed in each specimen, highlighted with red markings in the center zone. It should be noted, however, that pictures of specimen *S1* are not included in this collection, as the sensor data file associated with this specimen suffered from file corruption.

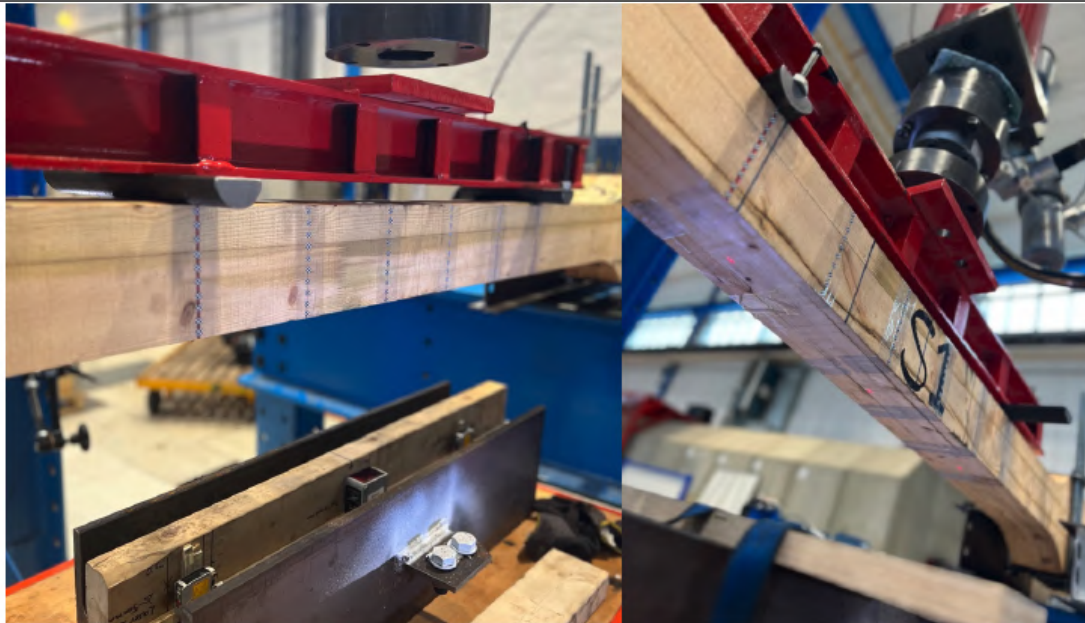
Test setup



Placement of markers for camera tracking



Laser distribution



Placement of lasers



Reinforcement with clamps of fractured parts from tension test



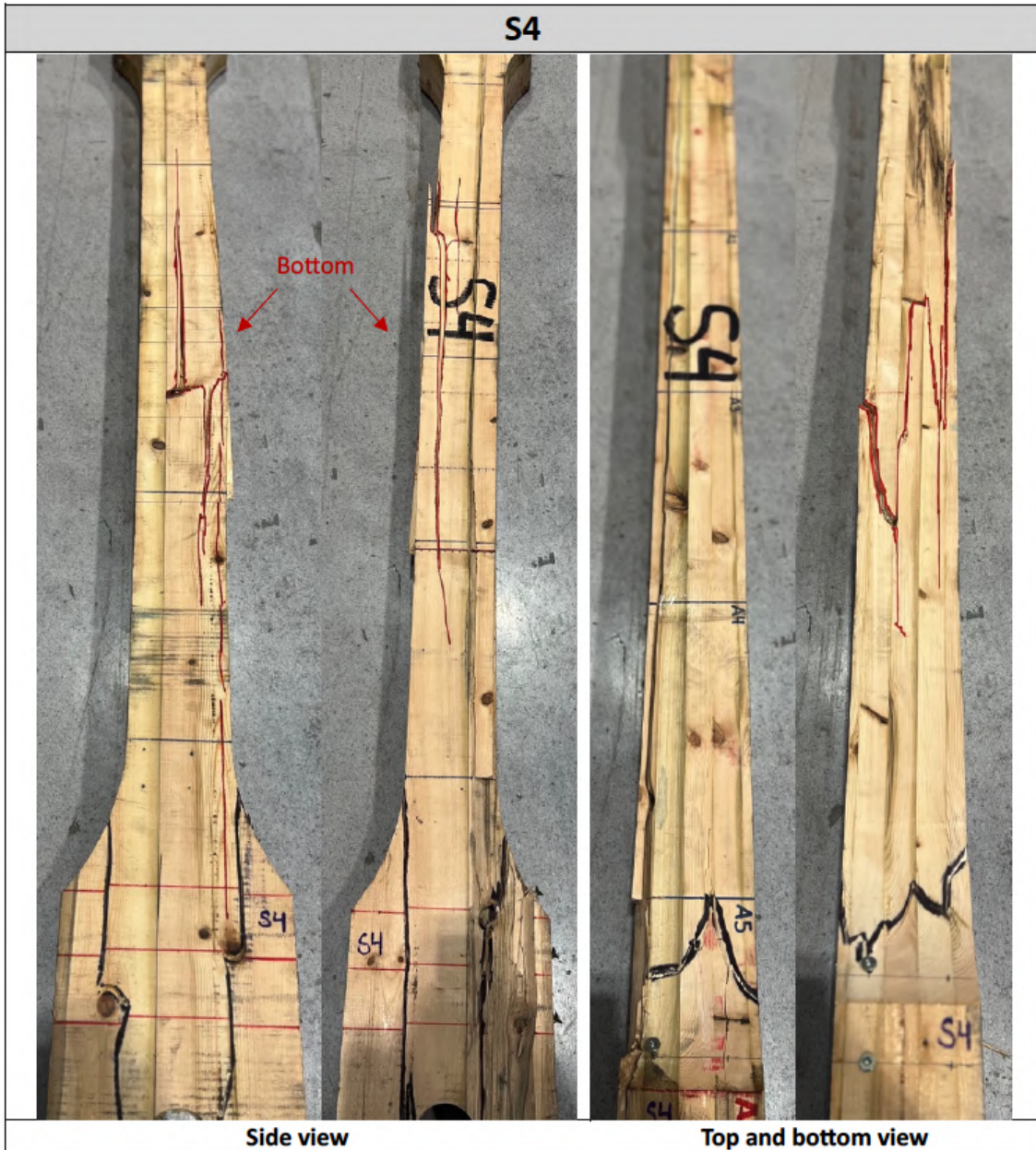
Horizontal beam secured with clamps and lasers protected from falling fracture parts



Complete setup with cameras on both sides







H Block from Tretten bridge

The appendix contains pictures of node 17B of the *Tretten* bridge, which is known as the lower node connected to diagonal 7 at the downstream axis. The remaining wooden parts from the block failure and the dowels were numbered and disassembled by NSIA, before being sent to NTNU. At NTNU, the dowels and wooden parts were successfully reassembled using the included manual.

Block from Tretten bridge









Overview picture of the node taken 29.09.2022 (NSIA)

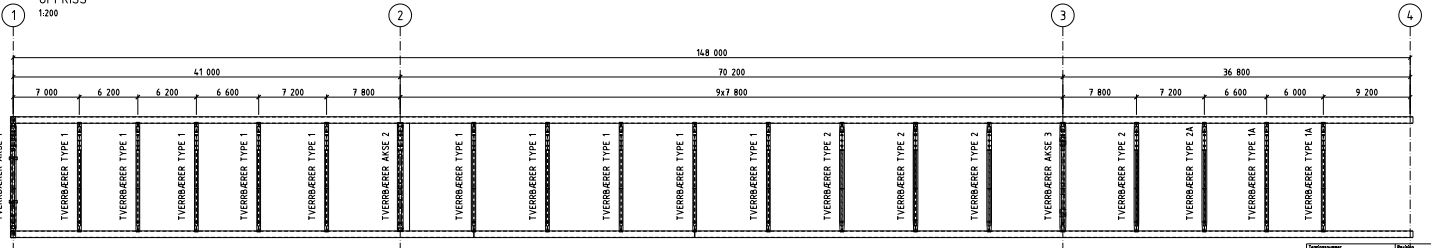
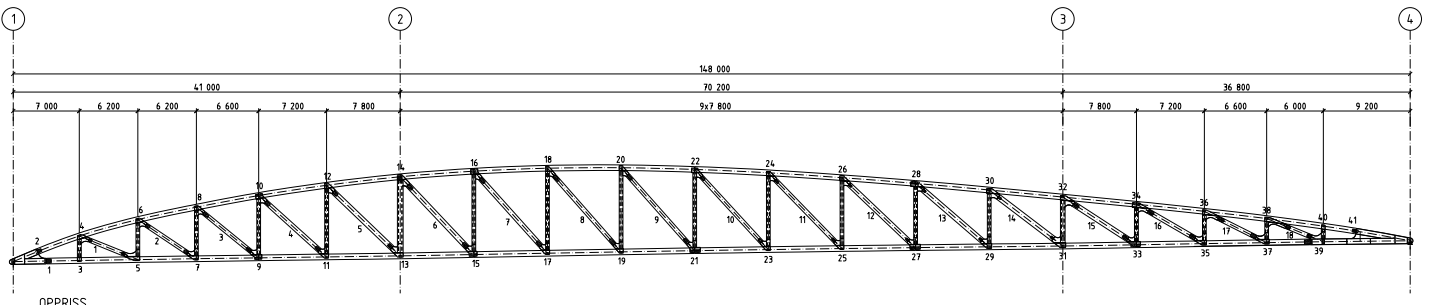


Overview picture of the node taken 15.11.2022 (NSIA)

I Drawings

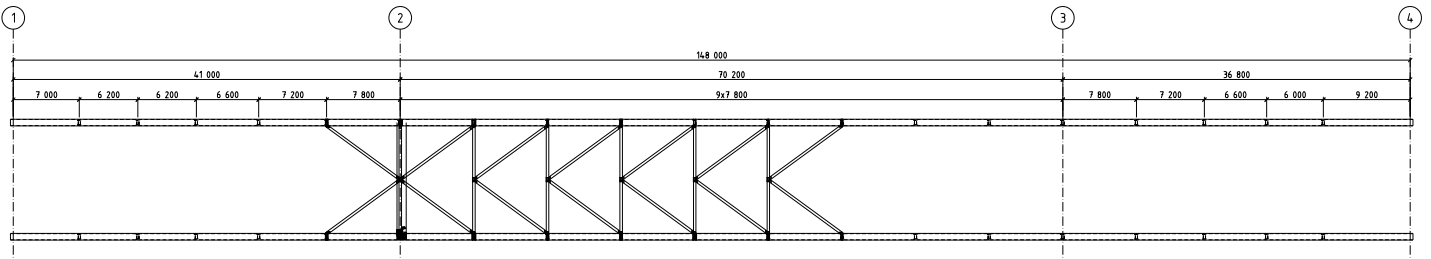
Following drawings were used for illustrations in this thesis. Note that the annotated scalings are not necessarily correct in an A4 format, and thus needs to be converted to A3. Including them as A3 in this *Master's thesis* would however impose challenges regarding printing, hence kept in A4 format. The borders indicates the A3 scale of the drawings. Nevertheless, they are included as illustrations.

I.1 Drawings of *Tretten*



PLAN TVERRBÆRERE
1:200

K300



PLAN VINDFAGVERK
1:200

FORKLARINGER:

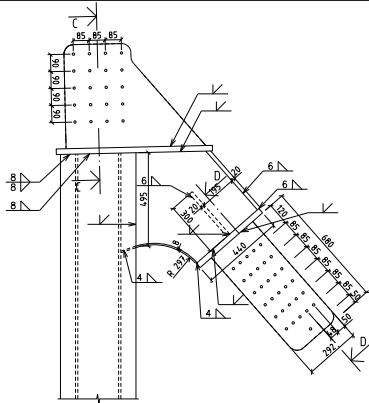
ANVISNINGER:

HENVISNINGER:

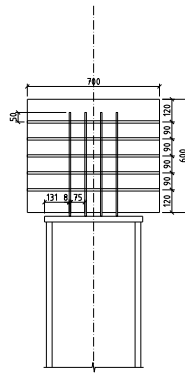
- 1. Oversikt
- 2. Fagverk

Se tegn. K100
Se tegn. K301-K370

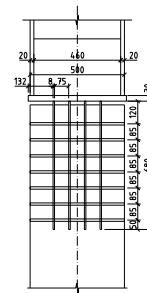
Revisjon	Revisjon gjelder	Dato	Av	Godkjent	Rev. dato
1	Som utført		JHE	FHE	HR
2	Godkjent som arbeidsplan. Ikke notat fra vegtrekontrollat		Skaar	2010/02/01-03/02	2011-10-24
			Skjerve	2010-05-28	
			Endre	FHE	
			Prosjekt led	Reigen	HR
			Opparbeid		
<p>Prosjekt: Fv 254-10-01 Fv 254-10-01 Prosjekt: Fv 254 Bruk nr: 05-1938 Tretten bru Fagverk Oversikt Plan og oppriss Form Som utført</p>					
<p>Prosjekt nr: 05-1938 Opparbeid av: JHE, FHE Godkjent av: HR Revisjonsnr: 521872 Prosjektleder: K300</p>					



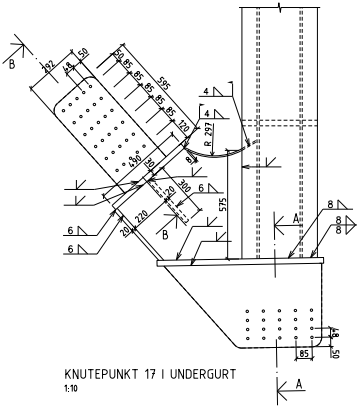
KNUTEPUNKT 18 I OVERGURT
1:10



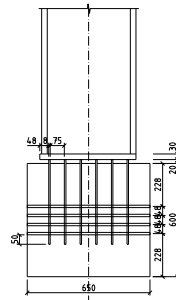
SNITT C-C
1:10



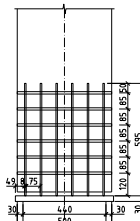
SNITT D-D
1:10



KNUTEPUNKT 17 I UNDERGURT
1:10



SNITT A-A
1:10



SNITT B-B
1:10

K338

FORKLARINGER:

BESTEMMELSER:

1. Krav til materialer og overflatebehandling, se materialiste, tegning K440

HENVISNINGER:

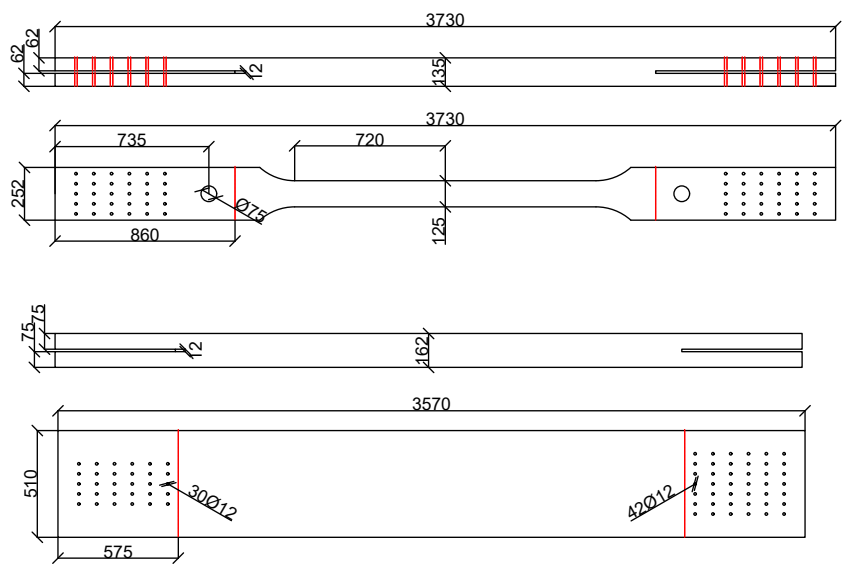
1. Fagverk. Oversikt. Plan og oppriss
2. Fagverk. Sammenstilling. Oppriss. Del 3
3. Knutepunkt 17 og 18. Snitt og detaljer del 1

Se tegn. K300
Se tegn. K312
Se tegn. K337

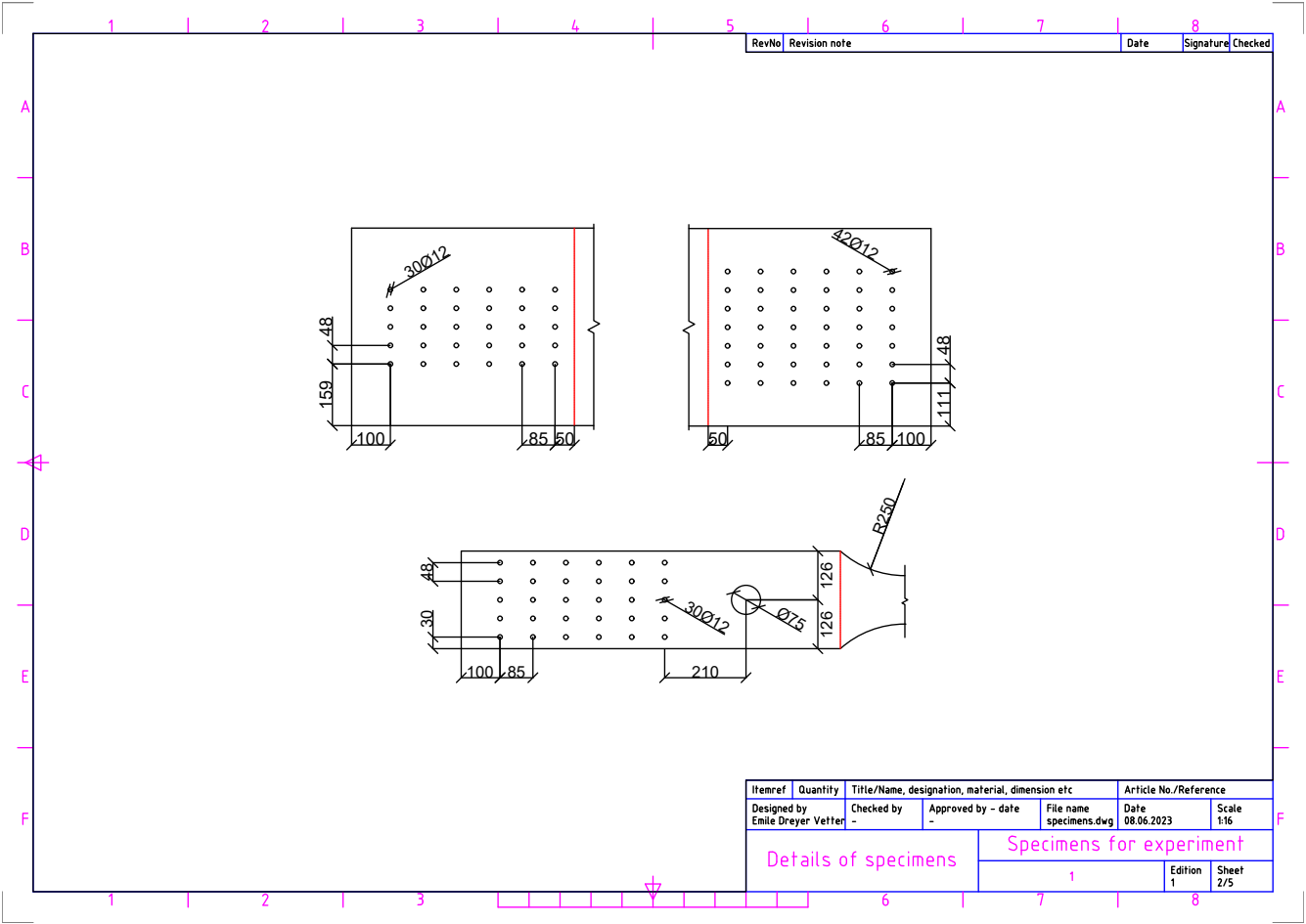
Revisjon	Revisjon gjelder	Dato	Av	Godkjent	Rev. dato
	Som utført		JHE	FHE	HR
	Godkjent som arbeiddokument. Ikke notat fra ingeniørkollegiet	Saksnr.	2010/02201-032		2011-10-24
		Sammenstilling	JHE		05-05-28
		Drømt	FHE		
		Prosjekt led	JHE		
		Drømt av			
<p>Fv 25a-10-01 Fase II Fv 25a Bru nr. 05-1838 Treften bru Innholdsfortegnelse 17 og 18 Slett og deler del 2 Som utført</p>					
<p>Norconsult</p>					
<p>PROJ-nummer: 0200006.102 Oppgjør: 05-1838 Målestokk: som vist</p>					
<p>Oppgjør av: JHE, FHE</p>		<p>Godkjent av: HB</p>		<p>Revisjonsnr.: 521872</p>	
				<p>Prosjektleder: K338</p>	

I.2 Drawings of specimens for experiments

RevNo	Revision note	Date	Signature	Checked
-------	---------------	------	-----------	---------



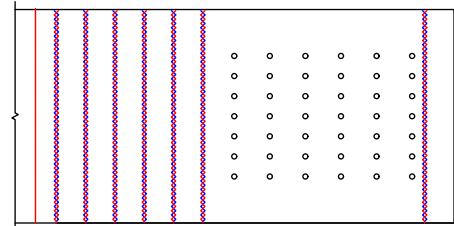
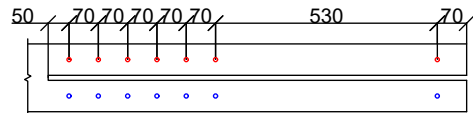
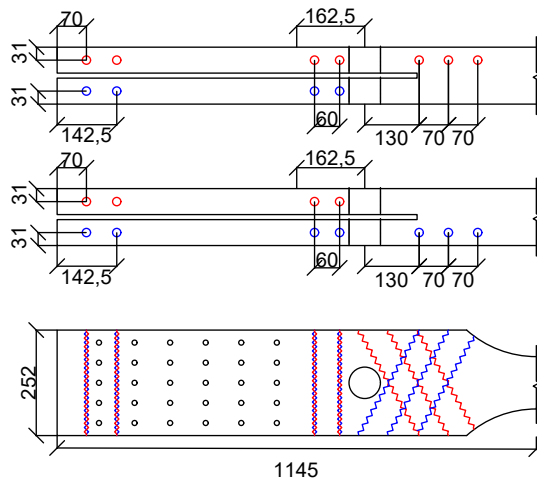
Itemref	Quantity	Title/Name, designation, material, dimension etc	Article No./Reference
Designed by Emile Dreyer Vetter	Checked by -	Approved by - date -	File name specimens.dwg
		Date 08.06.2023	Scale 1:16
Specimen S and B			Specimens for experiment
			1
		Edition 1	Sheet 1/5



RevNo	Revision note	Date	Signature	Checked

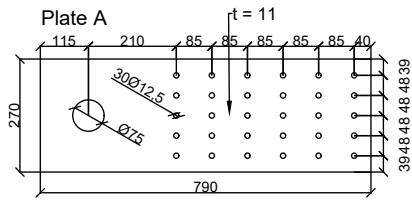
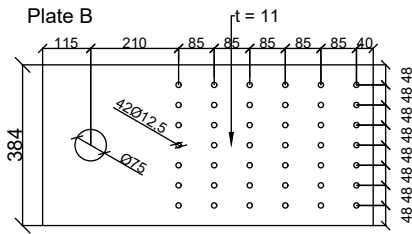
Itemref	Quantity	Title/Name, designation, material, dimension etc			Article No./Reference	
Designed by Emilie Dreyer Vetter		Checked by	Approved by - date	File name specimens.dwg	Date 08.06.2023	Scale 1:16
Details of specimens				Specimens for experiment		
				1	Edition 1	Sheet 2/5

RevNo	Revision note	Date	Signature	Checked



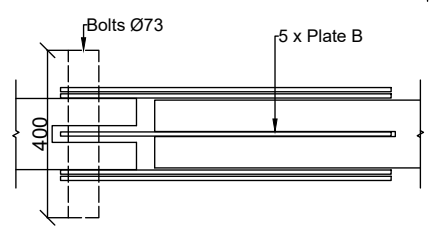
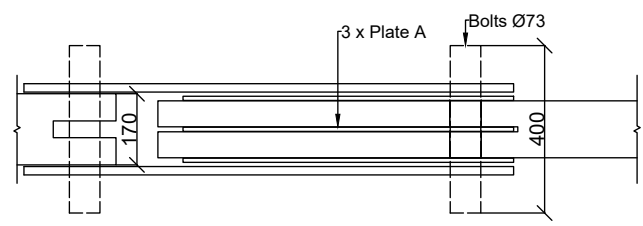
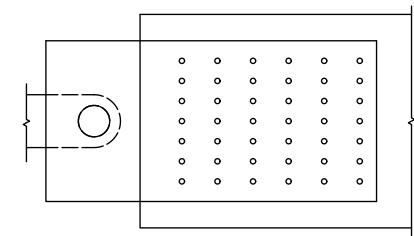
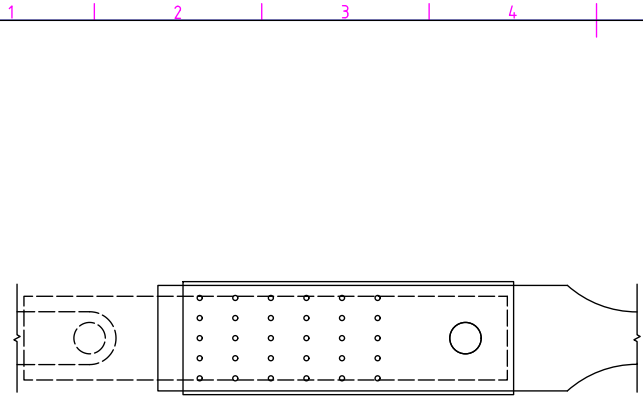
Itemref	Quantity	Title/Name, designation, material, dimension etc	Article No./Reference
Designed by Emile Dreyer Vetter	Checked by -	Approved by - date -	File name specimens.dwg
Reinforcement			Date 08.06.2023
Specimens for experiment			Scale 1:8
1			Edition 1
8			Sheet 3/5

RevNo	Revision note	Date	Signature	Checked



Itemref	Quantity	Title/Name, designation, material, dimension etc	Article No./Reference
Designed by Emile Dreyer	Checked by Vetter	Approved by - date -	File name specimens.dwg
Steel plates			Date 08.06.2023
Specimens for experiment			Scale 1:8
1			Edition 1
8			Sheet 4/5

RevNo	Revision note	Date	Signature	Checked



Itemref	Quantity	Title/Name, designation, material, dimension etc		Article No./Reference	
Designed by Emile Dreyer Vetter	Checked by -	Approved by - date -	File name specimens.dwg	Date 08.06.2023	Scale 1:8
Mounting			Specimens for experiment		
			1	Edition 1	Sheet 5/5

J Report

This report contains supplementary details regarding the conducted experiments. Certain information was not given priority to include in the thesis due to their detailed nature.



DEPARTMENT OF STRUCTURAL ENGINEERING

Report on experimental results for diagonal 13B

Authors:

Camilla Gunnesdahl Jensen, Emile Dreyer Vetter

June, 2023

Table of Contents

Abbreviations	III
Nomenclature	IV
1 Experimental test of Tretten bridge elements	1
1.1 Introduction to experiments	1
1.1.1 Background analysis of Tretten bridge	1
1.1.2 Diagonal elements of Tretten used for experiments	3
1.1.3 Details of dowel connections	4
1.2 Tension test of timber elements	7
1.2.1 Annotations and visual inspection of elements for tension test	7
1.2.2 Orientation and notation of <i>S-tests</i>	9
1.2.3 Preparation and reinforcement of <i>S-tests</i> prior to experiment	9
1.2.4 Mounting and equipment of <i>S-tests</i>	11
1.2.5 Method of <i>S-tests</i>	12
1.2.6 Results of <i>S-tests</i>	14
1.2.7 Discussion of tensile tests and concluding remarks	16
1.3 Block failure test	17
1.3.1 Annotations and visual inspection of elements for block failure test	17
1.3.2 Orientation and notation of <i>B-tests</i>	17
1.3.3 Preparation and reinforcement of <i>B-tests</i>	18
1.3.4 Mounting and equipment of <i>B-tests</i>	18
1.3.5 Method of <i>B-tests</i>	20
1.3.6 Result of <i>B-tests</i>	22
1.3.7 Discussion of block failure tests and concluding remarks	27
1.4 Compression tests	29
1.4.1 Annotations and orientation of <i>C-tests</i>	29
1.4.2 Preparations and mounting of <i>C-tests</i>	29
1.4.3 Method of <i>C-tests</i>	30
1.4.4 Results of <i>C-tests</i>	31
1.5 Four-point bending test	33
1.5.1 Annotations and orientation of bending test	33

1.5.2	Mounting and equipment of bending tests	33
1.5.3	Method of bending tests	34
1.5.4	Results of bending tests	35
1.6	Specimen moisture and density calculations	39
1.6.1	Density	39
1.6.2	Moisture content	41
2	Conclusion from experimental testing	42
	Bibliography	43

Abbreviations

B-test specimen for block failure test.

C-test specimen for compression failure test.

DOL duration of load.

EC5 EN 1995: Design of timber structures.

GL32c glued laminated timber, composite.

GLULAM glued laminated timber.

LVDT linear variable differential transformers.

MC moisture content.

MC-test specimen for moisture content and density determination.

NPRA Norwegian Public Roads Administration.

RH relative humidity.

S-test specimen for tension failure test.

Nomenclature

Δl	changes in length
Δl_0	changes in sectional length
ℓ_1	gauge length
$\rho_{05,i,min}$	lowest 5-percentile density of all subsamples
$\rho_{05,i}$	5-percentile density of subsample i
ρ_k	characteristic density
a_d	distance between a loading position and the nearest support in a bending test
A_{cs}	area of cross-section
A_{net}	net area
d_i	inner diameter
$E_{m,g}$	mean global modulus of elasticity
$E_{m,l}$	mean local modulus of elasticity
f_v	shear strength
$f_{c,0}$	compressive strength parallel to grain
$f_{c,el}$	elastic compression strength
$f_{c,pl}$	plastic compression strength
$F_{est,max}$	estimated maximum load
F_{Rk}	characteristic load-carrying capacity according to Johansen's theory
F_{Sk}	characteristic load-carrying capacity for splitting considering effective amount of dowels
$f_{t,0}$	tensile strength parallel to grain
G	shear modulus of elasticity
h	height of cross-section
I	second moment of inertia
I_{net}	net second moment of inertia
k_n	factor to adjust for number of subsamples in a density test
l	total length
l_0	gauge length
l_s	length between supports
L_{net}	total net length
l_{net}	sectional net length
M	moment

m_{init}	initial mass
m_{od}	oven dried mass
MC	moisture content
n	number of specimens
n_i	number of specimens in subsample i
n_s	number of subsamples
R_0	rotation around origin
t	specimen thickness
t_f	time until failure
w	width of cross-section

1 Experimental test of Tretten bridge elements

Prior to the collapse of the *Tretten* bridge in 2022, it was claimed to have a 100 year life expectancy utilizing an innovative but yet unconventional combination of timber and steel truss work (Hårstad-Evjen et al. 2013). Completed in 2012, this bridge was constructed to replace its predecessor, a steel truss bridge that had been in place since 1895, though only saw 10 years of service before collapse.

Tretten bridge was supposed to demonstrate a state of timber and steel in harmony (Hårstad-Evjen et al. 2013), but became an indicator of our lack of knowledge regarding complications arising when designing timber bridges. To further emphasize this point, the Perkolo bridge suffered a similar outcome due to the failure of the supervising engineer and the Norwegian Public Roads Administration (NPRA) to identify significant design flaws (Statens Vegvesen 2016). NPRA decided to close an additional ten bridges after the collapse of *Tretten* and terminate projects involving the use of timber in bridges, as more research needs to be done.

The objective of this report is to contribute on finding deviations of material properties for GL32c used in *Tretten* from specified ones in *EN14080*. By conducting tests in the laboratory on *T14.5* lamellas from downstream diagonal element number 13 (13B), the goal is to determine important strength parameters and compare them to projected values. The experiment will include four tension tests, three test related to block-failure, four four-point bending tests and an additional ten compression tests. From the latter, the objective is to determine the tension strength, compressive strength and find decisive failure surfaces that may be relevant in our understanding of the failure of the *Tretten* bridge.

1.1 Introduction to experiments

1.1.1 Background analysis of Tretten bridge

The *Tretten* bridge was a three spanned truss bridge consisting of components of steel and timber. The diagonal elements of the bridge consisted of GL32c identically angled with respect to the horizontal plane. The vertical steel components were connected to the timber with dowel connections. *Tretten* bridge measured a total of 148 metres with a main span of 70.2 metres. Figure 1 and Figure 2 illustrates the design of the bridge.

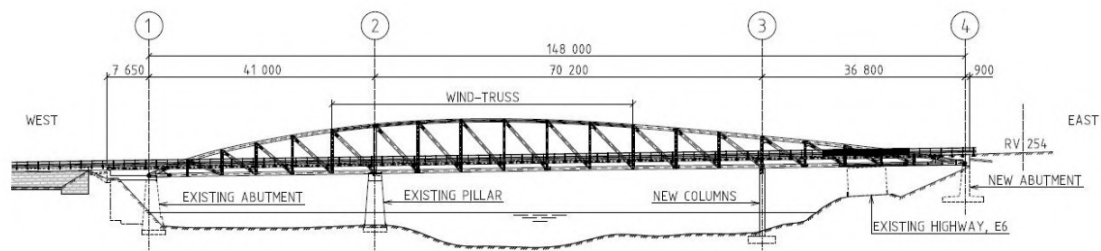


Figure 1: Dimensions of *Tretten* bridge (Hårstad-Evjen et al. 2013).

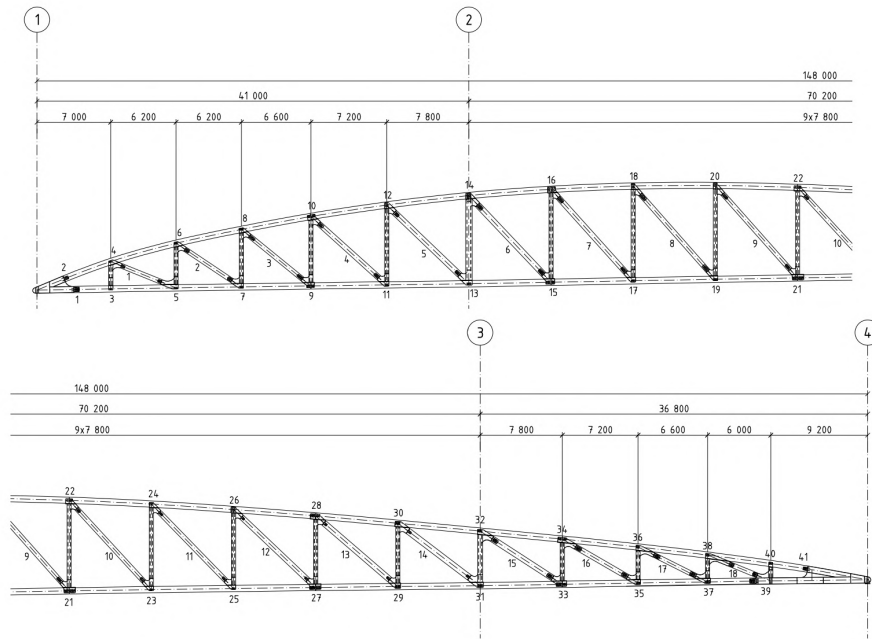


Figure 2: Details of *Tretten* bridge (Hårstad-Evjen et al. 2013).

The dimensions of the various components in the bridge depends on the the loads they are subjected to. The top and lower chord in the truss have a constant cross-section of 700×600 and 650×600 denoted in millimetres, respectively. Both the vertical steel components and diagonal timber elements have dimensions according to attributing loads. The GLULAM elements varies between 500×450 millimetres to 600×600 millimetres where the largest cross-sections are situated in the main span (Qvist and Soland 2022). The dimensions of the experimental test pieces does not coincide with the latter measurements, which will be elaborated in Section 1.1.2. The dowel connections in the bridge consists of 8 millimetres wide steel plates with a total of 32 dowels for elements subjected to largest loads.

Soland and Qvist carried out a parameterized structural 2D analysis of the bridge illustrating the distribution of forces and bending moments in the spans subjected to self-weight and a simple load scenario of a two-point axle load from a lorry. Figure 3 illustrates how the largest forces occurs over the nodes above the middle support.

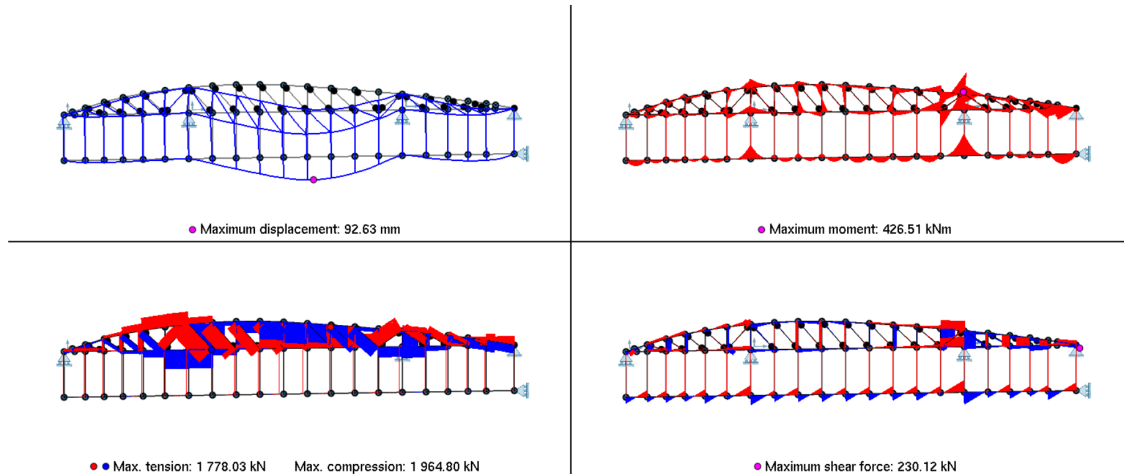


Figure 3: Result of structural analysis from *Tretten* bridge (Qvist and Soland 2022).

1.1.2 Diagonal elements of *Tretten* used for experiments

A total of seven specimens were sent to the department of structural engineering at NTNU for conducting experiments related to the failure of the *Tretten* bridge. All specimens consists of *T14.5* lamellas and have origin from downstream diagonal element number 13, referred to 13B where B denotes the downstream axis. Some diagonal elements were reportedly lifted out of the river of Grudbrandsdalslågen, hence likely contained various moisture content (MC). Before arrival to Trondheim, all the elements were shaped by *Moelven Limtre* according to dimensions required for experimental testing. At arrival in the laboratory, all specimens were placed in an environmental controlled room with $RH = 65\%$ and $20\text{ }^{\circ}\text{C}$.

Milling machines were used to shape the specimens for tension, and block failure tests, hereafter respectively referred to as *S-tests* and *B-tests*. Due to the specimens being cut from a larger element from the bridge diagonals, all the test pieces suffered from varying effects of swelling and shrinkage. For instance, a specimen with surfaces being directly exposed to water will contain vastly more water than a corresponding sample from the center due to the hygroscopic properties of timber. The latter induced minor deviations in dimension from provided measurements done by *Moelven Limtre*. The imposed alterations in the specimen length is assumed to have neglectable consequences for the sake of the tests, in opposition to the deviating width. The width is decisive for both tension and block failure hence needs to be accounted for. Nevertheless, provided specimen dimensions for tension (and later the bending test) and block tests are illustrated in Figure 4 and Figure 5, respectively. The uncertainties of the widths are measured to be ± 4 centimetres. All figures are drawn in millimetres.

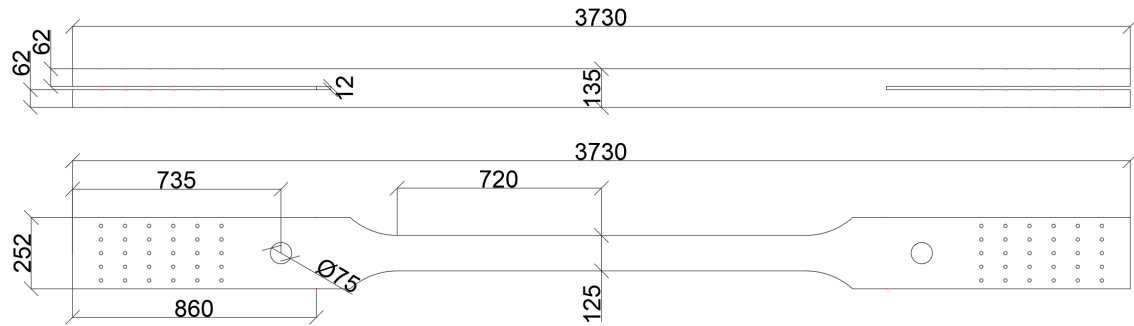


Figure 4: Dimensions of the 4 *S-tests* (used later for bending tests).

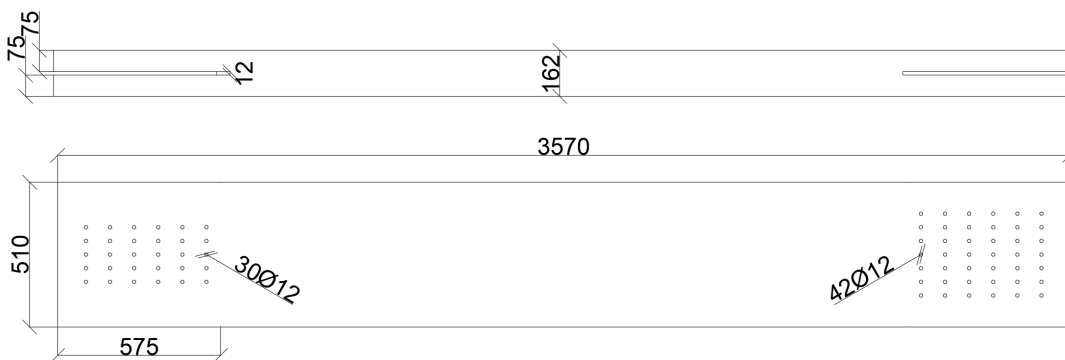


Figure 5: Dimensions of the 3 *B-tests*.

1.1.3 Details of dowel connections

The end-details of the dowel connection are illustrated in Figure 6 and Figure 7 in millimetres. Note that the *B-test* specimens are longitudinally asymmetric in order to obtain block failure in the weakest end, from now referred to as the "weak"-end. The *S-test* are however symmetric, hence both ends corresponds to the illustration in Figure 6.

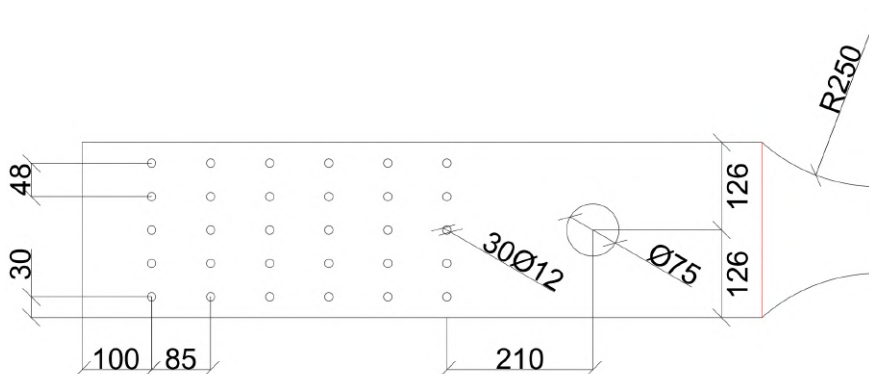


Figure 6: Dimensions of the 4 *S-test*.

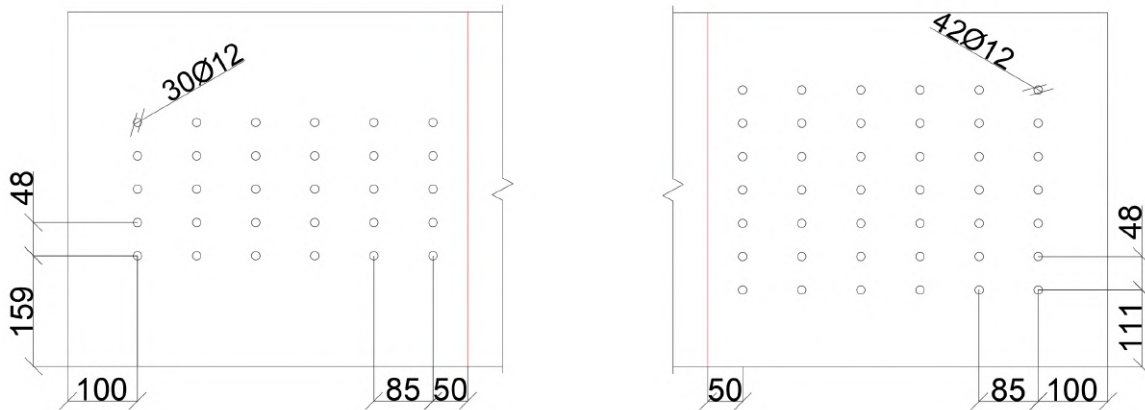


Figure 7: Dimensions of the 3 *B-test*.

The lengths of the dowels are defined according to the widths of each respective cross-section. The *S-test* and "weak"-end of the *B-test* will have connections with 30 $\text{Ø}12$ dowels, while the remaining "strong"-end of the *B-test* will have connections of 42 $\text{Ø}12$ dowels. The dimensions of the steel plates used for the experiments are defined according to Figure 8. Five of *Plate B* will be used for the strongest end of the block failure experiment. The connections are mounted with two outer plates on each side, and one in the center. Corresponding configuration with *Plate A* will be used for the "weak"-end of the block shear experiment. For the tension tests, three of *Plate A* will be used. Note that the connection are two-dimensionally identical for the *S-test* and one end of the *B-test* where only the widths of the specimens varies.

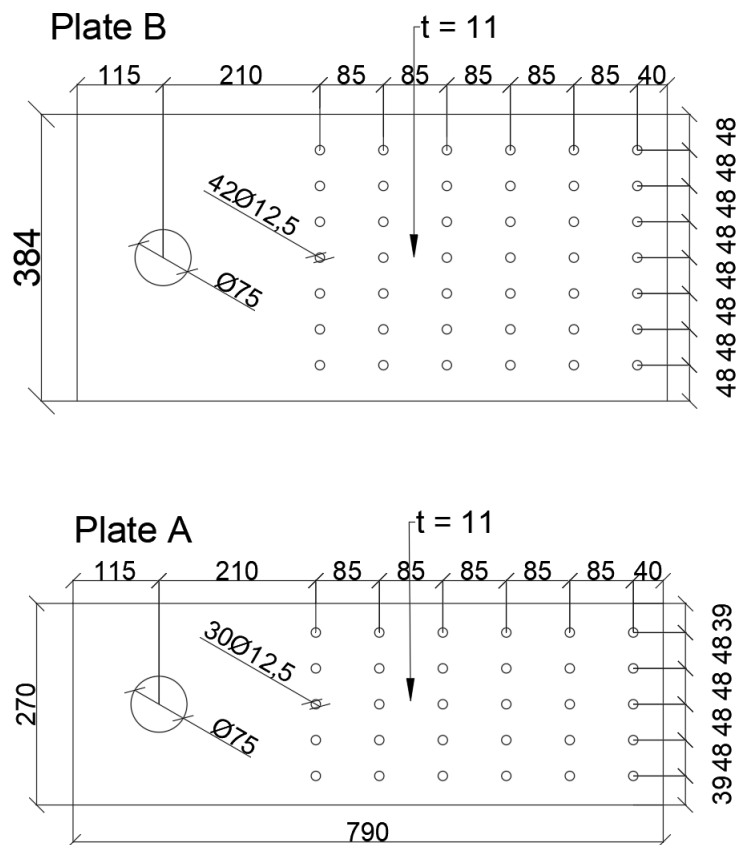


Figure 8: Dimensions of steel *Plate A* and steel *Plate B* in millimetres.

A total of 15 plates were provided for conducting the experiments, 5 of *Plate B* and 10 of *Plate A*. This implies that all the steel plates have to be reused for all the tests. Dowels on the contrary, will be changed for new ones between each test. Due to the symmetric nature of the connections, a mount configuration using 3 of *Plate B* can also be used for the *S-tests*. For the sake of efficiency, both *Plate A* and *B* were used for the mounting *S-tests*. Figure 9 illustrates the steel plates used for the experiments.



Figure 9: Steel plates for the experiments.

1.2 Tension test of timber elements

The objective of this experiment is to determine the tensile strength of the diagonal GLULAM elements, previously elaborated in Section 1.1.2. This chapter presents an experiment that examines the principles of tension testing for timber elements, including testing equipment, sample preparation, and data analysis of the results. Moreover, discussions of various factors that may significantly impact the experimental outcomes is visited to ensure accurate interpretation of the results.

1.2.1 Annotations and visual inspection of elements for tension test

The 4 specimens for tension test are annotated $S1$, $S2$, $S3$ and $S4$ and are hence referred to as S -tests. Each specimen was composed of a different configuration of lamellas accompanied by a variation of impurities such as knots illustrated by Figure 10. Note that $S4$ had a large crack parallel to grain prior to testing, this topic is elaborated in Section 1.2.2.



Figure 10: Annotation of specimens prior to tests.

Prior to failure, cross-sectional areas was measured with calipers in intervals of 360 millimetres in order to obtain relevant parameters for later calculations. The areas are denoted $A1 - A5$ and are divided symmetrically along the gauge length of $l_0 = 1440$ millimetres as described on Figure 11. Figure 12 illustrates how the height and width varies for each cross-section. Figure 13 describes the variation in corresponding areas. Exact measurements are provided in Section 2 in the appendix.

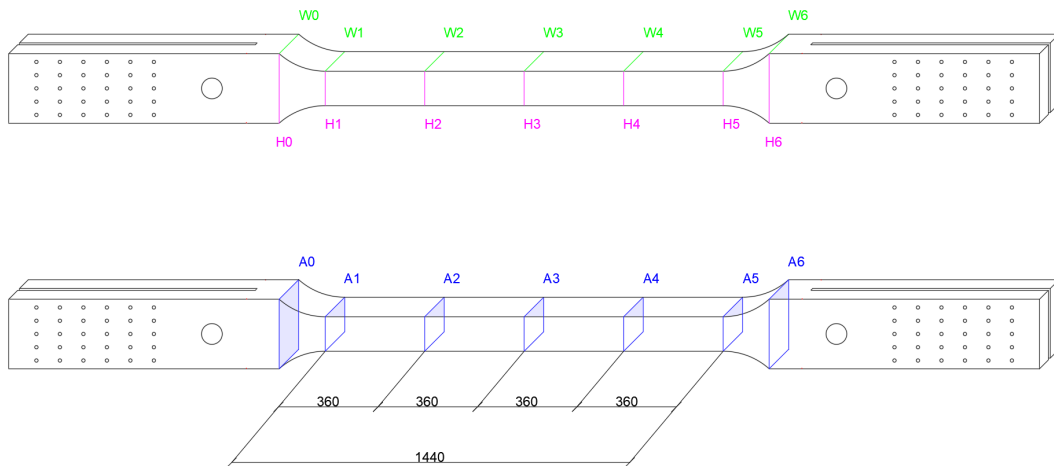


Figure 11: Annotations of cross-section areas.

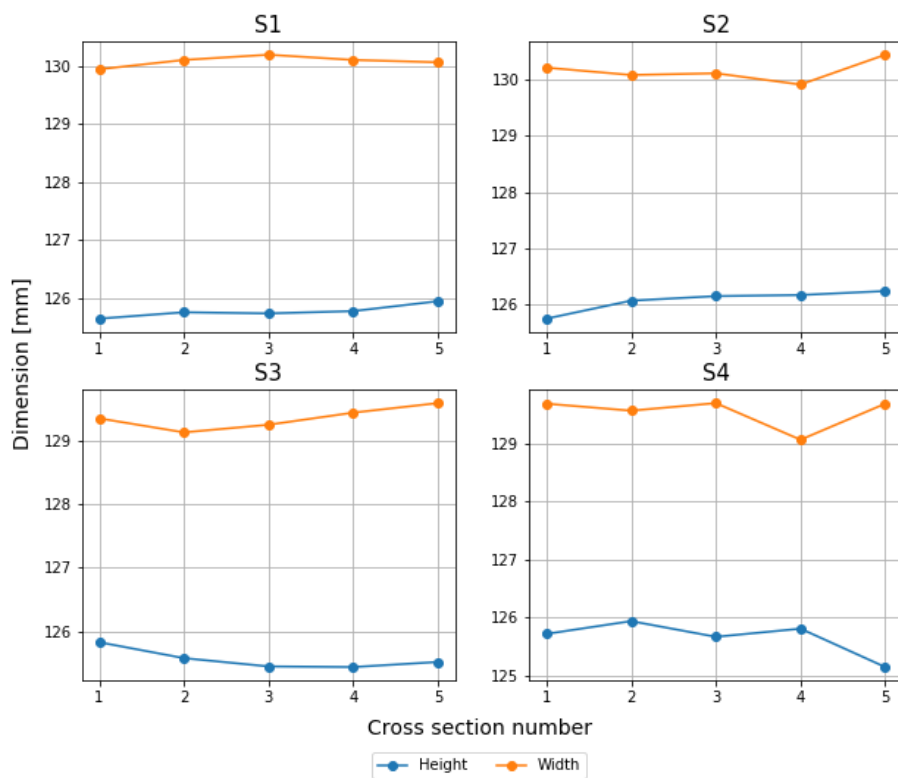


Figure 12: Heights and widths of tension-test elements from *Tretten* bridge.

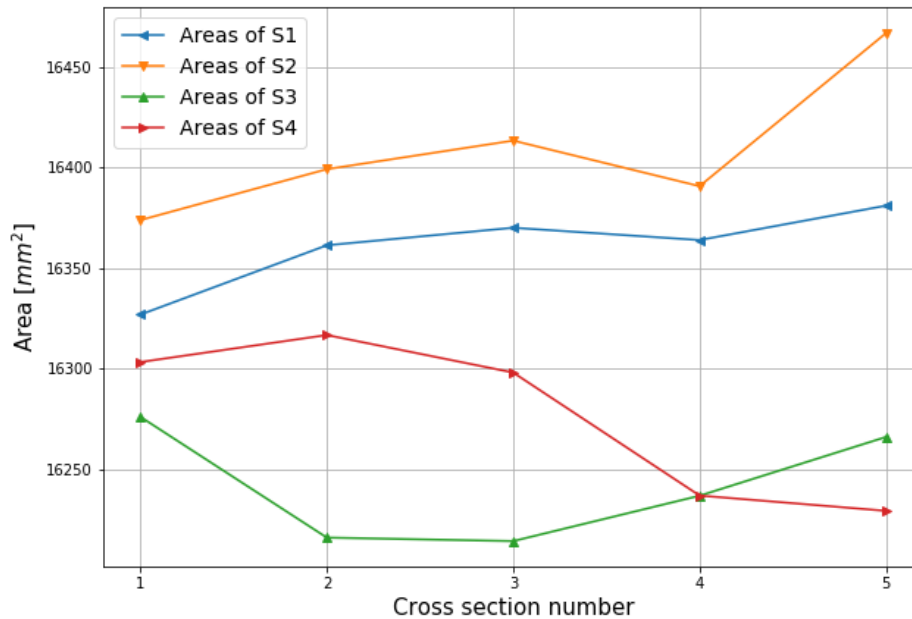


Figure 13: cross-section areas of tension-test elements from *Tretten* bridge.

1.2.2 Orientation and notation of *S*-tests

The tension test was conducted along the longitudinal axis of the specimens, which corresponds to force acting parallel to grain. An axial force acting on the normal plane of the first axis with a longitudinal orientation is denoted as LL. Conducting the experiment along the strong axis of the timber elements is suitable in regards of defining strength parameters for axially loaded diagonal elements in *Tretten* bridge.

Based on previous research, shear related failure for tension test of "dog-bone"-shaped specimens can not be disregarded (Jenssen and Vetter 2022). While the geometry of the specimens was designed for failure to happen between the narrowings, shear stress concentrations near the narrowings can be decisive for the capacity of the tension specimens. Shear stresses and failure acting perpendicular to the radial plane, caused by longitudinal axial loads, can be denoted with RL orientation. In an attempt of avoiding the latter failure mode, the specimens were reinforced.

1.2.3 Preparation and reinforcement of *S*-tests prior to experiment

To account for unforeseen and unwanted failure modes of the timber elements, given that the objective is to define the tensile strength of the material, reinforcement of the assumed weakest cross-sections is necessary. A total of 28 self tapping screws were used to reinforce each of the specimens. Screws with length $l = 300 \text{ mm}$ and inner diameter $d_i = 6 \text{ mm}$ were used to strengthen areas where failure was not desirable. Holes were pre-drilled with drill bits of diameter equal to their respective inner diameter.

Due to the symmetric nature of the *S*-test, it was necessary to include reinforcement in both ends of the specimen. For the latter test, crucial stresses would occur by the narrowing due to change in the grain orientation with respect to the propagation of stresses. Screws were hence drilled with a 60° angle in

attempt to counteract a potential failure in the narrowing. Vertical screws were used to strengthen the dowel connections. Figure 14 illustrates the reinforcement configuration of 8 vertical and 6 angled screws at one end of the specimen shown from the top, under and side.

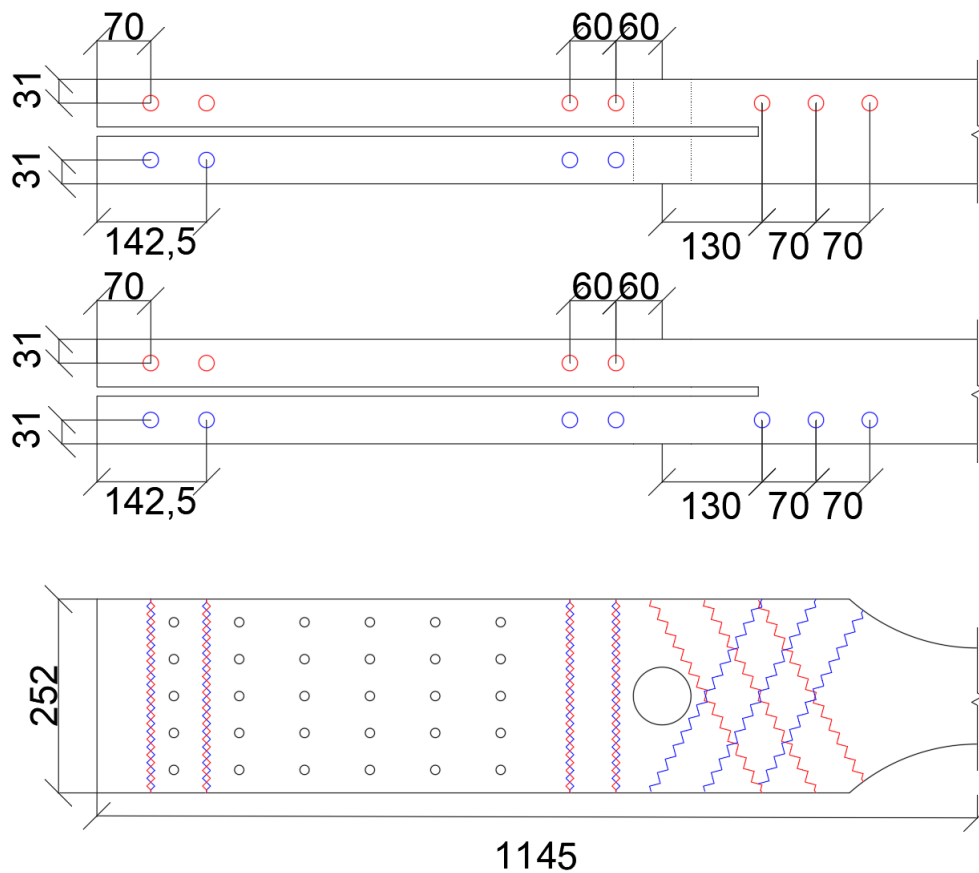


Figure 14: Reinforcement of *S-test*.

Complications regarding pre-drilling arose for specimens containing large amount of knots in sections that were to be reinforced. Knots, or alterations in the grain pattern, caused an angling of the drill bits. Consequently, some screws were instead positioned off-center through the pre-drilled holes as illustrated in Figure 15.

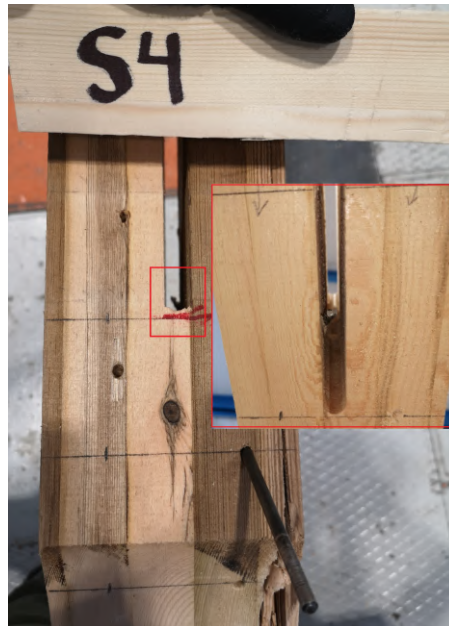


Figure 15: Angeled drill bit in *S4* due to knots.

As previously mentioned, *S4* is accompanied with large defects thus needed additional preparation before being subjected to tensile loads. A large crack parallel to the longitudinal axis of the specimen, likely caused by multiple knots, would reduce the effective area and hence the specimens capacity. The crack was filled with wood glue in order to conserve some strength and prevent further crack propagation. Figure 16 illustrates the crack before and while glue is applied.



Figure 16: Application of wood glue to the longitudinal cracks in *S4*.

1.2.4 Mounting and equipment of *S*-tests

The four tension tests were carried out using a horizontal configuration of an Instron machine. The specimens were fastened to the machine by a dowel connection and three steel plates of type *Plate A* (see Figure 8). Two sets of bolts were used to connect two additional thicker steel plates to the Instron as described in Figure 17. Furthermore, rolling boundaries were used beneath the specimens to elevate them in order to reduce friction and avoid asymmetrical loading due to the chain-effect.

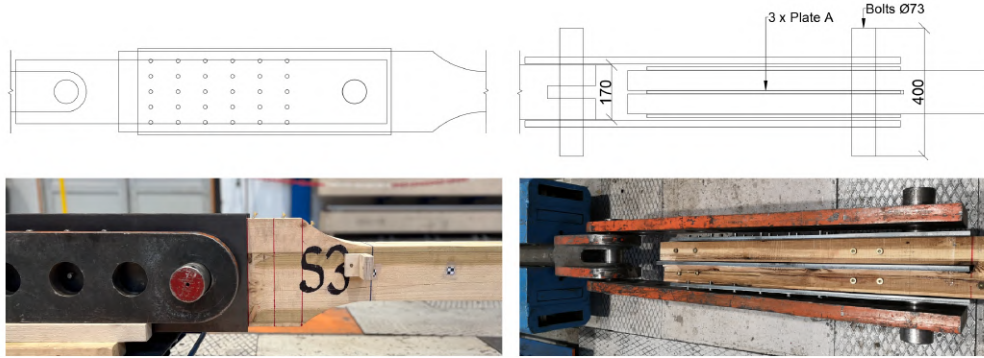


Figure 17: Mount of *S*-tests.

Longitudinal laser sensors were used for *S*-tests in order to evaluate the global displacement and compare it to the output from Instron. Lasers and non-reflective surfaces were mounted on both sides of the specimens at the location of $A1$ and $A5$, hence $\pm \frac{l_0}{2}$ or ± 720 millimetres from the middle origin, where l_0 denotes the gauge length.

Additionally, a camera was used to track the relative position of markers to obtain any local displacement variations. 8 markers were evenly distributed with a distance of 180 millimetres along the longitudinal axes of the element where the tension failure was assumed to occur, hence where the height of the specimen is 125 millimetres. Figure 18 illustrates *S3* mounted with lasers along with the non-reflective surfaces. Four out of eight markers for tracking displacement with camera is also visible in the figure.



Figure 18: Laser and non-reflective surface for measuring global displacement.

1.2.5 Method of *S*-tests

The determination of the modulus of elasticity in tension parallel to grain for *S* elements follows the guidelines in the standard *NS-EN 408* (CEN 2012), while the testing procedure is specified by *NS-ISO 6891* (ISO 1991). To find the estimated max load certain material properties had to be assumed. The mean tensile strength of GLULAM for the elements, $f_{t,0}$, was set equal to 15 MPa. Furthermore, the mean Young's modulus of the material, E_m is assumed to be 11000 MPa. The cross-sectional area, A_{cs} , was chosen conservatively from Figure 13 as 16250 millimetres squared. Equation 1 calculates the estimated maximum load of the *S*-tests which was needed to define the loading sequence.

$$F_{max,est} = A_{cs} \cdot f_{t,0} = 243.8 \text{ kN} \approx 250 \text{ kN} \quad (1)$$

This implies the following load parameters according to *NS-EN 408*.

$$\begin{aligned} 0.4F_{max,est} &= 100 \text{ kN} \\ 0.1F_{max,est} &= 25 \text{ kN} \end{aligned} \quad (2)$$

Both loads from Equation 2 were to be held for 30 seconds during the experiment and occurs respectively at the first local maxima and minimum for the load cycle. Hence the last unknown parameter is the linear load inclination. The latter can be approximated using Hooke's formula, with a bold assumption that timber is linear elastic, and the proportional relationship between displacement, strains and specimen length. Conservatively, the total change of length can be found by multiplying the result from Equation 3 with the ratio between the total and sectional length, assuming that displacements are constant over l . Thus, Equation 4 can be used as an approximation of total changes in displacement.

$$\Delta l_0 = \frac{0.4F_{max,est} \cdot l_0}{A_{cs} \cdot E_m} = \frac{100 \text{ kN} \cdot 1440 \text{ mm}}{16250 \text{ mm}^2 \cdot 11000 \text{ MPa}} = 0.8056 \text{ mm} \quad (3)$$

$$\Delta l = \Delta l_0 \cdot \frac{l}{l_0} = 2.086 \text{ mm} \quad (4)$$

Where,

Δl	is the total change in length;
Δl_0	is the change in gauge length;
l	is the total specimen length;
l_0	is the gauge length;
A_{cs}	is the cross-sectional area;
E_m	is the Young's modulus;
$F_{max,est}$	is the estimated max load.

Finally, the inclination of load or inclination of displacement is found by dividing the changes of load or displacement at the first local maxima, over the inclination of load duration. Based on *NS-EN 408*, the duration of inclination was set to 120 seconds. Results of Equation 5 implies a load configuration for the *S-tests* with an inclination of displacement of $0.018 \frac{mm}{s}$. The same value will be used for the declination of displacement after $0.4F_{max,est}$ is held for 30 seconds. Figure 19 summarises the calculated load configuration for *S-tests* plotted with force against time.

$$\begin{aligned} \frac{\Delta F}{s} &= \frac{100 \text{ kN}}{120 \text{ s}} = 0.833 \frac{\text{kN}}{\text{s}} \\ \frac{\Delta l}{s} &= \frac{2.086 \text{ mm}}{120 \text{ s}} = 0.018 \frac{\text{mm}}{\text{s}} \end{aligned} \quad (5)$$

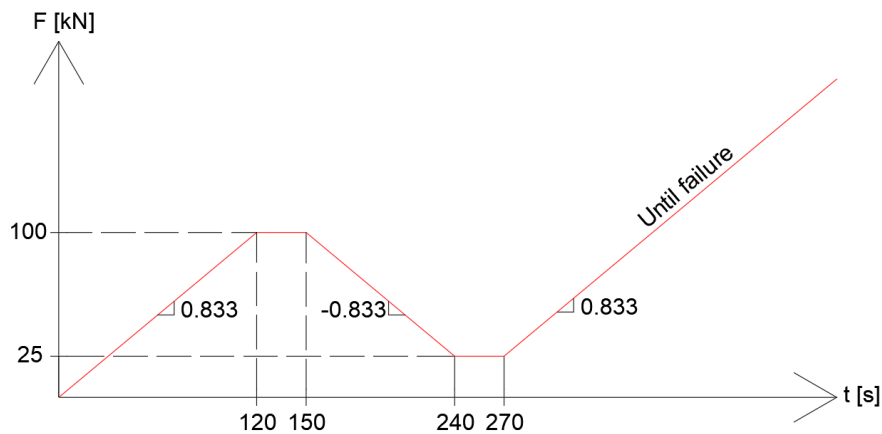


Figure 19: Load configuration for *S*-tests according to *NS-EN 408*.

1.2.6 Results of *S*-tests

All four *S*-tests tests produced similar failure patterns unrelated to tension failure, and hence the tension strength was difficult to obtain from this particular experiment. The results indicates that shear failure was more critical than tension, as illustrated on Figure 20. Regarding data acquired from the experiments, the laser sensors did not provide any useful information regarding displacement, hence not included in the results. The following results are based on displacement and force data acquired from the test machine.



Figure 20: Failure of *S4*.

By analysing the acquired data it is possible to see similar tendencies in specimen behaviour. The equivalent failure modes implies that the element capacity are equally similar. Note that *S4* was used as a test for instrumental and load configuration calibration and is hence excluded from further calculations. Nevertheless, Figure 21 illustrates all experimental results plotted with force against time and displacement. The data from the experiments contained multiple minutes with irrelevant data prior to the loading sequence, thus normalized with respect to time to reduce post-processing computational costs. Figure 22 illustrates average values from acquired data from the experiments. Table 1 includes force and displacement values at failure.

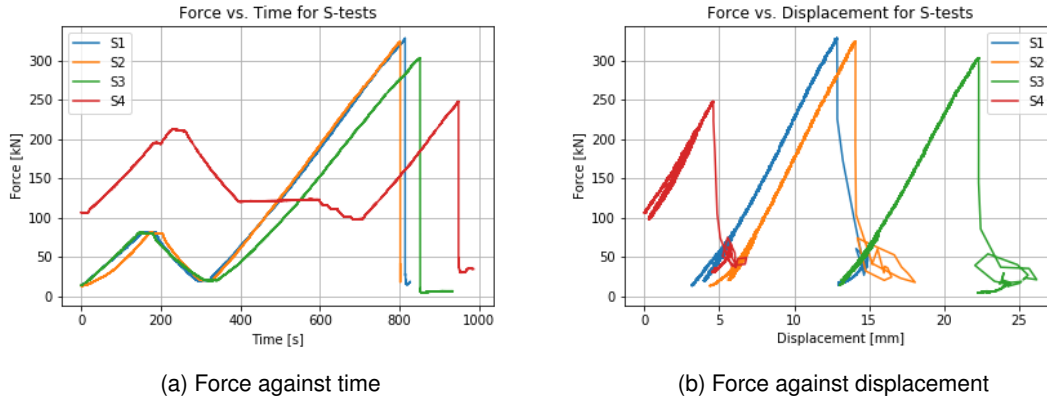


Figure 21: Data from all the *S*-tests.

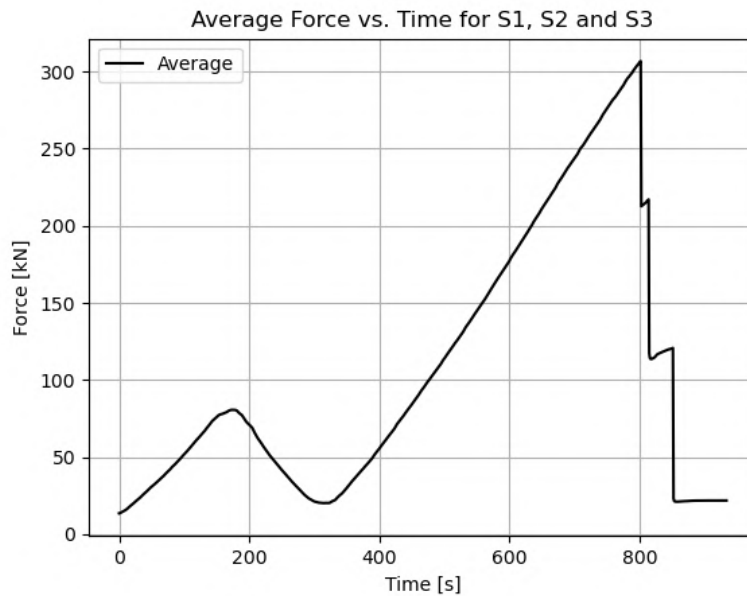


Figure 22: Average data of *S*1, *S*2 and *S*3.

Specimen	δ_{tot} [mm]	F_{max} [kN]	$A_{cs,min}$ [mm ²]	$f_{t,0}$ [MPa]
<i>S</i> 1	12.888	328.29	16326.96	20.11
<i>S</i> 2	14.106	323.98	16373.91	19.79
<i>S</i> 3	22.320	303.31	16214.41	18.71
Average values	16.438	318.53	16305.09	19.54

Table 1: Force and displacement at failure for *S*-tests.

From the test data it is possible to define the expected axial capacity for the specimen. Consequently, a bottom limit on mean tensile strength can be established. One could conservatively estimate the tensile strength by dividing the resisted axial force per respective smallest area according to Equation 6. The bottom limit of $f_{t,0}$ will be used as estimated tensile capacity for calculations in Section 1.3.5. Let $F_{max,i}$ and $A_{cs,min,i}$ denote max resisted force and minimum cross-section area with subscript referring to respective specimen number. The expected lower limit of $\bar{f}_{t,0}$ can hence be defined independent of

cross-sectional area.

$$\bar{f}_{t,0} \geq \frac{1}{3} \sum_{i=1}^3 \frac{F_{max,i}}{A_{cs,min,i}} = 19.54 \text{ MPa} \quad (6)$$

1.2.7 Discussion of tensile tests and concluding remarks

The *S-tests* did unfortunately not experience the desired failure mode, hence deemed unsuccessful for the sake of defining $f_{t,0}$. The specimens' load resistance along with angled screws used to reinforce the specimens did not provide enough resistance to shear loads. Based on the failure surfaces of the elements, it is likely that the hole for the bolt contributed to form a weak point for crack propagation along the fibres. Furthermore, sequences of knots caused reduction of capacity. This is emphasized by cracks patterns forming along the knots indicating their contribution to path of least resistance. This is clearly demonstrated on Figure 20.

On a better note, information acquired from the tests and failure patterns clearly illustrates similar material tendencies for the specimens. This implies that the capacity for the specimens is predictable to a certain extent and not solely dominated by unknown variables. If additional tests were to be conducted on similar specimens, it is likely that the data would give smaller standard deviation of capacity and more precisely define the expected value, in other words strengthen the tendency. Further testing is however not desirable, as the produced failure pattern is unrelated to tensile capacity.

To summarize the results of the *S-tests*, the specimens resisted a larger axial force than anticipated. The estimated tensile capacity of the elements were calculated to 250 kN, though *S1*, *S2* and *S3* resisted on average 318.5 kN. It is therefore possible to conclude that the mean tensile strength of the timber must be at least 19.5 MPa. The latter value will be used for capacity estimation for block failure tests.

1.3 Block failure test

The objective of this experiment is to demonstrate a possible critical failure mechanism of *Tretten* bridge. Based on ongoing research, samples sent from accident site and lack of restrictive guidance in *EC5* at the time of construction, block failure is likely a decisive cause of the structural collapse of *Tretten* bridge and hence an important topic of interest. By obtaining relevant parameters such as tensile and shear strength from other tests, corresponding sectional net areas from the fracture surfaces can be used to calculate the load-carrying capacity of elements.

1.3.1 Annotations and visual inspection of elements for block failure test

The 3 specimens for block failure test were annotated *B1*, *B2* and *B3* and are hence referred to as *B-tests*. As for the tension tests, the block failure test specimens were composed by a various distribution of lamellas including defects such as knots. Large longitudinal cracks, that likely occurred in the collapse of the bridge, dominates the strongest end of all the *B-tests*. These ends are hence dimensioned with 42 dowels and are regarded as the "strong"-end of the specimens. Figure 23 illustrates a large horizontal crack in *B2* that renders one row of dowels weak.



Figure 23: Horizontal crack in *B2* that weakens one dowel row.

1.3.2 Orientation and notation of *B-tests*

As for the tension test, the block failure tests are conducted along the longitudinal axis of the specimens. The elements were subjected to an axial tensile force parallel to grain direction to induce block failure at the "weak"-end of the specimens, hence denoted with orientation LL. Based on current studies regarding the reason of the collapse of *Tretten* bridge, this test configuration is deemed highly relevant.

In theory, block failure will induce three fracture planes for this kind of experiment. Two planes will have a positive and a negative normal vector parallel to the height (not referring to radial or tangential orientation as it depends on configuration of lamellas), and a plane with positive normal vector in global longitudinal axis. Accordingly, fracture planes will occur along the net shear and net tension area, respectively denoted as $A_{net,v}$ and $A_{net,t}$. These areas differs from the corresponding cross-sectional areas generally by subtraction of number of dowels in row or column multiplied by according dowel diameter.

For all practical purposes, failure planes will follow the path of least resistance. Consequently, impurities

such as knots and cracks will affect the results causing them to deviate from theory. The orientation of the failure planes are also affected by the latter, thus they will not necessarily have orthogonal relationships.

1.3.3 Preparation and reinforcement of *B*-tests

As for the tension tests, the *B*-tests needed to be reinforced prior to application of load. Even though the "strong"-end with 42 dowels is considerably stronger than the "weak"-end, the existence of defects can cause capacity reduction. The "weak"-end with 30 dowels, has relatively smaller net shear and net tension area and thus lower block failure capacity. However, to ensure that failure occurs in the "weaker" dowel connection, the "strong"-end was reinforced with screws perpendicular to the global longitudinal axis. All specimens were reinforced by two rows of 7 screws measuring $l = 500 \text{ mm}$ and with inner diameter $d_i = 8 \text{ mm}$. A drill bit with diameter equal to the screws' inner diameter was used to pre-drill holes in the specimens. Figure 24 illustrates the configuration of screws for reinforcement.

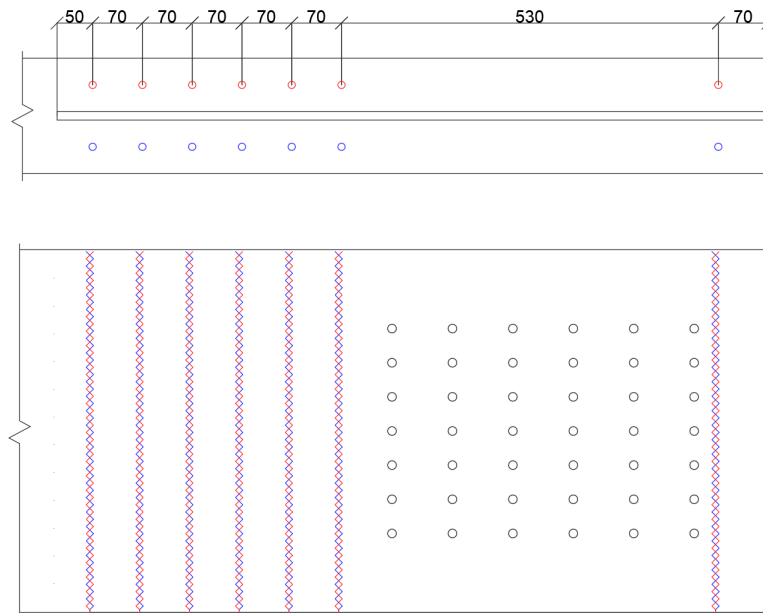


Figure 24: Reinforcement of *B*-test.

1.3.4 Mounting and equipment of *B*-tests

The three block failure tests were carried out using the same Instron machine as for the tension test. The "strong"-end and the "weak"-end were respectively fastened with five of *Plate B*, and five of *Plate A*. Additionally, bolts were used to fasten the plates to the test machine. As for the tension tests, rolling boundaries were used to avoid undesirable external forces on the system. Figure 25 illustrates how the ends were fastened to the machine.

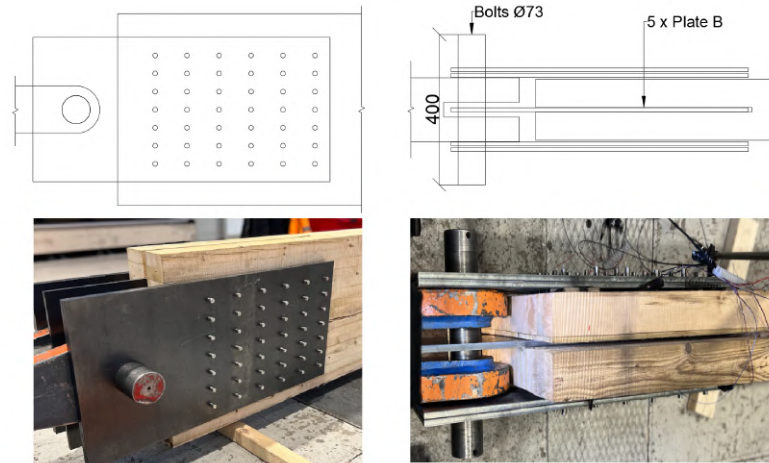


Figure 25: Mount of *B*-tests "strong"-end.

The *B*-tests were equipped with strain gauges and a pair of linear variable differential transformers (LVDT). *B3*, being the first specimen that is tested, is only equipped with strain gauges. For the sake of clarification, all sensors were mounted on the "weak"-end.

The specimens were mounted with four strain gauges at the inside of the outer steel plates to detect the order of which the fracture planes discussed in Section 1.3.2 occurs. Cyanoacrylate glue was used for gluing the strain gauges to the desired positions. The surfaces of the timber elements were considerably rough, so P60 followed by P120 sand paper was used to ensure cohesion between the glue and timber surface.

The fracture planes in the longitudinal axis were to be detected by two strain gauges mounted in a 45° angle between the 3rd and 4th dowel column. Two additional strain gauges were mounted parallel to the longitudinal axis between the 1st and 2nd, and the 4th and 5th dowel row, to detect the vertical fracture planes. Figure 26 illustrates the strain gauges mounted on *B3*.



Figure 26: Strain gauges on *B3*.

Additionally, a pair of LVDTs were mounted on each side to detect local displacements. The transformers are referred to as *LVDT1-LVDT4* in exported data. *LVDT1* and *LVDT2*, and *LVDT3* and *LVDT4* were mounted pairwise on each side of the specimen. Displacements and rotations can thus be computed independently, in average sizes, or combined by their respective locations on the specimens. Table 2 includes the distances between the transformers denoted with subscript of their respective

numbering. For instance, $l_{LVDT,12}$ corresponds to the distance between *LVDT1* and *LVDT2*. Figure 27 describes the configuration of LVDTs where annotations of the locations of the transformers are denoted as *L1-L4* for the respective number of the LVDTs.

<i>B1</i>	Distance [mm]
$l_{LVDT,12}$	401
$l_{LVDT,34}$	432
<i>B2</i>	Distance [mm]
$l_{LVDT,12}$	399
$l_{LVDT,34}$	387

Table 2: Distances between LVDTs.

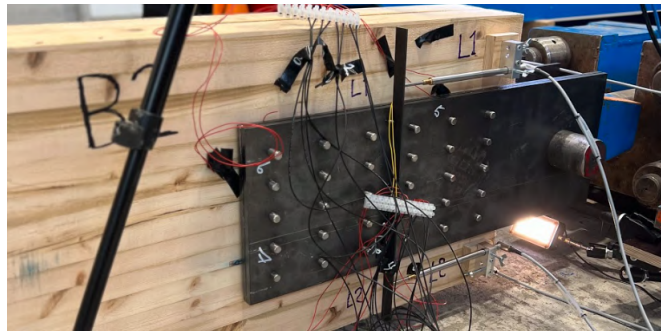


Figure 27: Configuration of strain gauges and LVDTs on *B2*.

1.3.5 Method of *B-tests*

The method of testing of *B-tests* is based on the same standards as for the tension test, though the input parameters for the test machine needed to be redefined. The lower limit of $f_{t,0}$ was previously estimated in Section 1.2.6 to approximately 20 MPa. Furthermore, the mean shear strength of the material, $f_{v,m}$, was assumed to be 5 MPa.

To find the estimated capacity of the block failure specimens, net tensile and net shear areas had to be calculated based on the connections' geometry according to Annex A in *EC5*. The the aforementioned parameters are defined by summations of net vertical and horizontal fracture planes according to Figure 28. Finally, estimated load capacity can be found by multiplying respective net areas and mean strengths according to Equation 9. For the sake of simplicity, multiplication factors $k_{bs,v} = 0.7$ and $k_{bs,t} = 1.5$ are assumed to be equal to unity.

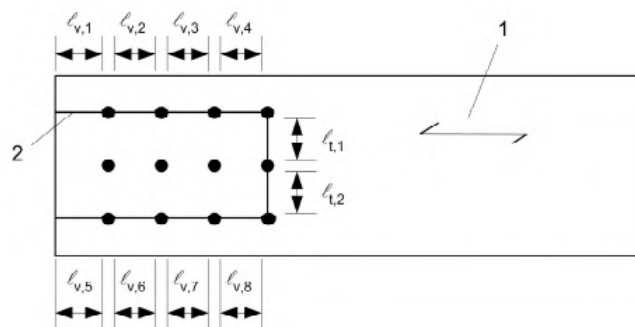


Figure 28: Parameters for calculating net area according to *EC5* (CEN 2010).

$$\sum_i l_{v,i} = 2 \cdot (100 \text{ mm} + 5 \cdot 85 \text{ mm} - 5.5 \cdot 12) = 918 \text{ mm}$$

$$\sum_i l_{t,i} = (4 \cdot 48 \text{ mm} - 4 \cdot 12 \text{ mm}) = 144 \text{ mm} \quad (7)$$

$$A_{net,v} = t L_{net,v} = t \sum_i l_{v,i} = (2 \cdot 75 \text{ mm}) \cdot 918 \text{ mm} = 137700 \text{ mm}^2$$

$$A_{net,t} = t L_{net,t} = t \sum_i l_{t,i} = (2 \cdot 75 \text{ mm}) \cdot 144 \text{ mm} = 21600 \text{ mm}^2 \quad (8)$$

$$F_{bs} = \max \begin{cases} A_{net,t} \cdot f_{t,0} \\ A_{net,v} \cdot f_v \end{cases} = \max \begin{cases} 576.0 \text{ kN} \\ 688.5 \text{ kN} \end{cases} \quad (9)$$

Where,

t	is the specimen thickness;
$L_{net,t}$	is the total net length of the tensile fracture area;
$L_{net,v}$	is the total net length of the shear fracture area;
$A_{net,t}$	is the net cross-sectional area perpendicular to the grain;
$A_{net,v}$	is the net shear area in the parallel to grain direction;
F_{bs}	is the block shear capacity.

$F_{max,est}$ was chosen conservatively as 600 kN, rather than the max value of the values according to EC5. Consequently, $0.4F_{max,est} = 240 \text{ kN}$ and $0.1F_{max,est} = 60 \text{ kN}$. Equation 10 calculates the changes in specimen length in order to find the required inclination of load. Variable notations are the same as provided for tensile test estimations. Finally, inclination of displacement of load could be defined according to Equation 11.

$$\Delta l = \frac{0.4F_{max,est} \cdot l}{A_{cs} \cdot E_m} = \frac{240 \text{ kN} \cdot 3700 \text{ mm}}{162 \text{ mm} \cdot 510 \text{ mm} \cdot 11000 \text{ MPa}} = 0.98 \text{ mm} \quad (10)$$

$$\frac{\Delta F}{s} = \frac{240 \text{ kN}}{2 \text{ min}} = 120 \frac{\text{kN}}{\text{min}}$$

$$\frac{\Delta l}{s} = \frac{0.98 \text{ mm}}{2 \text{ min}} = 0.5 \frac{\text{mm}}{\text{min}} \quad (11)$$

Note that for *B1* and *B2*, inclination of displacement and value of rest load deviates from calculated values. Latter alterations to the method was decided after noticing that $F_{max,est}$ was calculated conservatively low. Figure 29 illustrates the load configuration for *B-tests*.

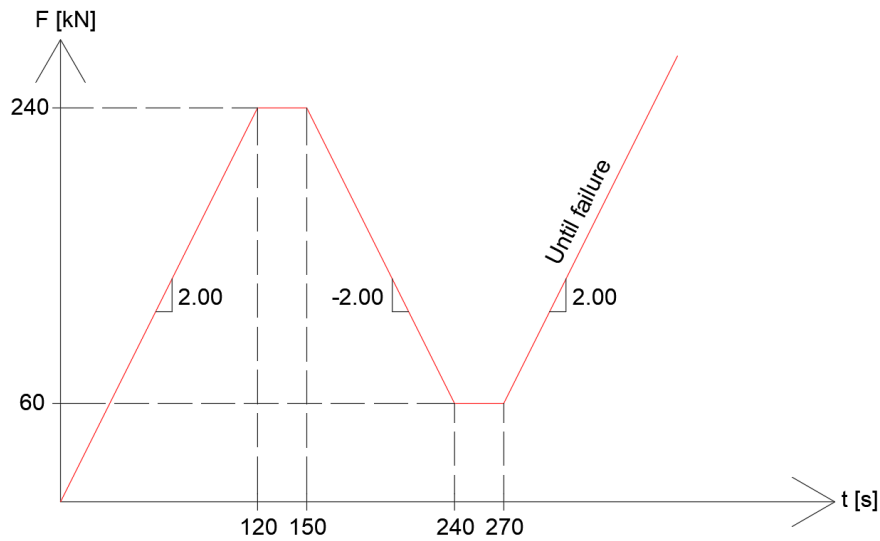


Figure 29: Load configuration for *B*-tests according to *NS-EN 408*.

1.3.6 Result of *B*-tests

All three *B*-tests yielded hypothetical failure patterns as illustrated on Figure 30, indicating successful testing outcomes. Failure surfaces of net tensile area is however highly dominated outside of the dowel zone, which equalates to a larger net area than provided for calculation of block failure capacity in *EC5*. The results suggests that yield surfaces exhibit a tendency to follow the path of least resistance, which is reflected upon the slight deviation of fracture surfaces on the net tension area from the theoretically calculated minimum area. This observation is further supported by the knots' contribution to crack propagation in the longitudinal mid-span of the element. In order to determine whether the ultimate failure was limited by shear or tension capacity, analysis from data required by camera must be performed. Block failure is dependent upon the interplay between both shear and tension capacity, such that the failure of one of the latter may result in the failure of the other, and vice versa.



Figure 30: Visualization of block failure surfaces.

Data lists acquired from the Instron of displacement, force and time were used to make graphs of all specimens as illustrated on Figure 31. Note that the load inclination for *B3* was half of the corresponding inclination of *B1* and *B2*.

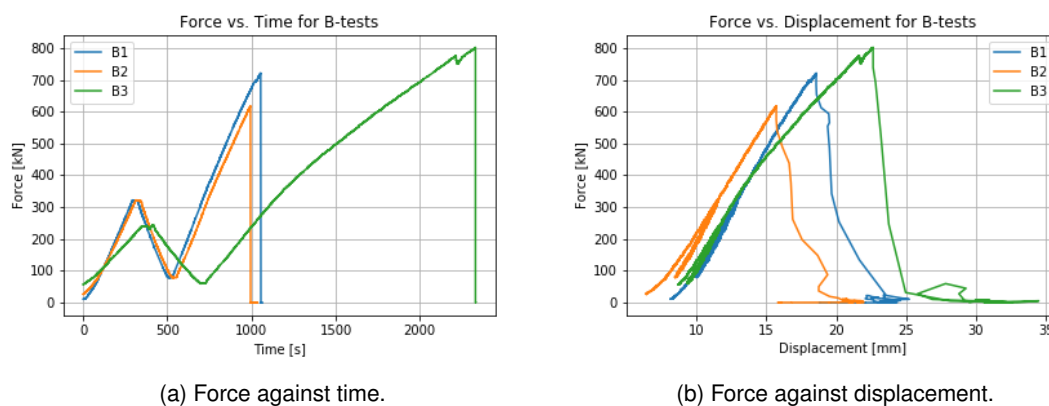


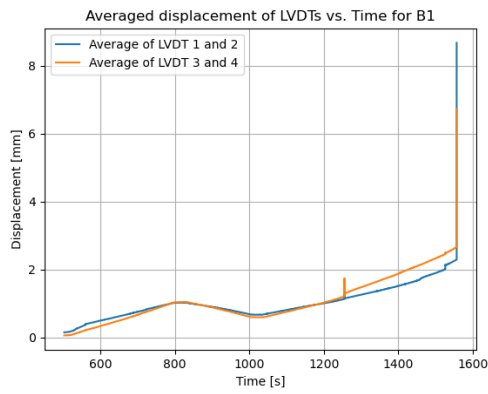
Figure 31: Data from all the *B*-tests.

Furthermore, the data acquired by the sensors were used to make multiple additional graphs. Data from the four LVDTs mounted on *B1* and *B2* were used to calculate average local displacement and rotations. Average displacement of the LVDTs is found by adding all measurements and dividing by number of sensors. Rotation around the middle point between the sensors, R_0 , is calculated according to Equation 12. The result is in radians.

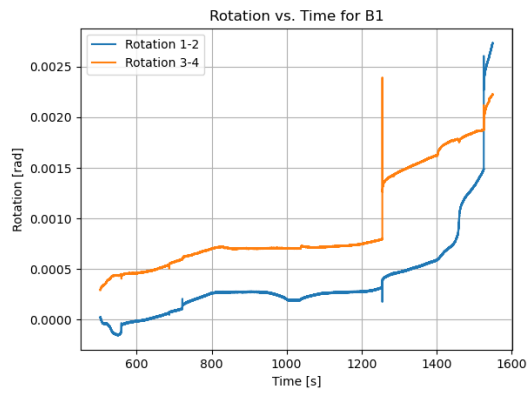
$$R_O = \frac{d_j - d_i}{l_{LVDT,ij}} \quad (12)$$

where $d_j - d_i$ is the difference in displacement readings of the lower and upper transformer. $l_{LVDT,ij}$ denotes the distance between the transformers. Lastly, subscripts refers to numerations of sensors according to Section 1.3.4.

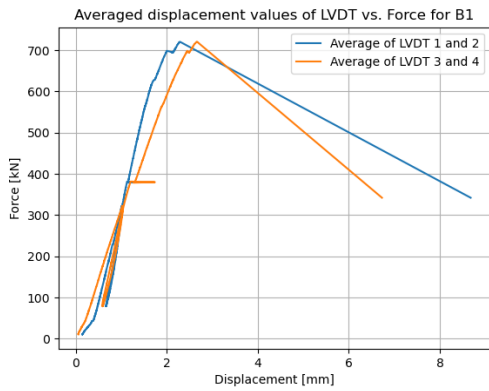
The data collected from the LVDTs are illustrated on Figure 32 and Figure 33. The graphs illustrates similar behaviour of local displacements from *LVDT* readings as for the previously presented total displacements, naturally with smaller magnitude. Note that both specimens seems to experience drastic changes of displacement and rotation at a timestamp around 1200 seconds. Indicators such as sudden dynamic changes in displacements or rotations can be relevant in the sake of establishment of unsymmetrical failure mechanisms. This topic is elaborated in Section 1.3.7.



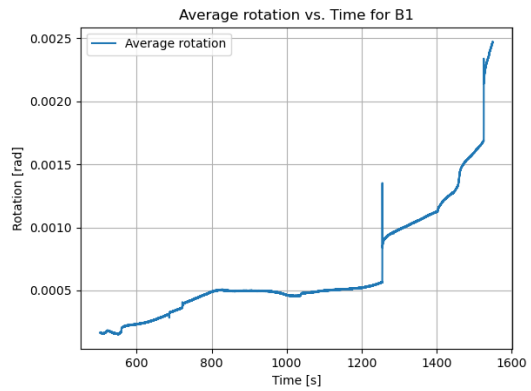
(a) Displacement against time for *B1*.



(b) Rotation against time for *B1*.



(c) Force and displacement for *B1*.



(d) Average rotation against force for *B1*.

Figure 32: Data from LVDTs on *B1*.



Figure 33: Data from LVDTs on *B2*.

Pictures taken from the cameras used in the block failure tests can provide valuable visual analysis of the failure modes, and possibly contribute to a deeper understanding of the specimen behaviour for block failure. Figure 34, Figure 35 and Figure 36 describes the changes of respective specimen *B1*, *B2*, and *B3* experiences from the start of the loading sequence, before, and after block failure has occurred. By analysing the angle of the steel plate, it is noticeable from the pictures that the test pieces experiences rotations before failure. Additionally, Figure 36 of *B3* provides information of great significance. Illustrated by the picture before failure, the specimen experiences an asymmetrical initial failure that eventually leads to block failure. An asymmetrical failure implies that the last resisting side have to carry a much larger load than originally intended.



Figure 34: Camera pictures at start, before and after block failure of *B1*.

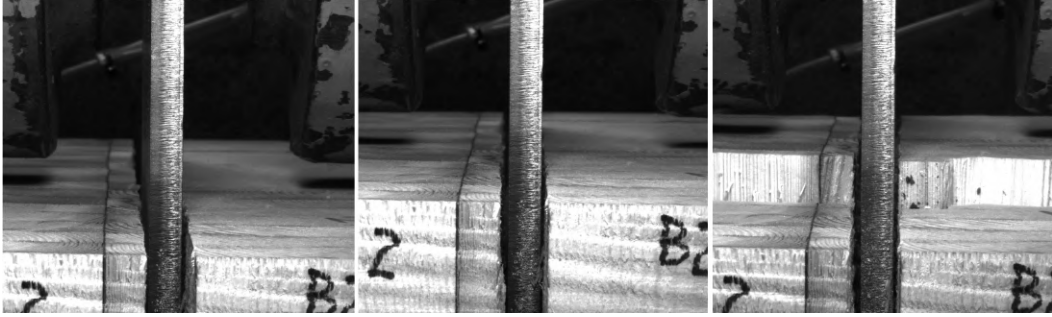


Figure 35: Camera pictures at start, before and after block failure of *B2*.

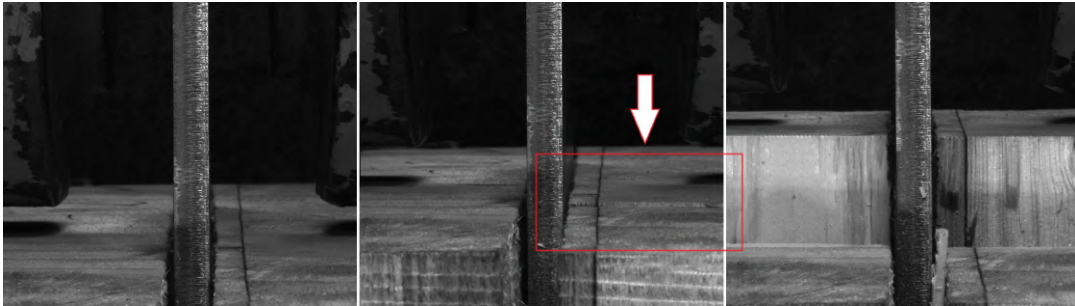


Figure 36: Camera pictures at start, before and after block failure of *B3*.

Table 3 includes all values acquired for time of failure, which is defined at the time F_{max} occurs. The latter can be used to estimate the tensile strength by division of calculated $A_{net,t}$ according to Equation 9. The total displacements are denoted by δ_{tot} . Furthermore, displacements from the LVDTs are presented as the average of four outputs and is hence denoted as $\bar{\delta}_{LVDT}$. Values of rotations are correspondingly the average of the values presented in Figure 32b and Figure 33b at failure. True orientation of displacements and rotations are illustrated in Figure 37.

Specimen	F_{max} [kN]	$f_{t,0}$ [MPa]	δ_{tot} [mm]	$\bar{\delta}_{LVDT}$ [mm]	\bar{R}_0 [rad]
<i>B1</i>	720.62	33.26	18.567	2.2970	0.002599
<i>B2</i>	617.30	28.58	15.718	1.5877	0.001048
<i>B3</i>	801.95	37.13	22.638	NA	NA
Average values	713.29	33.02	18.974	1.9424	0.001824

Table 3: Values at failure for *B-tests*.

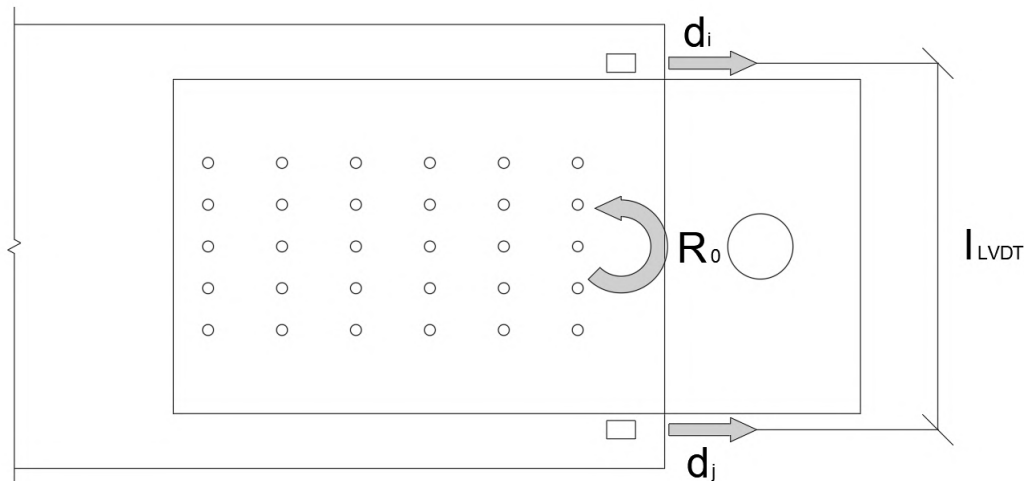


Figure 37: True direction of rotation and upper and lower LVDT displacement.

1.3.7 Discussion of block failure tests and concluding remarks

The results of the experiments indicate that all the test specimens experience similar tendencies before failure. All tests experienced hypothetical yielding patterns that, as anticipated, deviates slightly from theory due to the existence of defects in the timber material. It is however important to stress that all results are solely based on three tests, hence any conclusion potentially include large uncertainties.

The maximum axial load capacity of the beam was defined conservatively as 600 kN based on $f_{t,0}$ obtained from the tension test. Oppositely, the specimens resisted an average force of 713.3 kN that equivalates to around 120 % of estimated capacity. The average resisted force divided per $A_{net,t}$ indicates that the mean tensile strength is approximately 33 MPa . An ongoing separate investigation conducted by professor Kjell Arne Malo suggest similar values of the tensile strength as 33.5 MPa (Malo 2023). A comparison of $B1$ and $B2$ to $B3$ sheds light on timber's dependency on DOL. Being subjected to half the load inclination over a longer duration, $B3$ behaves differently than the other aforementioned specimens. Consequently, based on the characteristic behaviour of timber in regards of creep, $B3$ experiences larger displacement and hence also energy absorbance before failure. This implies more ductile behaviour for increased DOL. Oppositely, $B1$ and $B2$ experienced relatively more brittle failure modes.

Furthermore, the average total displacement observed during the block shear tests was measured as 19.0 millimetres at the point of failure. Analysis of the average values obtained from the LVDTs mounted on $B1$ and $B2$ revealed that 1.94 millimetres of this displacement was attributed to local displacements in close proximity to the point where block failure occurred. This corresponds to approximately 10 % of the total displacement observed during the tests.

At the same location, the rotations were averagely calculated to be approximately -0.002 radians for both specimens. The graphs collected from the LVDTs additionally indicates (at approximately 1250 seconds) that $B1$ and $B2$ experiences spikes in rotations around the horizontal axis. The calculated net average rotation, excluding the dynamic spike, indicates instantaneous changes of approximately 0.0004 and 0.0005 radians, respectively. This corresponds to 20 % and 50 % of the total observed rotations prior to failure for the respective specimens. Notably, the majority of the rotation was observed along the 3 – 4 LVDT axis. Dynamic responses such as the latter on symmetrically tensile-loaded specimens indicates segmented brittle behaviour with possible initial failure of the weakest net areas based on the true direction of rotation.

Equivalently as for the rotations, time correlation of the rotation graphs with Figure 32c and Figure 33c reveals a consistent pattern of failure. The displacements recorded by the LVDTs during the same time period exhibit a similar dynamic trend as observed in the rotations. Dominated by the 3 – 4 LVDT axis, the specimens experience sudden unsymmetrical jumps in displacement moments before failure, indicating partial weakening of the cross-section. Subsequently, the inclination of the displacement and rotation is increased, and block failure is imminent for further load increment.

Visual analysis of the pictures from the *B-tests* provides information of great significance that supports the statement from the rotation analysis that there is a great likelihood that the specimens experiences an unsymmetrical initial failure in one of the net areas. Though it is inaccurate to conclude this for all specimens, it is almost certain that *B3* experiences an initial failure of the right section demonstrated by Figure 36 prior to ultimate failure. Based on the similar tendencies of rotation and displacement for the other specimens, it is not unlikely that they experience similar failure modes.

Calculations on block failure capacity according to *EC5* is based on mean behaviour of the complex composition of tensile and shear strength around the dowel group. The experimental results have underscored the importance of incorporating the presence of defects or uneven cross-sectional areas that may result in unsymmetrical reduction of cross-sectional capacity in capacity calculations. Occurrence of partial or complete failure of one side of the dowel plane implies a non favorable load transfer such that the remaining side is subjected to a significantly higher axial load than anticipated. It is hence imperative, based on the results, that the ultimate bearing capacity is restricted by the weakest section, making it somewhat inaccurate to define block failure capacity based on a mean approach of evenly distributed tensile and shear strengths along the respective net areas.

1.4 Compression tests

The objective of this experiment is to determine both the compressive modulus of elasticity and the compressive strength parallel to grain of the diagonal GLULAM elements in *Tretten*. This will be achieved by analyzing the force and displacement data over time and applying Hooke's law to calculate the Young's modulus. In addition, the compressive strain data will be used to estimate the tensile strain since the tension tests resulted in a shear fracture rather than a tensile fracture. This chapter delves into important topics such as the fundamentals of compression testing for timber elements, testing equipment, sample preparation, and post-analysis of data from the results.

1.4.1 Annotations and orientation of *C-tests*

The specimens in the compression test are identified as *C-tests*, referring to the ten individual specimens labeled as *C1* to *C10*, shown in Figure 38. All of the specimens were obtained from the region of the tension specimens *S4* and *S3* that had been subjected to strain, with *C1* and *C2* being taken from *S4* and the remaining from *S3*. The compression test was carried out on the specimens' longitudinal axis, which indicates that the force is acting parallel to the grain, or the *LL* direction.



Figure 38: Annotation of *C-test* specimens prior to tests.

1.4.2 Preparations and mounting of *C-tests*

To ensure uniformity, all specimens were cut by a table saw to a cross-sectional area of $40 \times 40 \text{ mm}^2$ and a length of 240 millimetres. The test pieces consisted of a variety in timber structure, such as annual rings, knots and cracks, as well as number of lamellas.

The *C-tests* were carried out using Instron 5982, with a maximum load of 100 kN . The testing machine was equipped with smooth steel plates that were securely fastened to make a flat and frictionless surface. This configuration ensured that the testing machine could transfer force without introducing unwanted frictional effects, thereby enhancing the accuracy of the experimental measurements. However, it is inevitable that some friction will be present during the testing process. To minimize the influence of such frictional effects and ensure the accuracy of experimental measurements, the extensometer was attached at the center of the specimen's longitudinal axis where failure was most likely to occur. As the specimen undergoes compressive stress, the distance between the two contact points changes, and this variation was accurately detected and recorded by the extensometer. Figure 39 illustrates the test

setup, wherein the extensometer is attached to the right side of the specimen.



Figure 39: Mount of *C*-tests.

1.4.3 Method of *C*-tests

The method used in the *C*-tests follows the standard *NS-EN 408*. Prior to the final dimensions, a cross-section of $50 \times 50 \text{ mm}^2$ and length of 300 millimetres was chosen and tested. The estimated load capacity, based on an assumed characteristic compressive strength of the material, was found according to Equation 13.

$$F_{max,est} = A_{cs} \cdot f_{c,0} \quad (13)$$

With an assumed characteristic compressive strength of 30 MPa , the estimated maximum load was calculated to 75 kN . Consequently, the load parameters, described in *NS-EN 408*, were calculated according to Equation 14.

$$\begin{aligned} 0.4F_{max,est} &= 30 \text{ kN} \\ 0.1F_{max,est} &= 7.5 \text{ kN} \end{aligned} \quad (14)$$

The maximum load of 100 kN was set as the predetermined stopping point for the machine. Specimens did however not yield failure for this load, implying a compressive strength greater than 40 MPa , hence the dimensions had to be redefined. Consequently, redefined dimensions of the compressive tests were decided as $l = 240$ millimetres and $A_{cs} = 40 \times 40 \text{ mm}^2$. Finally, the mean modulus of elasticity, E_m was assumed to be 11000 MPa . In order to determine the required inclination of load, Equation 15 was used to calculate the changes in sectional length.

$$\Delta l = \frac{0.4F_{max,est} \cdot l}{A_{cs} \cdot E_m} = \frac{30 \text{ kN} \cdot 240 \text{ mm}}{1600 \text{ mm}^2 \cdot 11000 \text{ MPa}} = 0.0004 \text{ mm} \quad (15)$$

The final adjustments resulted in the load configuration and inclination of displacement as shown in Equation 16. The load configuration is illustrated in Figure 40.

$$\frac{\Delta F}{s} = \frac{30 \text{ kN}}{120 \text{ s}} = 0.25 \frac{\text{kN}}{\text{s}}$$

$$\frac{\Delta l}{s} = \frac{0.0004 \text{ mm}}{120 \text{ s}} = 3.33 \cdot 10^{-6} \frac{\text{mm}}{\text{s}}$$
(16)

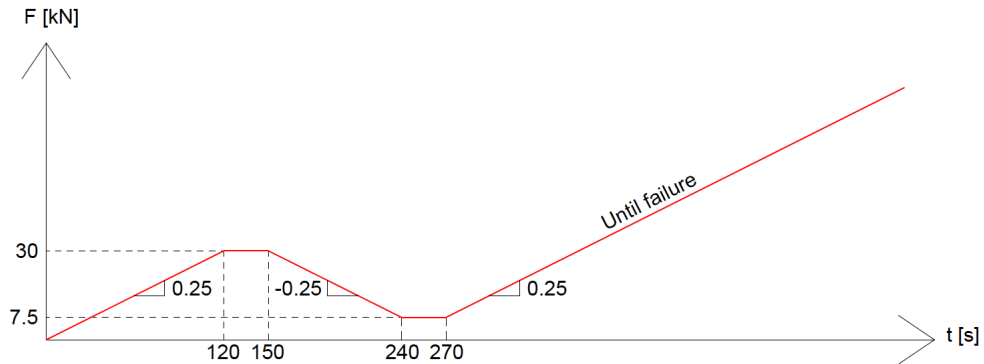
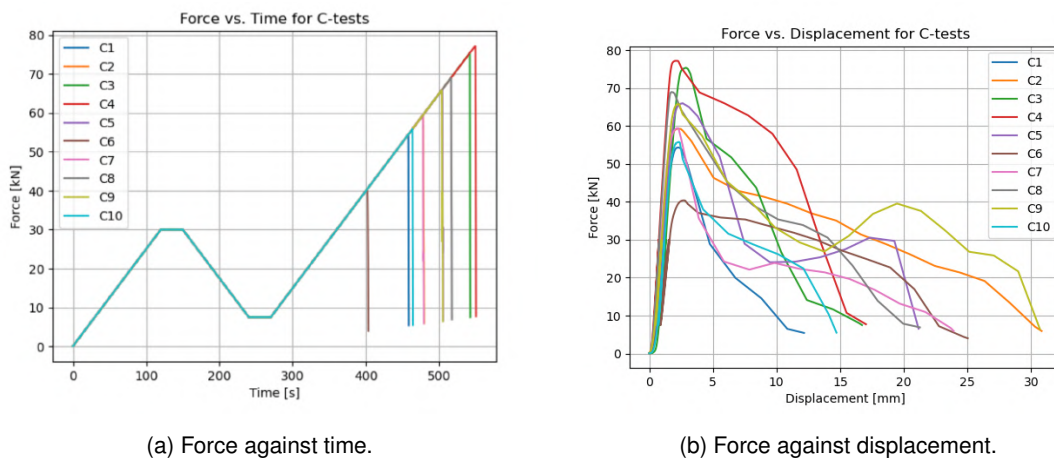


Figure 40: Load configuration for the *C*-tests.

1.4.4 Results of *C*-tests

All ten tests were performed with successful outcomes, meaning that failure was reached during the load sequence without unwanted failure mechanisms such as buckling. A plot of the load procedure for all *C*-tests is shown in Figure 41, as well as the displacement of the hydraulic head. The obtained test results are summarised in Table 4. In Section 2 individual graphs are shown, as well as graphs used to calculate the compressive modulus of elasticity in Table 5.



(a) Force against time.

(b) Force against displacement.

Figure 41: Data from all the *C*-tests.

Table 4 consist of data obtained from the *C-tests* and the calculated compressive strength. The total displacements are denoted by δ_{tot} , and the maximum strain reached is denoted as ϵ_{max} . The average compressive strength was found as 38.9 *MPa*.

Specimen	F_{max} [kN]	A_{cs} [mm ²]	δ_{tot} [mm]	ϵ_{max} [%]	$f_{c,0}$ [MPa]
<i>C1</i>	54.313	1598	12.159	1.529	33.988
<i>C2</i>	59.359	1601	30.830	0.450	37.076
<i>C3</i>	75.339	1604	16.715	0.341	46.969
<i>C4</i>	77.180	1602	17.026	0.986	48.177
<i>C5</i>	66.000	1597	21.157	0.399	41.327
<i>C6</i>	40.388	1596	25.021	0.292	25.306
<i>C7</i>	59.396	1601	23.918	0.468	37.099
<i>C8</i>	68.940	1598	21.262	0.384	43.141
<i>C9</i>	65.753	1599	30.694	0.342	41.121
<i>C10</i>	55.782	1602	14.709	0.277	34.820
Average	62.246	1600	21.349	0.547	38.902

Table 4: Results of the *C-tests*.

Based on the regression analysis, the objective was to determine two important properties, the compressive modulus of elasticity and the elastic compressive strength. In particular, the average value of the elastic compressive strength obtained from the regression analysis was found to be 35.7 *MPa*, as shown in Table 5. This value will be used in the subsequent calculation of the tensile strength, further discussed in Section 1.5.

In accordance with *NS-EN 14080*, it is specified that the *T14.5* strength class has a mean characteristic modulus of elasticity of 11000 *MPa*. The result obtained from the test was found to be an average value of 11420 *MPa*, which indicates that the stiffness was in the expected range.

Specimen	K_c [kN/mm]	$F_{c,0,el}$ [MPa]	$f_{c,0,el}$ [MPa]	$E_{c,0}$ [MPa]
<i>C1</i>	137.29	40.55	25.34	7365.8
<i>C2</i>	64.74	55.08	34.43	9710.9
<i>C3</i>	212.80	69.14	43.21	11638
<i>C4</i>	226.86	69.66	43.54	12407
<i>C5</i>	292.60	59.18	36.99	16002
<i>C6</i>	161.51	38.87	24.30	8832.6
<i>C7</i>	164.16	55.62	34.76	8977.6
<i>C8</i>	218.91	66.07	41.29	11972
<i>C9</i>	219.34	65.38	40.86	11995
<i>C10</i>	279.82	50.89	31.81	15303
Average	197.80	57.04	35.65	11420.4

Table 5: Results obtained from regression analysis.

1.5 Four-point bending test

As the *S-tests* failed to produce a single tension failure, the specimens still have the capacity to be tested differently. The objective of conducting this pure bending test is to obtain strength parameters that could not be derived from the tension test.

By analyzing the data from this experiment, moment, curvature and strain distribution can be used together with the compression strength to derive the tension strength of the elements. Using results from previous tests and post-data analysis of pure bending tests, it is anticipated that the last decisive strength parameters for the timber elements can be derived. This chapter will hence cover the test preparations, methods, and present the obtained results.

1.5.1 Annotations and orientation of bending test

The bending tests were conducted on the same specimens for the tension test, hence equally referred to as *S1 – S4*. The specimens were subjected to two point loads perpendicular to grain in order to induce a constant moment distribution between the point of applications. The reaction forces in the support are hence equally with orientation perpendicular to grain.

1.5.2 Mounting and equipment of bending tests

All the four 4-point bending specimens were mounted on an *RDP Howden* machine capable of producing 100 kN of axial load. The load was transferred to the specimen using a horizontal steel beam. The beam symmetrically divided the force into two point loads that induced a moment in the beam. Steel clamps were used to prevent lateral displacements of the specimen under the experiment in order to obtain valid test data from sensors.

The Instron machine was capable of tracing both force, time and displacement of the hydraulic press head. These measurements are important in order to define load condition, though they give little information of the stress and strain distribution in the cross-section. For strain calculations, a camera was used to track displacement of markers mounted as a 6×10 grid according to Figure 42. The longitudinal distance of the markers are $l_m = 150$ millimetres.

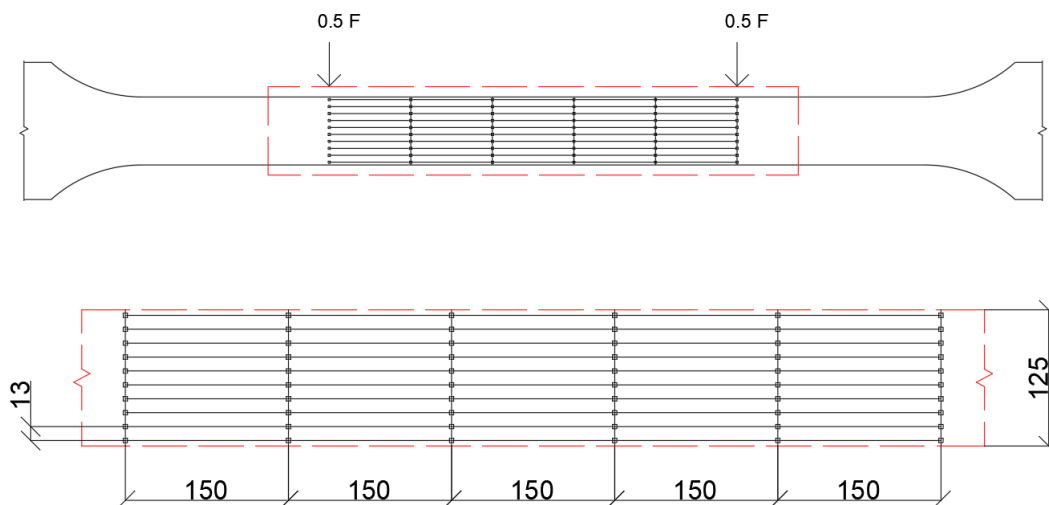


Figure 42: Placement of markers for camera tracking.

1.5.3 Method of bending tests

The 4-point bending tests were carried out according to the method provided in the standard *NS-EN 408*. Table 6 illustrates that all specimen requirements are fulfilled according to the aforementioned standard.

Location	Requirements [mm]	Specimen lengths [mm]
Specimen length	$l \geq 19h = 2375$	3730
Length between supports	$l_s \geq 18h \pm 3h = 2250 \pm 375$	2260
Gauge length	$l_0 \geq 5h = 750 \pm 187.5$	750

Table 6: Length parameters for 4-point bending test according to *NS-EN 408*.

The experiment was conducted with a load configuration provided in *NS-EN 408*, which specifies that the inclination of displacement shall not exceed $0.003h$ millimetres per second. Thus, the inclination was chosen as 10 millimetres per minute, which corresponds to 0.167 millimetres per second. The latter configuration implies a linear relationship between displacement and time throughout the DOL. The beam displacement induced a curvature that was measured using three lasers, two located directly under the point loads, and one at the middle at $\frac{l}{2}$. Theoretically, the lasers were placed such that an interpolation through the measured points would provide displacement as a second degree polynomial. Figure 43 illustrates the laser placements for bending test of *S4*.



Figure 43: Placement of lasers for curvature measurement.

Furthermore, local displacements in the grid of markers was tracked using two cameras on each side of the specimen. The frequency of captured images corresponds to three images per second per camera. One picture of the sequence produced for *S1* is illustrated on Figure 44.



Figure 44: One of 1503 pictures produced by one camera of *S1*.

1.5.4 Results of bending tests

The four tests were carried out successfully with failure occurring within the gauge length of the specimens. All sensor data, except for *S1*, which regrettably suffered from file corruption, was acquired without any impediments. All the specimens showed similar tendencies during the loading phase, a linear relationship between force and displacement, followed by minor slips resulting in a "stairway" shaped declination of load. Figure 45 illustrates the values and averaged values from the files that were not corrupted.

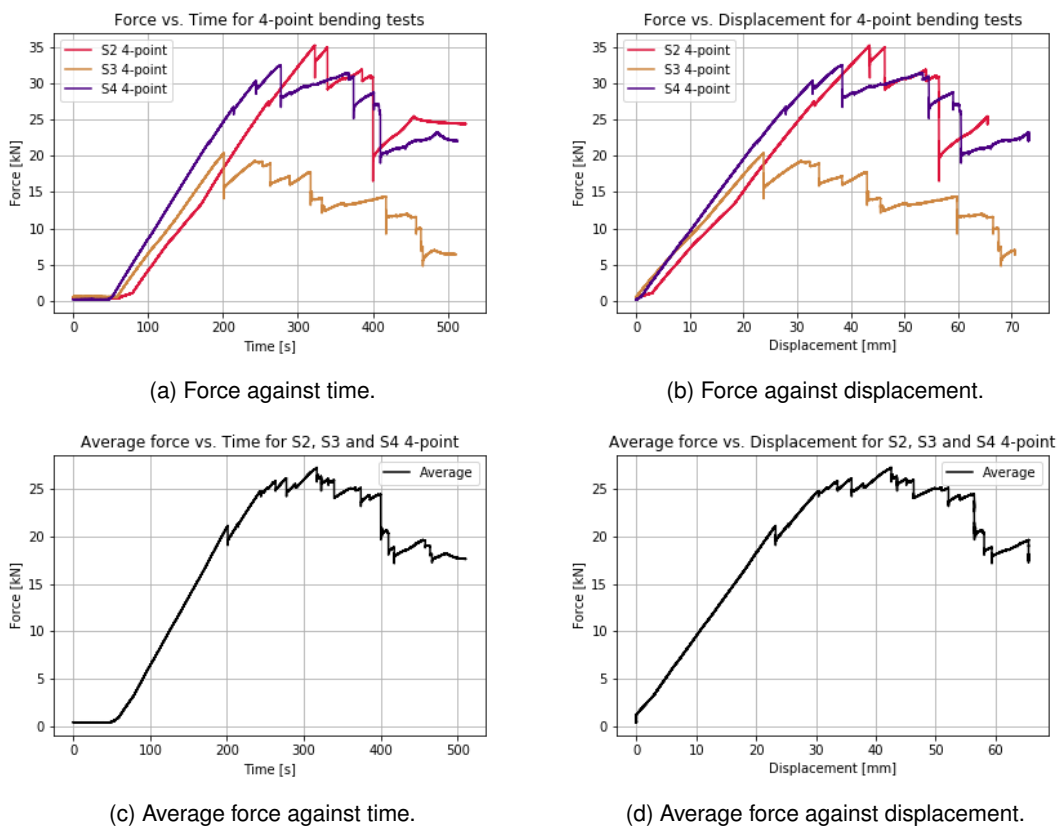


Figure 45: Data from 4-point bending tests.

A four-point bending experiment induces a constant moment distribution between the two point loads,

hence a failure is anticipated in the gauge length. Furthermore, symmetry and moment equilibrium can be used to calculate bending moment and cross-sectional strength parameters. Figure 46 illustrates how the moment distribution can be derived. Note that the force output from the acquired data is equal to the sum of the two point loads, which are hence denoted as $\frac{F}{2}$.

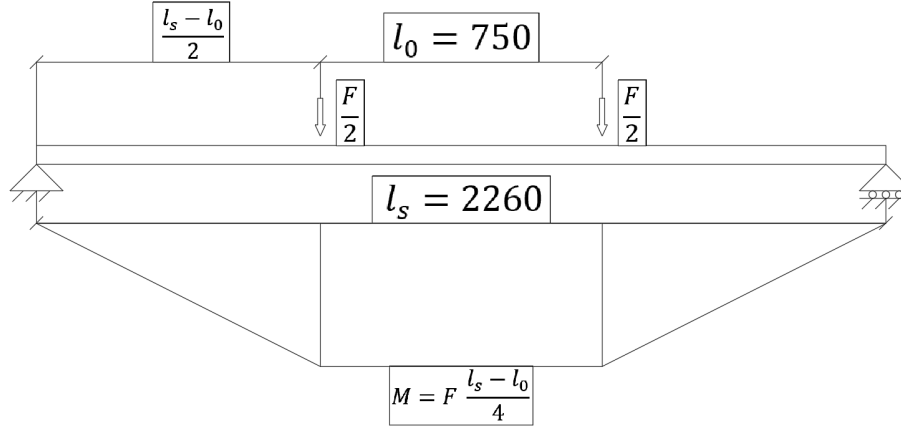


Figure 46: Moment distribution for 4-point test.

Equation 17 is obtained by moment equilibrium of the diagram on Figure 46. Based on previous gathered information from the compression tests, the material is expected to behave elastically for such tests. As the elastic compression strength, $f_{c,0,el}$, is greater than the tensile strength, failure will occur before the compression zone behaves non-linearly. Thus, the stress distribution in the cross-section is linear with a zero stress point at the centroid.

Additionally, the tension strength is calculated according to Equation 18, which is the same equation used to calculate bending strength in *NS-EN 384* (CEN 2022). The latter equations are used to obtain the relevant parameters when failure occurs on Table 7. To obtain the cross-sectional dimensions, w and h from *A3* is used as the reference point, which represents the cross-sectional area at the midpoint of the *S-test*, as defined in Section 2. a_d denotes the distance between the loading position and the nearest support, visualized as $\frac{l_s - l_0}{2}$ in Figure 46.

$$M = F \cdot \frac{l_s - l_0}{4} \quad (17)$$

$$f_m = \frac{3 \cdot F \cdot a_d}{w \cdot h^2} \quad (18)$$

Specimen	F_{max} [kN]	δ_{tot} [mm]	M [kNm]	$f_{t,0}$ [MPa]
<i>S2</i>	35.224	45.965	13.297	38.53
<i>S3</i>	20.352	25.676	7.683	22.66
<i>S4</i>	32.526	38.402	12.279	35.97
Average	29.367	36.681	11.086	32.39

Table 7: Values at failure for 4-point bending tests.

It is important to note that the average bending strength obtained from the tests is lower than the bending strength obtained for both *S2* and *S4*. This is mainly due to *S3*, which has significantly weaker

bending strength and is exerting a disproportionate influence on the overall average, as shown in Table 7. Additionally, the average compression strength calculated in Table 5 is lower than both $S2$ and $S4$, which suggests that there is a significant degree of uncertainty in determining the appropriate stress analysis approach, i.e., linear or non-linear. However, there was no indication of exceeding the elastic compressive capacity in the bending tests.

The determination of the global modulus of elasticity follows the method described in *NS-EN 408* (CEN 2012). Based on the experimental results, it was found that Laser 3 provided the most accurate deformation measurements compared to Laser 1 and Laser 2. This was clearly evident from the graphs plotted in Section 2, which showed the relationship between force and the deformation measured by each laser. The slope of the curve obtained from Laser 3 was found to be roughly constant, which allowed for a more accurate determination of the modulus of elasticity.

For the purpose of this analysis, the deformation measurements were taken at the center of the tension edge, which is located at the centre of the span. To ensure the highest possible correlation coefficient, the entire linear portion of the deformation curve was included in the analysis for the stiffness regressions, as shown in the graphs presented in Section 2. The graphs were created using Excel and the *trendline* function, which yielded a correlation coefficient of approximately 0.99.

According to *NS-EN 408*, the shear modulus is taken as infinity. However, coniferous wood species have a shear modulus of 650 MPa . Both results with and without the shear deformation correction were calculated, as prescribed by the standard. In line with *NS-EN 384*, when the shear modulus is taken as infinity, softwood specimens must be adjusted to the modulus of elasticity parallel to the grain, as described by Equation 19.

$$E_0 = E_{m,g} \cdot 1.3 - 2690 \quad (19)$$

Table 8 contains the stiffness and the computed global modulus of elasticity for two scenarios: when the shear modulus, G is set to a value of 650 MPa , and when it is set to infinity. In the latter case, the global modulus of elasticity is adjusted using the formula presented in Equation 19.

Specimen	K_b [kN/mm]	$E_{m,g}(G = 650)$ [MPa]	$E_{m,g}(G = \infty)$ [MPa]
$S2$	0.901	8830.76	8350.74
$S3$	0.914	9181.47	8776.85
$S4$	0.966	9637.20	9320.85
Average	0.927	9216.47	8816.15

Table 8: Stiffness and global modulus of elasticity from 4-point bending tests.

Wood exhibits a considerably lower shear modulus compared to its modulus of elasticity. This characteristic, combined with the typically large cross-sectional height of GLULAM components in relation to their span, can result in significant shear deformations in wooden constructions. To obtain precise results without incurring any extra costs or numerical issues, it is highly recommended to always consider shear deformations in calculations (Bell and Liven 2018). The observed failure patterns in the bending specimen indicate the presence of shear stresses. This is clear from the horizontal lines in Figure 47. In Figure 48, the strain is calculated from Hooke's law, using the average modulus of elasticity with a value of $G = 650 \text{ MPa}$, which indicates a presence of shear stresses. The value for σ_m at the extreme fibers is equal to $f_{t,0}$ in Table 7.

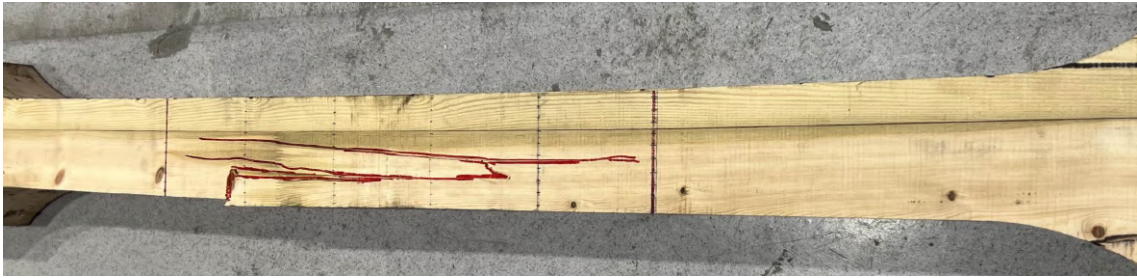


Figure 47: Failure in tension zone with secondary shear failure.

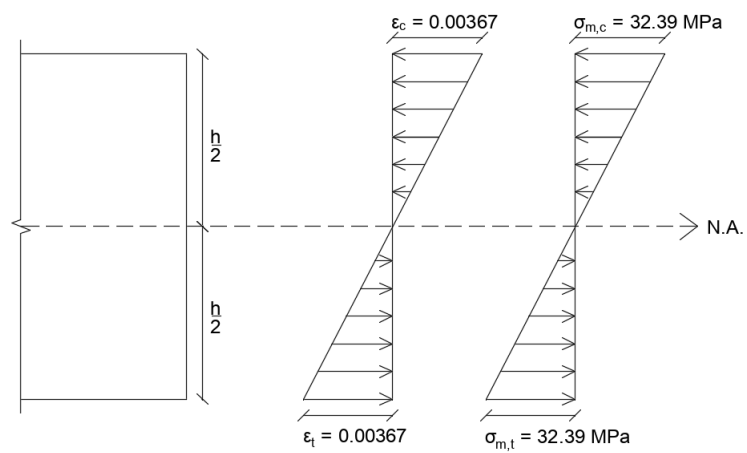


Figure 48: Stress-strain distribution across the cross-section of the beam.

1.6 Specimen moisture and density calculations

As previously discussed, structural behaviour of timber is largely dependent on MC and hence also density. In order to clarify the background of which all strength parameters in the previous tests are defined in, it is necessary to determine the MC and density of the tested specimens based on standardized methods. The ten specimens for both MC and density determination are identified as *MC-tests*. All specimens have origin from tension specimen *S4* and are labelled as *MC1-MC10* as illustrated on Figure 49.



Figure 49: Annotation of specimens from *MC-tests*.

1.6.1 Density

In *ISO 13061-2*, the procedure for determination of density is described (ISO 2014b). The dimensions of the test specimens were measured to the nearest 0.1 millimetre or to a precision of $\pm 0.3\%$, according to the standard. To ensure consistency between the *MC-tests*, measurements of the dimensions were taken from the same sides on each specimen, and the values can be found in Table 9. Following this, the density values were arranged in ascending order and presented in Table 10.

As all ten specimens were cut from the same subsample of *S4*, it can be concluded that $\rho_{05,i}$ is equivalent to $\rho_{05,i,min}$. Furthermore, the rank and the resulting 5-percentile density was calculated by interpolation, according to Equation 20.

Specimen	m_W [g]	b_W [mm]	d_w [mm]	h_W [mm]	V_W [mm ³]	ρ_W [kg/m ³]
MC1	33.1	55.2	34.0	30.8	57805.4	572.6
MC2	29.5	55.3	32.8	28.1	50968.9	578.8
MC3	28.5	55.5	33.0	27.2	49816.8	572.1
MC4	28.6	55.9	32.0	27.5	49192.0	581.4
MC5	28.3	57.0	31.5	26.9	48299.0	585.9
MC6	27.8	55.9	32.0	26.7	47761.0	582.1
MC7	29.4	55.3	31.8	28.1	49415.0	595.0
MC8	27.6	57.1	31.2	26.2	46675.8	591.3
MC9	28.8	56.5	31.6	27.5	49099.0	586.6
MC10	28.8	55.2	33.5	32.0	59174.4	486.7
Average values	29.0	55.9	32.3	28.1	50820.7	573.3

Table 9: Values for density in partially dry state.

Rank	1	2	3	4	5	6	7	8	9	10
ρ_W	486.7	572.1	572.6	578.8	581.4	582.1	585.9	586.6	591.3	595

Table 10: Values for density in ascending order and the corresponding ranks.

$$Rank = \frac{p}{100} \cdot (n - 1) + 1 = \frac{5}{100} \cdot (10 - 1) + 1 = 1.45$$

$$\rho_{05,i} = 486.7 + 0.45 \cdot (572.1 - 486.7) = 525.1 \frac{kg}{m^3}$$
(20)

The final calculation for the characteristic density is shown in Equation 21, where factor k_n set to be 0.88.

$$\rho_k = \min \left(1.1 \cdot 525.1 ; \frac{\sum_{i=1}^1 10 \cdot 525.1}{10} \right) \cdot 0.88 = 462.1 \frac{kg}{m^3}$$
(21)

1.6.2 Moisture content

The procedure for determination of moisture content is described in *ISO 13061-1* (ISO 2014a). The initial step of this procedure was to measure the weight and dimensions of the specimens. Once this was done, the specimens were placed in an oven set at a temperature of $(103 \pm 2)^\circ\text{C}$ for a period of 48 hours to completely dry them out. However, to ensure the accuracy of the measurements, the specimens were weighed thrice, with an interval of 8 hours in between, to confirm that there was a weight difference of less than 0.2 %. This step was crucial to ensure that the specimens were completely dried out and the weight remained constant. The moisture content results, including the initial mass, oven-dry mass, and moisture content for each specimen, are summarised in Table 11.

Specimen	$m_{init}[g]$	$m_{od_1}[g]$	$m_{od_2}[g]$	$m_{od_3}[g]$	MC[%]
MC1	33.1	29.4	29.3	29.3	13.0
MC2	29.5	26.3	26.2	26.1	12.6
MC4	28.5	25.4	25.3	25.2	12.6
MC4	28.6	25.3	25.3	25.2	13.0
MC5	28.3	25.1	25.1	25.0	13.2
MC6	27.8	24.7	24.7	24.6	13.0
MC7	29.4	26.2	26.1	26.0	13.1
MC8	27.6	23.5	24.5	24.4	13.1
MC9	28.8	25.6	25.6	25.5	13.0
MC10	28.8	25.6	25.6	25.5	13.0
Average values	29.0	25.8	25.8	25.7	13.0

Table 11: Values for MC.

2 Conclusion from experimental testing

As for all the tests on diagonal element 13B, it is imperative to stress the fact that all conclusions drawn are based on limited data obtained from a small number of tests. This inadequacy in sample size hampers the ability to accurately establish trends with minimal uncertainties. There is a sparse amount of material resources to conduct experimental tests, hence all collected data is considered valuable and significant. Additional uncertainties of MC and density were neither accounted for in calculations regarding estimated specimen capacity. On a final note, irregularities such as knots, differential swelling, and existing cracks contributed to diverse specimen quality. The latter is arguably a beneficial factor, as it more accurately describes the real situation in events such as the collapse of *Tretten* bridge.

Four tensile tests were conducted on the specimens sent to *NTNU* from the *Tretten* bridge. All four failed to produce failure modes related to tension, hence the tensile strength parallel to grain ($f_{t,0}$) could not be determined. The three specimens that exhibited the most consistent material behavior resisted on average a max tensile force of 318.5 kN . Divided by their respective areas, suggested that the timber used at *Tretten* had a mean tensile strength of at least 19.5 MPa . This value was later more accurately determined by conducting additional tests.

All three block failure tests experienced successful test results. In light of these, specimens mounted with LVDTs experienced sudden unsymmetrical rotation and dynamic displacement responses prior to failure. The latter in addition to visual analysis, suggests that the limitation of block failure capacity is highly influenced by unsymmetrical effects due to defects or uneven cross-sectional areas. Nevertheless, results indicate that the mean tensile capacity of the material ($f_{t,0}$) is approximately 33 MPa .

A total of ten compressive tests were conducted to determine compressive strength parallel to grain ($f_{c,0}$) and the stiffness (K_c) of the timber material. On average, the respective parameters were determined as 38.9 MPa and 197.8 kN/mm for the ten tests. The latter was used to find the corresponding elastic compressive strength $f_{c,0,el}$. As there were no indications of exceeding the elastic compressive capacity in the bending test, the possibility of non-linear compressive behavior was dismissed. Subsequently, a moment equilibrium analysis of the bending test results was utilized to ascertain the value of the tensile strength parallel to the grain ($f_{t,0}$) of the timber as 32.4 MPa . This value closely matches the one calculated from the block failure tests and the separate investigation carried out by Malo (2023), confirming its accuracy based on the experiments.

On a final note, the result indicates that the material quality of the lamellas *T14.5* used in diagonal 13B satisfies the qualities provided for GL32c in *EN14080*. The similarity between retrieved values from the bending tests and block failure test indicates accurate results for the experiment. Block failure is regarded as the failure mechanism that provides the least capacity against tensile loads, considerably lower than the capacity of the dowel group.

Table 12: Summary of experimental results of GL32c from *Tretten*.

Parameter	Value	Note
$f_{c,0}$	38.9 MPa	From compression test
$f_{c,0,el}$	35.7 MPa	From compression test
$f_{t,0}$	32.4 MPa	From bending test
$f_{t,0}$	33.0 MPa	From block failure test
$E_{c,0}$	11420.4 MPa	From compression test
ρ_k	$462.1 \frac{\text{kg}}{\text{m}^3}$	From density test
MC	13.0%	From MC test

Bibliography

- Bell, K. and H. Liven (2018). *Limtreboka - Bergeningsseksempler*. Trondheim/Moelv: Norske Limtreprodusenters Forening.
- CEN (2010). *Eurocode 5: Design of timber structures - Part 1-1: General - Common rules and rules for buildings*. CEN.
- (2012). *NS-EN 408:2010+A1:2012 Timber structures - Structural timber and glued laminated timber - Determination of some physical and mechanical properties*. CEN.
- (2022). *NS-EN 384:2016+A2 Structural timber — Determination of characteristic values of mechanical properties and density*. CEN.
- Hårstad-Evjen et al. (2013). 'Tretten Bridge – Timber and Steel in Harmony'. In: URL: https://intrans.iastate.edu/app/uploads/sites/12/2019/03/ID_100_Harstad-Evjen.pdf.
- ISO (1991). *NS-ISO 6891:1991 Timber structures - Joints made with mechanical fasteners - General principles for the determination of strength and deformation characteristics*. ISO.
- (2014a). *ISO 13061-1 Physical and mechanical properties of wood — Test methods for small clear wood specimens — Part 1: Determination of moisture content for physical and mechanical tests*. ISO.
- (2014b). *ISO 13061-2 Physical and mechanical properties of wood — Test methods for small clear wood specimens — Part 2: Determination of density for physical and mechanical tests*. ISO.
- Jenssen, C.G. and E.D. Vetter (2022). 'Introduction of fatigue behaviour of timber and processing experimental data'. Project thesis. NTNU.
- Malo, Kjell Arne (2023). 'Eksperimentelle undersøkelser av trematerialer fra Tretten bru'. Ongoing investigation for Havarikommisjonen.
- Qvist, S. and C. Soland (2022). 'Parameterstudie av Tretten bru'. Project thesis. NTNU.
- Statens Vegvesen (2016). 'Kollapsen av Perkolo bru – hva gikk galt?' In: URL: <https://www.vegvesen.no/globalassets/nyheter/bilder/komm/perkolo-bru---sluttfort-rapport.pdf>.



 **NTNU**

Norwegian University of
Science and Technology